

THESIS ON INFORMATICS AND SYSTEM ENGINEERING C97

Flow-Sensitive Robotic Fish: From Concept to Experiments

TAAVI SALUMÄE

TALLINN UNIVERSITY OF TECHNOLOGY
Faculty of Information Technology
Centre for Biorobotics

This dissertation was accepted for the defence of the degree of Philosophy in Engineering on December 22, 2014.

Supervisor: Prof. Maarja Kruusmaa
Centre for Biorobotics
Tallinn University of Technology
Tallinn, Estonia

Opponents: Prof. Kristin Ytterstad Pettersen
Centre for autonomous marine operations and systems
Department of Engineering Cybernetics
Norwegian University of Science and Technology
Trondheim, Norway

Prof. Gianluca Antonelli
University of Cassino and Southern Lazio
Cassino, Italy

Defence of the thesis: January 20, 2015, Tallinn

Declaration:

Hereby I declare that this doctoral thesis, my original investigation and achievement, submitted for the doctoral degree at Tallinn University of Technology has not been submitted for any academic degree.



European Union
European Social Fund



Investing in your future

Copyright: Taavi Salumäe, 2014
ISSN 1406-4731
ISBN 978-9949-23-732-6 (publication)
ISBN 978-9949-23-733-3 (PDF)

INFORMAATIKA JA SÜSTEEMITEHNIKA C97

**Voolutundlik robotkala:
ideest katsetusteni**

TAAVI SALUMÄE

CONTENTS

LIST OF PUBLICATIONS	7
INTRODUCTION	10
1 BACKGROUND	13
1.1 Traditional Marine robotics.....	13
1.1.1 Autonomous underwater vehicles and applications	15
1.1.2 Autonomous underwater vehicle technologies.....	18
1.2 Fish swimming and flow sensing	20
1.2.1 Fish propulsion mechanism.....	21
1.2.2 Fish flow sensing mechanism	22
1.2.3 Fish flow sensing behaviors	24
1.3 Biomimetics in underwater robotics.....	26
1.3.1 Linked fish robots	26
1.3.2 Compliant approach	27
1.3.3 Artificial lateral line sensors	28
1.3.4 Artificial lateral line sensing	29
1.4 Summary	29
2 COMPLIANT FISH-ROBOT DEVELOPMENT	30
2.1 Design criteria and limitations of previous studies.	30
2.2 Underlying questions of this chapter?	32
2.3 Design of the soft-bodied underwater vehicle.....	33
2.4 Mimicking passive properties of biological fish	37
2.4.1 Myometry-driven approach.....	38
2.4.2 Measuring the bending stiffness of a fish using a gravitational force	41
2.4.3 Biomimetic fin with continuous elasticity profile.....	43
2.4.4 Performance of the biomimetic fin.....	44
2.4.5 Conclusions about the bio-inspired stiffness profile	46
2.5 Experimental validation of model-based body design	47

2.6	Conclusions	50
3	FLOW-RELATIVE CONTROL	52
3.1	Artificial lateral line	52
3.2	Experimental setup	54
3.3	Robotic fish in steady flow	56
3.3.1	Rheotaxis	56
3.3.2	Flow speed detection	58
3.4	Robotic fish in turbid flow behind an object	62
3.4.1	Flow characterization	63
3.4.2	Detection of the presence of the upstream object	64
3.4.3	Estimation of the objects position	66
3.4.4	Station holding behind the object	68
3.5	Conclusions	69
4	CONCLUSIONS	70
	REFERENCES.....	72
	ABSTRACT.....	86
	KOKKUVÕTE.....	88
	APPENDIX A	91
	APPENDIX B	101
	APPENDIX C	109
	APPENDIX D.....	123
	APPENDIX E	131
	APPENDIX F	145
	APPENDIX G.....	153
	APPENDIX H.....	175
	CURRICULUM VITAE	183
	ELULOOKIRJELDUS	184

LIST OF PUBLICATIONS

Main contributing publications

This thesis is based mainly on work reported in following publications. All publications are reprinted in Appendix of this thesis. My contribution to each publication is described in the main part of the thesis. A brief summary of my contribution is also brought out at the end of the publications list.

- A. C. Fiazza, T. Salumäe, M. Listak, G. Kulikovskis, R. Templeton, O. Akanyeti, W. Megill, P. Fiorini, and M. Kruusmaa, “Biomimetic mechanical design for soft-bodied underwater vehicles,” in *Proc. OCEANS 2010 MTS/IEEE - Sydney*, 2010
- B. O. Akanyeti, A. Ernits, C. Fiazza, G. Toming, G. Kulikovskis, M. Listak, R. Raag, T. Salumäe, P. Fiorini, and M. Kruusmaa, “Myometry-driven compliant-body design for underwater propulsion,” in *Proc. IEEE Int. Conf. on Robotics and Automation (ICRA)*, 2010, pp. 84–89.
- C. T. Salumäe and M. Kruusmaa, “A Flexible Fin with Bio-Inspired Stiffness Profile and Geometry,” *J. Bionic Eng.*, vol. 8, no. 4, pp. 418–428, Dec. 2011.
- D. H. El Daou, T. Salumäe, G. Toming, and M. Kruusmaa, “A bio-inspired compliant robotic fish: Design and experiments,” in *Proc. IEEE Int. Conf. on Robotics and Automation (ICRA)*, 2012, pp. 5340–5345.
- E. H. El Daou, T. Salumäe, L. D. Chambers, W. M. Megill, and M. Kruusmaa, “Modelling of a biologically inspired robotic fish driven by compliant parts,” *Bioinspiration & Biomimetics.*, vol. 9, no. 1, p. 016010, Mar. 2014.
- F. T. Salumäe, I. Ranó, O. Akanyeti, and M. Kruusmaa, “Against the flow: a Braitenberg controller for a fish robot,” in *Proc. IEEE Int. Conf. on Robotics and Automation (ICRA)*, 2012, pp. 4210–4215
- G. T. Salumäe and M. Kruusmaa, “Flow-relative control of an underwater robot,” *Proceedings of the Royal Society. A*, vol. 469, no. 2153, 2013.
- H. M. Kruusmaa, G. Toming, T. Salumäe, J. Jezov, and A. Ernits, “Swimming speed control and on-board flow sensing of an artificial trout,” in *Proc. IEEE Int. Conf. on Robotics and Automation (ICRA)*, 2011, pp. 1791–1796.

Supporting publications

These papers are also published in the same field, but do not form a main part of this thesis and are therefore not added to the appendix.

1. T. Salumäe, R. Raag, J. Rebane, E. Ernits, G. Toming, M. Ratas, M. Kruusmaa, „Design principle of a biomimetic underwater robot U-CAT“ in *Proc. OCEANS'14 MTS/IEEE St. John's*, September 2014.
2. D. S. Jung, P. P. Pott, T. Salumäe, M. Kruusmaa, „Flow aided path following of an underwater robot“. in *Proc. IEEE Int. Conf. on Robotics and Automation (ICRA)*, 2013, pp. 4602 – 4607
3. G. Toming, T. Salumäe, A. Ristolainen, F. Visentin, O. Akanyeti, M. Kruusmaa, „Fluid Dynamics Experiments with a Passive Robot in Regular Turbulence“ in *Proc. IEEE International Conference on Robotics and Biomimetics (ROBIO)*, 2012 pp. 532 – 537
4. H. EL Daou, T. Salumae, A. Ristolainen, G. Toming, M. Listak, M. Kruusmaa, „A Bio-mimetic Design and Control of a Fish-like Robot using Compliant Structures“ in *Proc The 15th International Conference on Advanced Robotics*, 2011, pp. 563 – 568
5. O. Akanyeti, J. Brown, L. D. Chambers, H. El Daou, C. Fiazza, P. Fiorini, J. Ježov, D. S. Jung, M. Kruusmaa, M. Listak, A. Liszewski, J. L. Maud, W. M. Megill, L. Rossi, A. Qualtieri, F. Rizzi, T. Salumäe, G. Toming, R. Venturelli, F. Visentin, and M. De Vittorio, “FILOSE: a swanning robot,” *IEEE Robotics and Automation Magazine*, vol. 21, no. 3, pp. 51 – 62, 2014.

Personal contribution to publications

- A. Designed and constructed most of the robot. Planned and conducted the experiments
- B. Proposed the initial idea. Contributed to planning and conducting the experiments. Designed and constructed the tail models.
- C. Developed the methodology for measuring stiffness of fish. Developed fins with biological stiffness profiles. Developed experimental setup. Planned and conducted experiments. Analysed and discussed the data. Wrote the article.

- D. Developed methodology for experimentally validating theoretical model of robot dynamics. Developed experimental setup, planned experiments and conducted them.
- E. Developed methodology for experimentally validating theoretical model of robot dynamics. Developed experimental setup, planned experiments and conducted them.
- F. Identified the required parameters to develop controller. Developed the controller and identified its performance. Planned and conducted all the experiments. Analysed data and discussed results. Wrote the paper in cooperation with co-authors.
- G. Proposed the hypotheses, developed the methodology, ran the experiments, analyzed the results, discussed them, made the conclusions and wrote the article.
- H. Identified the relationship between the pressure drop and the flow speed. Characterized the actuation properties of the robotic platform by using the force feedback. Implemented a swimming-speed control with a pressure feedback. Contributed to writing of the “Force control” and the “Swimming control with the onboard flow/pressure sensing” sections.

INTRODUCTION

All the objects in water, including underwater robots, are affected by flow. Even very large robots working in oceans are constantly being carried by currents. For small robots, however, the flow influence is extreme. Especially if these robots have to work in rivers, streams, canals and other turbulent and fast-flowing environments. Therefore, it is clear that such autonomous underwater vehicles need to take flow into consideration. To do that, robots first need to be aware of the flow, and then they have to be able to adapt to the flow. Flow awareness means that the robots need to sense the water movement and they have to be able to understand how the movement will affect them. Adaption to the flow means that they need to change their behavior and movement according to what they sense.

At the moment there are no good methods available to sense the flow and to estimate its influence on the robot. The problem is partly solved for large vehicles by using acoustic flow measuring devices (acoustic Doppler current profilers). Unfortunately, these devices are not suitable for small and medium-sized vehicles because of the size and weight. Also, the influence estimation part of the problem remains largely unsolved, because the acoustic devices only measure the average bulk flow speed of the surrounding water, not the flow on the surface of the vehicle that actually affects it.

Researchers have tried to solve this problem by taking inspiration from fish. Fish are very aware of the water movement around them thanks to the lateral line organ. Using the lateral line they can feel the flow on their body and act according to what they feel. For example they can adapt to the direction and the speed of the flow. They are also able to detect other objects in flow and they are even able to harvest energy from the vortices created by these other objects. Inspired by these great abilities, researchers have tried to understand and copy the mechanism and the functionality of the lateral line. Artificial lateral lines that have been created are already able to localize and identify moving objects, detect vortices created by the bodies upstream and even increase the efficiency of propulsion by using these vortices. Most of these studies, however, have been conducted using static sensor arrays or platforms with very limited degrees of freedom. Also the algorithms that have been used are mostly too complex and inefficient to run in real time. Therefore, artificial lateral lines are today not in use to control underwater vehicles.

The lack of suitable sensing mechanisms also induces a problem with the flow adaption. The vehicle cannot be controlled according to the flow if there is no information about the flow. However, the flow adaptability does not have to be only active (control-based), but can also be passive. It means the robot can be mechanically adapting to the water movements. The underwater vehicles in use

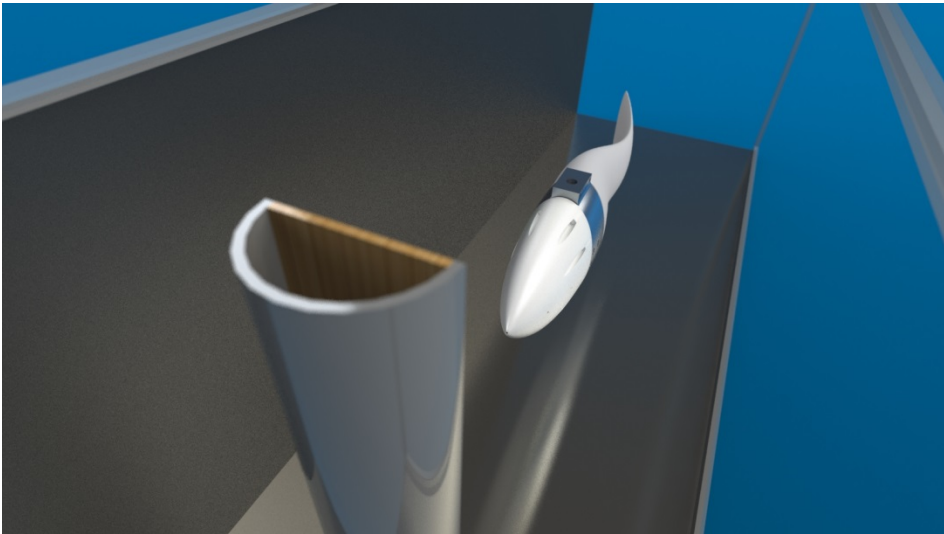


Figure 0.1 – Illustrative figure of the fish-robot developed in this thesis. The robot is swimming in a flow-tunnel in turbulent water behind a half-cylinder.

at the moment are rigid and therefore are not passively adapting to the currents and vortices. The current solution for making them less prone to be manipulated by the weaker currents is to make them larger and heavier. But this solution also makes them useless for many types of environments where these currents are the main problem. For example shallow riverbeds, rocky bottoms and between human-made underwater structures like bridges and dams are such kind of environments. However, if the vehicle was made soft and flexible, the vortices would bend the robot instead of moving the whole body. Soft underwater vehicle could therefore be much better solution for riverine environments. In rivers and canals there are many small eddies and currents that the soft vehicle could neglect thanks to its passive properties. Soft underwater vehicle could also be much safer to the surrounding environment, including the animals and humans swimming together with it. It would be more durable to collisions than rigid vehicles. Another advantage would be that it is much less likely to getting tangled in different water-plants and human-made objects that are common in rivers.

I propose an approach to address the flow awareness and the flow adaptability problems. I claim that an artificial lateral line can be simply and effectively used to control an autonomous underwater vehicle in real time. A small array of artificial lateral line pressure sensors is enough to navigate a rapidly moving vehicle in steady flow as well as in a wake of an object. I demonstrate this by developing a soft-bodied fish-robot. The robot carries 5 commercial pressure sensors that I show is enough to get information about flow speed, direction and regimen, and to navigate in a vortex street behind an object. The vehicle itself is propelled by a compliant tail that mechanically adapts to flow and is therefore suitable for rapidly flowing environments.

More specific scientific contributions of this thesis are following:

- Developing a novel type of fish-robot which incorporates soft-body actuation and artificial lateral line.
- Showing that fish-like swimming can be achieved with a compliant body whose geometry and elasticity distribution are mimicking these of a real fish. The body can be actuated from a single point instead of mimicking the distributed muscle actuation of biological fish.
- Proposing a Myometry-driven approach for identifying the fish body properties and using these properties in a design of biomimetic fins.
- Developing a gravity-based methodology for identifying the stiffness distribution of fish.
- Developing an experimental methodology for validating the dynamics models of the biomimetic oscillating fins used in our study.
- Proving that an artificial lateral line consisting of pressure sensors can be used for real-time control of underwater robot with respect to flow.
- Demonstrating a use of pressure-based Braitenberg control for achieving rheotactic behavior of an underwater robot
- Developing a methodology for identifying the flow velocity using artificial lateral line pressure sensors.
- Developing a methodology for controlling an underwater robot to hold station behind an upstream object using signals from artificial lateral line.
- Showing that this methodology helps underwater robot to save energy by using hydrodynamic shadow of an upstream object.

This thesis is divided into two main parts: compliant fish-robot development and flow-relative control. In the robot development part I concentrate on the design of an underwater vehicle with a single actuator and a soft tail. I will describe the methods used for building the vehicle and address the main problems arising with our design. The most important issue with compliant robotic fish tail is the design of its material and geometrical properties. I have used several different methods to find these properties. I describe and compare these methods in the robot development chapter.

In the flow-relative control part I show how the vehicle can be controlled using artificial lateral line pressure sensors. I implement station holding in a steady stream and in the wake of a bluff object. I also show navigation with respect to the flow in periodic turbulence and show that our method reduces vehicle's energy consumption.

The mentioned main parts of the thesis are preceded by the background research chapter to give an overview of the related studies and to emphasize the scientific importance and applicability of the current study. The author's publications, on which this thesis is based, are added to the Appendix.

1 BACKGROUND

Developing a compliant fish-like robot with an on-board biomimetic flow sensing is a topic that cannot be easily categorized into any specific research field. It is a multidisciplinary work that involves background from several seemingly very different areas. Robotics, biology, fluid dynamics and soft body modelling are all part of this study. Therefore, this chapter is not only a narrow overview of previous work done about fish-robots with flow-sensing. It instead gives a more general introduction to related topics to place the thesis into scientific context.

The Section 1.1 gives an overview of traditional underwater robotics that to this day does not use fish-like flow-sensing. We describe the current situation of underwater robotics, its challenges, and most importantly, methods for reckoning the flow. The Section 1.2 describes how the nature has done the things described in Section 1.1. We show how fish are swimming and how they take the flow into consideration. The Section 1.3 shows what people have taken from Section 1.2 to improve the work in Section 1.1. From there you can find out about fish-robots, artificial lateral lines and fishlike behaviors of robots.

1.1 Traditional Marine robotics

Underwater environment is one of the most difficult places for a man to be in. Mass of water creates a hydrostatic pressure that is not tolerable by the human organism. The maximum recommended technical diving limit using the most advanced technology is only 100 m. Beyond this limit human needs to use an atmospheric diving suit that has taken US navy diver to the maximum depth of 610 m [1]. Both of these numbers are just a small fraction of more than 10 km depths that we can find in our oceans. Therefore, without special vehicles, most of the underwater world remains inaccessible for people. Water, however, covers more than 70% of our planet. This 70% of course includes the majority of our planets natural resources, is a habitat for a huge amount of different and still unknown plants and animals and also conceals much of the human history. Therefore, there is a very strong motivation to develop robots that work in seas, lakes and rivers.

Marine robotics can be categorized into following groups:

- Unmanned surface vehicles (USV)
 - Autonomous surface vehicles (ASV)
 - Remotely operated surface vehicles
- Unmanned underwater vehicles (UUV)
 - Remotely operated underwater vehicles (ROV)
 - Autonomous underwater vehicles (AUV)
 - Intervention autonomous underwater vehicles (IAUV)



Figure 1.1 – Left: Typical remotely operated underwater vehicle Hercules ROV being deployed for mission (Public domain, Wikimedia Commons); Right: Autonomous surface vehicle Sonobot designed by Evologics. ¹

Unmanned surface vehicles are usually small boat-like crafts that are mostly used for bathymetric mapping and defense. Pioneering work on USVs has been done in MIT starting with their ARTEMIS robot developed in 1993 [2]. ARTEMIS was used to collect bathymetric data in the Charles River in Boston, MA [3]. Successful use of ARTEMIS has led MIT to the development of its successors ACES (Autonomous Coastal Exploration System) [4] and AutoCat [5]. USVs are nowadays commercially available and widely used. Some of the commercial examples are Evologics Sonobot [6] (Figure 1.1 right) and various products of ASV unmanned marine systems [7]. Such products are used for example as a moving long baseline navigation beacons [8], communication platforms, scientific survey vehicles or even as a naval targets for military trainings. Modern trends in scientific development of USVs is a use of wave [9], solar [10] and wind [11] energy to propel the vehicles during extra-long surveys.

Remotely operated underwater vehicles are the most common type of underwater robots. Most of them, however, are not actually robots at all according to the classical definition of this term. ROV's are teleoperated by a human from a surface vessel through a long cable. They are usually well-maneuverable vehicles for conducting different underwater inspection and manipulation tasks. To make operation as simple and intuitive as possible, ROVs are generally iso-actuated, have isotropic control properties and possess hovering capability [12]. Iso-actuation means that the vehicle is equipped with as many actuators as the number of the controlled degrees of freedom. Isotropic properties are ones that allow having equivalent system reaction capabilities in all the directions. Hovering capability allows the vehicle to stay steadily at a constant position. ROVs have already been in use since 60s. Early development was mostly funded by US Navy. They developed a "Cable-Controlled Underwater Recovery Vehicle" (CURV), which was used to recover objects

¹ All uncited images are made personally by the author of this thesis.

from the ocean floor [13]. Today classical ROVs are commercially widely available [14]. There are even open source projects that allow enthusiasts to build their own vehicles at home [15].

Even if classical ROVs cannot actually be called robots, it is not true for very modern vehicles that are developed nowadays. Modern ROVs combine properties of teleoperation and autonomy. They use data from various sensors and localization mechanisms to assist human operator or to carry out semi-autonomous tasks [16]. Recent ROV developments are concentrating on the improvements of the model-based control [17], visual servoing [18] and other image-based algorithms like 3D reconstruction of seabed [19].

1.1.1 Autonomous underwater vehicles and applications

Another class of UUVs is autonomous underwater vehicles (AUVs). AUVs are not tethered and they are fully on their own after deployed into water. They have to be able to conduct complicated underwater missions while running algorithms for navigation, localization, mapping etc. Human intervention is very limited due to the lack of fast and reliable underwater communication methods. Acoustic modems, which are used on these robots, allow sending very limited amount of data between the operator and the robot. Also the choice of sensor technologies that can be used under water is very narrow. When surface, aerial and terrestrial vehicles can rely on radio frequency devices (GPS, radio beacons) and different optical sensors (cameras, LIDARs), then underwater vehicles do not have this possibility. Radio frequencies do not propagate well in water and visibility is usually limited. AUVs have to deal mostly with acoustic signals. Artificial lateral line technologies are therefore most suitable for this class of marine robots.

The first known autonomous underwater vehicles (AUV's) were developed starting from the late 50s. One example is the SPURV (Self-Propelled Underwater Research Vehicle) developed in University of Washington [20]. Researchers used the vehicle to make conductivity and temperature measurements to support wave modeling [21]. SPURV displaced 480 kg, and could operate at 2.2 m/s for 5.5 hours at depths to 3 km. "The vehicle was acoustically controlled from the surface and could autonomously run at a constant pressure, sea saw between two depths, or climb and dive at up to 50 degrees" [12]. Another pioneer of underwater robotics was the Epaulard constructed in the 70s. Epaulard was able to dive 6000 m and operate for 7 hours with a velocity of 1 knot. It was equipped with acoustic positioning and communication and was designed for photographic and bathymetric survey of seabed [22].

From the end of 90s and the beginning of 2000s the availability of commercial AUVs and the development of new AUV technologies have greatly increased. The leading forces for the increase have been the defense and oil and gas



Figure 1.2 – Left: NESSIE AUV developed by the Ocean Systems Laboratory of the Heriot-Watt University; Right: REMUS 100 AUV by Hydroid.

industry. Also a civil protection and scientific institutions have played a big role [12].

In defense industry there are many applications where AUVs are extremely beneficial. In most of these applications AUVs help to reduce risk to manned vessels and thus help to save human lives. US navy has described the current applications and needs for AUV technologies in their UUV Master Plan 2004 [23] and US Department of Defense Unmanned Systems Integrated Roadmap 2013-2038 [24]. In the master plan they define nine high priority UUV navy missions, which in the order of priority are:

- Intelligence, Surveillance, and Reconnaissance (ISR)
- Mine Countermeasures (MCM)
- Anti-Submarine Warfare (ASW)
- Inspection / Identification
- Oceanography
- Communication / Navigation Network Nodes (CN3)
- Payload Delivery
- Information Operations (IO)
- Time Critical Strike (TCS)

At the moment the most mature technologies are available for mine countermeasures. For example U.S. Navy is using Hydroid’s REMUS 100 vehicle [25] (Figure 1.2) which was first in service during operation Iraqi Freedom in 2003 [26]. REMUS 100 is a compact torpedo-shaped AUV with a depth rating of 100 m. It is modular and can be equipped with different

navigation and payload sensors. Due to its military-proven reliability, REMUS 100 is widely used in many other fields except mine countermeasures. Some examples include Hydrographic surveys, harbor security missions, environmental monitoring, fishery operations etc. [27]. Other AUVs used in military service are for example HUGIN developed by Norwegian company Kongsberg [28], Battlespace Preparation AUV (BPAUV) by Bluefin [29] and Talisman by British company BAE systems.

Another leading force in AUV development, oil and gas industry uses AUVs mainly for surveys to locate deposits and for pipeline and oil rig inspection. Large scale AUVs like C&C ASV 6300 [30] and Furgo Echo Surveyor II [31] are used for surveys. These vehicles are able to travel long distances (48 to 70 hours with 4 knots operating speed) to map large areas of seabed. They use various sensors to detect areas of interest for oil companies. For pipeline inspection smaller and often more maneuverable AUVs are being used. Commercial software like SeeByte AutoTracker [32] is available for these platforms to automatically track the pipeline.

Current challenges for industrial AUVs include autonomous inspection of more complex underwater structures [33] and autonomous intervention tasks. The vehicles that are able to conduct such intervention tasks form their own class: Intervention Autonomous Underwater Vehicles (IAUV). Such robots are currently being developed for tasks like object recovery [34] and valve-turning [35].

Besides the industry and military, researchers are also motivated to use and develop AUVs. The main application of AUVs in research is hydrographic survey. During hydrographic surveys researchers often need to measure various water parameters in deep water, over long time or over large areas. This can be done also with manned research vessels or static measurement stations, but AUVs provide some significant advantages. Most important of them are lower cost, higher range and better accessibility.

High ranges and durations are achieved using gliders. Gliders do not use propellers to create thrust, but instead they change their buoyancy. Change in buoyancy creates up and down movement which is converted to forward motion using wings. The horizontal speed of gliders is typically around 1 km/h, but thanks to very low power consumption they are able to achieve great endurance. The Seaglider 1000 is able to travel up to 6000 km and has stayed in water for 292 days [36]. Other popular gliders, SLOCUM [37] and Spray [38] are capable for similar durations. SLOCUM also has a thermal version that harvests energy from temperature variations with ocean depth.

Better accessibility means that the AUVs can go to places that are very difficult to go with manned vessels. For example under ice explorations are one interest of research. Woods Hole Oceanographic Institution is using Remus 100 and

SeaBED vehicles to study conditions under polar ice [39][40]. These studies play a great role in understanding climate warming and ocean pollution. Also AUVs can collect survey data from depths that are difficult to achieve with towed vehicles. The deepest diving AUVs are REMUS 6000 [41] and Autosub6000 [42] that are rated for 6000 m missions.

The abilities of these available deep-diving and under-ice exploration AUVs is only a fraction of what is planned to be developed in following years. There are several projects going on to develop AUV technologies that could be used to explore the ocean of the Europa. Europa is one of the moons of the planet Jupiter. It is believed that the outer layer of the Europa is consisting of 100 km of salt-water covered with thick ice. This huge ocean is hypothesized to be one of the most probable places in our solar system to find extraterrestrial life form. To investigate these hypotheses, NASA has funded the projects VALKYRIE 1 and 2 [43] and ENDURANCE [44] through their ASTEP framework (Astrobiology Science & Technology for Exploring Planets). The goal of the VALKYRIE projects is to develop ice-penetrating robots that in the future could deploy underwater vehicles under ice. The ENDURANCE project aims to develop such underwater vehicles. Similar research is also funded by German Aerospace Center with the project EurEx (Europa-Explorer) [45]. EurEx project is using a Dagon-AUV [46] as an experimental platform to evaluate different Europa mission scenarios.

1.1.2 Autonomous underwater vehicle technologies

As mentioned earlier, radio frequencies and light do not travel well under water. Therefore, the list of available technologies that can be used is very limited. The navigation, localization and data collection of all the above described vehicles rely on the same short list of physical principles. These principles are mostly acoustic, inertial or magnetometric. Their use is pushed to limits with advancements in software algorithms and signal processing. The basic methods, however, have been the same for all the AUVs from the beginning of their era. This fact emphasizes the need for development of new technologies based on the physical principles, whose full potential is currently underused.

One of these most undeveloped principles is manometricity – measuring pressures. Every AUV carries a pressure sensor (Figure 1.3 right) to measure the hydrostatic pressure. Hydrostatic pressure is used to precisely calculate the depth of the vehicle. However, as explained later in this thesis, manometricity could be very well used to acquire much more information about the environment. Pressure distribution around the vehicle contains information about the flow, movement and objects around the vehicle. There are no traditional AUVs that use pressure measurements to get these data.

Acoustic and inertial principles are, however, very advanced and are used instead. Information about the flow is gathered using Acoustic Doppler Current Profiler (ADCP) [47] (Figure 1.3 left). ADCP estimates the velocity profiles of

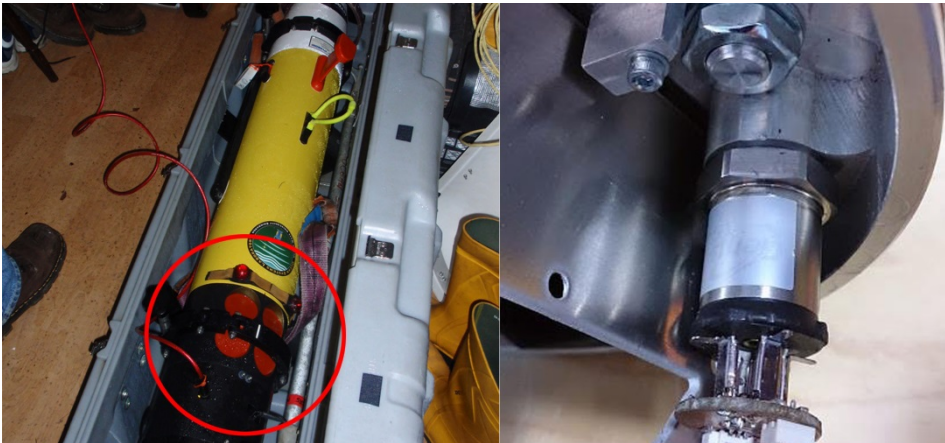


Figure 1.3 – Left: Acoustic doppler current profiler (marked by red circle) mounted on Remus 100 AUV; Right – Hydrostatic pressure sensor for measuring the depth of AUV. Image is taken from the inside of the U-CAT AUV developed in the Centre for Biorobotics in Tallinn University of Technology.

the water column. It estimates Doppler shift of sound waves scattering back from the particles in the water. ADCP can be used relatively well to measure the velocity of the vehicle with respect to the surrounding water. The problem with using the ADCP is that it measures the global currents at some distance from the transducer. The distance may usually be from 5 cm to hundreds of meters. So it is usually not possible to measure local flow that is actually affecting the vehicle. Also the device is large and expensive so it is usually not feasible to measure the flow at many different points around the AUV.

As the flow measurements are problematic on the AUVs, they usually rely on simpler and more reliable methods for navigation and localization. The navigation of AUVs is often based on dead-reckoning, meaning that the robot does not have any external references to measure its position. Position is instead calculated from a previously known position by integrating the velocities over time. Dead-reckoning AUVs use the following sensors:

- INS (Inertial Navigation System) – INS is composed of accelerometers, gyroscopes. Accelerometers provide estimation for linear accelerations and gyroscopes give data about angular position. INS includes the computer that runs sensor fusion algorithms to calculate the Euler angles of the vehicle. Modern INSs use fiber-optic gyroscopes which offer great accuracy. However, there will always be a drift in the estimation.
- Magnetic compass – is used to compensate for the drift in yaw angle.
- Doppler Velocity Log (DVL) – DVL improves the position estimation by providing the direct measurement of velocity. DVL measures Doppler shift in the acoustic pulses echoing back from the sea-bottom.

Most of the surveys AUVs use only the above described sensors for navigation. However, dead-reckoning is not precise enough for more demanding task. External position reference is often needed. This is usually provided by using the following systems:

- Long Baseline positioning (LBL) – Long baseline system consists of fixed beacons with a known position somewhere in the working area of the robot, and a transceiver on the robot. The robot uses acoustic signals to measure the distance from the beacons and then calculates its position using triangulation. The beacon may also be substituted with another AUV. In this case acoustic modems that are used for underwater communication are often used to measure distance from the other AUV.
- Short Baseline positioning (SBL) – The vehicle carries several acoustic transceivers. The system measures the distance of every transceiver with respect to a fixed transponder somewhere in the working area. It uses these distances to calculate the position of the vehicle. The bigger is the distance between the transceivers on the robot, the higher is the precision.
- Ultra-Short Baseline (USBL) – The vehicle carries an array of transceivers that are placed close to each other. Robot sends out an acoustic signal that is returned by a single fixed transponder. It finds the distance from the transponder by measuring the time delay. The direction is calculated by estimating the phase-shifts of the returned signals in the different transceivers.

Using the acoustic positioning system together with INS and DVL can give the vehicle a very precise positioning. Such vehicles will perform well in open waters and they are widely used, but they cannot be used in places with obstacles or near sea-bottom. Robots that have to work in such conditions always carry sensors for obstacle avoidance. Various types of sonars are used for this purpose. The simplest one is an echo sounder that is only able to measure distance to the reflecting surface. Scanning sonars are more advanced devices than incorporate an echo sounder moved by a motor. Multi-beam imaging sonars provide an acoustic image of the surrounding. The capability of all these devices to see obstacles is very dependent of the material and surface of the obstacle.

1.2 Fish swimming and flow sensing

Underwater robot technologies and their applications described in previous section are all evolved during the last century. Nature, however, has had time to develop solutions to similar problems for millions of years already. The methods and materials that nature has used during that time are also different and often much more complex. They have given very different solutions to the underwater problems. Locomotion of the above described marine robots is based on rotating propellers, while water organisms are mostly moving using

flapping or oscillating motion. Marine robots use acoustic, visual and inertial sensors for navigation and localization, but fish also have lateral line flow sensors, tactile sensors [48] and in some cases electric field sensors [49]. Both, natural and technological solutions have their own advantages and limitations. However, natural ones outperform the technological ones usually in many aspects. Efficiency of fish swimming can be as high as 97% [50]², while efficiency of propellers does not generally exceed 70% [51]. Navigation of fish allows them to maneuver in complex environments together with lots of different species of animals, from whom some have to be avoided and some have to be pursued to stay alive. Navigation of marine robots is still limited to relatively simple tasks like lawnmower surveys or primitive obstacle avoidance. Fish also have supremacy in maneuverability, accelerations and adaptability. Such outperformance demands us to study the locomotion and navigation of nature's created fish to improve the abilities of underwater robot technologies.

1.2.1 Fish propulsion mechanism

There are many different principles of biological underwater propulsion. For example jellyfish and squid practice jet propulsion, scallop claps its shells open and closed, and shrimp paddles with its legs. With fish the selection is much narrower. Fish swimming is usually categorized into two groups: body and/or caudal fin locomotion (BCF) and median and/or paired fin locomotion (MPF) [52]. MPF swimming fish flap their pectoral, pelvic, dorsal and anal fins. BCF swimming fish propel forward by creating an undulating wave in their body and caudal fin (tail) [53]. 85% of fish use BCF swimming, but usually they are able to use MPF as well. The first one is used for cruising and fast movements, while the latter one is helpful for maneuvering and backward propulsion.

BCF swimming fish species use different amount of their body for moving forward. Eel for example creates a traveling wave in all of its body. Tuna, on the other hand, only actuates a small portion of its body just in front of the tail fin. The ratio of actuated body to still body defines the class of BCF swimming. Rainbow trout, who is the main biological model in this thesis, belongs into a subcarangiform class. It creates a traveling wave in 3/5 of its body (Figure 1.4).

Even though the general principles of fish locomotion are well known, there is still a lot that remains unknown. It is not yet fully understood, how fish can generate high thrust while still being extremely efficient. Fish dynamics models, such as Lighthill's elongated body theory [54] are able to estimate the thrust forces based on the well-known kinematics. The estimated forces, however are much lower than those actually created by fish. Therefore, it is believed that fish use complex interactions with flow patterns created by other animals, environment, and itself. Recent studies with modern particle image velocimetry methods have revealed the interactions between the tail fin and the vortices created by the anal and dorsal fins [55]. The total thrust generated by all the fins

² As estimated by analyzing the wake behind a steadily swimming Mullet.

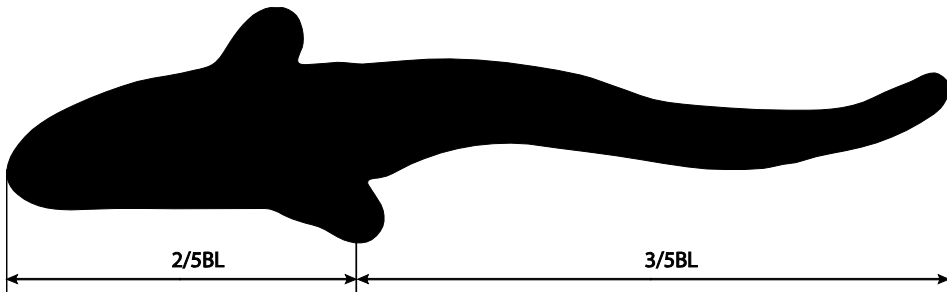


Figure 1.4 – Snapshot of a subcarangiformBCF swimming motion of a juvenile trout. The first $2/5$ of the body is rigid, while the rear $3/5$ is generating an undulating wave with an increasing amplitude towards the tip of the tail.

together is higher than the sum of thrust generated by them separately. Another aspect that helps to increase performance is that fish are able to use the passive properties of their bodies very efficiently. They can tune their body stiffness to optimize the mechanical cost of generating an undulating wave [56]. The effect of body stiffness and damping is actively studied analytically [57] and by using biomimetic mechanisms [58][59]. The body properties and the vortex interactions are also strongly linked. The tail stiffness plays a role in the production of wake patterns [60]. Fluid interaction, body properties and muscle activity are combined together in complex neuromechanical models of fish swimming [61].

1.2.2 Fish flow sensing mechanism

The flow interactions are not only important for propulsion, but also on a much more global scale. The natural water environment is in a constant movement. The movement exists from a molecular level up to ocean streams with a length of thousands of kilometers. It is caused by temperature variations, potential energy and pressure variations, differences in magnetic field, wind, moon, animals etc. It is affected by all the surrounding solids like rocks, bottom and ice. The information about all these reasons and influencers is contained in the flow. It is like a type of memory that stores data about the variables of a very complex function. The animals living in water are strongly influenced by flow and thus it is beneficial for them to be able to read this huge amount of stored information.

All fishes are able to sense and process hydrodynamic events using the lateral line organ. [62]. Also some crustaceans [63] and aquatic mammals have flow sensing organs [64]. The lateral line of a fish is visible as a faint line running lengthwise on the both sides of the fish. The line contains thousands of hair-cell like elements called neuromasts, which are bent by water movement. The bending is felt through an electrochemical signals sent to the brain over nerve fibers [65]. Although the organ is called a lateral line, the neuromasts are not actually located only on the visible line, but can be distributed all over the body. The design of the neuromasts and their number and placement can vary greatly

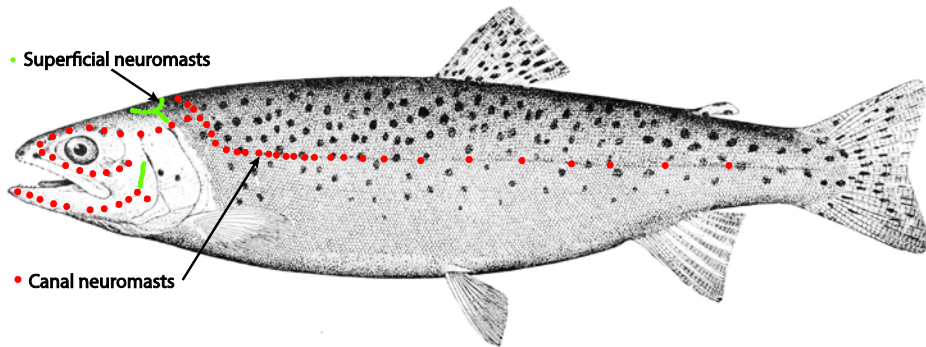


Figure 1.5 – Lateral line of a Rainbow Trout. The head of trout is densely covered by the canal and superficial neuromasts. The canal neuromasts on the side of the fish form a visible part of the lateral line. (Modified public domain image from Wikimedia Commons)

among different fish species [66]. For example the neuromasts on the rainbow trout are located on the visible line and densely on the head, while on the rest of the body is sparsely covered (Figure 1.5). The reason for differences in the lateral line design is not clear. It has been hypothesized, that the design is depending on the hydrodynamic conditions in the habitat. However, no direct relationship has been found between the number and distribution of the neuromasts and the habitat of the species [67].

The neuromasts of the lateral line exist in four different configurations: superficial neuromasts (SN), canal neuromasts (CN), spiracular organs, and vesicles of Savi [68]. All the fish species have the superficial and canal neuromasts, while the spiracular organs and vesicles of Savi are specific to some species, not including rainbow trout.

Superficial neuromasts (Figure 1.6 – left) occur free-standing on the skin, in pits, or on pedestals raised above the skin [62]. They consist of mechanosensory hair-cells that are covered with a cupula. The cupula is affected directly by the water flowing over the body. Therefore the SN directly measures the velocity on the surface of the fish body. The hair cells in the neuromast are oriented antagonistically so that the SN can sense the positive and negative flow in a single direction. To measure the flow in various directions, the neuromasts with different polarization axis are grouped together [69]. The SNs can sense flow speeds as low as $10 \mu\text{ms}^{-1}$ [70] and they respond to frequencies up to 100 Hz [62], indicating that the lateral line works also in the audible range [71].

Canal neuromasts are located in small canals under the fish skin. The canals are coupled to the surrounding water through canal pores (Figure 1.6 - right). The flow acceleration creates a different pressure between different canal pores. The pressure difference creates a proportional flow in the canal, which is felt by the CNs. Therefore, the CN can be described as a differential pressure sensor

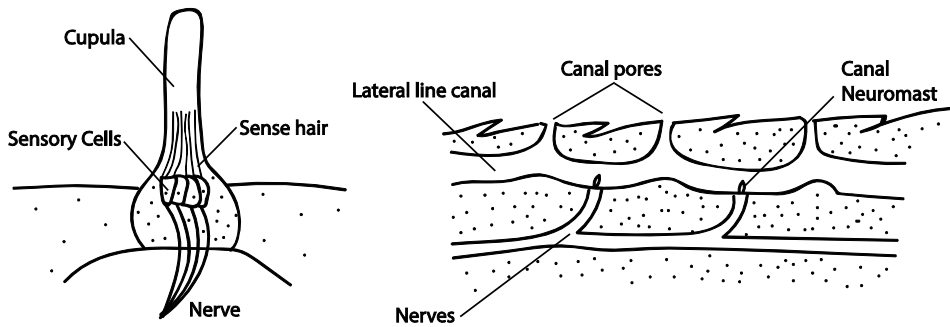


Figure 1.6 – Left: Superficial neuromast; Right: Lateral line canal with canal neuromasts.

between different canal pores [72]. The CNs are generally located on the visible part of the lateral line and on the head. Their sensitivity is in the range of $0.1 \dots 1$ *mPa* [70].

Spiracular organs and vesicles of Savi are specialized mechanoreceptors of some fish classes [73]. Spiracular organs are associated with the gills and consist of a tube or pouch lined with sensory neuromasts. The tube is sometimes opened to the water but may also be isolated. Neuromasts are stimulated by flexion of the cranial-hyomandibular joint [74], which is a joint associated with the movement of jaws and gills. The biological role of spiracular organ is not clear, but studies indicate that it plays a role in proprioceptor sense – a sense of the relative position of neighboring parts of the body. Vesicles of Savi consist of neuromasts enclosed in small isolated pouches on the ventral surface of some fish species like sharks and rays [75]. As neither of these organs is directly imposed by the water, their function in hydrodynamic sensing is still not understood.

1.2.3 Fish flow sensing behaviors

The lateral line is related to various fish behaviors. These behaviors are triggered either by abiotic or biotic sources. Abiotic sources are water movements caused by the environment, like the running water in river, currents in sea and wakes created by rocks. Biotic sources are generated by the self-motion of the fish or by the movements of other animals.

One of the best known abiotic flow sensing behaviors of fish is the rheotactic behavior – the fish orienting itself towards the water current. Orienting with respect to flow is important behavior in fish for upstream migration or for holding a position in a favorable place in the stream to detect odors and food carried with the flow. When there are no visual cues, like in the case of a blind Mexican cavefish, the rheotaxis is entirely based on the superficial lateral line [76]. In most cases however, the fish uses a combination of superficial lateral line and vision. The rheotaxis is also strongly linked to the fish ability to detect the flow velocity by sensing the fluctuations in the currents [77].

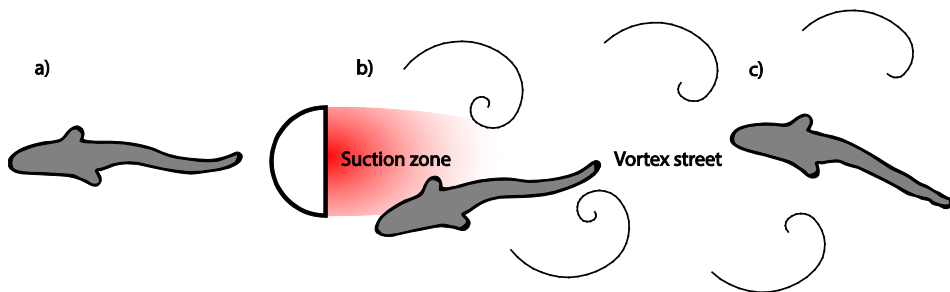


Figure 1.7 – Three preferred positions of a trout around the vortex street generated by a half-cylinder. a) bow wake in front of the cylinder; b) suction zone just behind the cylinder; c) well-developed Kärman vortex street.

Another set of very useful abiotic flow related behaviors is seen when a fish is swimming in flow in the vicinity of an object – for example rock or bridge pole in the river. It has been proven that fish are able to use the turbulence created by the object to consume less energy and to make their swimming more efficient [78][79]. This ability is one of the key factors that help some fish to migrate upstream thousands of kilometers in fast rivers. The most used approach to study the behaviors in unsteady flows is to use Kärman vortex street (KVS). The KVS is a repeating pattern of periodically shed vortices behind the blunt body in flow [80]. KVS can be reproduced in laboratory conditions with well-defined parameters. Half-cylinder is usually used as a blunt body. Vortex shedding frequency and the wake wavelength can be modified by changing the flow velocity and cylinder diameter.

Studies with rainbow trout in KVS have shown that trout uses 3 regions around the cylinder for station-holding: the vortex street (Figure 1.7 c), the edge of the suction zone just behind the cylinder (Figure 1.7 b) and the bow wake in front of the cylinder (Figure 1.7 a). In the first case the trout swims in the area behind the cylinder where the periodic vortices have fully developed. They adopt a distinct pattern of movement, called the Kärman gait [81]. During Kärman gating the trout tunes its movement according to the vortices. The body amplitude and curvature increase greatly and the tail-beat frequency matches the vortex shedding frequency of the cylinder. As a result the muscle activity and thus the cost of locomotion decrease [82]. The high efficiency of swimming in the vortex street is well demonstrated by the fact that even a dead fish is propelled upstream thanks to the passive properties of the body [83]. Alive fish only has to sense the flow and make some corrective movements to stay in the street [84].

The second preferred station holding behavior for trout is to entrain the flow in the edge of the suction zone (Figure 1.7 b). Suction zone is an area just behind the cylinder, where the flow is in the opposite direction with the surrounding flow due to lower pressure in the shadow of the cylinder. Objects placed into this area will be sucked against the cylinder. Fish stays on the side of the suction zone, balancing the suction force and the drag force to hold station [85].

The third option for fish is to use the increased pressure area in the bow wake in front of the cylinder [84] (Figure 1.7 a). In front of the cylinder there is a stagnation point where the flow velocity is zero. Around the stagnation point the flow velocity is lowered due to the increased pressure. Therefore, the drag force there is smaller and fish has to spend less energy to hold station [86].

Although during all the three station holding behaviors the muscle activity and oxygen consumption is reduced [79], it has been hypothesized that the bow wake is the most energetically favorable region [81]. However, experiment done in [87] shows that trout prefers to spend equal time (28%) in the bow wake and in the entraining zone. The time spent in the Kärman gait zone was only 8%.

Apart from the environmental flow sensing behaviors, fish also exhibit flow sensing behaviors triggered by other animals. One example is the ability of fish to discriminate between different surface waves and to detect and locate the prey on the surface [88]. It has also been proved that fish are able to detect and localize the waves generated under the surface by the vibrating dipole source [89]. They can also detect larger scale movements of the passing objects [90] and the hydrodynamic trail of other fish [91], which may be visible even 3 minutes after the fish has passed [92].

1.3 Biomimetics in underwater robotics

Great swimming and flow sensing performances of fish have inspired many research groups to mimic them. This mimicking is driven by two main goals. First goal is to develop better underwater vehicles. Fish outperform traditional marine robotics in most aspects. By understanding what the mechanisms behind this high performance are, it is possible to apply them on underwater vehicles. Another reason for biomimicry is to learn more about fish themselves. Research with living animals is difficult because it is often not possible to change the experiment's parameters independently. For example we cannot force the fish to change some of its body kinematics parameters while leaving everything else constant. Also it is hard to isolate fish senses from each-other to study behaviors. Therefore it is wise to develop robotic models that mimic fish swimming and sensing to study the locomotion and behaviors.

1.3.1 Linked fish robots

Most of the body and/or caudal fin swimming robotic fish are based on a linked structure. Their posterior body is composed of series of rigid links, which are actuated independently by many actuators or by a single actuator with separate transmission mechanisms for every link. One of the first and best-known of such robots is the MIT's RoboTuna [93]. RoboTuna is a 1.25 m long, 6-link tuna-shaped robot. It was used to show that the drag of an actively swimming fish-like body is significantly lower than the drag of the same body towed at the same speed [94]. MIT also developed RoboPike to study the hydrodynamics related to the fast-starting and maneuvering [95]. The first autonomous mission-scale fish-like swimming robot was the Vorticity Control Unmanned Undersea

Vehicle (VCUUV) developed in Draper Laboratory [96]. VCUUV is a 2.4 m, 174 kg fully autonomous vehicle that was used to study the foil interaction with K arman street vortices. Results indicated that the correct interaction with vortices may lead to improved efficiency and reduced wake signature, proving that the energy harvesting apparent in fish can also be used on a fish-robot. The University of Essex has developed series of autonomous robots to study the possible tail mechanisms and control algorithms to perform complex 3D maneuvers like C-shape turning [97][98]. Similar goals were set for the RoboSalmon project of Glasgow University [99]. RoboSalmon uses a tendon mechanism mimicking the distributed actuation of fish. Attempts have also been made to take the fish-like actuation out from the lab to the real-world environment. Beihang University has developed series of marine robots called SPC-I to SPC-III, that are incorporating fish-tail propulsion [100]. SPC robots carry traditional marine robot technologies, but have better maneuvering capabilities.

The fish-robots described above are mainly developed to improve the capabilities of underwater vehicles. There are many fish-like propulsion mechanisms that are developed to study the actuation and behaviors of biological fish. One example is an ongoing study about the coupling of electrical sense and mechanical system of an electric knifefish in the Northwestern University [101]. Also there are series of studies made in the Lauder Laboratories in Harvard, where robotic mechanisms are used to examine the fin and body kinematics and hydrodynamic function during locomotion [59].

1.3.2 Compliant approach

The mechanisms described above are composed of several links. By separately controlling the movement of each link, the desired kinematics of the body can be easily achieved. The similarity of the kinematics to that of a real fish is limited by the number of links. More links give higher precision. However, the complexity of the mechanism also increases. Robot needs to have more actuators, gears and bearings, resulting in higher friction and smaller reliability. To overcome these problems, researchers have developed compliant fish-like robots. Compliant robots are usually using one or a few actuators to flap a soft tail. The fish-like performance is achieved by choosing the right actuation parameters, geometry and material properties of the tail. A set of such compliant robots was developed by Pablo Valdivia y Alvarado at MIT [102]. The robots had a rigid head and a silicone body, which was actuated by the steel cables casted into it. The bodies were modeled by a cantilever beam actuated from a single point. The study hypothesized that that the exact kinematics of the fish can be copied by analytically calculating the elastic and viscous properties of the tail. Another compliant fish robot developed at MIT is based on a fluidic actuation [103]. Its silicone tail has air-channels, which are being filled with compressed air to actuate the tail. The robot is self-contained, and it is capable of rapid, continuum-body motion, such as escape maneuvers. Silicone tails were

also used by McHenry *et al.* who showed that body stiffness can be used to control the swimming kinematics and performance of elastic models of pumpkinseed sunfish [104]. Alben *et al.* studied the relationship between the rigidity and performance of the soft foils. They found peaks in a swimming speed at certain parameters.

1.3.3 Artificial lateral line sensors

Apart from mimicking the swimming mechanism of fish, researchers have also mimicked the lateral line system of fish. The aim for this is to better understand biological principles of fish sensing and to give underwater vehicles a sense of flow. The flow sensors like ADCP described in a traditional marine robotics section 1.1 are large devices that are not suitable for small vehicles. They are especially unsuitable for fish-like robots whose body is not fully rigid. Also ADCP is not capable of measuring the local flow at different places on the body of the robot.

To overcome these problems, researchers have tried to copy the sensing principles of both, superficial and canal neuromasts. Artificial superficial neuromasts are based on a miniature cantilever beam, whose deformation by the flow is being measured, exactly as it is with a biological fish. In [105]–[107], the deformation is being measured using piezoresistive strain gauges, while in [108]–[111] capacitive sensors are used. Artificial neuromasts using piezoresistive sensors are larger in size and are usually designed to be sensitive to flow only in a single direction. Multiple hair-cells are needed to measure flow in different directions, but the size sets the limit on designing such array. Capacitive sensors can be designed to be sensitive to flow in every direction and also they can be placed densely together, as the measurement units are small and can be fitted on a common electrode array. The main problem with the artificial superficial neuromast sensors is the fragility. The sensors are optimized to be sensitive enough to measure very small flow speeds, but the tradeoff is that the sensors saturate or break at higher velocities or when they collide with larger particles in water. McConney *et al.* have tried to overcome this problem by covering the hair-cells with a hydrogel cupula [112]. They have reported a sensitivity of $2.5 \mu\text{ms}^{-1}$, which is in the same order of magnitude with the biological lateral line sensors.

Research on artificial canal neuromasts is not as thorough as on artificial superficial neuromasts. Yang *et al.* used piezoresistive hair-cells that were mounted into canal with pores to achieve a fishlike differential pressure sensing [113]. Some other researchers, however, have placed arrays of flat pressure sensors on the underwater vehicle surface to directly measure the pressure [114], [115]. This method is somewhat different from fish lateral line sensing, as the sensors do not measure the differential pressure, but the absolute pressure instead.

1.3.4 Artificial lateral line sensing

Mimicking the mechanical action of the fish lateral line sensors is somewhat easier task than copying the signal processing and behavioral processes of it. Nevertheless, there are several ways how the artificial lateral lines have been used to achieve fish-like sensing behaviors. One of the best-studied sensing tasks is the dipole source detection and localization. Dipole source creates a distinct excitation pattern in an array of artificial lateral line flow sensors [116]. It has been demonstrated with different types of flow sensors and experimental configurations, that by processing these patterns, the position and nature of the source can be precisely identified [117]–[119]. It is also possible to identify the objects passing the sensor array. By using an array of MEMS pressure sensors, the velocity of the passing object can be detected with an average error of 2.5% [115]. Fernandez *et al.* demonstrated that also the shape and the size can be identified [120].

Another flow sensing task that has gained attention is the detection of turbulent flows. The goal of this task is to localize the vehicle with respect to the object generating vortices. This would allow achieving higher efficiency of the vehicle by using the energy of the flow, exactly as the fish does. As with fish studies, the K arman vortex street is also in the main focus here because of the high controllability and well determined parameters. Yang *et al.* used an array of 16 artificial superficial neuromast sensor to show that the fluctuations caused by the vortices are well distinguishable [116]. They were able to spatially map the wake signature behind the cylinder. Akanyeti *et al.* used a DPIV analysis to emulate the signals acquired by the flow sensor array and got a similar spatial map [121]. They also proposed a method to estimate the relative position of the sensor array with respect to the vortex formation point. Klein and Bleckmann extended the results by experimentally validating that the position of the upstream cylinder can be estimated by using only two artificial lateral line canal sensors on each side of their test platform [122]. The study was conducted using a static measurement array placed in various positions in the wake.

1.4 Summary

From this chapter it can be concluded that the complexity of current biomimetic systems is limiting their application in underwater robotics. We saw that plenty of robotic fish have been developed. However, all the marine robots used in natural environments are still rigid and use screw propellers. Also there are many artificial lateral lines created and successfully tested for various situations, but they have not been included in the control of any underwater vehicles. The reason is that most of the biomimetic technologies we saw lack the robustness and maturity required for underwater vehicles. From the traditional marine robotics section we saw, that these criteria are extremely important, as the marine robots have to conduct extremely responsible tasks in very complex environments. Therefore, technical approaches we choose in this thesis are such which in principle are more robust and simpler to apply. We emphasize the simplicity and usability rather than the biological adequacy.

2 COMPLIANT FISH-ROBOT DEVELOPMENT

In this chapter we describe the design of soft-bodied fish-robot. The rear 3/5 of the robots body is composed of compliant silicone which is being actuated by a single motor. The goal of implementing such a system is to improve the performance and applicability of fish-inspired robots by developing new methodologies for designing soft fins with minimal mechanical complexity. We introduce three novel approaches for finding the suitable design parameters, i.e. material properties for the soft body. Two of the methods are empirical and are based on mimicking the actual properties of a fish. The third method is based on theoretical modelling of the robot's body dynamics.

The robot described here also serves as a platform for studying flow-relative control of underwater vehicles in Chapter 4. The vehicle is carrying an artificial lateral line which we used in the European Commission FP7 project FILOSE (Fish Locomotion and Sensing) [123] to study how fish sense the flow around them, how they react to what they sense, and how the sensing and reactions can be mimicked on an underwater robot.

This chapter is organized as follows. In Section 2.1 we set the requirements for the fish-robot and discuss the limitations of the previous studies to meet these requirements. Specifically we show why the rigid linked fish-robots are not suitable and what the main problems with designing soft robots are. In Section 2.2 we propose the underlying questions of this chapter that we are going to answer to improve the performance of the compliant robot. In Section 2.3 we will present the prototype. In Section 2.4 we describe the empirical methods based on mimicking the body properties of fish and in Section 2.5 we describe a verification of a theoretical approach for predicting a body's motion. We draw the conclusions in Section 2.6.

2.1 Design criteria and limitations of previous studies.

The vehicle that has to operate in turbid underwater environments like rivers, canals etc. need to meet some very strict requirements. These requirements set the design guidelines of the biomimetic propulsion system. These guidelines are:

1. Applicability. The principle of the mechanism has to be simple enough for being used on underwater vehicles. Complex mechanisms usually require more space, are expensive and difficult to manufacture and lack reliability.
2. Flow-adaptability. The passive mechanical properties have to be such that the tail of the robot can be freely moved by the water. Such mechanism can passively adapt to light vorticity and turbulence by damping the forces generated by them.

3. Durability. A robot that has to operate in fast-flowing waters between many different objects like rocks, poles etc. is definitely going to crash against these objects. The mechanism has to be able to survive these crashes.
4. Efficiency. The propulsion system has to be reasonably efficient so that it would be in principle usable for actual autonomous robot tasks, where battery capacity is limited.
5. Velocity. The underwater vehicle has to be able to cope with the oncoming current and has to be able to swim upstream
6. Maneuverability. The vehicle has to be well controllable to effectively carry on different real-life operations.
7. Fish-like kinematics. The motion of the robotic fish tail developed here has to be similar to that of the actual fish. This requirement is important for the fish-like flow-sensing studies. If the robot and fish move in a similar way, comparative studies can be made between the sensing and behavior of these two [123].

Fish overcome man-made systems in terms of all of these requirements. Applicability, adaptability, durability and fish-like kinematics are of course natural to all fish, but fish are also faster, more efficient and better maneuverable than most of the man-made analogues. Therefore, as was described in the background chapter, researchers have developed several robotic-fish systems. All these systems have their own limitations when looking at the design criteria listed above.

The linked systems, such as RoboTuna [93] , RoboPike [94] and Essex fish [97], [98], are very well able to mimic the fish kinematics. By increasing the number of links involved, the motion can be made relatively precise. The Essex fish demonstrated that these systems can also be very well maneuverable. SPC-II vehicle by Beihang university showed that they even can develop relatively high speeds (1.2 Bl/s) [100]. However, these abilities are achieved by increasing the complexity of the mechanism and thus reducing the efficiency, durability, applicability and flow-adaptability. The efficiency is limited because of the high number of motors, transmission and other moving components. Durability and applicability are reduced for the same reason. Multi-part complex systems are difficult and expensive to build and are besides very prone to wear out and break. Moreover, including multiple motors and details requires more space in the vehicle and also makes it heavier. The linked systems thus reduce the possibility to include payload equipment like cameras and other sensors. Lastly, the multi-link fish-robots do not have flow-adaption ability. Their tail does not have a passive motion due to water movement.

Compliant biomimetic robotic tails such as the ones developed by Alvarado [102], McHenry [104] and Riggs [124] lack many of the problems of linked designs. These mechanisms are in principle very simple, incorporating only one actuator and a passively moving soft tail. Therefore, they are much easier and

cheaper to manufacture, are much more durable, and do not have a problem of internal friction and wear. The compliant materials are also passively adapting to the flow. Additional benefits are that they can be usually made quieter because of the smaller number of moving elements and they are safer to the surrounding environment. Based on all these benefits we can already say that the compliant robotic fish tails have more potential to become into use on actual underwater vehicles.

Of course there are some problems that have to be overcome before the compliant fish tails are mature enough for real-world applications. The main problem is the actual performance of these tails. Even though in theory the artificial fish-like locomotion can create high thrust and is more efficient than propellers, the current studies do not prove that. The robotic tuna of Alvarado *et al.* was able to swim at the maximum velocity of 1 BL/s [125], while his target velocity at the same actuation parameters was 2.5 BL/s. Also the error between the target kinematics and the actual measured kinematics was large. To design the vehicles, Alvarado *et al.* used an analytical approach by modelling the fish tail as a compliant beam. Even though the model was relatively detailed, the actual reaction of the tail was very different from the target action. This indicates that the current theoretical knowledge of nonlinear compliant vibrating systems with water interactions is not advanced enough to accurately describe the kinematics and dynamics of the system.

Other researchers have tried several empirical approaches to avoid using the imprecise analytical modelling. Their goal has been to improve the performance of the flapping fins by mimicking the properties of an actual fish. McHenry *et al.* [104] used a fishlike geometry and showed that body stiffness controls swimming kinematics and therefore the performance of elastic fish-like fins. Riggs *et al.* [124] casted silicone fins with biomimetic stiffness profile and compared the performance with regular NACA profiles. They showed that mimicking the properties of actual fish indeed improves the performance of the flapping fins. However, the studies were limited in various aspects. They isolated the biomimetic properties from each-other and did not study the influence of geometry and stiffness together. They also did not use the exact values of stiffness but only mimicked the chordwise stiffness profile. Also, the studies were made on a static platform instead of an actual robotic fish. Therefore, the performance of these studies in terms of the velocity, maneuverability and efficiency could not be estimated.

2.2 Underlying questions of this chapter?

To extend the knowledge required to improve the performance of compliant fish robots, being inspired by the limitations of the current studies, this chapter concentrates on two main questions.

1. If the passive properties of the biomimetic oscillating fin are more similar to these of an actual fish, will the performance of the fin increase? This question is studied in Section 2.4
2. How to improve the experimental methods that help to extend the theoretical knowledge about modelling the compliant robotic tail. This question is addressed in the Section 2.5

Before going to these questions, the Section 2.3 will describe the design of the robotic fish platform.

The model animal, on which the robotic fish of this study is based on, is rainbow trout (*Oncorhynchus mykiss*). When choosing the properties of the tail, the target kinematics and also when studying the flow sensing behavior in the next chapter, this species is taken as inspiration. The first reason is that a trout is very capable in turbulent waters. It swims hundreds of kilometers upstream in very difficult and raging water to its spawning grounds. Moreover, it does not eat on their journey, meaning that its locomotion is extremely efficient. Various studies show that this efficiency is greatly thanks to its skillful energy harvesting of upcoming vortices [78], [79], [81]–[84]. This brings out the other main reason for using trout as a subject specimen: it has very advanced lateral line sensing. Moreover, as the trout also lives in seas, it is also a very universal fish. It can survive in very different environments. Therefore, it is likely that the studies of trout locomotion can lead to more general solutions towards the biomimetic design of propulsion mechanisms. Also the principle of trout's locomotion is very suitable for underwater robots. It is a subcarangiform swimmer, meaning that it uses 3/5 of its posterior body for swimming, while the 2/5 of the anterior body is relatively rigid. While designing the robot, this rigid part can be used to enclose the electronics, actuators, sensors and other stiff, but vital components of the underwater vehicle.

2.3 Design of the soft-bodied underwater vehicle

The general principle of the actuation mechanism of our robot is based on the design of Alvarado [126] - a single servomotor pulls two cables that are connected to the rigid plate inside the soft tail. The design is partially published also in my master thesis [127]. The master thesis includes only the initial design that differs from the one described here in many aspects. All the internal components have been redesigned and replaced. Also, the main part of the robot, the compliant tail, is different.

One intermediate step of the robot design is also published in the 2010 IEEE OCEANS conference article “Biomimetic Mechanical Design for Soft-Bodied Underwater Vehicles” [128]. The article is attached into the Appendix A. My contribution to this article is the general design principle of the robot, design and manufacturing of some of the robots internal components, the design and manufacturing of all the silicone tails, and conducting the experiments.

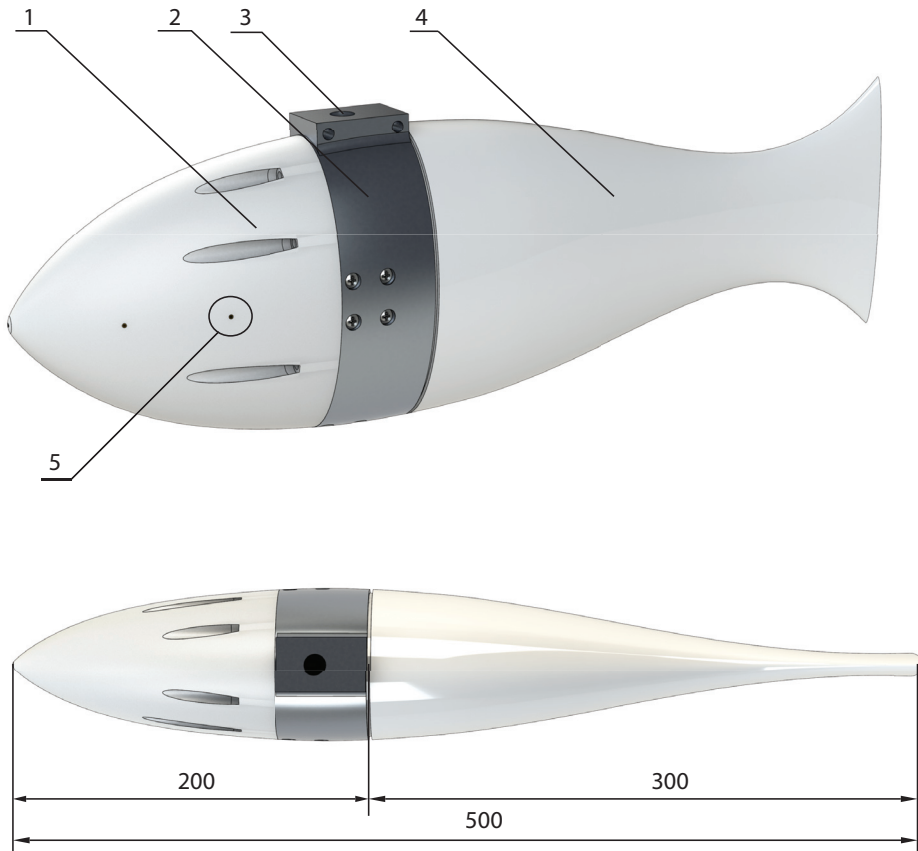


Figure 2.1 - The external design of the robotic fish. 1 – Plastic nose cover printed using selective laser sintering method; 2 – Aluminum chassis for holding all the main components of the robot; 3 – A screwpiece for mounting the robot to different experiment setups; 4 – The compliant body casted from 2-component silicone; 5 – Pressure port.

This chapter concentrates on the newer and improved version of the robot. My contribution to this robot version is the design of all the robots mechanical components and the development of the experiment software. The electrical design was made by the engineers of Centre for Biorobotics and the other partners of the FILOSE project.

The external design of the fish robots body is shown in Figure 2.1. The shape of the body is derived from a 3D scan of an actual rainbow trout. To get an analytical description of the body, we approximated the shape using elliptical cross-sections. The robot is made symmetrical in sagittal (right) and frontal (top) plane, while the actual fish is somewhat asymmetrical. The robot is also slightly wider to make room for the actuators, sensors and electronics. The length of the device is 0.5 m, of which the fore 0.2 m is rigid and the rear 0.3 m is compliant.

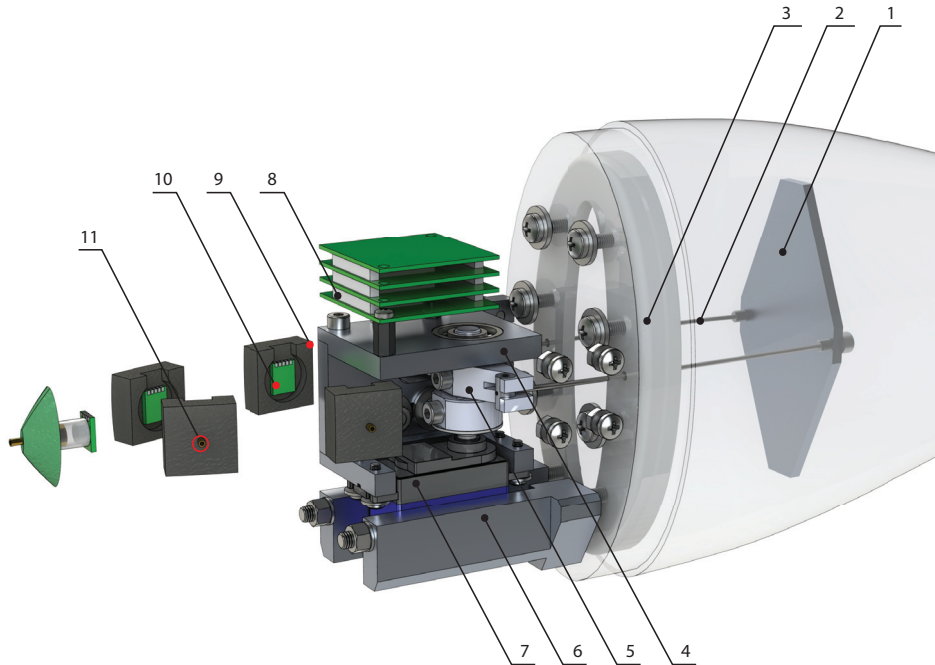


Figure 2.2 – The design of the internal components of the robotic fish. 1 – actuation plate casted inside the silicone; 2 – steel cables connected to the actuation plate; 3 – aluminium plate for mounting the tail to the chassis of the robot; 4 – Adjustable motor mounting for setting the pretension of the cables; 5 – cable pulley; 6 – heat conductors; 7 – Servo motor; 8 – ARM computer; 9 – Rubber casings glued on the internal wall of the nose cover for mounting pressure sensors; 10 – Pressure sensor with amplifier and ADC; 11 – Pressure port.

The exterior body of the vehicle consists of three main components: nose cover (Figure 2.1 - 1), middle chassis (2) and the tail (4). The middle chassis is the central part of the robot, holding together most of the other components. The chassis is manufactured from a corrosion resistant aluminum alloy using a 3-axis CNC milling machine. The rear end of the chassis holds the silicone tail, which is attached using 8 bolts through the fixing plate casted inside the tail. The flat front part of the tail seals the chassis from the rear side. The front side of the chassis is enclosed by a polyamide nose cover, which was 3D printed using a selective laser sintering method. The even surface between the chassis and the nose cover is lubricated with a silicone grease to guarantee the waterproofness of the body.

The compliant part of the robot is casted from a two-component platinum-cure silicone. In the initial tail we used Dragon Skin 10 by Smooth-On. However, during the development we have used various different products from different manufacturers. Finding the properties of the soft body is described in the following sections of this work. We used CNC machined plastic molds and

developed the proper casting techniques required for every specific fin design described later in the work.

Inside the tail there is an aluminum actuation plate (Figure 2.2 - 1), which is casted into the silicone during the molding process. The actuation plate is connected to the servomotor (7) through two stainless steel cables (2). When the motor turns, one of the cables will pull the actuation plate to bend the tail. As the cables are flexible, the cable on the opposite side will loosen and will not exert a significant force. The servomotor itself is attached on the chassis with a fixing mechanism (4). The mechanism allows adjusting the pre-tension of the steel cables by moving the motor front- or backwards. We use a Futaba BLS152 brushless metal gear servomotor. It was chosen because of a high reliability and very high torque (3.5 Nm) compared to the regular hobby servomotors. The metal body of the motor is placed between two aluminum heat sinks (6). The other end of the heat sinks is connected to the aluminum chassis to transfer heat from the motor to the surrounding water. Effective cooling is necessary to stabilize the temperature inside the robot. Stable temperature in turn is required to improve the precision of the pressure measurements.

The fish robot is equipped with five piezoresistive silicon absolute pressure sensors (10) that form an artificial lateral line. The reasoning behind choosing the specific sensors, their positioning and a more thorough description of their characteristics is given in Chapter 3. Here we just show that the sensors are pressed into the rubber casings (9) that are glued onto the interior wall of the plastic nose cover. The rubber casings are connected to the bronze tubes (11) glued into the plastic cover. The back walls of the rubber casings are covered with a thick tape to provide shielding from thermal radiation from the motor and the electronics (not drawn on the figure).

The sensors and the motor are connected to the 400 MHz ARM computer running dedicated software on a Linux operating system. The computer acquires the pressure sensor data and controls the servomotor. In our study the robot is not working autonomously, so that the on-board computer is not actually running any real-time data analysis. Its main task is to communicate with an external PC over a serial interface through a cable. The frequency of the communication and thus also the data acquisition frequency is limited to 100 Hz. The cable is chosen as flexible and small-diameter as possible to minimize its effect on the robots movement. However, the minimum size is dictated by the power requirements of the robot, as the cable also provides a 24V power supply for the robot. The 24V is converted to 5V inside the robot with two separate regulators - one for the motor and other for the computer and sensors.

The real-time robot control software operates on external computer running dedicated software developed in LabVIEW. The software is responsible for analyzing the pressure sensor signals and generating the corresponding control

signal. The software is also managing the camera, force measurements and any other tasks described in the following sections.

The robots motor is actuated using sinusoidal motion

$$\varphi = A \cdot \sin(2\pi ft) + \varphi_0 \quad (2.1)$$

,where φ is the motor angle, A is the actuation amplitude, f is the frequency and φ_0 is the motor angle offset. The velocity can be changed by changing the actuation frequency of the amplitude. To turn the robot, the offset φ_0 can be added to the actuation signal. This turning method does not allow fast maneuvers with small turning radius, but is enough to steer the robot for the purpose of our study. For more complex maneuvers the vehicle can be equipped with additional pectoral fins.

The lack of additional fins also restricts the movement of the vehicle only to a single horizontal plane. However, for the studies described here, this is sufficient. To restrict the vertical movement, we fix a buoyant bar on top of the robot. The robot itself is negatively buoyant so it hangs on the buoyant bar at a certain depth below the water surface.

The initial compliant tail of the robot was casted with a uniform stiffness profile along the length of the body. The body was made using a two-component silicone Dragon Skin 10 by Smooth-On. The initial tail was used to validate the viability of the biomimetic fish robot and to test its suitability for further research tasks. The results showed that the vehicle is capable to swim and turn as expected. However, the performance of the robot in terms of the maximum velocity was low. The vehicle with a constant elasticity profile was not able to achieve velocities higher than 0.2 BL/s. For comparison, the velocities of a biological rainbow trout may be as high as 8.5 BL/s

2.4 Mimicking passive properties of biological fish

To improve the performance of the compliant fin, we first hypothesize that by copying the stiffness profile and the geometrical properties of a biological fish body, we are able to achieve motion similar to real fish. We assume that as a result of increasing kinematic similarity, also the performance will increase. The hypothesis is based on biological evidence that fish use mostly their anterior muscles for steady swimming while the caudal part of the body is passive. This passive part acts as a carrier of energy, transferring the momentum to the surrounding water. Such evidence was found by McHenry *et al.* [53], who used electrical stimulation of the posterior muscles of pumpkinseed sunfish, *Lepomis gibbosus*, to investigate how the travelling waves are generated in the fish's body. Another reason to mimic the body of a fish is the fact that fish use the passive properties of their bodies to save energy while swimming upstream. As already mentioned above, Beal *et al.* [83] have demonstrated that a dead rainbow trout is able to swim upstream in a wake of a cylinder.

The general methodology to test the hypothesis consisted of the following steps:

1. Identification of the rainbow trout's body properties
2. Design and construction of the compliant bodies that have the same passive properties as the biological fish
3. Characterization of the fins performance in terms of the kinematic similarity and thrust.

To identify the body properties, it is first essential to understand which passive properties play a key role in the propagation of a travelling wave in a fish body. This question has been issued by Cheng *et al.* in [129]. They modelled the fish swimming and the passive properties of the fish body using a continuous dynamic beam model. A similar approach was used later in [102]. The analyses revealed that the parameters affecting the travelling wave most are the spatial distribution of the inertia, viscosity and elasticity. Viscosity and elasticity are both equally important as the tissues of fish have viscoelastic properties. Also the external geometry plays a crucial role in the dynamics due to the water-solid interactions on the fish body.

We developed two novel methods to identify the material properties of the fish body. The first one is by using a Myoton device that is used in medicine to estimate the properties of human muscle. Another method is by directly measuring the stiffness of the body using a gravitational force.

2.4.1 Myometry-driven approach

A detailed description of using Myoton device to measure the properties of a fish is given in the article “Myometry-Driven Compliant-Body Design for Underwater Propulsion” [130], which can be found from the Appendix B. My role in this article is proposing the initial idea of using Myoton device, participating in the preparation of the Myoton measurements and doing some of the measurements. I also made the silicone tails for validation and participated in running the experiments of validation. Writing the article, analyzing the data and developing the main idea, the discussion and the conclusions were left to the other authors.

Myoton is a hand-held digital palpation tool that measures the properties of a soft material by applying a mechanical impulse and then measuring the feedback oscillation [131]. The corresponding method is called Myometry. It is generally used for *in vivo* measurements of muscle tissue properties in medicine [132], [133]. From the oscillation, the Myoton calculates the following tissue parameters [134]:

- Natural oscillation frequency [Hz]
- Logarithmic decrement of natural oscillation
- Dynamic stiffness [N/m]
- Mechanical stress relaxation time [ms]

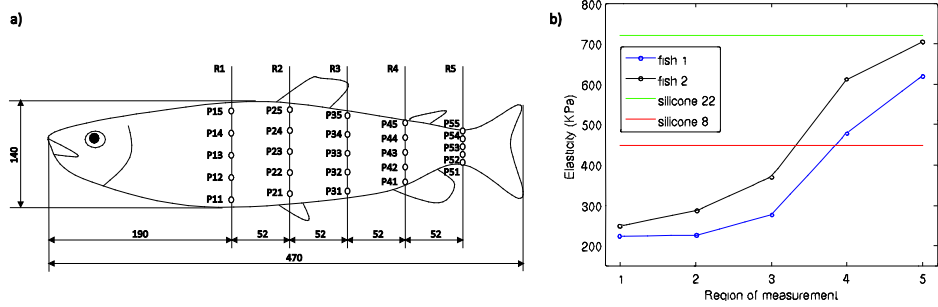


Figure 2.3 – Myometry measurements on a Rainbow Trout. a) points where the measurements were taken from; b) the resulting Young’s moduli of 2 fish of same size. For comparison the moduli of 2 silicones used for casting the prototypes are added.

- Ratio of deformation and relaxation time (Deborah number)

As we can see, these parameters match very well the properties that play the key role in fish body dynamics. Especially relevant are the dynamic stiffness to describe the elastic properties and the mechanical relaxation time and Deborah number to describe the viscoelastic properties, namely creep. The problem is that these parameters do not describe only the properties of the muscle tissue, but the properties of a much more complex system consisting of the tissue, skin, backbone, internal organs and also the supporting surface of the fish under measurement. Therefore, it is important to understand the relation between the Myoton output and the design parameters of the silicone tail.

In our study we concentrated only on the elasticity distribution of the fish body. We found the relation between the measured dynamic stiffness and the young’s modulus of the measured material by calibrating the device on a test piece. The test piece was a silicone body with a decreasing elliptical cross-section towards the end of the tail resembling the shape of fish. Its material properties are known and therefore its actual stiffness can be calculated. We modelled the relation between the Myoton output k and the materials Young’s modulus E using the following empirical relation:

$$k = \alpha \frac{EA}{w} \quad (2.2)$$

,where k is the measured dynamic stiffness, E is the materials Young’s modulus, A is the area of the measurement probe, w is the width of the test piece at the measurement point and α is an empirical scaling coefficient. A more detailed explanation about the calibration is given in the original article.

After calibrating the device for our application we determined Young’s modulus of rainbow trout’s body. We used two fresh-water rainbow trout’s caught from a fish farm. The fish were 40 cm and 50 cm in length, approximately matching

the size of the designed robot. We performed Myometry shortly after execution to minimize the effect of *rigor mortis*. Every measurement was repeated 10 times. The measurement points are shown in Figure 2.3a. The measured Young's modulus profiles are shown in Figure 2.3b. From the results it can be seen that the young's modulus of the fish increases greatly towards the tail. That is an important fact to take into consideration when designing biomimetic fins.

The next step was to develop biomimetic fins with different elasticity distributions for comparison. We developed three main prototypes:

1. A fin with an average Young's modulus approximately the same as the trout
2. A fin with much higher Young's modulus
3. A fin which has a lower modulus in the anterior part and a higher modulus in the posterior part to mimic the stiffness profile of a trout.

We estimated the performance of the fins based on their kinematic similarity to an oscillation of a dead trout. The prototypes were attached on a waterproofed motor inside a flow-tunnel. They were actuated with sinusoidal motion using different amplitudes, frequencies and flow-speeds. The resulting travelling wave in the fins was recorded with an overhead camera. The video footage was analyzed using custom-made automated LabVIEW software. The same procedure was repeated on a dead trout of a similar size. The kinematic similarity between the prototypes and the dead trout was then estimated by comparing the mean absolute lateral motion difference and the Spearman rank correlations between the prototype and the fish. A more detailed description about the experiments and data analysis can be found from the article in the Appendix B.

The results demonstrated in the paper show that the prototype composed of 2 different silicones performed slightly better than single-component prototypes. Therefore, we conclude from the study that the biomimetic stiffness profile increases the tails kinematic similarity to the biological trout. We can also conclude that myometry is a promising approach for developing such biomimetic fins. We were able to use it to identify the body properties of a biological trout. This in turn led to the improved performance of the oscillating fin.

However, our conclusions are adequate for a relatively limited scenario. Estimating the performance only based on the kinematics analysis does not give much information about the actual applicability of the fin on an underwater robot. The first parameter to optimize the fin for in real applications is thrust. However, better kinematic similarity does not necessarily lead to higher thrust. Therefore, thrust has to be measured separately to get a better overview of the fins performance. Moreover, in our study we used a dead trout on a motor as a motion reference. Unfortunately there are no studies that prove the motion

similarity of such system to a living trout. Our comparative experiments only show that our fin and a trout behave similarly when actuated in the same way, but we cannot claim that neither of these systems moves in the same way as a swimming fish.

More limitations are related to the Myoton measurements. We calibrated the Myoton output on a single dummy for a very specific situation. The calibration is certainly valid only for the measurements of very similar silicone bodies. We do not know how precise the results are when measuring the biological trout. A real fish is a complex system composed not only of a soft tissue but also a backbone, skin etc. Therefore, the Myoton calibration should be validated separately for this system by measuring the stiffness of the trout using some other method.

None of the prototypes followed the actual stiffness distribution measured by Myoton. The two-component body was close to a real trout, but still failed to follow the Young's modulus values along most of its length. Therefore, there is a chance that when the stiffness similarity is increased more, the performance will actually decrease. We cannot make strong conclusions based only on a single biomimetic prototype.

2.4.2 Measuring the bending stiffness of a fish using a gravitational force

To overcome the issues related to the previous study, we propose a different approach for identifying the fish body properties. This approach allows us to validate the results acquired using myometry. A detailed explanation about the method is given in the article "A Flexible Fin with Bio-Inspired Stiffness Profile and Geometry", which was published in the Journal of Bionic Engineering [135] (Appendix C). My contribution to the article is developing the methodology for stiffness measurements, designing and constructing the fin, developing the methodology for performance analysis, running all the experiments and writing the article. Co-author Maarja Kruusmaa was supervising the study. The work published in the article was partly done already during my master thesis and the results have been also partially published there. The article was written during my PhD studies and I include it here for the sake of integrity of my whole study about the robotic fish design.

The first step is the characterization of the fish body properties. As we described in the previous sub-section, it is difficult to estimate the separate properties of the muscle tissue, backbone, etc. Another way is to measure the properties of the whole system together. Again we are concentrating only on the elastic properties, leaving aside the viscoelasticity. Therefore, the main parameter of interest is again the stiffness. It is known that the bending stiffness $\kappa(x)$ along the fish longitudinal axis x is the ratio of applied moment $M(x)$ and the resulting body curvature $k(x)$.



Figure 2.4 - An example of photos used to identify the bending curvature of the fish. The red line marks the automatically extracted midline.

$$\kappa(x) = \frac{M(x)}{k(x)} \quad (2.3)$$

In our method we are directly measuring both, the applied moment and the curvature. Instead of using a complex rig with force sensors and actuators to apply moment, we use gravity.

We used a 50 cm rainbow trout caught from a fish farm. Shortly after execution by farmer, the trout was mounted horizontally in a fixture by its anterior body. The fish was in the fixture on its side so that its posterior body was hanging freely. The body was bent downwards by the gravitational force. The body of the trout was photographed on a contrast background using a spatially calibrated camera system (Figure 2.4). The images were analyzed using custom-made LabVIEW software. The software extracted the midline of the trout's body, which was used to find a function describing the body's curvature.

After measuring the curvature the mass distribution of the trout was identified. The fish was sliced longitudinally into 20 mm pieces. Weight, width and height of every piece were measured. From weight we found the mass of the trout per unit length and from the dimensions we identified the geometry. From the curvature and the mass distribution we calculated the bending stiffness profile of a trout. We approximated the geometry with ellipses to be able to calculate the area moment of inertia $I(x)$ of the fish cross-sections. From the area moment of inertia and the bending stiffness we can find an average young's modulus of the fish cross-section

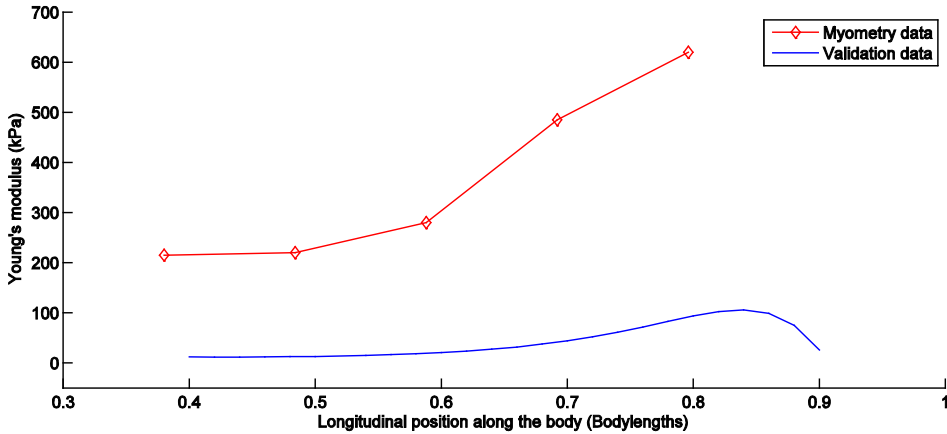


Figure 2.5 - Distribution of the Young's modulus along the body of the Rainbow Trout estimated using two different methods.

$$E_A(x) = \frac{\kappa(x)}{I(x)} \quad (2.4)$$

The average modulus is shown in Figure 2.5 together with the modulus found using Myoton.

The results show that the average Young's modulus is increasing towards the tail as was predicted basing on the previous studies and the Myoton results. However, the absolute values measured using the gravity-based approach are smaller from these acquired with the Myoton. The difference is approximately in a range of one order of magnitude. This bias proves that there is a systematic error in one of the approaches. To identify the faulty method, we conducted a simple verification test. The verification test was similar to the curvature measurement of a real trout. The tail designed using a myometry-driven approach was placed horizontally on the rig and its bending curvature was observed. It was clear that the prototype bends much less than the real trout and has thus a much higher average Young's modulus. Therefore, we can now state that the method we used to calibrate the Myoton is not sound. The reason is probably related to the fact that the Myoton was calibrated on a monolithic silicone dummy composed of an isotropic material. Fish in the other hand has a complex structure of multiple materials. Also, the Myoton does not measure the average dynamic stiffness values through the whole fish cross section. It instead creates an oscillation only in a certain portion of the fish body. This portion may include different materials depending on the specific location where the measurement was taken from.

2.4.3 Biomimetic fin with continuous elasticity profile

We continued the study with the Young's modulus values achieved from the gravity-based method. The next step was to develop a fin whose stiffness profile matches that of a trout as closely as possible. As the geometry is fixed, we

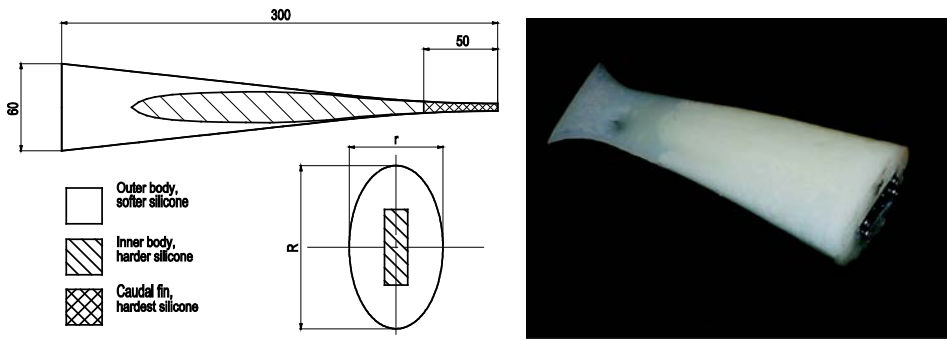


Figure 2.6 – Left: a top view and a cross-sectional view of the composite silicone tail schematics; Right: A casted composite silicone tail prototype.

needed to change the average Young’s modulus of the cross-section’s along the length of the fin. To do this we came up with a composite fin design seen in Figure 2.6. The fin is composed of two concentrically casted silicone materials with different Young’s moduli. By varying the cross-section of internal, harder material, the total average stiffness can be modified. The 50 mm part in the end of the fin is casted of harder silicone to mimic a relatively rigid caudal fin of a trout. As the fish tissue is very soft, conventional silicone rubbers were not enough to achieve a low stiffness of a fish. Therefore, as the external material of the prototype we used a two-component silicone foam (“Soma Foama” by Smooth-On). During a casting process the foam was covered with a thin layer of silicone rubber to avoid the absorption of water into the foam.

2.4.4 Performance of the biomimetic fin

The performance of the fin was identified in the flow-tunnel of the Centre for Biorobotics. The fin was actuated with different frequencies and amplitudes, and its motion was again captured with an overhead camera. To improve the precision of the motion-capture, black markers were placed on the back of the fin. The generated thrust and lateral forces were measured using a force-plate mounted under the motor which moves the fin. We also tried to give an approximate estimation of the swimming velocity of vehicle with such a fin. For that we implemented a PI controller that controlled the tail-beat frequency to balance the thrust and drag forces. We changed the flow-speed and recorded an average frequency needed to balance the forces at certain speed. This method of course gives only an approximate result as the systems movement is constrained. A freely swimming robot fish can also rotate and move sideways while swimming.

We characterized the kinematics of the tail by the length of the propulsive wave and the trailing edge amplitude. These parameters allow us to compare the motion of the composite tail to the motion of a swimming trout. The reference motion is published by Webb *et al.* in [136]. The kinematic parameters of our fin compared to the biological values are shown in Figure 2.7. Figure 2.8 shows the estimated swimming velocity at the corresponding actuation parameters.

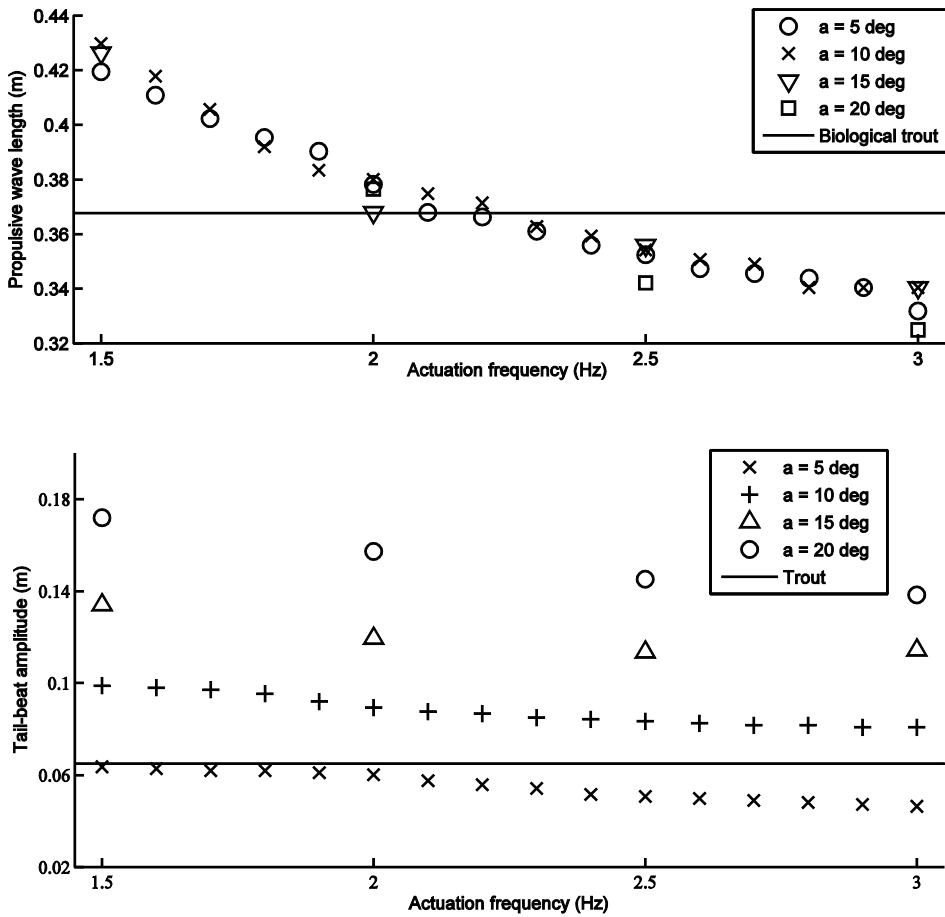


Figure 2.7 – Propulsive wave length and tail-beat amplitude of the composite tail at different actuation parameters. The corresponding values for a biological trout are marked with a solid line.

From the propulsive wave length graph it can be seen that the wavelength of our compliant tail is very similar to that of a trout with a same size. The maximum deflection from the biological value in the whole actuation frequency range is only 16 %. We can also see that with our fin, the wave length is related to the actuation frequency while the wave length of a swimming trout is constant. The tail-beat amplitude graph shows that when choosing the right actuation amplitude, we can also achieve an exact match of the tail-beat amplitude. However, the amplitude is again dependent on the actuation frequency.

The swimming speed results show that the estimated velocity of a robotic fish with the bio-mimetic tail reaches well the biological values in our frequency range. However, our main interest in the light of our hypothesis is the velocity at the actuation parameter values which give the most similar kinematics to trout. The velocity of our tail at these parameter values (6.6 degree amplitude

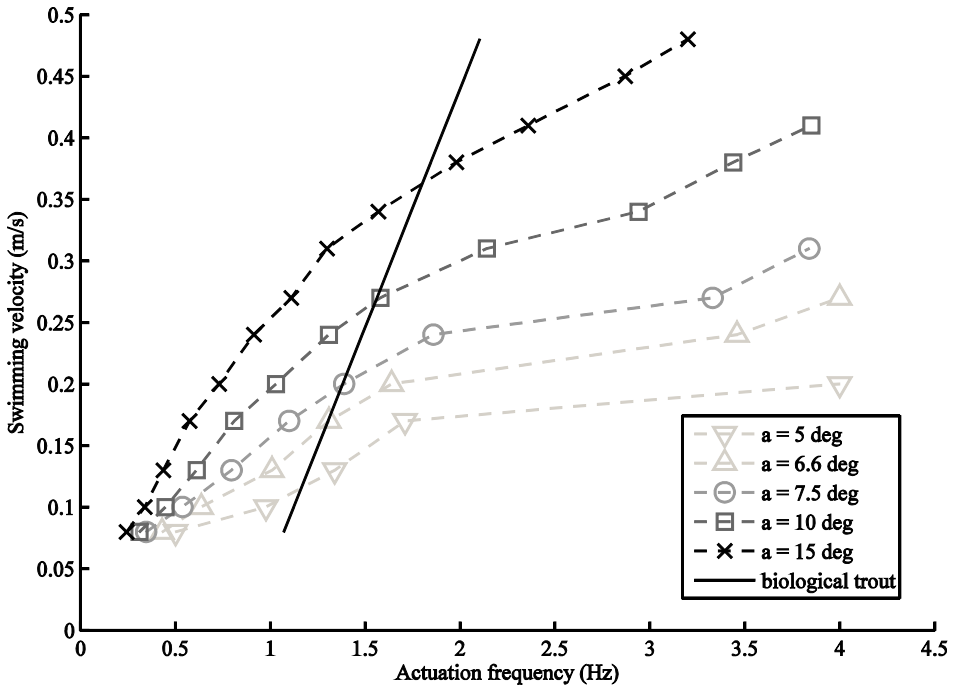


Figure 2.8 – Swimming velocity of a composite tail at different actuation parameters. Swimming velocity of a biological trout is marked with a solid line.

and 2.3 Hz frequency) is in the range of $0.2 \dots 0.24 \text{ m}\cdot\text{s}^{-1}$ ($0.4 \dots 0.48 \text{ BL}\cdot\text{s}^{-1}$). This is only 30% to 37% of that of a real trout with same size.

2.4.5 Conclusions about the bio-inspired stiffness profile

As our results showed, the kinematic parameters of our composite fin almost precisely match these of a freely swimming trout. This proves the first part of our hypothesis. Fish-like swimming can be achieved by mimicking the stiffness profile and geometry of the rainbow trout on the pitching fin. However, the results also show that our assumption about the generated thrust forces is not true. Even though the kinematics is similar to the fish, the thrust forces generated by the fin are only a fraction of the forces generated by a trout. The reason for this could be the small number of kinematic parameters used in analysis. We used only the wavelength and tail-beat amplitude, but these parameters do not fully define the motion of the fin. They do not give any information about the lateral and rotational motion of the whole fish body, which presumably play an important role in the fish swimming dynamics. Literature provides an in-depth characterization of the lateral and rotational motion, but only for a relatively small trout [81]. It has not been studied, how the kinematics scales up to a large, 50 cm trout that is being used as a reference in our work. Therefore, to follow up the proof of our hypothesis, more detailed kinematical references have to be acquired.

Another limitation of our approach to mimic a biological stiffness profile is that we use only a passive stiffness as a reference, while living fish also actively vary their stiffness. They use muscles to change the stiffness and thus the natural frequency of their bodies [56]. This active control allows fish to tune their body properties for different situations, i.e. steady swimming, escape maneuver, K arman gaiting etc. Also they can optimize their cost of transportation by matching the swimming frequency to their natural frequency. The importance of the frequency is also visible in the results of our study. All the kinematic parameters we used are depending on the actuation frequency. The low thrust performance of our fin is probably also related to the fact that the optimum body stiffness for steady swimming is not equal only to the passive stiffness but to the combination of active and passive.

2.5 Experimental validation of model-based body design

To improve the thrust of the fin by optimizing its stiffness profile for a certain swimming parameters, there are two general approaches – experimental and model-based. Experimental approach would include developing a series of prototypes, whose performance in terms of desired target parameters can be measured. The results of the experiments would give the relationship between the design parameters, for example material properties, and the parameters under optimization, for example thrust at certain actuation assumptions. This approach, however, is very time-consuming as it requires large amount of prototypes. Also, the experimental approach does not give the explanation for the actual principles behind the empirical relations.

The problem with a model-based approach is that the dynamics of our system includes large-amplitude oscillations of the viscoelastic soft body which is interacting with a surrounding fluid. As we described in the limitations of previous studies in Section 2.1, the current theoretical models are not able to describe such systems with a satisfactory precision. Therefore, we have also contributed to improve the current models.

An in-depth description of the compliant robotic fish modelling is given in the article “A Bio-inspired Compliant Robotic Fish: Design and Experiments” [137], which is published in the proceedings of the 2012 IEEE International Conference on Robotics and Automation (Appendix D). A continuation of this study is presented in the article “Modelling of a biologically inspired robotic fish driven by compliant parts” [138] which is published in IOP Journal of Bioinspiration and Biomimetics in 2014 (Appendix E). The two main parts of both papers are modelling the dynamics of the compliant body and validating the models through experiments. The modelling and the theoretical work are fully done by the first author of the paper Hadi El Daou. My contribution is the development of experimental methods for model parameter identification and experimental validation. This includes developing the methodology, the experimental setup and conducting the experiments.

In the first of these articles an added mass is used to define the hydrodynamic forces on the compliant robot's body. The second article elaborates the model by using Lighthill's elongated body theory [54], which is more general and better suited for the geometry and dynamics of subcarangiform swimming. An assumed modes method was used to derive the equations of motion and to compute the relationship between the applied moment and the resulting lateral deflections. Rayleigh proportional damping was used in both articles to model the damping, but a more general solution was used in the second paper.

The experimental work required for modelling included two main parts: 1) estimation of the natural frequencies of the compliant tail and 2) verification of the theoretical model by comparison of experimental and theoretical lateral deflections. The natural frequencies were required to compute the Rayleigh damping coefficients used in the model. Comparison of the lateral deflections was used to show that the predicted kinematics of the tail and the actual kinematics are in good agreement and thus the model is valid to predict the motion of the tail at given actuation properties.

To estimate the natural frequencies and to measure the kinematics, we developed an experimental measurement device. The device oscillates the robotic tail at different frequencies and measures the resulting torque. The frequencies with minimum resulting torques are considered to be natural for a system. An alternative approach would be to actuate the system and measure the amplitude of resulting oscillations. At the natural frequencies the amplitude is largest. However, in practice this approach can only be used to find the first natural frequency. Identifying the higher modes of oscillation from the video is unfeasible, as the oscillations at higher harmonic frequencies are too small.

The schematic of the measurement system is presented in Figure 2.9. The compliant body under measurement is mounted together with a chassis of the robot inside a water tank (4). The internal servo-motor of the robot is replaced by an external servo-motor (1), which is connected to the actuation cables of the tail through a vertical shaft (3). In between the shaft there is a custom-built torque sensor (2) which is connected to a strain-gauge amplifier. To estimate the kinematics of the compliant body, the silicone body is marked using black dots (6) attached on its top midline. The position of the dots is tracked using an overhead camera (5) at 50 frames per second. The whole system and data recording is controlled through a PC running LabVIEW.

The minimum actuation torque was measured at frequencies 3.30 Hz and 9.96 Hz, which are the first and the second resonance frequency of the compliant body in air. The third resonance frequency is predicted to be close to 34 Hz. However, our experimental setup was not able to actuate the tail at such high frequencies and thus only the first two resonant frequencies could be identified. We used these two frequencies to calculate the Rayleigh damping coefficients needed to identify the model parameters. After measuring the frequencies in air

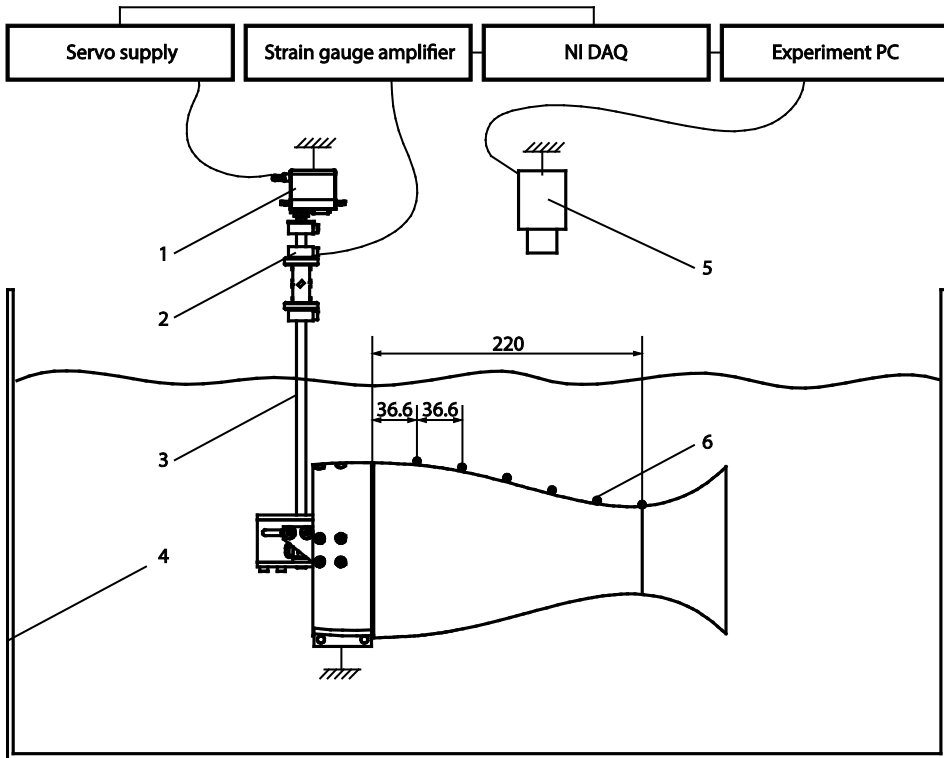


Figure 2.10 - Experimental setup for measuring the natural frequencies of the compliant body and estimating its lateral deflections. 1 – Servomotor; 2 – Torque sensor; 3 – Shaft; 4 – Tank; 5 – Overhead camera; 6 – Markers on the tail.

we ran a resonant frequency validation experiment in water to verify our methodology. We immersed the robot by filling the tank with water and repeated the experiment. The first resonant frequency in water is predicted to be close to 0.8 Hz, which is too low to be measured as the torque resulting from the hydrodynamic drag is too high. The second resonant frequency was measured to be 3.37 Hz. The second calculated resonant frequency was 3.1 Hz. The error between the model-predicted and measured value is equal to 8%. Therefore, our methodology is validated.

To further verify the model, we also measured the lateral deflections of the compliant body and compared them to model-predicted values. We actuated the robot by a sinusoidal signal using a known torque at series of different frequencies. We recorded the lateral deflections using the overhead camera and compared them to these predicted by the model. The comparison of the calculated and measured maximum lateral deflections at different frequencies and different locations on the tail are presented in Figure 2.11. The results show that the maximum percentage of absolute errors between the model-predicted and the measured deflections for the tip of the body for frequencies 0.7 Hz and

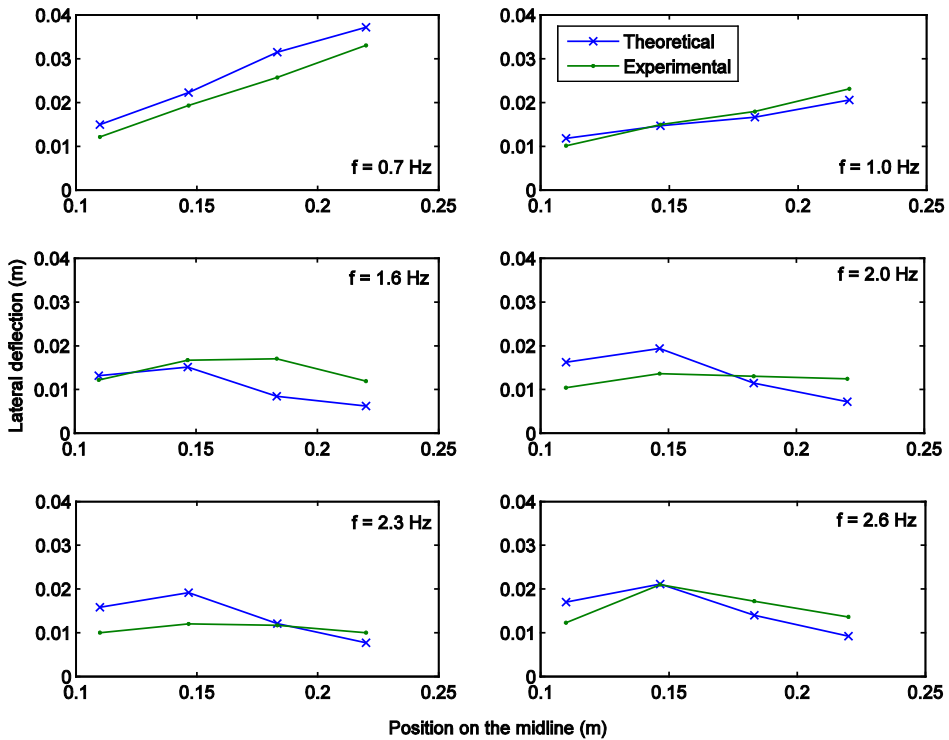


Figure 2.11 – Lateral deflections of the robots compliant tail at different frequencies. Blue line marks the theoretical model-predicted values. Green line marks the experimentally measured values. The markers show the position of the black dots on the tail.

1 Hz are 12% and 11%. At higher frequencies the error increases (48%, 42%, 28%, and 32% for frequencies 1.6 Hz, 2.0 Hz, 2.3 Hz, and 2.6 Hz respectively).

From the results we can conclude that the presented model is very well able to predict the kinematics of the compliant oscillating body at lower frequencies. It is predicted that the error at higher frequencies could be reduced by measuring also the higher resonant frequencies to get a more precise estimate of the damping ratios for the higher harmonics.

2.6 Conclusions

In this chapter we described the novel design methodology of the compliant-bodied robotic trout. Even though the general locomotion principle of the robot is based on previous similar robots [102], we have developed different, novel approaches for finding the optimal properties of the silicone tails. The robot is also unique as it carries an artificial lateral line.

By designing and testing the robot we proved that the compliant approach is a good alternative to fish-robots with rigid links. Our design meets most of the design requirements we set for the robots that have to work in turbulent waters. The technology is applicable, durable and passively adapts to the flow. The results showed that the robot, depending on the specific tail design, was able to swim at the velocities of 0.4 body lengths per second and was able to achieve kinematics similar to real trout.

We introduced a novel approach of designing the compliant tail of the robot by mimicking the body properties of a real trout. We proved that in terms of kinematic similarity this approach is valid. To identify the body properties of trout we proposed two new approaches. The myometry-driven approach is a very promising method that in theory can be used to estimate most of the parameters used while designing viscoelastic bodies. However, the methodology has to be improved by developing sound measuring models that can be validated on large sets of biological and dummy specimens. Until now this work has only been done to measure human tissue properties, but never for fish. To overcome the current limitations of the Myoton-approach, we proposed another novel approach for identifying the passive properties. By using a gravitational force we were able to identify the required parameters. We used these parameters to develop a new type of an oscillating fin with a continuous stiffness profile throughout the body. The motions of this fin were very similar to the motions of a swimming fish.

In addition to the experimental methods for designing the compliant body, we also contributed to verification and development of a novel theoretical model describing our system. The described model was able to predict the motions of a compliant-bodied robot with high accuracy. The verification proves that this model can be used to improve the performance of the robot. The material and geometrical parameters of the tail can be used to calculate the deflections of the robot without measuring them on a prototype.

3 FLOW-RELATIVE CONTROL

As we pointed out in the introduction, the flow awareness and adaptability can be either passive or active. Whereas the last chapter concentrated on the passive properties of our robotic fish, the emphasis of this chapter is on the active flow awareness and adaptability. The goal is to develop an artificial lateral line system simple enough to be used for real-time control of an underwater vehicle.

In the background chapter we gave an overview of different artificial lateral lines (subsection section 1.3.3). We also described how these lateral lines have been used to detect different events in the flow or to identify various flow patterns (subsection 1.3.4). From the perspective of our task, all these studies have one major limitation. Their methods and algorithms have been developed for and tested only on static measurement platforms or platforms with very few degrees of freedom. There have been no studies where the artificial lateral line is in use to control a freely swimming underwater vehicle.

In this chapter we first describe the design rationale and the implementation of the lateral line system that is most suitable for real-time control. After that we describe the experimental setup where the system has been tested. From there we go on to the control of the robot using the artificial lateral line.

In Sections 3.3 and 3.4 we concentrate on mimicking the fish lateral line based behaviors that would be most beneficial for a small-scale underwater vehicle operating in rapidly flowing waters. We try to find simple control laws that are easily applicable and usable in real time. The capabilities we are implementing on our fish-robot are:

- Identification and discrimination of flow regimens
- Detecting the orientation of the robot with respect to the flow direction
- Measuring the flow speed
- Estimating the position of the robot in the wake of an object

3.1 Artificial lateral line

Before implementing the control, the most suitable sensing principle has to be chosen. Again, we start by identifying the criteria that the lateral line system has to meet. The first criterion is defined by our main requirement, which is the applicability of the system in the future in real-world applications. This means that the sensor technology has to be reliable enough to handle the rough environmental conditions which may occur when the vehicle is used outside the lab. The sensors should not break when they bump against other objects. Also they should be able to work in salty or dirty water. The other criterion is that the sensors characteristics have to be such that the system can be used for real-time control. This means sufficient precision, resolution and sampling frequency. In

addition, the lateral line sensors have to be miniature enough to be placed into our small-sized vehicle.

The solution with the highest biological similarity would be to use the artificial superficial neuromast sensors [105]–[111]. Superficial neuromast sensors are also extremely small and therefore large arrays of sensors with tens or hundreds of artificial neuromasts could be placed on an underwater vehicle. They also provide very high sensitivities up to $2.5 \mu\text{ms}^{-1}$. However, the major limitation of using the artificial superficial neuromasts is that they are extremely fragile. They are usually tested only in deionized clean water. Even the sediment particles in water may damage the sensor, not to mention walls, rocks etc. Therefore, these sensors are not suitable for our application. The same problem occurs with hot-wire anemometry sensors that have been used by some authors [118], [139].

Another solution would be to use flat MEMS pressure sensor arrays mounted on the surface of the robot. Such sensors have been developed and their preliminary application in the artificial lateral line has been demonstrated in [114], [115]. The sensors developed in these studies are sensitive and they can be used to build dense sensors arrays. These arrays would be extremely useful as they would allow mapping the whole pressure field on the body of an underwater vehicle. However, the MEMS arrays are not yet mature enough for application. They are not available off-the-shelf and their production is a complex process requiring special equipment. The authors also don't report the reliability and robustness of their sensors. Therefore, we believe that at the moment the technology readiness level is not high enough. However, this technology is extremely promising for using in flow-based control of underwater vehicles.

The third option is to use single commercial pressure sensors distributed on the body of the vehicle. This approach has been chosen in various other studies made in the framework of the FILOSE project [123]. Ježov for example has developed 3 static platforms with an artificial lateral line consisting of piezoresistive off-the-shelf pressure sensors [140]. These sensors can be mounted inside the vehicle so that they are almost fully separated from the external environment. The only connection to the external environment is the pressure port between the sensor and the surface of the vehicle. Therefore they are robust and reliable even if the vehicle is operating in natural environments. The sensors used by Ježov have been sensitive and fast enough to detect various hydrodynamic events such as the vortices generated by the cylinder [141]. Even though the size of the piezoresistive pressure sensors is not comparable to the size of MEMS pressure sensor arrays, they are made in relatively small package so that several of them can be fitted inside our fish-robot. Because of these reasons the piezoresistive pressure sensors are most suitable for our study with the freely-swimming robotic fish.

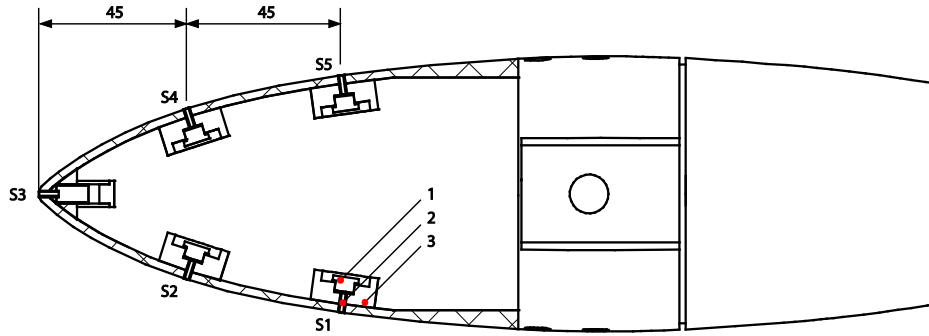


Figure 3.1 – Pressure sensors in the head of the robot (top view). 1 – Sensor with amplifier and ADC; 2 – Pressure port; 3 – rubber casing. S1 to S5 show the numbering of the sensors.

As we already briefly mentioned in the vehicle design Subsection 2.3, there are 5 piezoresistive pressure sensors mounted on the head of the robot - one on the tip of the nose and 2 on each side (Figure 3.1). We use Intersema MS5407-AM miniature low-noise, high-sensitivity, and high-linearity piezoresistive sensors. Each sensor is mounted on a separate PCB that includes also a 22-bit differential analog-digital converter. The ADC gives us a sensitivity of 0.1 Pa. As the pressure sensors are sensitive to the temperature variations, each PCB also includes a temperature sensor for compensation. The pressure and the temperature values are transferred to the robot's computer over SPI interface.

The sensors are mounted into the special rubber casings that are glued on the inner wall of the fish plastic nose cover. The pressure sensitive area of each sensor is connected to the outer surface of the robot through a 1.2 mm bronze tube.

3.2 Experimental setup

All the experiments with the robotic fish and its artificial lateral line were conducted in the flow tunnel of the Centre for Biorobotics. The flow-tunnel is of a submerged closed-top type. It is built into a water tank with a length of 4 m, width of 1.5 m and height of 1.5 m. The image of the tank can be seen in Figure 3.2. Image also shows the flow-tunnel which is submerged into the tank. The tunnel has a 1.5 m long working section with the width and height of 0.5 meters. The working section is preceded by the collimator and flow guides that are designed to assure a uniform flow velocity in the whole working area. The flow is created by a propeller driven by an AC motor with a frequency inverter. The maximum flow velocity in the tunnel is 1.0 m/s.

The robot is placed into the flow tunnel so that it can freely move on a horizontal plane while its vertical movement is constrained (Figure 3.3). It is mounted to the buoyant floater by the rod on the top of the robot. The robot is heavier than water so that it hangs on the floater. The floater itself is sliding on

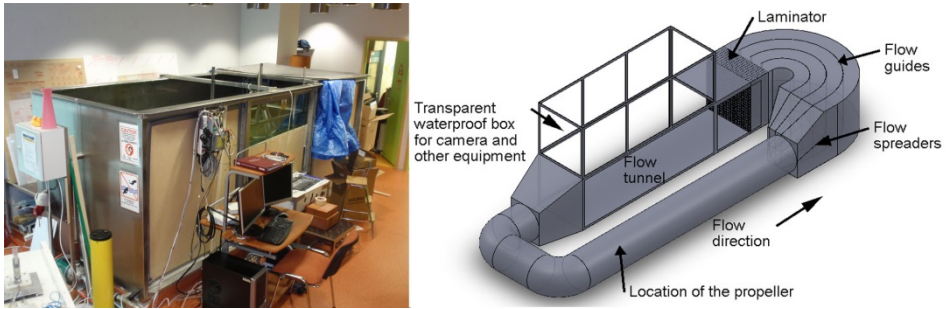


Figure 3.2 – Test tank of Centre for Biorobotics. Left – general view; Right – the submerged flow tunnel built into the tank (Image courtesy of Gert Toming).

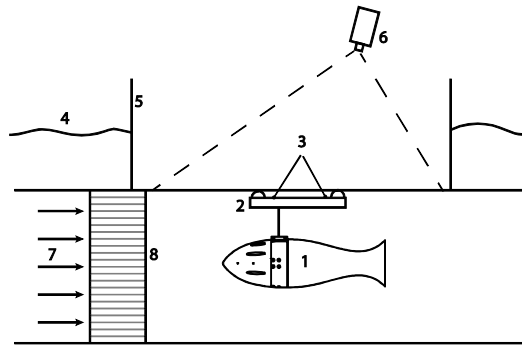


Figure 3.3 – The experimental setup for flow-relative control. 1 – robot; 2 – buoyant floater; 3 – LED markers; 4 – water level; 5 – Transparent box for filming; 6 – overhead camera; 7 – flow direction; 8 – collimators.

the upper glass wall of the flow tunnel to allow horizontal movements. The contact points between the floater and the glass are two round plastic tips that help to minimize the friction. Also the buoyancy of the system is precisely balanced for that purpose. We constrained the vertical movement because the fish-robot at the moment is not designed to be neutrally buoyant or to control its depth. This setup also helps to analyze the pressure sensors signals. The hydrostatic pressure changes caused by the changes in depth are eliminated and we can concentrate only on the hydrodynamic pressure.

The robots position was tracked using an overhead camera. The camera was fixed above the flow tunnel and it filmed the robot through the upper glass wall of the tunnel. For precise tracking, the floater on top of the robot was equipped with two LED's – one in the front and one in the back. The position of these LEDs was extracted in real-time using custom-made LabVIEW software running on the experiment PC. Before the experiments, the camera was spatially calibrated to acquire position of the fish in real-world coordinates with respect to the corner of the flow-tunnel.

The experiment PC that tracked the fish was also responsible for analyzing the pressure sensor data and controlling the vehicle. It communicated with the robots PC over a serial interface through a cable. We use a thin cable to minimize the force it is exerting to the robot.

3.3 Robotic fish in steady flow

We use the developed artificial lateral line to achieve different real-fish rheotropism behaviors on our fish-robot. Rheotropism is a tendency of water animals to react to mechanical stimuli of the flow [142]. By mimicking these behaviors we try to identify simple control laws that can be useful for the flow-related navigation of underwater vehicles. We begin with the reactions seen in fish while swimming in steady flow.

3.3.1 Rheotaxis

The first behavior we are concentrating on is the rheotaxis. As was described in Subsection 1.2.3, during rheotaxis the fish orients itself towards the oncoming flow. This means that the fish is able to detect the direction of the flow. Such ability would be also beneficial for an underwater vehicle. Therefore, the first step is to understand the relation between the artificial lateral line readings and the direction of the oncoming flow. As the second step we implement a rheotactic behavior on our fish-robot.

The implementation of the rheotactic behavior of the fish-robot is described in detail in our article “Against the flow: A Braitenberg controller for a fish robot” [143]. The article was published in the 2012 IEEE International Conference on Robotics and Automation and it can also be found from the Appendix F. I contributed to the article by characterizing the angle-pressure relation, implementing the Braitenberg controller and testing the performance of it. I designed and prepared all the experiments and ran them. The writing of the article was partially done by other authors. The rheotaxis problem is also addressed in our other article “Flow-relative control of an underwater robot” published in the Proceedings of the Royal Society A: Mathematical, Physical & Engineering Sciences in 2013 [144]. This article can be found from the Appendix G.

Our assumption is that when the robot is rotated with respect to the flow direction, there will be a pressure difference on the two sides of the robots. This pressure difference can be detected by the artificial lateral line pressure sensors. Through the measured difference the angle of the robot with respect to the flow can be estimated. We ran an experiment to validate our assumption. The robot was placed in a steady flow and its orientation with respect to the flow was varied. The experiment was repeated with three different flow speeds. We recorded the pressure data and found the pressure difference between the left and right side of the robot. The results are shown in Figure 3.4.

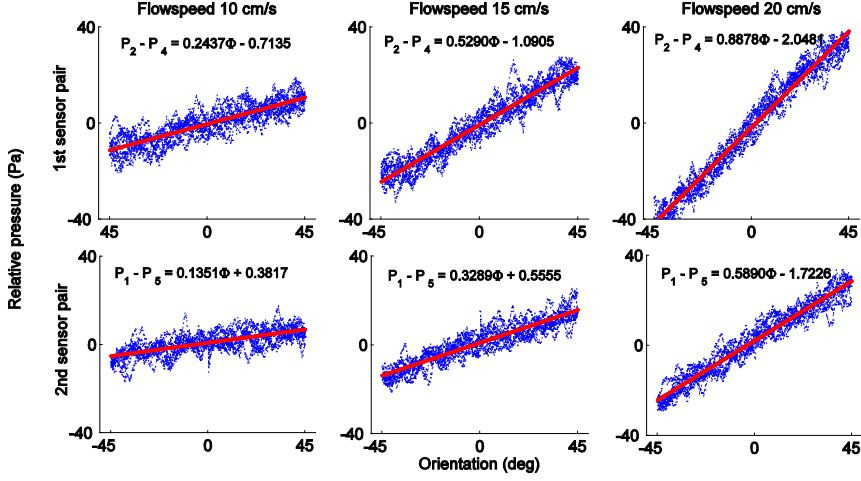


Figure 3.4 – Pressure difference between the left and right side of the robot in relation to the orientation of the robot with respect to the flow. Measurements are taken with the sensor pair S2 and S4 (1st pair) and S1 and S5 (second pair) at three different flow speeds.

The results show that there is a significant correlation between the pressure difference and the robot's orientation. In our orientation range ($-45^\circ \dots 45^\circ$) the relation can be well fitted with a linear function. The slope of the trend increases with the increasing flow speed and is larger for the anterior sensor pair (S2 and S4).

A strong linear relationship lets us assume that the pressure difference can be well used to control the orientation of the robot in flow. To validate that assumption we implement a rheotaxis controller using a Braitenberg vehicle approach. Braitenberg vehicles are vehicles whose sensors are in principle directly connected to the actuators [145]. One example of such a vehicle is a light-following agent called the Braitenberg vehicle 2b. The vehicle 2b always orients itself towards the light source (stimulus). In our case the stimulus is the source of the flow. By orienting itself towards the source of the flow, the robot will always stay parallel to the streamlines. We used a proportional controller whose input is the pressure difference on the right and on the left side of the robot. Such controller will always try to equalize the pressure on each side of the fish-robot:

$$\varphi_0 = [\theta_s - (P_r - P_l)]K_\varphi \quad (3.1)$$

Where φ_0 is the robot tail offset that turns the vehicle, P_r and P_l are the pressures on the right and left side of the vehicle, K_φ is a proportional gain. θ_s is the robot orientation set point angle. In our case the set point is 0° as we want the robot to orient itself towards the flow.

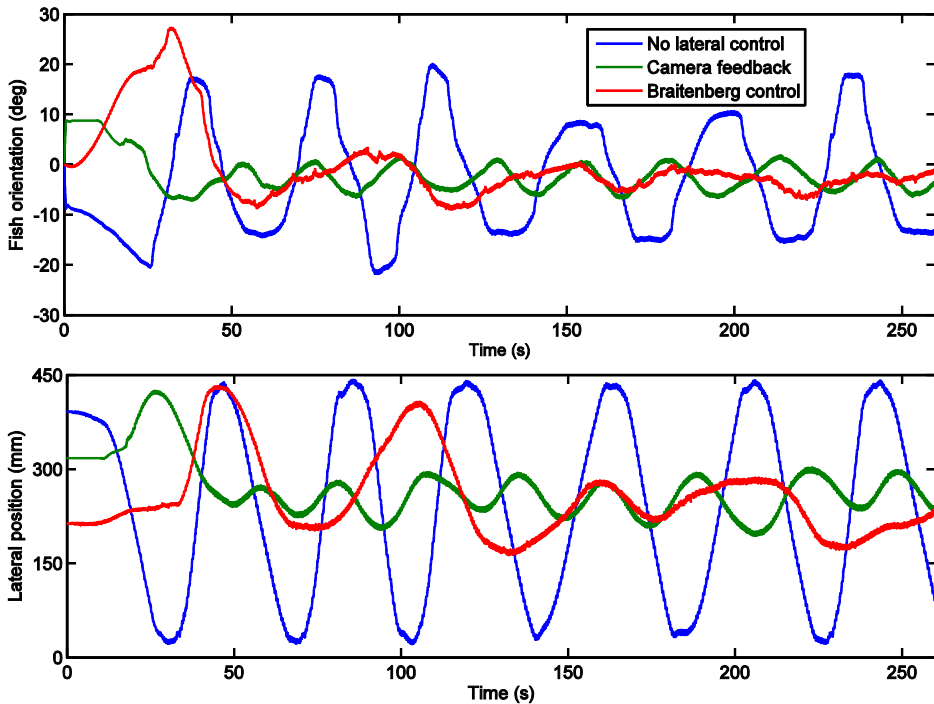


Figure 3.5 – Heading (above) and lateral position (below) of the robot in time. The experiment was done using 2 different controllers – flow-based and camera feedback. For comparison a behavior of the robot without any control is given.

We tested the rheotaxis behavior in the flow tunnel with different controller parameters and flow-speeds. The downstream position of the robot in the tunnel was controlled automatically using the position feedback from the overhead camera. For comparison we also tested the robots behavior in two other cases: 1) without any orientation control and 2) with an automatic proportional orientation control based on a feedback from the camera. The results can be seen in Figure 3.5.

The experimental results show that the robot without any orientation control started oscillating between the sides of the flow tunnel. Its orientation was unstable. The robot with the Braitenberg controller on the other hand was able to maintain a steady orientation towards the direction of the flow. Its performance was similar to the performance of a robot controlled using the camera-feedback. These results prove that the rheotaxis behavior of an underwater robot can be achieved using a very simple proportional control based on the artificial lateral line pressure sensors.

3.3.2 Flow speed detection

Another lateral line related ability of fish is to detect the velocity of the flow [146]. It has been hypothesized that they detect the velocity by sensing the propagation of flow fluctuations along their body [77]. Ježov *et al.* have studied

the identification of such fluctuation propagation using artificial lateral line pressure sensors similar to ours [141]. They were able to detect the passing vortices generated by an upstream cylinder. However, their data lets us assume that detecting much weaker fluctuations that exist in flow without upstream cylinders is not feasible. The pressure sensors are not sensitive enough for this task.

We have developed another method to measure flow speed with our lateral line. The velocity of the vehicle is estimated using the pressure distribution on its surface. One example of similar application is the Pitot tube that is being used widely to measure the wind speed or the velocity of aircrafts. A detailed explanation of our flow speed estimation approach is given in our article “Swimming Speed Control and on-board Flow Sensing of an Artificial Trout”, which was published in the 2011 IEEE International Conference on Robotics and Automation [147]. The article is also included in Appendix H. In the paper we use a different static platform. However, it uses the same artificial lateral line sensors. We estimate the flow speed using the pressure drop on the side of the robot. We then use that estimated flow speed to control the tail-beat frequency of the robot so that the thrust and drag forces are balanced. Using the experimental results we prove that the pressure drop on the sides of the robot gives a good estimation of the flow speed. Such speed estimation can be well used to control the swimming speed of the robot. I contributed to the article by 1) identifying the relationship between the pressure drop and the flow speed, 2) characterizing the actuation properties of the robotic platform by using the force feedback, 3) implementing a swimming-speed control with a pressure feedback, 4) writing the “Force control” and the “Swimming control with the onboard flow/pressure sensing” sections.

In the described article the velocity measurement was done with a static platform fixed to a rod. Our fish robot, however, is freely moving on a horizontal plane. It is also constantly oscillating while it is swimming. Such movements can affect the pressure distribution on the body of the vehicle. Therefore, the velocity measurement approach has to be validated also on our fish-robot. We have done that in the article “Flow-relative control of an underwater robot”, which was published in the Proceedings of the Royal Society A in 2013 [144] (Appendix G). My contribution to the article is proposing the hypotheses, developing the methodology, running the experiments, analyzing the results, discussing them and making the conclusions.

To validate the velocity measurement on a moving fish-robot, we first found the relationship between the pressure readings and the flow speed for our robot. We used two slightly different methods. First, we analyzed the pressure difference between the nose and the sides. Second estimation is acquired by using only the pressure drop on the sides of the vehicle. The resulting relations can be seen in Figure 3.6.

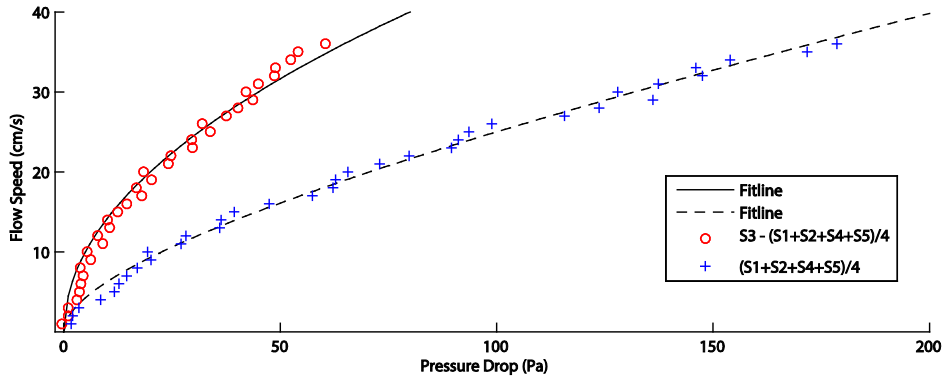


Figure 3.7 – Flow speed with respect to pressure drop measured using two different approaches.

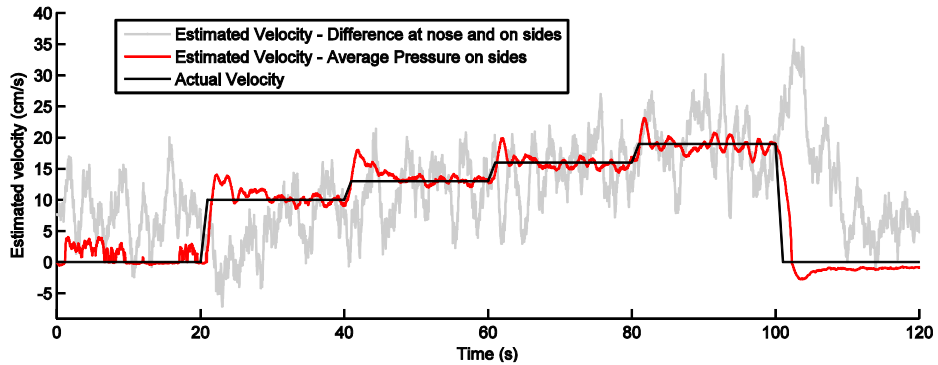


Figure 3.6 – Flow speed estimated using two different approaches. The flow speed is increased after every 20 seconds. The actual flow speed is shown in black.

It is important to understand if these two relations can be used to estimate the flow speed relative to an actively swimming robot. To investigate this issue, we ran a validation experiment. We placed the robotic fish into the flowing water. The robot was actuated and its downstream position was kept constant using a PID controller with an overhead camera feedback. This controller assured that the fish-relative flow speed equals the flow speed in the tunnel. We gradually changed the flow speed during the experiment and recorded the pressure data. Using this data we estimated the flow speed using the methods described above. Figure 3.7 shows the actual flow speed and the estimated speeds during the experiment. The results show that the average pressure on the sides of the robot gives a stable and precise estimation of the flow speed. The estimation from the difference between the pressure on the nose and the sides, however, is very unstable.

As we can see, our artificial lateral line can be well used to estimate the flow speed while the robot is actively swimming. As a next step we will make a simple validation test to ascertain the usability of the speed estimation for

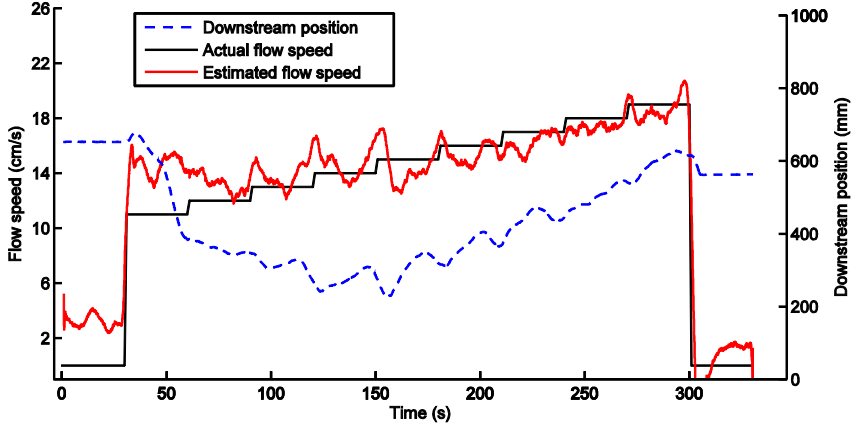


Figure 3.8 - Downstream position of the robot controlled by the station-holding controller while the flow speed is gradually increased over 270 s. The actual flow speed and the estimated flow speed are marked on the left axis and the downstream position is marked on the right axis.

controlling the underwater robot. We developed a controller that matches the robots speed U to the estimated flow speed V . In an ideal case such controller would keep the robot in a constant downstream position. In a real case, of course there is an odometry error that creates a drift away from the initial position. This drift is a parameter that shows the goodness of the velocity estimation.

To show the robustness of the method, the controller is as simple as possible. The robots tail beat amplitude A is adjusted to match the swimming speed of the robot U to the surrounding flow speed V .

$$A = 1.56V - 9.1 \quad (3.2)$$

The relationship between the robot swimming speed U and the tail-beat amplitude A was identified experimentally.

The robot with the speed-matching controller was placed in the flow tunnel. It was freely swimming while the flow-speed was gradually changed. The initial flow speed was 0.11 ms^{-1} and it was increased after every 30 s by 0.01 ms^{-1} up to 0.19 ms^{-1} . Figure 3.8 shows the flow speed, estimated flow speed and the robot's downstream position during a 300 s long experiment. The results show that in the beginning of the experiment the robot was overestimating the flow speed so that it started moving upstream. However, shortly after that the downstream position of the robot became very stable. Later during the experiment the robot started slowly drifting downstream. Even though some drift exists, it is notable that the range of the drift throughout the experiment was approximately 0.4 m, which is only 4/5 of the robots body length. The

downstream drift in the end of the experiment was 0.1 m. The results of the validation experiment suggest that the lateral-line based speed measurement can provide an accurate enough odometry estimate to be used in case of an absent global reference.

3.4 Robotic fish in turbid flow behind an object

Even though the rheotaxis and the flow speed detection in uniform flow can be extremely useful for underwater vehicles, the real benefits of the lateral line appear in the vicinity of other objects. These other objects, such as rocks, poles, ships, other animals and fish create turbulence in the flow. This turbulence can be used by fish to collect useful information about its surroundings. In reaction to the collected information fish show several behaviors of vital importance. These behaviors were explained in the Subsection 1.2.3 about the background of the fish flow sensing. One set of the behaviors appear when the fish is swimming behind a blunt object. As was explained, some fish are able to use the turbulence generated by the upstream object to save energy. Such ability would be beneficial also for an underwater robot that is working in flowing waters. Finding the objects and using their vortices to save energy would allow the vehicles to operate for longer periods on a battery power.

As we described, there are three different behaviors that fish use to save energy in the vicinity of an object. The first is the Kàrman gaiting, in which the fish is synchronizing its swimming movements with the oncoming vortices. To mimic such behavior on our robotic fish we would need to first identify the position of the vehicle with respect to the object. After that we have to detect the vortices with artificial lateral line and precisely adapt the robots movements. Detecting the position and the vortices with pressure sensors has been attempted by Venturelli *et al.* in [148]. They used a frequency domain analysis to find the dominant frequencies in pressure readings. They were able to detect the presence of the vortex street and to identify its various properties. However, their methods do not work in real time. Frequency-domain analysis requires data from longer period of time including multiple vortex shedding periods. Therefore, it is not suitable for using on our robot. A different approach that is also working in real time was used by Ježov *et al.* [141]. They used a fixed robotic fish-like platform with pressure sensors and moving tail to harvest energy from the vortices. Instead of frequency-domain analysis they identified extremes in pressure signals. They were able to show that synchronizing the tail movement to the vortices increased the efficiency up to 23%. However, such approach works well if the robots position in the vortex street is constrained to a single point. Their algorithm was tuned for very specific conditions only and it has to be retuned if these conditions, i.e. position, will change. Therefore, this approach is also not suitable for real-time control of freely swimming robot behind an object.

Another energy saving behavior that fish use is swimming in the bow wake in front of the object. To mimic this behavior on a fish robot, we could detect the

increased pressure area in front of the cylinder with the artificial lateral line pressure sensors. However, the downstream length of the increased pressure area is approximately in the range of 1...2 diameters of the object creating the wake. And as our fish robot has pressure sensors mounted only on the head, with this method it is theoretically possible to detect only very large objects. With objects much smaller than the robot itself the bow wake does not reach the sensors on the head of the robot.

The third behavior that fish use when swimming close to an object is entraining the flow in the edge of the suction zone behind the cylinder. Suction zone is an area behind the object where the flow is in the opposite direction with respect to the free-stream flow. Objects placed in this area are sucked against the object. Fish are able to balance the suction force to the downstream drag force to hold station and rest behind the object.

We show that this station holding behavior can also be mimicked on our fish-robot. The object in flow creates a distinct pressure field behind itself. We used the artificial lateral line pressure sensors to navigate in this pressure field and to achieve an energy-saving suction-zone entraining behavior. A detailed explanation of the study is given in Section 3 of our article “Flow-relative control of an underwater vehicle” [144] (Appendix G).

3.4.1 Flow characterization

To study the station-holding of the fish-robot, we used two different objects. The first was the vertical half-cylinder, which is widely used in real fish studies. The half-cylinder is usually used because it creates a well-developed Kàrman vortex street whose properties are predictable, repeatable and described thoroughly in the literature [149]. The second object was a cuboid. The cuboid was chosen because it creates less perfect and thus more natural flow conditions. These conditions were used to test the functionality of our methods in a more complex situation.

Before the experiments with the robotic fish, we characterized the flow behind the two different objects using the digital particle image velocimetry (DPIV) system. Figure 3.9 shows the mean downstream velocity and the vorticity behind the cylinder and the cuboid. The appropriate parameters are given in *Table 1*. The average velocity behind the cylinder clearly shows that a distinct suction zone area exists. The image also shows the reduced flow area, where the flow speed is significantly slower from the free-stream flow. The border of these two areas is the most favorable either for fish or our fish robot. The vorticity data shows that there is also a well-developed vortex street, meaning that the flow-pattern behind the cylinder is stable and consistent. The flow behind the cuboid is much more chaotic. There is no well-developed vortex street. Also, the suction zone is much smaller and the reduced flow area is narrower. Thus, the robot holding station behind the cuboid has to stay within

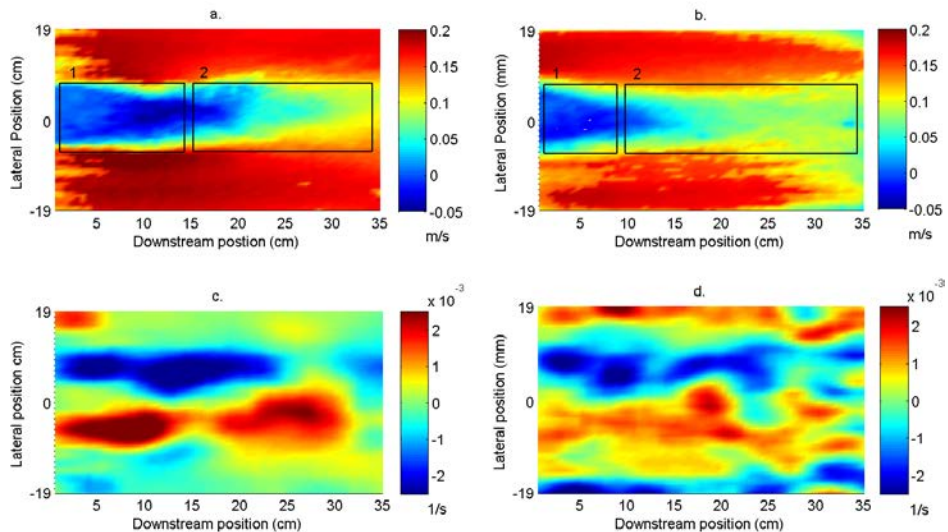


Figure 3.9 - Results of the DPIV analyses. (a,b) The mean downstream velocity behind the cylinder (a) and the cuboid (b). (c,d) The vorticity behind the cylinder (c) and the cuboid (d). On the mean velocity (a,b): 1, suction zone; 2, reduced flow area.

Table 1 – Flow parameters

	Behind the cylinder	Behind the cuboid
Incoming flow speed (cm s^{-1})	15	15
Tank width (cm)	50	50
Object width (cm)	10	10
Vortex shedding frequency (Hz)	0.4	0.3
Vortex street width (cm)	13.7	14.8
Suction point (cm)	13.7	6.5
Vortex shedding point (cm)	42.4	35.5
Mean velocity inside KVS (cm s^{-1})	9.4	6.1
Mean velocity outside KVS (cm s^{-1})	16.4	14.4

a much more limited area to successfully entrain the flow on the edge of the suction zone.

3.4.2 Detection of the presence of the upstream object

Before implementing the station holding, we look at the possibilities for detecting the presence of the upstream object. Ability of detecting the presence of the object is crucial if the station-holding is applied on underwater robots. It allows the vehicle to switch between different behaviors depending of if the task is to hold station and save energy or to pass the object and swim forward.

Two different approaches for discriminating a K arman vortex street from a free-stream flow are presented in [148]. The first method is using a frequency

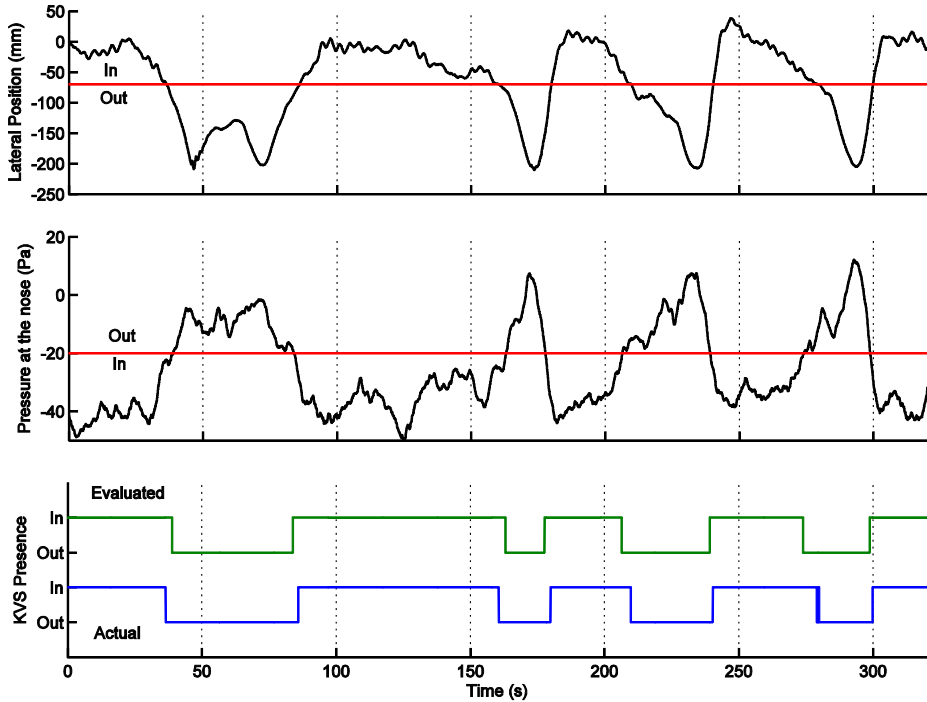


Figure 3.10 - KVS detection using the pressure at the nose. (Upper) The lateral position of the robot with respect to the KVS midline. (Middle) the corresponding pressure at the nose of the robot. The thick solid line on (Upper) is the limit of the KVS and on (Middle) it is marking a threshold below which the robot is considered to be in the KVS. (Lower) Whether the robot is actually in the KVS and its evaluation about the presence of the KVS.

spectrum analysis. This method involves analyzing the periodic pressure pulses created by the oncoming vortices using the fast Fourier transform. The second method is based on analyzing the turbulence intensity using the standard deviation of the pressure readings. Authors claim that with a static platform both of these approaches can be used to successfully distinguish the KVS. Our interest is, if the methods described in literature also work on a moving robotic fish. We implemented the algorithms presented in [148] and validated their functionality on our robot. We were able to verify the reported results on our robot while it was still. After verifying that the methods work as described by authors, we ran some experiments with swimming robot in the vortex street. The robot was controlled manually to steadily hold station. Our tests showed that it was possible to identify the presence of the Kàrman vortex street. However, the time window needed for analysis was at least 30 s. This is a clear mark that the previously presented methods in current form are not suitable for real-time control.

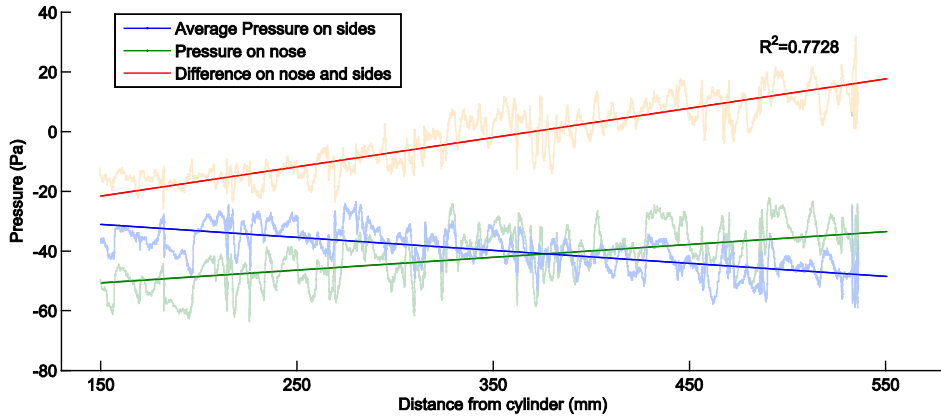


Figure 3.11 - Pressure data in KVS with respect to the distance from the cylinder.

We propose a more robust approach for upstream object detection. As we described above, there is a distinct reduced pressure area behind the object in flow. This pressure drop can be used to quickly detect the object. We conducted an experiment to test the usability of such approach. We placed the robot into the vortex street. Its downstream distance from the object was held constant at 50 cm using a controller based on the camera feedback. The tail-beat offset was manually controlled to repeatedly guide the robot into the vortex street and out again. The pressure at the tip of the nose during the experiment can be seen in Figure 3.10. The graphs show that the pressure data correlates very well with the presence of the vortex street. We also set a threshold to distinguish the presence of the object. From the lower graph we can see that using the pressure threshold is a precise method to detect the upstream object in our experimental conditions.

3.4.3 Estimation of the objects position

The next step after detecting the presence of the upstream object is to identify its position. We conducted a series of experiments to find the relationship between the robots position with respect to the upstream cylinder and the lateral line readings. The robot was placed into 0.15 ms^{-1} flow behind the half-cylinder. In the first experiments we varied its downstream distance while recording pressure data. In the second experiment the downstream distance was fixed and the lateral position with respect to the cylinder midline was changed.

The pressure readings with respect to the distance from the cylinder are shown in Figure 3.11. We see that when approaching the cylinder, the average pressure on the sides of the robot is increasing. This is caused by the lower flow speed behind the cylinder that reduces the pressure drop. Another trend that can be seen is the pressure drop at the tip of the nose of the robot. This is also an expected result as the static pressure behind the cylinder is lower compared with the free-stream pressure. To estimate the distance from the object, we use the

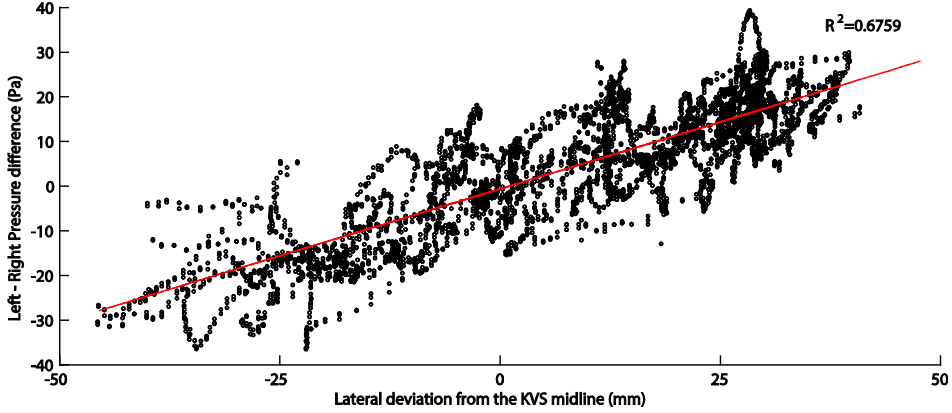


Figure 3.12 - Pressure difference on the left- and on the right-hand sides of the fish robot head versus the lateral deviation from the midline of the KVS.

sum of these two trends. In other words, the linear fit of the pressure difference between the nose and the sides.

$$D_{xe} = \frac{(P_3 - P_{avg}) + 36.29 + C}{0.09815} \quad (3.3)$$

,where D_{xe} is estimated distance from the cylinder; P_3 is the pressure at the nose and P_{avg} is the average pressure on the sides. The constant C takes into account the reduced dynamic pressure at the nose resulting from the lateral oscillation of the head. We identified it by actuating the robot in still water and comparing the sensor signals with a steady robot and the actuated robot.

When the robot moves laterally with respect to the cylinder, we expect to see an asymmetry in the pressure on the left- and on the right-hand side. The reason for the asymmetry is that the outer sensor starts to move out from the lower pressure area behind the cylinder while the inner sensor is still in the low pressure. Figure 3.12 shows the pressure difference on the left and right side of the robot with respect to the lateral deviation from the cylinder midline. From the figure we see that the expected asymmetry exists. To estimate the robot's lateral position with respect to the cylinder midline, we approximated the pressure difference on the left and right side using a linear function

$$D_{ye} = \frac{(P_l - P_r) + 0.63}{0.59} \quad (3.4)$$

where D_{ye} is the deviation from the midline of the vortex street; P_l is the average pressure on the left-hand side of the robot and P_r is the average pressure on the right side of the robot.

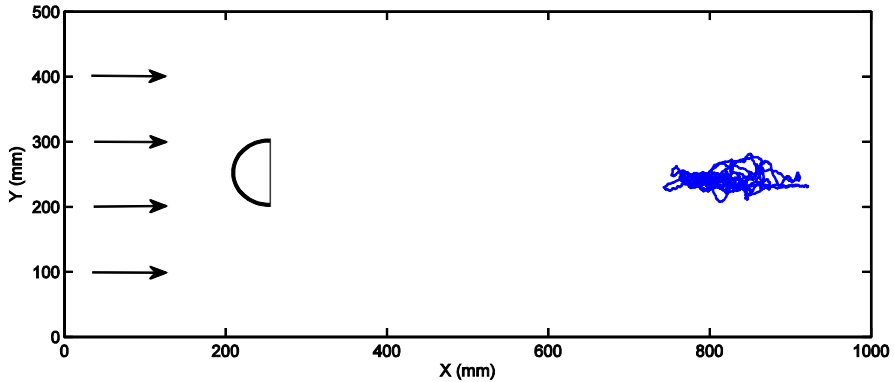


Figure 3.14 - Centre of mass trajectory of a robotic fish over 270 s in a KVS generated by the cylinder with a station-holding control in action. Flow direction and a position of the cylinder are marked on the graph.

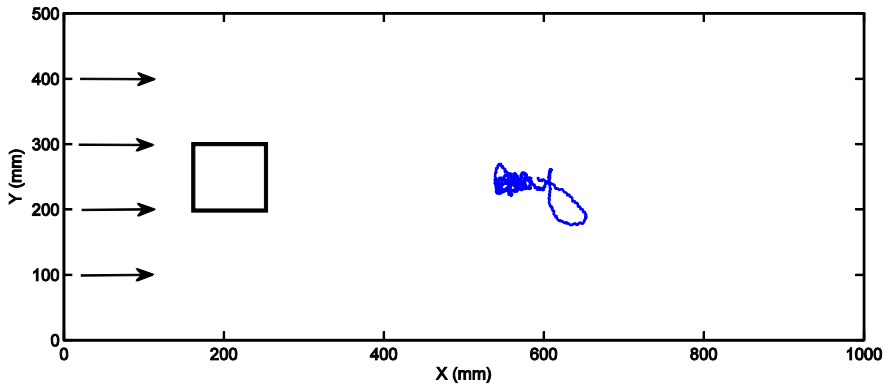


Figure 3.13 - Trajectory of the robot's centre of mass over 270 s holding station behind a cuboid.

3.4.4 Station holding behind the object

Using the relations described above, we implemented a station holding controller for the fish-robot. The controller consists of 2 parts: downstream distance control and the lateral position control. The aim of the downstream distance controller is to keep the vehicle at the edge of the suction zone. We chose the set point using the flow characterization results described above and the experiments with manual control. We manually controlled the robot to approach the cylinder. When moving further from certain point, the robot was rapidly sucked against the cylinder. The optimum set point is just slightly downstream from that suction point. The task of the lateral controller is to keep the robot aligned with the cylinder's midline. A more detailed description of the controllers is given in the Appendix G.

We tested the same controller behind the cylinder and the cuboid in a 0.15 m/s flow. Typical robot trajectories over 270 s are shown in Figure 3.14 and Figure 3.13. The images show that in both cases the robot is able to hold the position during the whole experiment. During the experiments we also measured the power consumption of the robot and compared them to the consumption in free flow. The results revealed that during the station holding behind the cylinder the robot used 7 % less energy and behind the cuboid it used 17 % less.

3.5 Conclusions

In this chapter we demonstrated a real-time flow-based control of an underwater vehicle using an artificial lateral line. By doing this we showed that a pressure-sensing artificial lateral line can be well used on underwater vehicles that have to work in rapidly flowing environments. We also proved that mimicking flow-related behaviors of fish can give extremely beneficial and directly applicable control methods for underwater robotics. For example rheotaxis and flow-speed detection would allow robots to hold station in the flow when other positioning references, like acoustic beacons, have been lost. Station holding, in the other hand, would help to save energy during long missions.

Of course the methods we described need further study before they can be used in real-world applications. We only tested the basic functionality of the principles in controlled laboratory conditions. However, the results of our studies let us assume that the methods can be well expanded for using in more complex scenarios.

4 CONCLUSIONS

In this thesis we addressed the problems of flow awareness and flow adaption of a small-sized underwater vehicle for turbid environments. We demonstrated that a bio-mimetic approach is useful for finding solutions to both of these problems.

Artificial lateral line sensors mimicking the canal neuromasts of fish can be used to improve the awareness. The artificial lateral line, as described in this thesis, does not have to be near to the complexity of its biological analogue. Off-the-shelf pressure sensors are already enough to be used for a real-time control of a rapidly moving vehicle in steady flow as well is in a wake of an object [144]. To prove this point we developed a novel type of fish-robot that incorporated both, fish-like actuation and fish-like sensing [128], [137], [138], [143], [144]. We proposed various control-principles to control the robot with respect to flow using feedback from its artificial lateral line. Starting with the steady current, we developed methodology to measure the orientation of the vehicle with respect to the flow and showed that even a simple Braitenberg controller can be used to achieve stable rheotactic behavior [143]. Also, we developed approach for estimating flow speed and holding down-stream position [144], [150]. Moving from steady flow to disturbed flow, we developed an approach to identify and localize the upstream object using an artificial lateral line. We demonstrated that by holding station in the hydrodynamic shadow of upstream object, the energy consumption of the vehicle reduced. [144]. The controllers were based on behaviors of a biological fish, proving that not only the sensing principles of the lateral line can be used for underwater engineering, but also the controllers can benefit from biomimetic approach.

Our solution to the problem mainly differs from the previous similar studies as it uses an actual freely-swimming underwater robot, not a constrained measurement platform. Therefore, this approach is much closer to industrial applications. The artificial lateral line with pressure sensors could serve as a good alternative for acoustic flow measurement devices used on the industrial underwater robots at the moment. It would expand the capabilities of autonomous underwater vehicles by providing data about the flow on their surface directly affecting them. The physical part of lateral line is miniature and can be installed on almost any vehicle. Of course the study has to be greatly extended before the results can be applied in real-world applications. In this thesis we only gave the proof of concept of the flow-based control. We showed that our control principles can be used even with simplistic controllers. However, to control a robot in more complex environments where the parameters of the objects and the flow are not predefined, more advanced control methods have to be developed. For example, adaptive controllers are a part of our future work.

In addition to mimicking fish sensing and behaviors, we also mimicked fish locomotion. We developed a novel approach for designing the compliant tail of our robotic fish. We demonstrated that fish-like swimming can be achieved by neglecting the distributed muscle actuation of biological fish and creating a compliant body whose geometry and elasticity distribution are mimicking these of a real fish [135]. To identify the elasticity distribution of fish, we proposed 2 novel approaches: by using Myometry [130] or by applying moment to soft body using gravity [135]. In addition to empirical approach to the tail-design we also contributed to model-based methods by developing an experimental methodology for validating the dynamics models of the biomimetic oscillating fins [137].

Even though we demonstrated that by mimicking the passive properties of a trout helps us to improve the kinematical similarity of the robot to biological fish, we saw that only passive properties are not enough to achieve high thrust and efficiency of the compliant-bodied robot. We have to tune the passive properties of the robot to match the properties of a live swimming fish. The tuning of these properties could be done with the help of new analytical models, such as the one we validated in this thesis. Another solution, which can be a part of future work, would be to develop a compliant fish robot with variable stiffness control. The stiffness control would allow tuning the body parameters in real time to optimize them for the specific swimming scenario.

The combination of the soft-bodied fish robot and its flow-based control provides a new approach for designing underwater systems for turbulent waters. This system adapts to the flow both passively and actively and has therefore many advantages with respect to traditional rigid underwater vehicles with no sense of flow.

REFERENCES

- [1] M. G. Logico, "Navy Diver Sets Record with 2,000 foot Dive," *military.com*, 2006. [Online]. Available: <http://www.military.com/features/0,15240,108883,00.html>. [Accessed: 12-Feb-2014].
- [2] J. E. Manley, "Unmanned surface vehicles, 15 years of development," *Ocean*. 2008, pp. 1–4, 2008.
- [3] T. W. Vaneck, C. D. Rodriguez-Ortiz, M. C. Schmidt, and J. E. Manley, "Automated bathymetry using an autonomous surface craft," *Navigation*, vol. 43, no. 4, pp. 407–417, 1996.
- [4] J. E. Manley, "High fidelity hydrographic surveys using an autonomous surface craft," Massachusetts Institute of Technology, 1998.
- [5] J. E. Manley, A. Marsh, W. Cornforth, and C. Wiseman, "Evolution of the autonomous surface craft AutoCat," in *Oceans 2000 MTS/IEEE Conference and Exhibition*, 2000, vol. 1, pp. 403–408.
- [6] Evologics, "Sonobot Autonomous Hydrographic Survey Vehicle." [Online]. Available: <http://www.evologics.de/en/products/sonobot/index.html>. [Accessed: 17-Feb-2014].
- [7] ASV, "ASV Unmanned Marine Systems." [Online]. Available: <http://www.asvglobal.com/>. [Accessed: 17-Feb-2014].
- [8] J. Curcio, J. Leonard, J. Vaganay, a. Patrikalakis, a. Bahr, D. Battle, H. Schmidt, and M. Grund, "Experiments in Moving Baseline Navigation using Autonomous Surface Craft," *Proc. Ocean. 2005 MTS/IEEE*, pp. 1–6.
- [9] J. Manley and S. Willcox, "The Wave Glider: A persistent platform for ocean science," *Ocean. Ieee Sydney*, pp. 1–5, May 2010.
- [10] G. Romeo, G. Frulla, and E. Cestino, "Design of a high-altitude long-endurance solar-powered unmanned air vehicle for multi-payload and operations," *Proc. Inst. Mech. Eng. Part G J. Aerosp. Eng.*, vol. 221, no. 2, pp. 199–216, 2007.

- [11] H. Erckens, G.-A. Büsser, C. Pradalier, and R. Siegwart, "Navigation Strategy and Trajectory Following Controller for an Autonomous Sailing Vessel," *IEEE Robotics and Automation Magazine*, no. March, pp. 45–54, 2010.
- [12] L. Lionel, *Underwater Robots Part I: Current Systems and Problem Pose*. Pro Literatur Verlag, 2006, pp. 335–360.
- [13] P. Ridao, M. Carreras, E. Hernandez, and N. Palomeras, "Underwater Telerobotics for Collaborative Research," in *Advances in Telerobotics SE - 21*, vol. 31, M. Ferre, M. Buss, R. Aracil, C. Melchiorri, and C. Balaguer, Eds. Springer Berlin Heidelberg, 2007, pp. 347–359.
- [14] SAAB, "SAAB Seaeye." [Online]. Available: <http://www.seaeye.com/>. [Accessed: 18-Feb-2014].
- [15] "Open ROV project." [Online]. Available: <http://openrov.com/>. [Accessed: 18-Feb-2014].
- [16] S. Cohan, "Trends in ROV development," *Mar. Technol. Soc. J.*, vol. 42, no. 1, pp. 38–43, 2008.
- [17] M. Corradini, "An actuator failure tolerant control scheme for an underwater remotely operated vehicle," *Control Syst. Technol. IEEE Trans.*, vol. 19, no. 5, pp. 1036–1046, 2011.
- [18] G. C. Karras, S. G. Loizou, and K. J. Kyriakopoulos, "A visual-servoing scheme for semi-autonomous operation of an underwater robotic vehicle using an IMU and a Laser Vision System," *2010 IEEE Int. Conf. Robot. Autom.*, pp. 5262–5267, May 2010.
- [19] T. Kwasnitschka, T. H. Hansteen, C. W. Devey, and S. Kutterolf, "Doing fieldwork on the seafloor: Photogrammetric techniques to yield 3D visual models from ROV video," *Comput. Geosci.*, vol. 52, pp. 218–226, Mar. 2013.
- [20] W. E. Nodland, "A general description of the self-propelled underwater research vehicle," 1968.
- [21] T. E. Ewart, "Observations from straightline isobaric runs of SPURV," *Proc. IAPSO/IAMAP PSII*, pp. 1–18, 1976.
- [22] J.-L. Michel, P. Borot, and H. Le Roux, "Epaulard: Experience and developments," *ROV 1984*, pp. 360–363, 1984.

- [23] U.S. Navy, “The Navy Unmanned Undersea Vehicle (UUV) Master Plan.” U.S. Navy, 2004.
- [24] U.S. Department of Defense, “Unmanned Systems Integrated Roadmap 2013-2038,” 2013.
- [25] C. von Alt, “REMUS 100 transportable mine countermeasure package,” *Ocean. 2003. Proc.*, pp. 1925–1930, 2003.
- [26] P. Ryan, “Mine countermeasures a success,” *PROCEEDINGS-UNITED STATES Nav. Inst.*, vol. 129, no. 5; ISSU 1203, p. 52, 2003.
- [27] Kongsberg, “REMUS 100 AUV,” 2014. [Online]. Available: <http://www.km.kongsberg.com/ks/web/nokbg0240.nsf/AllWeb/D241A2C835DF40B0C12574AB003EA6AB?OpenDocument>. [Accessed: 20-Feb-2014].
- [28] R. Marthiniussen, “HUGIN-AUV concept and operational experiences to date,” *Ocean. MTT/IEEE*, pp. 846–850, 2004.
- [29] J. W. Rish, S. Willcox, R. Grieve, I. Montieth, and J. Vaganay, “Operational testing of the Battlespace Preparation AUV in the shallow water regime,” *MTS/IEEE Ocean. 2001. An Ocean Odyssey. Conf. Proc.*, vol. 1, pp. 123–129, 2001.
- [30] C&C, “C&C ASV6300.” [Online]. Available: <http://www.cctechnol.com/site337.php>. [Accessed: 21-Feb-2014].
- [31] Furgo, “Echo Surveyor II datasheet.” [Online]. Available: http://www.fugrogeoservices.com/related/auv_datasheets/echosurveyorII.pdf. [Accessed: 21-Feb-2014].
- [32] J. Evans, P. Patron, and B. Privat, “Autotracker: Autonomous inspection—capabilities and lessons learned in offshore operations,” in *Proceedings of the IEEE OCEANS Conference*, 2009.
- [33] F. Maurelli, T. Larkworthy, D. Lane, G. C. Karras, C. P. Bechlioulis, and K. J. Kyriakopoulos, “Pose-based and Velocity-based Approaches to Autonomous Inspection of Subsea Structures.”
- [34] G. Marani, S. K. Choi, and J. Yuh, “Underwater autonomous manipulation for intervention missions AUVs,” *Ocean Eng.*, vol. 36, no. 1, pp. 15–23, Jan. 2009.

- [35] S. R. Ahmadzadeh, P. Kormushev, and D. G. Caldwell, "Autonomous robotic valve turning: A hierarchical learning approach," *2013 IEEE Int. Conf. Robot. Autom.*, pp. 4629–4634, May 2013.
- [36] C. C. Eriksen, T. J. Osse, R. D. Light, T. Wen, T. W. Lehman, P. L. Sabin, J. W. Ballard, and A. M. Chiodi, "Seaglider: A Long-Range Autonomous Underwater Vehicle for Oceanographic Research," vol. 26, no. 4, pp. 424–436, 2001.
- [37] D. C. Webb, P. J. Simonetti, and C. P. Jones, "SLOCUM: An Underwater Glider Propelled by Environmental Energy," *IEEE J. Ocean. Eng.*, vol. 26, no. 4, pp. 447–452, 2001.
- [38] J. Sherman and R. Davis, "The autonomous underwater glider 'Spray,'" *IEEE J. Ocean. Eng.*, vol. 26, no. 4, pp. 437–446, 2001.
- [39] A. Kukulya, A. Plueddemann, T. Austin, R. Stokey, M. Purcell, B. Allen, R. Littlefield, L. Freitag, E. Gallimore, J. Kemp, K. Newhall, and J. Pietro, "Under-ice Operations with a REMUS-100 AUV in the Arctic," in *Autonomous Underwater Vehicles (AUV), 2010 IEEE/OES*, 2010.
- [40] C. Kunz, C. Murphy, H. Singh, C. Pontbriand, R. A. Sohn, R. Camilli, and J. Bailey, "Toward Extraterrestrial Under-Ice Exploration: Robotic Steps in the Arctic," *J. F. Robot.*, vol. 26, no. 4, pp. 411–429, 2009.
- [41] M. Purcell, D. Gallo, G. Packard, M. Dennett, M. Rothenbeck, A. Sherrell, and S. Pascaud, "Use of REMUS 6000 AUVs in the search for the Air France Flight 447," in *OCEANS 2011*, 2011, pp. 1–7.
- [42] S. McPhail, "Autosub6000: A Deep Diving Long Range AUV," *J. Bionic Eng.*, vol. 6, no. 1, pp. 55–62, Mar. 2009.
- [43] NASA, "VALKYRIE: Phase 2." [Online]. Available: <http://astrobiology.nasa.gov/astep/projects/nra/nnh11zda001n-astep/valkyrie-phase-2/>. [Accessed: 27-Feb-2014].
- [44] Stone Aerospace, "ENDURANCE." [Online]. Available: <http://www.evl.uic.edu/endurance/>. [Accessed: 27-Feb-2014].
- [45] German Research Centre for Artificial Intelligence, "EurEx." [Online]. Available: <http://robotik.dfki-bremen.de/en/research/projects/eurex-1.html>. [Accessed: 27-Feb-2014].

- [46] M. Hildebrandt, C. Gaudig, L. Christensen, S. Natarajan, P. Paranhos, and J. Albiez, “Two years of experiments with the AUV dagon - a versatile vehicle for high precision visual mapping and algorithm evaluation,” *2012 IEEE/OES Auton. Underw. Veh.*, pp. 1–9, Sep. 2012.
- [47] C. Ordonez and R. Shearman, “Obtaining absolute water velocity profiles from glider-mounted Acoustic Doppler Current Profilers,” in *OCEANS, 2012 - Yeosu*, 2012.
- [48] a. O. Kasumyan, “Tactile reception and behavior of fish,” *J. Ichthyol.*, vol. 51, no. 11, pp. 1035–1103, Dec. 2011.
- [49] G. von der Emde and S. Fetz, “Distance, shape and more: recognition of object features during active electrolocation in a weakly electric fish,” *J. Exp. Biol.*, vol. 210, no. 17, pp. 3082–3095, Sep. 2007.
- [50] U. Müller, B. Heuvel, E. Stamhuis, and J. Videler, “Fish foot prints: morphology and energetics of the wake behind a continuously swimming mullet (*Chelon Labrosus Risso*),” *J. Exp. Biol.*, vol. 2906, pp. 2893–2906, 1997.
- [51] D. G. M. Watson, *Practical ship design*, vol. 1. Gulf Professional Publishing, 2002.
- [52] C. M. Breder, *The locomotion of fishes*. 1926.
- [53] J. Long, M. Mchenry, and N. Boetticher, “Undulatory Swimming: How Traveling Waves Are Produced and Modulated in Sunfish (*Lepomis Gibbosus*),” *J. Exp. Biol.*, vol. 192, no. 1, pp. 129–45, Jul. 1994.
- [54] M. J. Lighthill, “Large-amplitude elongated-body theory of fish locomotion,” *Proc. R. Soc. London. Ser. B. Biol. Sci.*, vol. 179, no. 1055, pp. 125–138, 1971.
- [55] B. E. Flammang, G. V. Lauder, D. R. Troolin, and T. E. Strand, “Volumetric imaging of fish locomotion,” *Biol. Lett.*, vol. 7, no. 5, pp. 695–8, Oct. 2011.
- [56] J. L. Jr, “The importance of body stiffness in undulatory propulsion,” *Am. Zool.*, vol. 694, pp. 678–694, 1996.
- [57] R. G. Root and C. W. Liew, “Computational and mathematical modeling of the effects of tailbeat frequency and flexural stiffness in swimming fish,” *Zoology (Jena)*, vol. 117, no. 1, pp. 81–5, Feb. 2014.

- [58] O. M. Curet, N. a Patankar, G. V Lauder, and M. a MacIver, “Mechanical properties of a bio-inspired robotic knifefish with an undulatory propulsor.,” *Bioinspir. Biomim.*, vol. 6, no. 2, p. 026004, Jun. 2011.
- [59] C. J. Esposito, J. L. Tangorra, B. E. Flammang, and G. V Lauder, “A robotic fish caudal fin: effects of stiffness and motor program on locomotor performance.,” *J. Exp. Biol.*, vol. 215, no. Pt 1, pp. 56–67, Jan. 2012.
- [60] B. E. Flammang, G. V Lauder, D. R. Troolin, and T. Strand, “Volumetric imaging of shark tail hydrodynamics reveals a three-dimensional dual-ring vortex wake structure.,” *Proc. Biol. Sci.*, vol. 278, no. 1725, pp. 3670–8, Dec. 2011.
- [61] E. D. Tytell, C. Hsu, T. L. Williams, A. H. Cohen, and L. J. Fauci, “Interactions between internal forces, body stiffness, and fluid environment in a neuromechanical model of lamprey swimming,” *Proc. Natl. Acad. Sci.*, vol. 107, no. 46, pp. 19832–19837, 2010.
- [62] J. Mogdans and H. Bleckmann, “Coping with flow: behavior, neurophysiology and modeling of the fish lateral line system.,” *Biol. Cybern.*, vol. 106, no. 11–12, pp. 627–42, Dec. 2012.
- [63] E. J. Denton and J. Gray, “Lateral-Line-Like Antennae of Certain of the Penaeidea (Crustacea, Decapoda, Natantia),” *Proc. R. Soc. London. Ser. B. Biol. Sci.*, vol. 226, no. 1244, pp. 249–261, Dec. 1985.
- [64] G. Dehnhardt, B. Mauck, and H. Bleckmann, “Seal whiskers detect water movements,” *Nature*, vol. 394, no. July, pp. 235–236, 1998.
- [65] J. Montgomery, S. Coombs, and M. Halstead, “Biology of the mechanosensory lateral line in fishes,” *Rev. Fish Biol. Fish.*, vol. 5, no. 4, pp. 399–416, 1995.
- [66] J. F. Webb, J. C. Montgomery, and J. Mogdans, “Bioacoustics and the lateral line system of fishes,” in *Fish bioacoustics*, Springer, 2008, pp. 145–182.
- [67] M. Beckmann, T. Erős, A. Schmitz, and H. Bleckmann, “Number and Distribution of Superficial Neuromasts in Twelve Common European Cypriniform Fishes and Their Relationship to Habitat Occurrence,” *Int. Rev. Hydrobiol.*, vol. 95, no. 3, pp. 273–284, Jun. 2010.

- [68] S. Coombs, P. Görner, and H. Münz, “A Brief Overview of the Mechanosensory Lateral Line System and the Contributions to This Volume,” in *The Mechanosensory Lateral Line SE - 1*, S. Coombs, P. Görner, and H. Münz, Eds. Springer New York, 1989, pp. 3–5.
- [69] A. Schmitz, H. Bleckmann, and J. Mogdans, “Organization of the superficial neuromast system in goldfish, *Carassius auratus*,” *J. Morphol.*, vol. 269, no. 6, pp. 751–61, Jun. 2008.
- [70] S. M. van Netten, “Hydrodynamic detection by cupulae in a lateral line canal: functional relations between physics and physiology,” *Biol. Cybern.*, vol. 94, no. 1, pp. 67–85, Jan. 2006.
- [71] M. S. Weeg, A. H. Bass, and B. R. Land, “Frequency Response Properties of Lateral Line Superficial Neuromasts in a Vocal Fish , With Evidence for Acoustic Sensitivity,” *J. Neurophysiol.*, vol. 88, no. 3, pp. 1252–1262, 2002.
- [72] S. Coombs, M. Hastings, and J. Finneran, “Modeling and measuring lateral line excitation patterns to changing dipole source locations,” *J. Comp. Physiol. A*, vol. 178, no. 3, pp. 359–371, 1996.
- [73] R. Hueter and D. Mann, “Sensory biology of elasmobranchs,” in *Biology of sharks and their relatives*, 2004, pp. 325–368.
- [74] M. Barry, D. Hall, and M. L. Bennett, “The elasmobranch spiracular organ,” *J. Comp. Physiol. A*, vol. 163, no. 1, pp. 85–92, 1988.
- [75] K. P. Maruska, “Morphology of the mechanosensory lateral line system in elasmobranch fishes : ecological and behavioral considerations,” *Dev. Environ. Biol. fishes*, vol. 20, pp. 47–75, 2001.
- [76] J. C. Montgomery, C. F. Baker, and A. G. Carton, “The lateral line can mediate rheotaxis in fish,” *Nature*, vol. 389, no. October, pp. 960–963, 1997.
- [77] B. P. Chagnaud, C. Brücker, M. H. Hofmann, and H. Bleckmann, “Measuring flow velocity and flow direction by spatial and temporal analysis of flow fluctuations,” *J. Neurosci.*, vol. 28, no. 17, pp. 4479–87, Apr. 2008.
- [78] C. L. Cook and D. J. Coughlin, “Rainbow trout *Oncorhynchus mykiss* consume less energy when swimming near obstructions,” *J. Fish Biol.*, vol. 77, no. 7, pp. 1716–23, Nov. 2010.

- [79] M. Taguchi and J. C. Liao, "Rainbow trout consume less oxygen in turbulence: the energetics of swimming behaviors at different speeds.," *J. Exp. Biol.*, vol. 214, no. Pt 9, pp. 1428–36, May 2011.
- [80] R. D. Blevins, "Flow-induced vibration," *New York, Van Nostrand Reinhold Co., 1977. 377 p.*, vol. 1, 1977.
- [81] J. C. Liao, "The Karman gait: novel body kinematics of rainbow trout swimming in a vortex street," *J. Exp. Biol.*, vol. 206, no. 6, pp. 1059–1073, Mar. 2003.
- [82] J. C. Liao, D. N. Beal, G. V. Lauder, and M. S. Triantafyllou, "Fish exploiting vortices decrease muscle activity.," *Science*, vol. 302, no. 5650, pp. 1566–9, Nov. 2003.
- [83] D. N. Beal, F. S. Hover, M. S. Triantafyllou, J. C. Liao, and G. V. Lauder, "Passive propulsion in vortex wakes," *J. Fluid Mech.*, vol. 549, no. -1, p. 385, Feb. 2006.
- [84] J. C. Liao, "The role of the lateral line and vision on body kinematics and hydrodynamic preference of rainbow trout in turbulent flow.," *J. Exp. Biol.*, vol. 209, no. Pt 20, pp. 4077–90, Oct. 2006.
- [85] P. Webb, "Entrainment by river chub *nocomis micropogon* and smallmouth bass *micropterus dolomieu* on cylinders," *J. Exp. Biol.*, vol. 201 (Pt 16), pp. 2403–12, Aug. 1998.
- [86] H. Bleckmann, A. Przybilla, A. Klein, A. Schmitz, S. Kunze, and C. Brücker, "Station holding of trout: behavior, physiology and hydrodynamics," in *Nature-inspired fluid mechanics*, Springer, 2012, pp. 161–177.
- [87] A. Przybilla, S. Kunze, A. Rudert, H. Bleckmann, and C. Brücker, "Entraining in trout: a behavioural and hydrodynamic analysis.," *J. Exp. Biol.*, vol. 213, no. Pt 17, pp. 2976–86, Sep. 2010.
- [88] H. Bleckmann, G. Tittel, and E. Blübaum-Gronau, "The Lateral Line System of Surface-Feeding Fish: Anatomy, Physiology, and Behavior," in *The Mechanosensory Lateral Line SE - 25*, S. Coombs, P. Görner, and H. Münz, Eds. Springer New York, 1989, pp. 501–526.
- [89] J. Mogdans and I. E. Nauroth, "The oscar, *Astronotus ocellatus*, detects and discriminates dipole stimuli with the lateral line system.," *J. Comp.*

- Physiol. A. Neuroethol. Sens. Neural. Behav. Physiol.*, vol. 197, no. 10, pp. 959–68, Oct. 2011.
- [90] D. Vogel and H. Bleckmann, “Behavioral discrimination of water motions caused by moving objects,” *J. Comp. Physiol. A Sensory, Neural, Behav. Physiol.*, vol. 186, no. 12, pp. 1107–1117, Feb. 2001.
- [91] K. Pohlmann, F. W. Grasso, and T. Breithaupt, “Tracking wakes: the nocturnal predatory strategy of piscivorous catfish.,” *Proc. Natl. Acad. Sci. U. S. A.*, vol. 98, no. 13, pp. 7371–4, Jun. 2001.
- [92] W. Hanke, C. Brücker, and H. Bleckmann, “The ageing of the low-frequency water disturbances caused by swimming goldfish and its possible relevance to prey detection.,” *J. Exp. Biol.*, vol. 203, no. Pt 7, pp. 1193–200, Apr. 2000.
- [93] K. Streitlien, G. S. Triantafyllou, and M. S. Triantafyllou, “Efficient foil propulsion through vortex control,” *Aiaa J.*, vol. 34, no. 11, pp. 2315–2319, 1996.
- [94] D. Barrett and M. Triantafyllou, “Drag reduction in fish-like locomotion,” *J. Fluid Mech.*, vol. 392, pp. 183–212, 1999.
- [95] J. Kumph, “Maneuvering of a Robotic Pike,” Massachusetts Institute of Technology, 2000.
- [96] J. M. Anderson and P. A. Kerrebrock, “The vorticity control unmanned undersea vehicle (VCUUV)-An autonomous vehicle employing fish swimming propulsion and maneuvering,” in *International Symposium on Unmanned Untethered Submersible Technology*, 1997, pp. 189–195.
- [97] I. Dukes, “Novel mechatronics design for a robotic fish,” *2005 IEEE/RSJ Int. Conf. Intell. Robot. Syst.*, pp. 807–812, 2005.
- [98] J. Liu, “Mimicry of Sharp Turning Behaviours in a Robotic Fish *,” in *IEEE International conference on Robotics and Automation*, 2005, no. April, pp. 18–23.
- [99] E. McGookin and C. Watts, “A biomimetic underwater vehicle design concept,” Institution of Engineering and Technology, 2012.
- [100] J. Liang, T. Wang, and L. Wen, “Development of a Two-Joint Robotic Fish for Real-World Exploration,” *J. F. Robot.*, vol. 28, no. 1, pp. 70–79, 2011.

- [101] I. D. Neveln, Y. Bai, J. B. Snyder, J. R. Solberg, O. M. Curet, K. M. Lynch, and M. a MacIver, “Biomimetic and bio-inspired robotics in electric fish research.,” *J. Exp. Biol.*, vol. 216, no. Pt 13, pp. 2501–14, Jul. 2013.
- [102] P. V. y Alvarado and K. Youcef-Toumi, “Design of machines with compliant bodies for biomimetic locomotion in liquid environments,” *J. Dyn. Syst. Meas. Control*, vol. 128, no. 1, pp. 3–13, 2006.
- [103] A. D. Marchese, C. D. Onal, and D. Rus, “Autonomous Soft Robotic Fish Capable of Escape Maneuvers Using Fluidic Elastomer Actuators,” *Soft Robot.*, vol. 1, no. 1, pp. 75–87, Mar. 2014.
- [104] M. Mchenry, C. Pell, and J. Jr, “Mechanical control of swimming speed: stiffness and axial wave form in undulating fish models,” *J. Exp. Biol.*, vol. 198, no. Pt 11, pp. 2293–305, Jan. 1995.
- [105] Z. Fan, J. Chen, J. Zou, D. Bullen, C. Liu, and F. Delcomyn, “Design and fabrication of artificial lateral line flow sensors,” *J. Micromechanics Microengineering*, vol. 12, no. 5, pp. 655–661, Sep. 2002.
- [106] C. Tucker, J. M. Engel, and S. Pandya, “Design and Characterization of Artificial Haircell Sensor for Flow Sensing With Ultrahigh Velocity and Angular Sensitivity,” *J. Microelectromechanical Syst.*, vol. 16, no. 5, pp. 999–1014, Oct. 2007.
- [107] a. Qualtieri, F. Rizzi, M. T. Todaro, a. Passaseo, R. Cingolani, and M. De Vittorio, “Stress-driven AlN cantilever-based flow sensor for fish lateral line system,” *Microelectron. Eng.*, vol. 88, no. 8, pp. 2376–2378, Aug. 2011.
- [108] J. J. Van Baar, M. Dijkstra, R. J. Wiewerink, T. S. J. Lammerink, and G. J. M. Krijnen, “Fabrication of arrays of artificial hairs for complex flow pattern recognition,” *IEEE Sensors*, pp. 332–336, 2003.
- [109] M. Dijkstra, J. J. Van Baar, R. J. Wiewerink, T. S. J. Lammerink, J. H. De Boer, and G. J. M. Krijnen, “Artificial sensory hairs based on the flow sensitive receptor hairs of crickets,” *J. Micromechanics Microengineering*, vol. 15, no. 7, pp. S132–S138, Jul. 2005.
- [110] a M. K. Dagamseh, C. M. Bruinink, H. Droogendijk, R. J. Wiewerink, T. S. J. Lammerink, and G. J. M. Krijnen, “Engineering of biomimetic hair-flow sensor arrays dedicated to high-resolution flow field measurements,” *2010 IEEE Sensors*, pp. 2251–2254, Nov. 2010.

- [111] N. Izadi, M. J. de Boer, J. W. Berenschot, and G. J. M. Krijnen, "Fabrication of superficial neuromast inspired capacitive flow sensors," *J. Micromechanics Microengineering*, vol. 20, no. 8, p. 085041, Aug. 2010.
- [112] M. E. McConney, N. Chen, D. Lu, H. a. Hu, S. Coombs, C. Liu, and V. V. Tsukruk, "Biologically inspired design of hydrogel-capped hair sensors for enhanced underwater flow detection," *Soft Matter*, vol. 5, no. 2, p. 292, 2009.
- [113] Y. Yang, A. Klein, H. Bleckmann, and C. Liu, "Artificial lateral line canal for hydrodynamic detection," *Appl. Phys. Lett.*, vol. 99, no. 2, p. 023701, 2011.
- [114] V. I. Fernandez, S. M. Hou, F. S. Hover, J. H. Lang, and M. S. Triantafyllou, "Development and application of distributed MEMS pressure sensor array for AUV object avoidance," in *16th Int. Symp. on Unmanned Untethered Submersible Technology*, 2009.
- [115] a G. P. Kottapalli, M. Asadnia, J. M. Miao, G. Barbastathis, and M. S. Triantafyllou, "A flexible liquid crystal polymer MEMS pressure sensor array for fish-like underwater sensing," *Smart Mater. Struct.*, vol. 21, no. 11, p. 115030, Nov. 2012.
- [116] Y. Yang, J. Chen, J. Engel, S. Pandya, N. Chen, C. Tucker, S. Coombs, D. L. Jones, and C. Liu, "Distant touch hydrodynamic imaging with an artificial lateral line.," *Proc. Natl. Acad. Sci. U. S. A.*, vol. 103, no. 50, pp. 18891–5, Dec. 2006.
- [117] a. M. K. Dagamseh, T. S. J. Lammerink, M. L. Kolster, C. M. Bruinink, R. J. Wiegerink, and G. J. M. Krijnen, "Dipole-source localization using biomimetic flow-sensor arrays positioned as lateral-line system," *Sensors Actuators A Phys.*, vol. 162, no. 2, pp. 355–360, Aug. 2010.
- [118] J. Chen, J. Engel, and N. Chen, "Artificial lateral line and hydrodynamic object tracking," *19th IEEE Int. Conf. Micro Electro Mech. Syst.*, no. January, pp. 694–697, 2006.
- [119] Y. Yang, N. Nguyen, N. Chen, M. Lockwood, C. Tucker, H. Hu, H. Bleckmann, C. Liu, and D. L. Jones, "Artificial lateral line with biomimetic neuromasts to emulate fish sensing.," *Bioinspir. Biomim.*, vol. 5, no. 1, p. 16001, Mar. 2010.

- [120] V. Fernandez, S. Hou, and F. Hover, “Lateral-line-inspired MEMS-array Pressure Sensing for Passive Underwater navigation,” in *15th Int. Symp. on Unmanned Untethered Submersible Technology*, 2007.
- [121] O. Akanyeti, R. Venturelli, F. Visentin, L. Chambers, W. M. Megill, and P. Fiorini, “What information do Karman streets offer to flow sensing?,” *Bioinspiration biomimetics*, vol. 6, no. 3, p. 036001, 2011.
- [122] A. Klein and H. Bleckmann, “Determination of object position, vortex shedding frequency and flow velocity using artificial lateral line canals.,” *Beilstein J. Nanotechnol.*, vol. 2, pp. 276–83, Jan. 2011.
- [123] O. Akanyeti, J. Brown, L. D. Chambers, H. El Daou, C. Fiazza, P. Fiorini, J. Ježov, D. S. Jung, M. Kruusmaa, M. Listak, A. Liszewski, J. L. Maud, W. M. Megill, L. Rossi, A. Qualtieri, F. Rizzi, T. Salumäe, G. Toming, R. Venturelli, F. Visentin, and M. De Vittorio, “FILOSE: a swanning robot,” *IEEE Robotics and Automation Magazine*, 2014.
- [124] P. Riggs, A. Bowyer, and J. Vincent, “Advantages of a Biomimetic Stiffness Profile in Pitching Flexible Fin Propulsion,” *J. Bionic Eng.*, vol. 7, no. 2, pp. 113–119, Jun. 2010.
- [125] B. P. Epps, P. Valdivia y Alvarado, K. Youcef-Toumi, and A. H. Techet, “Swimming performance of a biomimetic compliant fish-like robot,” *Exp. Fluids*, vol. 47, no. 6, pp. 927–939, Jun. 2009.
- [126] P. V. y Alvarado, “Design of biomimetic compliant devices for locomotion in liquid environments,” Massachusetts Institute of Technology, 2007.
- [127] T. Salumäe, “Design of a Compliant Underwater Propulsion Mechanism by Investigating and Mimicing the Body of a Rainbow Trout (*Oncorhynchus mykiss*),” Tallinn University of Technology, 2010.
- [128] C. Fiazza, T. Salumäe, M. Listak, G. Kulikovskis, R. Templeton, O. Akanyeti, W. Megill, P. Fiorini, and M. Kruusmaa, “Biomimetic mechanical design for soft-bodied underwater vehicles,” in *Proceedings of OCEANS 2010 MTS/IEEE - Sydney*, 2010.
- [129] J. Cheng, “A continuous dynamic beam model for swimming fish,” *Philos Trans R Soc L. B Biol Sci.*, vol. 353, no. 1371, pp. 981–997, 1998.
- [130] O. Akanyeti, A. Ernits, C. Fiazza, G. Toming, G. Kulikovskis, M. Listak, R. Raag, T. Salumäe, P. Fiorini, and M. Kruusmaa, “Myometry-

- driven compliant-body design for underwater propulsion,” in *Proc. 2010 IEEE International Conference on Robotics and Automation (ICRA)*, 2010, pp. 84–89.
- [131] Myoton AS, “Myoton Muscle Diagnostics - Innovation for Muscle Health and Performance.” [Online]. Available: <http://www.myoton.com/>. [Accessed: 29-Jul-2014].
- [132] T. Rätsep and T. Asser, “Changes in viscoelastic properties of skeletal muscles induced by subthalamic stimulation in patients with Parkinson’s disease.,” *Clin. Biomech. (Bristol, Avon)*, vol. 26, no. 2, pp. 213–7, Mar. 2011.
- [133] L. Aird, D. Samuel, and M. Stokes, “Quadriceps muscle tone, elasticity and stiffness in older males: reliability and symmetry using the MyotonPRO.,” *Arch. Gerontol. Geriatr.*, vol. 55, no. 2, pp. e31–9, 2012.
- [134] Myoton AS, “Myoton Method of Measuring.” [Online]. Available: <http://www.myoton.com/en/Technology>. [Accessed: 29-Jul-2014].
- [135] T. Salumäe and M. Kruusmaa, “A Flexible Fin with Bio-Inspired Stiffness Profile and Geometry,” *J. Bionic Eng.*, vol. 8, no. 4, pp. 418–428, Dec. 2011.
- [136] P. W. Webb, P. T. Kostecki, and E. D. Stevens, “The effect of size and swimming speed on locomotor kinematics of Rainbow Trout,” *J. Exp. Biol.*, vol. 95, pp. 77–95, 1984.
- [137] H. El Daou, T. Salumäe, G. Toming, and M. Kruusmaa, “A bio-inspired compliant robotic fish: Design and experiments,” *Robot. Autom. (ICRA), 2012 IEEE Int. Conf.*, pp. 5340–5345, 2012.
- [138] H. El Daou, T. Salumäe, L. D. Chambers, W. M. Megill, and M. Kruusmaa, “Modelling of a biologically inspired robotic fish driven by compliant parts.,” *Bioinspir. Biomim.*, vol. 9, no. 1, p. 016010, Mar. 2014.
- [139] J. Chen, Z. Fan, J. Zou, J. Engel, and C. Liu, “Two-Dimensional Micromachined Flow Sensor Array for Fluid Mechanics Studies,” *J. Aerosp. Eng.*, no. April, 2003.
- [140] J. Ježov, “Pressure sensitive lateral line for underwater robot,” Tallinn University of Technology, 2013.

- [141] J. Jezov, O. Akanyeti, L. D. Chambers, and M. Kruusmaa, “Sensing oscillations in unsteady flow for better robotic swimming efficiency,” in *Proceedings of the 2012 IEEE International Conference on Systems, Man, and Cybernetics*, 2012, pp. 91–96.
- [142] G. P. Arnold, “Rheotropism in fishes,” *Biol. Rev.*, vol. 49, no. 4, pp. 515–576, 1974.
- [143] T. Salumäe, I. Ranó, O. Akanyeti, and M. Kruusmaa, “Against the flow: a Braitenberg controller for a fish robot,” *Robot. Autom. (ICRA), 2012 IEEE Int. Conf.*, pp. 4210–4215, 2012.
- [144] T. Salumäe and M. Kruusmaa, “Flow-relative control of an underwater robot,” *Proc. R. Soc. A*, vol. 469, no. 2153, 2013.
- [145] V. Braitenberg, *Vehicles: Experiments in synthetic psychology*. MIT press, 1986.
- [146] H. Bleckmann, “Role of the Lateral Line in Fish Behaviour,” in *The Behaviour of Teleost Fishes SE - 7*, T. Pitcher, Ed. Springer US, 1986, pp. 177–202.
- [147] M. Kruusmaa, G. Toming, T. Salumäe, J. Jezov, and A. Ernits, “Swimming speed control and on-board flow sensing of an artificial trout,” *2011 IEEE Int. Conf. Robot. Autom.*, pp. 1791–1796, May 2011.
- [148] R. Venturelli, O. Akanyeti, and F. Visentin, “Hydrodynamic pressure sensing with an artificial lateral line in steady and unsteady flows,” *Bioinspir. Biomim.*, pp. 1–21, 2012.
- [149] M. M. Zdravkovich, “Flow around circular cylinders, vol. 1. Fundamentals,” *J. Fluid Mech.*, vol. 350, pp. 377–378, 1997.
- [150] M. Kruusmaa, G. Toming, T. Salumäe, J. Jezov, and A. Ernits, “Swimming speed control and on-board flow sensing of an artificial trout,” in *IEEE International Conference on Robotics and Automation*, 2011, pp. 1791 – 1796.

ABSTRACT

Fishes have a flow-sensing organ called the lateral line. In this thesis we argue that a man-made copy of a lateral line is an excellent tool for flow-relative control of an underwater robot. A simple biomimetic flow-sensor array can be effectively used to control a rapidly moving vehicle in steady flow as well as in a wake of an object. To prove our argument, we demonstrate a soft-bodied fish-robot with an array of pressure sensors mounted on its head. We use these pressure sensors to mimic different flow-related behaviors of fish on the robot. By implementing these behaviors we also show that bio-mimetic approach can be directly used to design control principles that are well applicable on underwater robots. In addition to the flow-based control, we use the developed soft-bodied fish-robot to advance the current knowledge about the biomimetic fin design. We demonstrate novel design approaches that help to improve the performance of fish-like compliant bodies. The combination of the soft-bodied fish-robot and the flow-based control provides a novel design approach for underwater robots working in rapidly flowing waters like rivers, canals etc.

The work is motivated by the fact that underwater robots at the moment are not able to adapt to the flow to the sufficient degree. There are some methods, like acoustic Doppler current profiling, that can be used to measure the flow movement around the vehicle. However, these methods require large devices that are not suitable for miniature vehicles. Therefore, at the moment the possibilities for making small vehicles for riverine environments are extremely limited.

We approach the problem by taking inspiration from fish. All fishes are capable of sensing the flow and adapting to it. They use their lateral line to feel how the water is moving around their body and they actively react to the movements. In addition to the active reactions they also show passive reactions to the water movements. It means they have compliant bodies that bend in the flow, reducing the effect of vortices and smaller water motions on the movement of the whole fish. Our goal is to develop an underwater robot that also is able to react to the flow both passively and actively.

The active reactions and artificial lateral line flow-measurements have been studied rather extensively by different authors. There have been several studies where the artificial lateral line sensors have been used. It has been proven that artificial lateral lines can be used to detect passing objects, identify the position of dipole sources and so on. However, up to our knowledge, all the previous studies have been done using constrained platforms. Their applicability on real-world scenarios has not been extensively studied. We look the problem from more application-oriented point of view. We use an actively swimming robotic-fish and study, how the artificial lateral line can be used to control it in different

flow conditions. We develop principles for measuring the flow speed and direction, holding station in steady flow, detecting the presence and the position of an upstream object and holding station in the wake of that object to save energy.

Also the compliant fish-like bodies have been studied before. There are different analytical models available to estimate the behavior of the viscoelastic bodies. However, we analyze some empirical approaches to design better fins. We mimic the body properties of an actual fish to increase the performance of a robot. We develop two new methods to estimate the properties of a real fish. In addition we demonstrate some experiment methodologies to improve the analytical modelling of viscoelastic compliant bodies.

KOKKUVÕTE

Kõikidel kaladel on küljejoon – organ, mis võimaldab neil tunda vee liikumist enda keha pinnal. Küljejoonelt saadud informatsiooni kasutavad kalad ümbritseva veekeskonna tajumiseks, näiteks teiste veeloomade liikumise ja asukoha tuvastamiseks, vee voolukiiruse ja suuna määramiseks, voolavas vees leiduvate objektide asukoha hindamiseks jne. Selline ümbruskonna tajumise viis oleks äärmiselt kasulik ka allvee robotitele. Paraku aga ei kasuta tänapäevased allvee robotid küljejoonele sarnaseid andureid. Käesolevas töös väidame, et bioloogilise küljejoone tehnoloogilist analoogi, niinimetatud kunstlikku küljejoont, on võimalik edukalt kasutada ka allvee robotile kasuliku informatsiooni hankimiseks. Veelgi enam, saadud info põhjal on võimalik allvee robotit reaalselt juhtida.

Lisaks kala küljejoone kopeerimisele on allvee robotite konstrueerimisel mõistlik eeskuju võtta ka kalade liikumismehhanismist. Kalalaadset liikumist on võrreldes klassikalises inseneerias kasutusel olevate sõukruvidega terve hulk eeliseid. Kalad suudavad oma uimede abil liikuda oluliselt efektiivsemalt, manööverdada paremini, saavutada väga suuri kiirusi ja kiirendusi. Seetõttu panustame käesolevas töös ka kalalaadset liikumist põhinevate allvee robotite väljatöötamisele. Väidame, et voolavas vees opereerivatel allvee robotitel on mõistlik kasutada ühe mootoriga liigutatavaid pehmeid uimi, mille materjaliomaduste valimisel võetakse eeskujuks bioloogilise kala keha materjaliomadused.

Oma väidete kinnitamiseks konstrueerime kunstliku küljejoonega varustatud voolutundliku robotkala. Küljejoon kujutab endast väga lihtsat, viiest roboti pähe paigaldatud rõhuandurit koosnevat seadet. Hoides küljejoone lihtsana, näitame, et roboti voolu järgi juhtimiseks ei ole vaja kasutada keerukaid, paljudest anduritest koosnevaid sensorsüsteeme. Võttes eeskuju kalade voolutunnetusel põhinevatest käitumismaneeridest, töötame roboti jaoks välja erinevaid juhtimisprintsippe ning katsetame nende toimivust erinevates voolava vee tingimustes. Näitame, et kunstliku küljejoonega varustatud robot on võimeline hindama vee kiirust ja suunda ning tuvastama ülesvoolu jääva objekti olemasolu. Objekti olemasolul on ta suuteline määrama selle asukohta ning liikuma objekti varju, et säästa energiat. Kunstlikke küljejooni on loomulikult uuritud ka varem, kuid meie lähenemine erineb eelnevatest selle poolest, et kasutame esmakordselt küljejoont reaalse roboti juhtimiseks. Senistes töodes on erinevaid kunstliku küljejoone tehnoloogiaid katsetatud äärmiselt staatilistes tingimustes, kinnitades neid näiteks fikseeritud platvormide külge. Nii aga jääb piisava tähelepanuta tehnoloogia reaalse rakendatavus päris elus tekkivate probleemide lahendamiseks.

Ka robotkala mehaanika välja töötamisel oleme arvesse võtnud rakendatavust. Selle asemel, et kasutada jäikaid, mitmete lülide, mootorite ja ülekandemehhanismidega keerukaid lahendusi, kasutame ühe mootori abil liigutatavaid pehmeid uimi. Keskendume nende uimede materjaliomadustele. Valides sobivad materjaliomadused, on võimalik uimi võnkuma panna selliselt et nende liikumine on sarnane ujuva kala kehas tekkivate lainetega. Töös oleme välja töötanud erinevaid uudseid lahendusi sobivate materjaliomaduste valimiseks.

APPENDIX A

C. Fiazza, T. Salumäe, M. Listak, G. Kulikovskis, R. Templeton, O. Akanyeti, W. Megill, P. Fiorini, and M. Kruusmaa, “Biomimetic mechanical design for soft-bodied underwater vehicles,” in *Proc. OCEANS 2010 MTS/IEEE - Sydney*, 2010

Biomimetic Mechanical Design for Soft-Bodied Underwater Vehicles

C. Fiazza¹, T. Salumäe², M. Listak², G. Kulikovskis³, R. Templeton⁴, O. Akanyeti¹, W. Megill⁴, P. Fiorini¹, M. Kruusmaa²

Abstract—This paper describes a biomimetic underwater fish robot prototype and its design methodology. The key question directing our design is the transfer of functionality from fish to a fish robot with respect to efficient mobility. We want to minimize mechanical complexity and achieve a low-cost fabrication. We argue for the case of morphological computation, i.e. achieving high mobility and efficiency by duplicating fish physical body structure. In this way, a possibly large part of the fish motion ability is outsourced to the embodiment, i.e. achieved by the interaction of the fish body parts and the water flow. This approach makes us focus on the material properties of a compliant tail propulsion mechanism. The tail is actuated by a single motor and we want to make it efficient by exploiting the energy propagation from the body to the surrounding fluid. We explain our design constraints, material choices and describe the design process. We draw conclusions about the relevance of our design parameters and design choices.

I. MOTIVATION AND SCOPE

It has been known for at least half a century that autonomy would become indispensable for successful underwater robotics. So far, this challenge has not been met in full. In order to develop effective underwater autonomous vehicles, further progress with respect to mobility is needed in the following key areas: i) agility in motion; ii) variety in information types that can be acquired and possibly also used during operation; iii) low cost and fast production line and iv) effective context-driven control strategies.

In order to successfully realize such features, the following aspects need to be synergistically addressed: i) mechanical design of the robot must be adequate to support the functionalities; ii) the sensor system must be sufficiently rich to carry significant information on the external environment; iii) signals should be processed so as to recognize the hydrodynamic patterns in the environment, identify their salient elements and allow for the proper control action to be selected.

We focus on a bio-inspired design for underwater robots. Key features of our approach are: soft-bodied design; innovative sensing technologies mimicking the functionalities of the lateral line in fish and employed both as a support for motion and for information gathering; effective exploitation of common materials, so as to realize low-cost design; bio-inspired sensorimotor integration, to guarantee contextually-driven control. We treat mechanical design as the development of a platform capable of supporting all such aspects.

In this paper, we present our progress on mechanical design; we show innovative design solutions for bio-inspired soft-bodied vehicles that have the potential of being refined into the underwater search vehicle of the future. Our design is suited for complex task environments, such as in-shipwreck search, underwater marine cave exploration or shallow-water near-coast inspection.

We also take a stance on the key question in biomimetics: to what extent does biomimesis entail replication? We would like to achieve a technological transfer of functionality, while keeping to simple design. With one actuator only, instead of distributed actuation, we can still achieve an adequate locomotor functionality. As a general guideline, we will try to copy embodiment shape and wave propagation mechanics, to gain the benefits of morphological computation found in fish.

Therefore, we address the following questions:

- 1) Partially vs. fully compliant design: are there any sections that we can safely treat as rigid?
- 2) How can we identify an appropriate elasticity distribution? How can such a distribution be realized in the embodiment?
- 3) How can we reconcile the concept of compliant body with the use of rigid electromechanical components?
- 4) Is it truly advantageous to envision a non-uniform elasticity distribution and a tuning mechanism?
- 5) How can we actuate compliant bodies?

We answer these questions by showing how we have progressed from a simple, single-material design to multi-layered prototypes; we summarize the experimental test data that has oriented us towards our current prototype.

II. FROM BIOLOGICAL FISH TO ROBOTIC FISH

We first turn to fish for inspiration concerning the global concept. We are particularly interested in subcarangiform swimming (trout-like), as it embodies a good balance between speed and maneuverability. Subcarangiform swimmers are generalists and can be found in almost every ecological niche. Their minimum turning radius is very contained (on average 20% of the bodylength) – a tenfold improvement with respect to best maneuvering ships, and without having to slow down ([3]). In addition to their agility, these fish are also efficient at sustained swimming. This natural design possesses all the qualities of an ideal underwater device for exploration in complex environments.

¹Dept. of Computer Science, University of Verona, Italy

²Center for Biorobotics, Tallinn University of Technology, Estonia

³Dept. of Theoretical Mechanics, Riga Technical University, Latvia

⁴Dept. of Mechanical Engineering, University of Bath, UK

A. Three-component approximation

In first approximation, we consider three macrosections – head, body and tail. We initially keep a rigid head; fish do have a rigid part – the skull. In fish, the head constitutes less than 20% of the body length, but the propulsive role of the anterior part of the body is rather contained. In steady swimming, the anterior musculature is recruited only at high swimming speeds; the preferred muscle groups for subcarangiform swimming are located in the posterior region; progressively more anterior musculature is additionally recruited at higher swimming speeds ([4], [9]). On the other hand, the tail is flexible to exploit the mechanics of tail-water interaction developed by Nature. The central section accommodates the transmission mechanism, so that actuation effectively occurs within the compliant tail. We think that the key point lies in ensuring smooth transitions between sections, rather than focusing on life-like, all-compliant design.

We have designed the central section to adhere to the organization of biological agents, even when accommodating some rigid mechanical parts. It is quite unnatural to implant a rigid mechanism in an embodiment that is meant to be soft and compliant. To reduce the impact of rigid components on the operation of the flexible parts, we have thought of accommodating sensing-related electronics in volumes that in fish contain the inner organs and are thus not involved in propulsion. The actuator is placed within the rigid head and motion is simply transmitted through the middle part; we have preferred this solution to directly embedding a motor in soft regions, thus altering their concept.

B. Operation

The key idea is operation through bending wave propagation. We do not generate the wave through distributed actuation – we generate it in a single location and then tune the propagation. Tuning occurs both at the design level and through control, in such a manner as to induce thrust via non-stationary waves.

Under different swimming conditions (flow regimens and flow speeds) and depending on swimming mode and intended action (steady state, turning, fast start), the bending curves in fish can look markedly different. It is important for our autonomous device to be able to adapt to different hydrodynamic circumstances and support different control actions. However, this kind of flexibility needs to be explicitly designed for. Designing an embodiment that can support a range of bending styles is not a trivial accomplishment. It involves taking simultaneously into account both the properties of the embodiment and the actuation (type of actuation, localization and actual signal).

Ebbs et al. ([6]) have shown that localized actuation of a compliant body can mimic the bending behavior of fish. Alvarado ([5]) posits a single operational frequency and realizes embodiment/actuation design to yield a desired kinematics at the operational frequency – the resonant frequency of the resulting embodiment. In a recent paper ([6]), testing of the prototype so designed shows that the prototype can operate well in a range of frequencies, although it does

not fully achieve its design objectives in terms of extent of bending (approximately 25% of the target). Alvarado's work shows clearly that, with compliant body design and localized actuation, achieving different bending curves may require very different material distributions. Since we cannot change material distribution during operation, it is apparent that there is need to design for a baseline range of bending behaviors and make room for methods to change stiffness adaptively.

We believe that much can be accomplished by designing the embodiment to react in a qualitatively different manner as a function of the features of the actuation signal (waveform, frequency, amplitude). So our strategy consists of tuning the material properties in design.

C. Compliant body vs. multi-link design

Designs based on multiple actuated links are not suited for our purposes. Multi-link design is an engineering solution that is feasible and has given amazing results (Robotuna [3], Essex robot [8]), but that requires forcing the interaction with the flow: the body takes the lead and shapes the flow. The fish-flow boundary is governed with an a-priori strategy, in order to test hypotheses and elucidate the principles of fish behavior. It is, on the other hand, very difficult with this kind of design, to *observe* the effects of the environmental flows and react to them. In a sense, we wish to look at the fish-flow boundary (here the bending curve) as the result of the interaction between material and water, not as the result of pre-defined purposeful action. We are looking for a support to realize innovative improvements in efficiency through flow adaptation, not limited to efficient propulsive vortex generation.

III. TAIL DESIGN: ELASTIC PROPERTIES

We initially concentrate on tail design. Elasticity and geometry are known to affect heavily the performance of hydrofoils, hence we consider them parameters worthy of careful tuning.

Analytical methods to estimate design parameters become very complicated when realistic shapes are considered. In [1], we report on a novel method to identify the elasticity profile in fish, using myometry for direct investigation. Results (in Figure 1) show that elasticity increases towards the tail and provide an average value to consider for soft-bodied design. We identified silicon-based materials that could capture the average (pink) and maximum (green) values.

We have casted a selection of compliant tails (in Fig. 2) to explore if adhering to the biological elasticity distribution is advantageous to accomplish fish-like passive kinematics. We actuated each prototype and a dead fish with a servomotor at 5 frequencies (1-5 Hz) in three laminar flow speeds (0, 0.25, 0.5 m/s). We recorded video data for each experiment and extracted the midbody line for comparison.

Prototype 6 shown in Figure 2 is hybrid and represents a 2-value approximation of the trend found in fish. Even though the approximation is very rough, P6 exhibits non-negligible improvement with respect to the other fish-shaped prototypes. We interpret this result as a confirmation that designing for

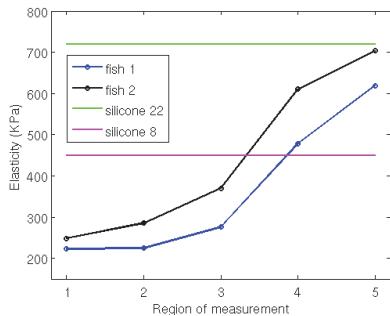


Fig. 1. Elasticity distribution as measured through myometry on two freshly killed trout *Oncorhynchus mykiss* (blue and black lines) and elasticity values for the pink and green materials used in the artificial tails of Figure 2. The pink material is Elite Double 8 (E8, Shore A scale: hardness 8, elasticity 450KPa) and the green material Elite Double 22 (E22, Shore A scale: hardness 22, elasticity 720KPa). [1]



Fig. 2. Six compliant tail prototypes of varying elasticity (E8, E22) and shape (cylinder, truncated elliptical cone and elliptical cone with tail). The cylinder is taken as analytical reference and the cones serve as an intermediate step towards the more realistic fish-like shapes [1]

non-uniform elasticity is indeed beneficial in realizing fish-like kinematics.

We also evaluated the interplay of geometry and material. The initial results show that geometry and elasticity should not be considered independently. The mutual effects on bending performance are such that as one design parameter approaches the values found in fish, performance does not improve even if all other factors are kept constant. Average elasticity also does not affect all shapes in the same manner. In short, the searchspace of heuristic design methods is not regular.

IV. TAIL DESIGN: WAVE PROPERTIES

In our eyes, the difficulty in understanding the searchspace might be related to the fact that we have chosen mechanically relevant parameters that do not, however, encapsulate a cohesive picture of fish-flow interaction. In fact, we have focused on factors that are related to the *method* by which the fish outsources computation to the embodiment and governs such interaction; the method can be either hard-wired structurally (through evolution of a shape fit for the strategy) or in real time (through stiffness control, occurring through differential muscle contraction).

In order to orient design, we need to understand, on the other hand, the fundamental traits of the *strategy* governing the fish-flow interaction, as opposed to the mechanics ruling the interaction’s features. A clear indication that we have understood something fundamental about how compliant bodies are successfully employed in water lies in the ability to identify a unifying factor able to relate to performance in adhering to the biological bending profile.

We change approach and look at bending in terms of a propulsive wave that travels along the body – as opposed to the spatial localization of the body during operation. This approach seems sound because the main descriptors of the bending wave have been extensively employed to convert the kinematics into estimates for forces, power and Froude efficiency ([12], [13], [14], [15], [16]). With the advent of DPIV technology, it has been possible to validate such relations experimentally; in particular, Tytell shows that estimates for power and Froude efficiency are reasonably accurate, whereas force can be underestimated by as much as 50% ([10], [11]).

Design parameters such as shape and elasticity have an immediate translation in terms of the wave picture: shape affects the proportion of the propulsive wave that is reflected into the embodiment at the posterior boundary, whereas elasticity has a very natural interpretation in terms of wave speed. Interestingly, this perspective allows capturing also some characteristics of the environment.

A. Bending vs speed of the propulsive wave

Further analysis of the bending performance for the prototypes in Figure 2 shows that higher laminar flow speeds result in higher speeds of wave propagation and in a more contained bending – as if the flow provided an “added stiffness” to the embodiment. This effect should be considered when designing a prototype tail for deployment in environments where noticeable flow is expected.

Figure 3 shows the wavespeed profiles and amplitude envelopes of the three fish-shaped prototypes, compared to a dead trout. The hybrid prototype is closest to the biological reference also according to wavespeed, taken as an additional criterion of kinematic similarity. None of the prototypes achieves a bending extent comparable to the trout, even though the wave speed for the hybrid tail matches very closely.

There seems to be a tradeoff between amplitude and wavespeed, if elasticity is the only design parameter. Interestingly, a similar result can be deduced from [6], where the propulsive wave speed closely matches the target speed, but bending is only 25% of the target. Fish seem to escape this tradeoff, as they possess the ability to transmit the propulsive wave at a high speed, while still achieving high body bending.

One possible explanation is that the traveling wave that can be observed on the fish-flow boundary is a resultant wave – and that the effective wave traveling down the fish body is much faster. This hypothesis seems to be corroborated by the fact that the muscle actuation wave also runs much faster than the bending wave. Having taken elasticity to be uniform within the cross-section may account for the artificial prototypes’ failure to reach the performance of fish. If we allow for elasticity to

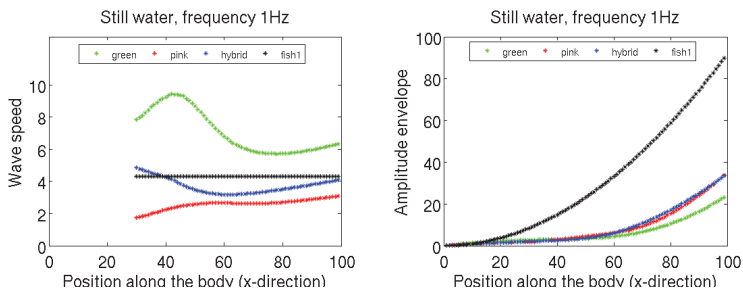


Fig. 3. The wave speed profile and amplitude envelope along the body for the fish-shaped prototypes in Fig. 2 (hybrid, pink and green), actuated at 1Hz in still water. The values for wave speed in the anterior part of the body are not considered reliable due to considerable numerical noise and are therefore not represented. In black, we show values for a dead trout actuated in the same conditions; we report only the average value of wave speed, because calculations were carried out with a different method.

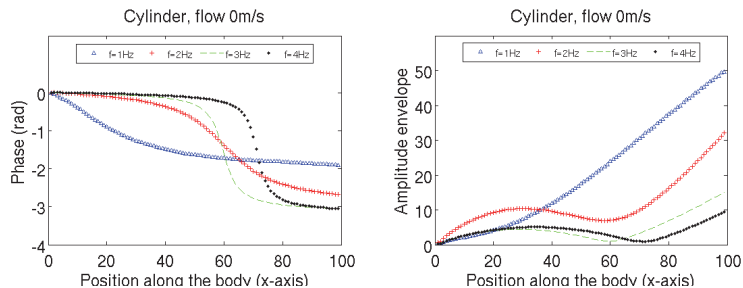


Fig. 4. Phase ϕ and amplitude envelope for the cylinder-shaped prototype of Figure 2, when fitted with the model $h(t, x) = A(x) \cos(\omega t + \phi(x))$ (left). Data refers to actuation frequencies 1-4Hz in still water.

vary within the cross-section, a simple two-value approximation yields a salient feature of the biological organization: a region of markedly higher stiffness – a backbone. Under this perspective, fish transmit the actual traveling wave along the backbone – the stiffest part of the body; on the other hand, the softer surrounding tissues allow bending to greater extents.

B. Standing wave on cylinder prototype

In this section we highlight the importance of tail shape in motion efficiency. In Fig. 4 we show the behavior of the pink cylindrical prototype in still water and under a sinusoidal actuation of different frequencies. The presence of a propulsive traveling wave translates in terms of the phase picture as a monotonically decreasing trend. This trend is apparent at 1Hz, but disrupted at higher operational frequencies. In fact, with increasing frequency the phase graphs look progressively closer to a sigmoid function, which captures a transition between two constant values. Inspection of the bending behavior confirms that the cylinder exhibits a standing wave during most of the body. The situation is reflected in the amplitude envelope, where we see positions approximating the behavior of nodes, located in the transitional region.

The reason for the appearance of standing waves lies in the posterior body-flow boundary: there is a flat surface that allows the reflection of the traveling wave. In such circumstances, the cylinder can only transfer a minor part of the energy in an

orderly fashion, resulting in very poor propulsive efficiency. The phenomenon, albeit less severe, is present also in the cone-shaped prototypes. The experimental data shows that, although it is very convenient to reduce analytical complexity by resorting to simple shapes during design, the impact of having reflecting surfaces simply cannot be ignored.

V. TAILS WITH BACKBONE

The previous discussions in Sections III and IV encourage us to design a tail with backbone to achieve more fish-like behaviour and therefore higher propulsion efficiency. We believe that such design permits achieving a high propagation wave speed together with a high bending amplitude. The stiffer backbone would permit faster wave propagation while softer material surrounding it would permit a higher bending amplitude. Moreover such design also allows us to get an increasing elasticity profile along the body.

The previous discussion also reveals that the geometry plays an important role in how the traveling wave is propagated to the surrounded medium (flow) or reflected back. Since the fish tail geometry appeared to be efficient with that respect we decided to fix the geometry of a subcarangiform swimmer and tune the elasticity profile based on the ratio between backbone and softer material which is determined by the shape of the tail.

We designed molds with fish tail geometry using the mathematical representation of the fish outer shape. We then checked

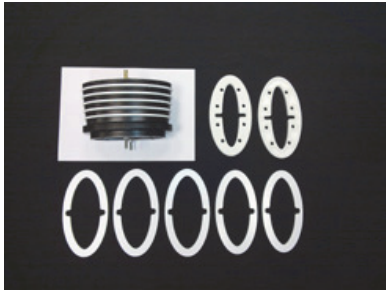


Fig. 5. The cross-section of Dragon Skin A10 tail with hollow mid-section (above). The ribs are used to support the skin as well as functioning as a backbone (below).

the availability of silicone materials—in terms of elasticity values—that can enable us to design a tail with backbone within the average elasticity range of biological fish (Figure 1). We cast a tail prototype using the Dragon Skin A 10 material which was the least stiff silicone available at that time. The initial testing with the casted tail revealed that even with the least stiff silicone, high torque was needed to bend the tail.

To overcome this problem, hollowness inside the tail was needed to reduce the bending stiffness. To maintain the stability we had to keep the material in the center; but remove some from the sides while keeping the outer surface untouched (skin) (Figure 5 above). To reduce the unpredictable bending of the skin, the rib structure was designed (Figure 5 below).

While testing the new prototype we however discovered that it has a problem of lateral buckling as shown in Figure 6. Therefore we looked for a solution how to reduce it. As a solution a new tail was casted from a foam (Soma foama 15 by Smooth on). In comparison to the Dragon Skin (or other silicone materials) of the previous prototype tail, foams have very different properties regarding energy storage, reactivity and compressibility. With this choice of materials, we can effectively exploit an additional element, which plays the structural role of a backbone and guides the propagation wave.

The foam prototype was realized using Dragon Skin A20 for the backbone (which is a stiffer version than Dragon Skin A10), the foam for the body and covering the tail with a thin layer of Dragon Skin A10 (Figure 7). The outer skin will prevent the foam from absorbing water and swallowing up. This prototype has also an advantage that its elasticity distribution is much closer to the biological fish and the foam is almost neutrally buoyant.



Fig. 6. The lateral buckling problem for the tail made of Dragon Skin A10 with hollow mid-section.



Fig. 7. The foam prototype with backbone design.

a) The preliminary experiments with foam prototype:

Having designed the foam prototype, we are currently testing it in our flow tank. Figure 8 illustrates series of images showing motion of the foam prototype in one cycle when it is actuated at $f=3\text{Hz}$ in still water. The evaluation of the prototype in terms of wave propagation and propulsion efficiency is currently under progress for different flow regimes, operational frequencies and different actuation waveforms.

VI. COMPONENT INTEGRATION AND PLATFORM DESIGN

Besides having worked with the design of compliant tails, we also investigated how to integrate the tail prototypes to the rest of the robot platform. The design requirements we had for the fish robot prototype were the following: i) the head should be fish-shaped to reduce the drag but big enough to contain the onboard electronics, ii) the fish tail is actuated by a single-point actuator. However, we also wanted to investigate the performance of different actuators and therefore the design should permit changing them without making modifications in the rest of the prototype, iii) the tails should be easily changeable because we want to use the platform to investigate different propulsion mechanisms and their effect to swimming efficiency and iv) the outer shell should be waterproof because we did not want to be concerned about water-proofing every component individually.

Taking those requirements into account, the head is manufactured with rapid prototyping. However, we had to compromise and make the head bigger than the head of a biological fish to accommodate the electronics and motors. All the main components (head, tail and motor) are attached to the middle part. Choosing the appropriate design of the middle part was the most important issue to achieve proper sealing. The fastest solution was to make the middle part from aluminum using CNC milling. A later version was made of polyamide

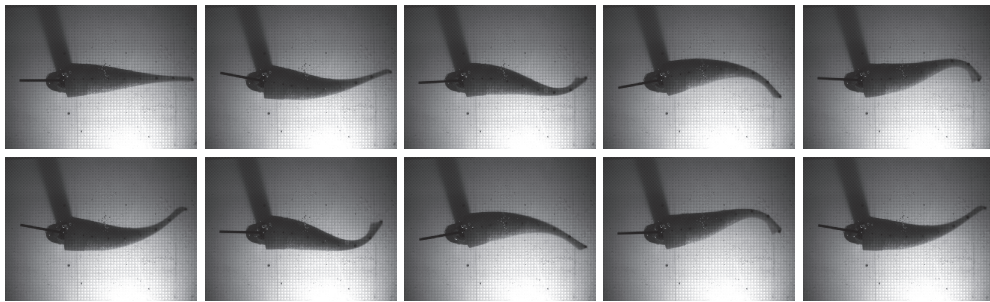


Fig. 8. The series of snapshots taken while foam prototype is being tested ($f = 3Hz$, in still water).

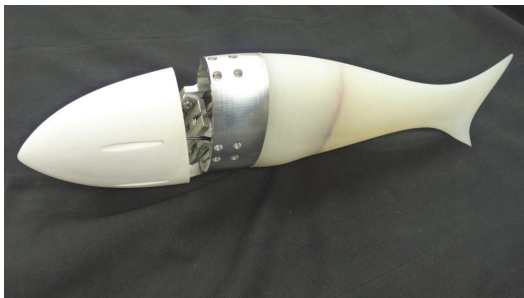


Fig. 9. Prototype in Dragon Skin. The rib structure is located in the central section and helps maintain shape around the hollow.

using rapid prototyping. Moving from external actuation of the tail to internal actuation, we realized two kinds of actuation mechanism.

A. Actuation mechanisms

In both cases the actuator itself is placed in the head of the fish and motion is transferred to the tail by actuating a plate casted in the silicon. In the first case the actuation is achieved with a single rigid link. In the second case it is achieved with a pair of rods pulling the plate (Figure 10).

The constructional complexity of both methods is rather similar, however, the second method is more interesting for several reasons. We expect that it transfers forces better along the tail and minimize the propagation along the normal of the surface.

Also the actuation mechanism pulls the strings and lets the silicon do the reverse work. Call-back mechanisms in biology can be purely passive and outsourced to the morphology – relying on the mechanical properties of the material and the environment for instance breathing out. Also the newest generation of hybrid passive walkers has purely passive swing phase and actuated lift phase. The comparison between the actuation mechanisms enables us to investigate the interplay between the forces and the material. We can also investigate and make conclusions on how much the efficiency of the propeller depends on the properties of the body and the actuation style.

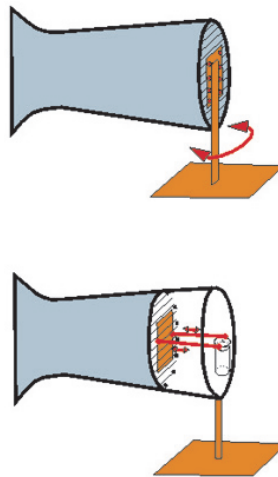


Fig. 10. Two actuation mechanisms; rotational actuation around fixed axis (above), actuating plate casted inside the tail and actuated by pully-strings (below).

One of the areas which we are planning to investigate with the described platform is to test the role of actuation mechanism in terms of waveforms, parameters of waveforms (frequency, phase and amplitude) and actuation styles. Such analysis may lead to interesting conclusions about embodiment-actuation interaction to design more robust underwater robots. The proposed form of work is under progress in our research-lab.

VII. CONCLUSIONS

In this paper we describe a case for biomimetic design of a fish robot and explain our design choices that led us to the current prototype. Our driving factor for the design is simplicity without conceding motion capabilities of biological fish. We therefore explore different solutions on prototype realization using a compliant tail actuated with a single actuator. We

argue that undulatory motion of designed prototypes depends on the embodiment and in particular, we investigate how the stiffness, stiffness distribution and wave propagation can be used to orient the design. Based on these findings we propose a new tail design based on realizing the elasticity distribution through a composite tail with a backbone. We believe that such design should also permit optimizing both for the traveling wave speed and the bending. We also explore methods of actuating the tail as well as a waterproof robot platform to integrate the actuation with the embodiment.

VIII. ACKNOWLEDGEMENTS

This work is carried out under the FILOSE project, supported by the European Union, seventh framework programme (FP7-ICT-2007-3). We thank Andres Ernits for his contributions on electronics and development of the flow tank.

REFERENCES

- [1] O. Akanyeti, A. Ernits, C. Fiazza, G. Toming, G. Kulikovskis, M. Listak, R. Raag, T. Salumäe, P. Fiorini, M. Kruusmaa, Myometry-Driven Compliant-Body Design for Underwater Propulsion, *IEEE International Conference on Robotics and Automation (ICRA)*, 2010, (accepted for publication).
- [2] Webb, P. W., Speed, Acceleration and Manoeuvrability of two Teleost Fishes, *Journal of Experimental Biology*, vol. 102, pp. 115-122, 1983.
- [3] Triantafyllou, M. S., and Triantafyllou, G. S., "An efficient Swimming Machine", *Scientific American*, 272(3), 1995.
- [4] Coughlin, David J. and Spiecker, Amy and Schiavi, Jonathan M., "Red muscle recruitment during steady swimming correlates with rostral-caudal patterns of power production in trout", *Comparative Biochemistry and Physiology - Part A: Molecular and Integrative Physiology*, vol 137(1), pp 151-160, 2004.
- [5] Pablo Valvidia y Alvarado, "Design of Biomimetic Compliant Devices for Locomotion in Liquid Environments", *Ph.D. Thesis*, MIT, 2007.
- [6] Epps, Brenden P. and Valdivia y Alvarado, Pablo and Youcef-Toumi, Kamal and Techet, Alexandra H., "Swimming Performance of a Biomimetic Compliant Fish-like Robot", *Experimental Fluids*, 2009.
- [7] Barrett, D. S. and Triantafyllou, M. S. and Yue, D. K. P. and Grosenbaugh, M. A. and Wolfgang, M. J., "Drag Reduction in Fish-like Locomotion", *Journal of Fluid Mechanics*, vol 392, pp. 183-212, 1999.
- [8] J. Liu and H. Hu. Novel Mechatronics Design for a Robotic Fish. *IEEE/RSJ International Conference on Intelligent Robots and Systems (IROS)*, Edmonton, Canada, pp. 2077-2082, 2005.
- [9] G. V. Lauder, E. D. Tytell. Hydrodynamics of Undulatory Propulsion. *Fish Biomechanics. Fish Physiology*, R. E. Shadwick, G. V. Lauder, Eds., Academic Press, San Diego, vol. 23, pp. 425-468, 2006.
- [10] Tytell, E. D., "The hydrodynamics of eel swimming II. Effect of swimming speed." *J. Exp. Biol.* vol 207, pp 3265-3279, 2004.
- [11] Tytell, E. D., and Lauder, G. V., "The hydrodynamics of eel swimming. I. Wake structure.", *J. Exp. Biol.*, vol 207, pp 1825-1841, 2004.
- [12] J.J. Videler and F. Hess, "Fast Continuous Swimming of two Pelagic Predators, Saithe (*Pollachius virens*) and Mackerel (*Scomber Scombrus*): A Kinematic Analysis". *J. Exp. Biol.* vol 109, pp 209-228, 1984.
- [13] B. C. Jayne and G. V. Lauder, "Speed Effects on Midline Kinematics during Steady Undulatory Swimming of Largemouth Bass, *Micropterus Salmoides*". *J. Exp. Biol.* vol 198, pp 585-602, 1995.
- [14] Hess and Videler, 1984; Hess, F., and Videler, J. J., "Fast continuous swimming of saithe (*Pollachius virens*): A dynamic analysis of bending moments and muscle power.". *J. Exp. Biol.*, vol 109, pp. 229-251, 1984.
- [15] Daniel, T. L., and Webb, P. W., "Physics, design and locomotor performance." In "Comparative Physiology: Life in Water and on Land" (Dejours, P., Bolis, L., Taylor, C. R., and Weibel, E. R., Eds.), pp. 343-369. Liviana Press, Springer Verlag, New York, 1987.
- [16] Müller, U. K., and Stamhuis, E. and Videler, J., "Riding the waves: The role of the body wave in undulatory fish swimming.", *Integr. Comp. Biol.* vol 42, pp. 981-987, 2002.

APPENDIX B

O. Akanyeti, A. Ernits, C. Fiazza, G. Toming, G. Kulikovskis, M. Listak, R. Raag, T. Salumäe, P. Fiorini, and M. Kruusmaa, “Myometry-driven compliant-body design for underwater propulsion,” in *Proc. IEEE Int. Conf. on Robotics and Automation (ICRA)*, 2010, pp. 84–89.

Myometry-Driven Compliant-Body Design for Underwater Propulsion

O. Akanyeti¹, A. Ernits², C. Fiazza¹, G. Toming², G. Kulikovskis³,
M. Listak², R. Raag², T. Salumäe², P. Fiorini¹, M. Kruusmaa²

Abstract—Within the broader scope of underwater biomimetics, in this paper we address the relevance of factors such as shape and elasticity distribution in the ability of a compliant device to imitate the kinematic behaviour of a fish. We assess the viability of myometry as a tool to determine candidate mechanical parameters without relying solely on analytical models; we show that we can obtain elasticity distributions that are both consistent with previous theoretical investigations and experimentally better adherent to the passive kinematics of a biological embodiment (rainbow trout).

I. INTRODUCTION

The overall goal of our work is to design a biomimetic underwater propulsion system with higher power-thrust efficiency and maneuverability than current underwater vehicles. The biological inspiration is steadily swimming fish. In order to reproduce the dynamics of a fish during its steady swimming, in particular sub-carangiform swimming in rainbow trouts, we first study its structural morphology. Our starting point is assessing the properties of the device's structure, examining in particular the following three questions:

- 1) Which characteristics of fish morphology enable fish to achieve high swimming performances?
- 2) Which mechanical design approach is most suited to develop an underwater vehicle with similar characteristics?
- 3) In the chosen approach, which design parameters are most relevant? What methodology can we successfully employ to determine values for such parameters?

The first question is answered in literature. Previous research on fish swimming ([1], [2], [3], [4], [5]) stresses the importance of few key features in achieving high swimming efficiency: i) undulating motion mechanics, in which a body wave travels downstream with phase speed greater than the fish's swimming speed; ii) the ability to alter the body wave speed, by adjusting tail beat frequency and/or body wavelength; iii) the ability to tune the body wave in terms of amplitude and phase.

In light of this set of competences, we address the following question "What is the simplest mechanical design that can accomplish this overall functionality?". Traditionally, robots that mimic fish ([6], [7], [8]) are built with rigid components connected by joints. This design style leads to complex mechanisms with inevitable controllability difficulties.

¹Dept. of Computer Science, University of Verona, Italy

²Center for Biorobotics, Tallinn University of Technology, Estonia

³Dept. of Theoretical Mechanics, Riga Technical University, Latvia

A. Modelling fish as visco-elastic bodies

We have decided to use the visco-elastic compliant-body approach recently proposed in [9]. This approach is inspired by [10], in which the body of a real fish is modeled as a visco-elastic beam. In this approach, devices are compliant continuous flexible bodies, in which material distribution allows a minimal set of input functions to exploit resultant modes of vibration for locomotion.

Locomotion-inducing waves travelling along the elastic body are achieved through phase differences between subsequent points in the body; phase depends on viscosity and timing is critical. Hence, two important design parameters emerge in affecting device performance: spatial distribution of elasticity and of viscosity. These design parameters encapsulate i) geometry of the body (shape and size), ii) material distribution along the body, and iii) visco-elastic characteristics of each constituent material.

1) *Analytical Approach*: A promising way of computing these parameters is through analytical models. The standard model for fish comes from slender-body theory ([1]), which has been developed for small displacements but can be extended further. In recent studies ([10], [11]), the fish body has been modeled as a visco-elastic beam and analyzed in the domain of Euler-Bernoulli/Timoshenko beam theory. Lateral motion is described by the solution of the partial differential equation (PDE) associated to the visco-elastic beam. Given a geometry, the desired kinematics and the set of available actuation signals, a PDE model can relate prototype behavior to the target parameters. For simple geometries and uniform material distributions these equations can be solved to obtain reliable values ([12]). Moreover, PDE models can be used to determine favorable operating conditions — such as optimal operational range of frequencies and position of the excitation point.

However, PDE models, in general, suffer from an enormous increase in computational complexity with increasing dimensionality. As the number of parameters increases for geometries with tail, fins and non-uniform material distributions, the models get more complex and it is extremely difficult to solve their characteristic equations. This leads to over-simplified models which perform poorly when compared to biological fish.

2) *A myometry-based approach*: In this paper, we propose an alternative method and test its viability. We wish to obtain design parameters from direct investigation of real fish bodies. For direct analysis, we perform myometry on fish. Myometry is a method for non-invasive measurement of biomechanical properties of the muscles; myometry data

can enable us to better understand how the visco-elastic properties of fish muscles change along the body. If successful, this method allows bypassing analytical difficulties. In this paper, we focus in particular on the elastic properties of fish; we attempt to identify the elasticity distribution and employ it as values for soft-bodied robot design.

The main benefits of the proposed design method are: i) It is a simple, fast and efficient method for computing the desired modelling parameters. ii) It requires few theoretical assumptions. This enables us to design more realistic models with complex shapes and non-uniform material distributions. iii) Moreover, the method can be used to crossvalidate the analytical modelling approach and complement it; for instance, findings from myometry can be used as boundary conditions for analytical models or to reduce the dimensionality of unknown model parameters.

B. Paper methodology

Our methodology can be decomposed into four phases:

- 1) We perform myometry on biological specimens, measuring muscle properties along the body. We derive estimates for the elasticity distribution for real fish.
- 2) On the basis of geometry and estimated elasticity, we estimate the target properties of our biomimetic device: geometry, material properties, material distribution.
- 3) We manufacture prototypes for comparative experiments; prototypes vary in elasticity, elasticity distribution and geometry.
- 4) We conduct experiments to verify the kinematics of the prototypes against a real trout. We assess the kinematic similarity between prototype performance and real fish. We describe similarity by correlating body bending; we also evaluate the differences in point-wise displacement.

II. FISH MYOMETRY

To perform myometry we employ a Myoton, a device developed by Müomeetria AS. ([13]). The device operates by locally stimulating the tissue with a small impact and recording the resulting dampening oscillation through an accelerometer. A microprocessor analyzes the signals to output tone (frequency of the oscillation in Hz), logarithmic decrement (logarithm of the ratio of consecutive peaks) and stiffness of the tissue (in N/m) ([14]). Tone characterizes muscle tension, whereas decrement quantifies a muscle's ability to restore its initial shape after contraction. Stiffness refers to the muscle's resistance to changes in shape due to external forces.

Myometry is generally used to measure human skeletal muscles ([15]-[16]). In measuring relatively smaller-sized muscles (such as fish muscles), we expect that the Myoton readings do not depend solely on local muscle properties, but up to a certain distance ("the effective depth") also on the neighboring materials along the direction of the applied force (Figure 1). However, so far no data is available in the literature to establish with precision what the effective depth is. When tested on a homogeneous material with varying

thickness, the myometer's stiffness readings are found to be affected by the width at the point of measurement. We can consider the myometer readings k in terms of an "equivalent stiffness": $k = \frac{EA}{w(x)}$, where E is Young's modulus, A is the area associated to the applied force and $w(x)$ is the width at the point of measurement. We have also tested the myometer on a homogeneous cone with known elasticity, and compared myometer readings with the theoretical values for elasticity. We found that the myometer follows

$$k = \alpha(x) \frac{EA}{w(x)}, \quad (1)$$

where $\alpha(x)$ is a scaling coefficient with value approximately 0.5, and that adherence to theoretical values is poor when material thickness is very small (sensibly less than 5 cm). In terms of fish measurements, this means that fish is in the range of reliable thickness in the central section (see Figure 2, regions R1 – R4).

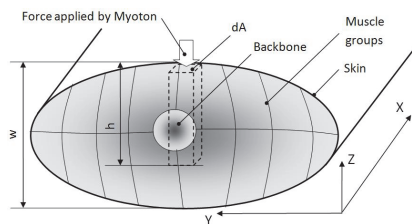


Fig. 1. Cross sectional view of fish body during myometry.

A. Experiments with Trout

For myometry experiments we used two fresh-water trouts. One fish measured approximately 40cm and the other approximately 50cm in length. Myometry was performed shortly after death, to minimize intervening changes in muscle properties. During measurements, the specimen were placed on a soft pillow-like surface. For each fish, we chose 25 sample points, to cover the surface of the body in the regions of interest. Sampling points are grouped in 5 regions (from midsection (R1) to tail (R5)), each containing 5 measurement points; each measurement was repeated 10 times. Figure 2 shows location of the sampling points for the second specimen. We take measurements only on 5 points per region to contain the duration of the myometry experiments, to avoid changes in stiffness due to rigor mortis.

B. Results and Analysis

Table I summarizes myometry data and elasticity estimates. Figure 3 shows that in fish E increases towards the tail. The measurements in Region 5 should be considered less reliable because the width is very small and interference from the underlying material is not negligible.

We believe the increase in E is related to the decrease in muscle-bone ratio of the body — as we approach the tail, the relative effect of bones on stiffness measurements increases.

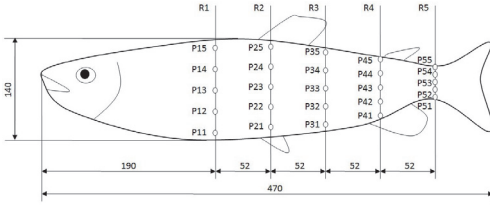


Fig. 2. Measurement points in myometry experiments (fish 2)

TABLE I
MYOMETRY READINGS AND ELASTICITY ESTIMATES.

	log. dec.	freq. (1/s)	stiff. (N/m)	elas. (KPa)
Fish 1				
R1	2.1 ± 0.1	15.4 ± 0.9	347.8 ± 18.4	222.6
R2	2.2 ± 0.1	16.9 ± 0.5	359.4 ± 24.8	224.8
R3	2.4 ± 0.1	19.0 ± 0.5	414.5 ± 26.5	275.7
R4	2.7 ± 0.1	21.4 ± 1.0	422.0 ± 19.7	478.3
R5	2.8 ± 0.1	13.4 ± 0.6	340.0 ± 17.7	618.5
Fish 2				
R1	1.4 ± 0.2	22.0 ± 2.6	466.9 ± 57.1	247.9
R2	1.2 ± 0.2	23.7 ± 2.4	519.7 ± 53.3	285.0
R3	1.2 ± 0.2	25.7 ± 2.3	569.9 ± 54.1	370.9
R4	1.3 ± 0.2	31.3 ± 1.9	629.1 ± 22.1	610.3
R5	2.2 ± 0.1	35.8 ± 2.4	505.0 ± 24.6	703.2

As bone is stiffer than muscles, E locally increases. Moreover, near the tail muscles are more tightly packed and there is more cartilage and tendon at the tail. This is also coherent with the theoretical models described in [10].

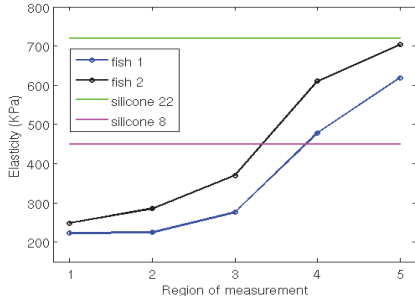


Fig. 3. Elasticity distributions of two fish. Elasticity values for two silicone materials are also plotted. Both materials are used during manufacturing prototypes (see Section III).

III. COMPLIANT-BODY DESIGN

Using myometry data, we have thus identified a candidate distribution of elasticity for our biomimetic device (figure 3). Direct investigation of fish has provided information on both a desirable trend – increase E towards the tail – and a desirable value for average elasticity.

The next step is to identify materials whose Young’s modulus lies in the biological range. We employ silicone-based materials Elite Double 8 (E8, Shore A scale: hardness

TABLE II
GEOMETRY, LENGTH (L) AND ELASTICITY (E) VALUES FOR MANUFACTURED PROTOTYPES. ELASTICITY VALUES: $E_1 = 454.4KPa$ AND $E_1 = 722.0KPa$. SHAPES: CYLINDER (A), ELLIPTICAL TRUNCATED CONE (B) AND FISH-LIKE (C). GEOMETRY: r_1 AND r_2 ARE MAJOR AND MINOR RADII FOR THE ELLIPTICAL CROSS SECTION AT THE LARGEST EXTREMITY.

Prot. #	E (Pa)	Shape	L (cm)	Geometry (cm)
P1	E_1	A	25	$r_1 = 4.5, r_2 = 2.25$
P2	E_2	B	25	$r_1 = 6, r_2 = 3$
P3	E_1	B	25	as P2
P4	E_2	C	30	as P2
P5	E_1	C	30	as P2
P6	E_1, E_2	C	30	as P2

of 8, elasticity $450KPa$) and Elite Double 22 (E22, Shore A scale: hardness of 22, elasticity $720KPa$). Figure 3 shows the elasticity values of the two silicone materials along with the biological distributions obtained via myometry. E8 lies in the middle of the biological range ($200-700 KPa$) and can be considered representative of the average elasticity of fish, whereas E22 approximates the highest value measured in fish.

The goal of our experimental procedure is assessing the passive kinematic similarity of biomimetic devices with respect to a fish body. For comparative experiments, we employ three different geometries (cylinder, truncated elliptical cone and elliptical cone with tail).

Prototype P1 is a cylinder made of E8. This prototype is used as analytical reference, because a solved partial differential equation describing its dynamics is available in [9]. Prototypes P2 and P3 (made of E22 and E8, respectively) are designed as elliptical truncated cones. This geometry can be seen as intermediate in complexity between a cylinder and a realistic fish-shape. Prototypes P4 to P6 are elliptical cones terminating with a tail (“fish-shaped” prototypes). Prototypes 4 and 5 are made from E22 and E8, respectively. To approximate an increasing elasticity distribution and mimic the trend found from myometry, prototype P6 is hybrid: the first part of the body is made of E8 and the posterior section, tail included, is fabricated out of E22. See Table II for physical properties of prototypes displayed in Figure 4. In total, we have 6 prototypes available for comparative experiments — with varying elasticity, elasticity distribution and geometry.

A. Fabrication of Prototypes

The manufacturing process comprises two steps: mould making and casting. For truncated elliptical cone-shaped bodies, a positive mould was cut out of expanded polystyrene (EPS) using electrically heated wire. After smoothing the surface with polyvinyl acetate (PVA) glue, the positive mould was covered with glass fiber cloth and painted with epoxy resin to obtain the negative mould. More complex moulds were milled on a computer numerical controlled (CNC) machine. As the silicone we used is virtually impossible to



Fig. 4. Compliant prototypes used in the experiments. The prototypes are manufactured using two different silicone materials: i) Elite Double 22 (green) and Elite Double 8 (pink). The elasticity values for E8 and E22 are, respectively, around 450KPa and 720KPa .

glue or fix with screws after curing, actuator mounts were inserted into the moulds during casting. The mounts are rigid plates with threaded holes for mounting and holes or pores to form a strong interface with silicone.

IV. COMPARATIVE EXPERIMENTS

A. Experimental Setup

The experiments were conducted in the flow tank of Tallinn University of Technology. The size of the tank is $(4 \times 1.5 \times 1.5)\text{m}^3$, with working section volume $(0.5 \times 0.5 \times 1.5)\text{m}^3$ and cross sectional area $(0.5 \times 0.5)\text{m}^2$. The tank is aerated and powered with an electric motor to generate a laminar water flow. The tank is equipped with a Doppler sonar velocity log system to measure the laminar flow speed.

We tested all 6 prototypes (Figure 4) and one rainbow trout (*Oncorhynchus mykiss*), immediately after death. Test objects were oriented with their main axis along \hat{x} and up along \hat{z} – with gravity lying in $-\hat{z}$. Objects were supported using a vertical rod along \hat{z} and a rotational joint. A waterproof DC-motor was used to actuate the body in the transverse direction (xy -plane). The applied torque was a sinusoidal signal with fixed amplitude (1Nm). Each object was tested in three flow conditions: static water and two laminar flows, with speeds 0.25ms^{-1} and 0.5ms^{-1} . The static water regimen serves as a reference condition, as the corresponding equations have already been analyzed [11], whereas the highest laminar flow speed is close to the cruising speed of rainbow trouts.

For each flow condition, each prototype was tested under applied torques of different frequencies (1-5 Hz). This corresponds to 105 experiments in total. In all cases, we tracked the kinematics of the models for approximately 30 seconds. Movement was captured by an overhead camera recording the test object against a lighted background. The camera images were logged with frame rate 60 Hz ; images were postprocessed to obtain point-wise lateral displacement, bending curvature, phase velocity and bending moment distribution for each test object. Figure 5 shows two sets of sample images (a trout and the hybrid prototype P6), recorded in static water with operating frequency 1 Hz .

In order to generate a good design for our biomimetic device, we investigate if tuning elasticity distribution and geometry can bring the prototype closer in behaviour to

TABLE III
AVERAGE SPEARMAN RANK CORRELATION AND AVERAGE DIFFERENCE IN LATERAL DISPLACEMENT. LEFT: ACROSS ALL TEST SCENARIOS; RIGHT: AVERAGED FOR FREQUENCIES IN THE 1-4 Hz RANGE. 5 Hz IS NOT IN THE BIOLOGICAL RANGE OF ACTUATION.

	All tests		Reduced range (1-4 Hz)	
	Spr.	Lmd.	Spr.	Lmd.
P1	0.29 ± 0.06	9.11 ± 0.35	0.33 ± 0.06	9.15 ± 0.38
P2	0.36 ± 0.05	13.76 ± 0.60	0.36 ± 0.06	13.83 ± 0.66
P3	0.22 ± 0.07	13.41 ± 0.74	0.29 ± 0.06	13.62 ± 0.84
P4	0.63 ± 0.05	5.97 ± 0.46	0.68 ± 0.04	6.10 ± 0.56
P5	0.65 ± 0.06	3.99 ± 0.12	0.73 ± 0.04	3.98 ± 0.15
P6	0.71 ± 0.06	3.94 ± 0.18	0.77 ± 0.05	3.95 ± 0.22

our biological reference. Better adherence to the passive kinematics of the trout is considered better performance. Correlation between the prototypes and the reference specimen with respect to kinematic characteristics can verify if our myometry-based design method is a useful tool. We use Spearman rank correlation coefficients to relate the bending performance of prototypes to fish (curvature distribution); we also measure the difference in lateral displacement between prototypes and fish and evaluate the mean absolute lateral motion difference.

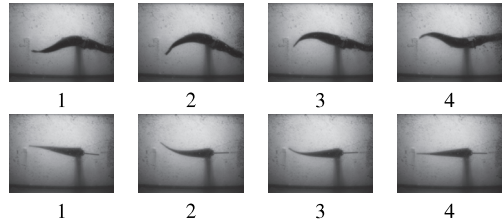


Fig. 5. Two sets of images captured by overhead camera (xy -plane) during experiments in static water at 1 Hz . First row: rainbow trout; second row: hybrid prototype (P6). The time interval between consecutive snapshots in the set is 100 ms .

B. Results

a) Complex interplay between geometry and elasticity:

Figure 6 presents Spearman rank correlation coefficients and mean position difference. In Table III we summarize performance results across the 15 test conditions. In all test scenarios, prototypes with fish-like geometry (P4, P5 and P6) perform significantly better than the rest. However, contrary to our expectation, cone-shaped prototypes did not perform better than the cylinder; the cylinder outscored both P2 and P3 consistently on error and P3 also on correlation. Thus, geometry is an important factor in achieving fish-like swimming, although by itself it cannot predict relative performance. The principle that, as geometry gets closer to the geometry of fish, performance does too, does not necessarily hold even if elasticity is not allowed to vary.

We also observe that the hybrid prototype (P6) performed slightly better than P4 and P5. P6 has the highest number of

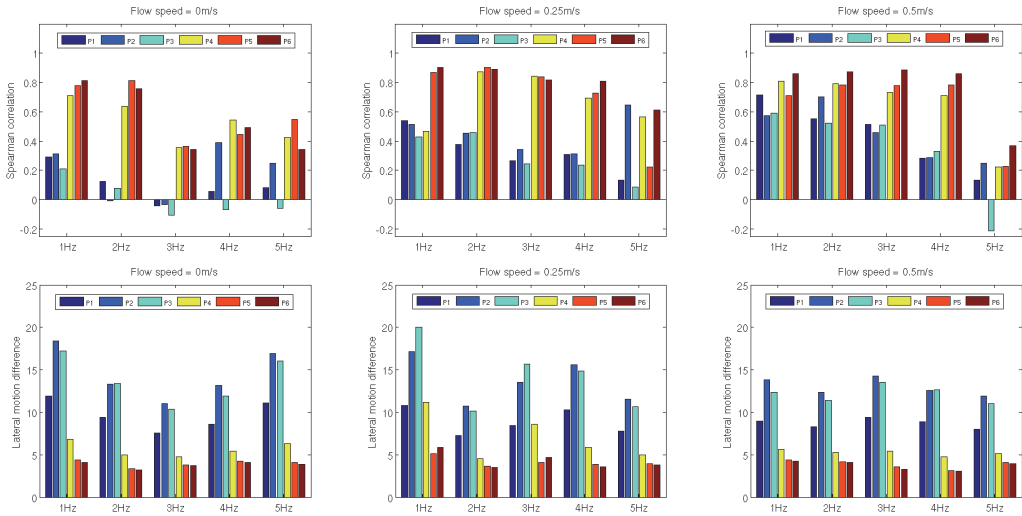


Fig. 6. Experimental results. Row 1: Spearman rank correlation (similarity in bending behaviour), all correlation coefficients presented in graphs are statistically significant ($p < 5\%$). Row 2: lateral motion difference (dissimilarity in amplitude behaviour).

best performances for both similarity criteria (8 w.r.t curvature and 10 w.r.t amplitude). Non-negligible improvement (6-8% across all tests and 4-9% in the reduced 1-4 Hz range) arises even from a crude 2-value approximation to the experimentally determined elasticity distribution. This confirms that designing compliant prototypes with varying elasticity is a key technology for biomimesis of fish.

Turning attention to the role of average elasticity, we now consider prototypes with the same shape. The soft fish (P5) performs better than the hard fish (P4), but the hard cone (P2) performs better than the soft cone (P3). This contradicts the expectation that a change in average elasticity affects all shapes in the same manner. Also, the principle that, as average elasticity gets closer to the elasticity of fish, performance does too, does not necessarily hold even if shape is not allowed to vary. All these observations suggest a complex relationship between geometry and elasticity.

b) Fish torso is overdamped beyond 3Hz in static water:

In static water, the similarity between prototypes and real fish decreases with increasing input frequency. The phenomenon is more evident after 3Hz. The kinematic behaviour of fish changes distinctly after 3Hz; the anterior part of the body hardly bends and bending amplitude increases very slowly towards the tail. Figure 7 illustrates the bending motions of the fish body at two different frequencies (1Hz and 4Hz). The results are coherent with previous research reporting that the fish body is overdamped at high frequencies ([10]). Although the natural frequency of the prototypes is in the range of the fish's natural frequency, no such overdamping is observed for prototypes. At higher frequency, the overall type of motion does not change for prototypes aside from the

obvious reduction in amplitude. This observation suggests that fish are mechanically engineered to operate at lower frequencies and this feature does not rest solely on geometry but requires tuning elasticity and viscosity distribution along the body. Overdamping of this sort can be observed also for experiments in laminar regimen, although the trend is far less clear than in still water.

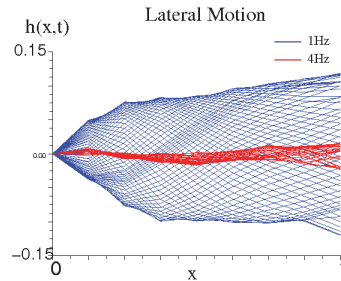


Fig. 7. Lateral motion $h(x,t)$ of a trout body at 1Hz (blue) and at 4Hz (red). Note that at 4Hz the body torso hardly bends.

c) Observations on Passive Bending Moments: We now examine the distribution of the elastic bending moment M_E in fish and fish shaped prototypes (P4, P5 and P6). M_E is obtained as $M_E = EI \frac{\partial^2 h(x,t)}{\partial x^2}$ and is shown in Figure 8 for one cycle in static water at 1Hz. M_E decreases gradually and approaches zero at two thirds of the body length. This trend is consistent with the reduction in passive visco-elastic bending moments predicted in [10], except for position of the peak amplitude for M_E . In free swimming fish, the peak amplitude is just before the mid-part of the body, whereas

in our case M_E is highest at the origin. This is due to the actuation style: in our experiment the fish body is subject to sinusoidal torque input at one extremity. In other words the boundary conditions are not the same: $M(0) \neq 0$. This shows that favorable effects arise in the hydrodynamic moment even when actuation is localized. Moreover, in prototypes there is a lateral asymmetry in the distribution of elastic bending moments, which is completely absent in the biological reference. Asymmetry seems to stem from the actuated extremity, so it might be possible that the phenomenon is at least partly originated by the fact that prototypes lack a head.

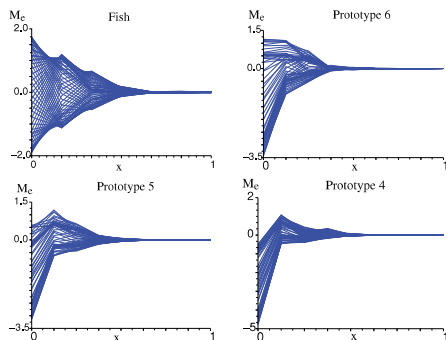


Fig. 8. The elasticity bending moment distribution ($M_E(x)$) along the body (x) of fish and fish-shaped prototypes (P4, P5 and P6). The experiments were conducted in static water at 1Hz.

V. CONCLUSIONS

In this paper, we conduct comparative experiments to investigate the relevance of factors such as geometry and elasticity, in a visco-elastic body's ability to imitate the kinematics of real fish. We also test the viability of myometry in orienting the design of biomimetic devices. The outcomes of our experiments are listed below:

Myometry is an interesting tool and can be used to obtain more information about the biomimetic reference that we are trying to mimic. In particular, we demonstrate this fact by estimating the elasticity distribution of biological fish.

There is a complex relationship between geometry and stiffness. Tuning one of them independently from the other does not always guarantee an improvement in performance. This limits the application of heuristic design methods — based on trial and error processes — and suggests that formal design methodologies, such as using myometry, are needed to optimize our biomimetic devices.

The torso in fish is overdamped after 3 Hz. This indicates that the viscosity distribution plays an important role in regulating bending moments along the fish body. It also suggests that the structure itself generates stability for swimming. Therefore, if the task is to replicate efficient fish swimming, a noticeable component of stabilization derives from the embodiment itself. We expect that the task of control shall not be entirely in charge of guaranteeing stability.

The hybrid prototype performed better than other fish-shaped prototypes. We believe that it is the increasing elasticity that grants P6 an edge.

Future Work: To approximate the elasticity distribution of fish we manufactured the body of the hybrid prototype (P6) in two sections using two different materials. This is a crude 2-value approximation and the performance is affected by the discontinuity. We are, therefore, investigating ways of designing prototypes with continuously-varying elasticity. We are also examining the following question: “how can myometry readings be used to improve and/or simplify the analytical models?”. We are looking for ways of employing myometry with live fish and working on developing a simple method to estimate the viscosity distribution from myometry experiments.

VI. ACKNOWLEDGEMENTS

This work is carried out under the FILOSE project, supported by the European Union, seventh framework programme (FP7-ICT-2007-3).

REFERENCES

- [1] M. J. Lighthill, Note on the swimming of slender fish, *Journal of FluidMech.*, 1960, vol. 9, 305-317.
- [2] M. J. Lighthill, Large Amplitude Elongated Body Theory of Fish Locomotion, *Proceedings of the Royal Society, Biological Sciences*, vol. 179, 1971, pp. 125-138.
- [3] F. Hess, and J. J. Videler, Fast Continuous Swimming of Saithe (Pollachius Virens): A Dynamical Analysis of Bending Moments and Muscle Power, *Journal of Experimental Biology*, vol. 109, 1984, pp. 229-251.
- [4] M. S. Triantafyllou, and G. S. Triantafyllou, and D. K. P. Yue, Hydrodynamics of Fish-like Swimming, *Journal of Fluid Mechanics*, 2000, vol. 32, pp. 33-55.
- [5] George V. Lauder and Peter G. A. Madden, Learning from Fish: Kinematics and Experimental Hydrodynamics for Roboticians, *International Journal of Automation and Computing*, vol. 4, 2006, pp. 325-335.
- [6] Michael S. Triantafyllou, and George S. Triantafyllou, An Efficient Swimming Machine, *Scientific American*, vol. 272:3, 1995, pp. 272-3.
- [7] D. S. Barrett, M. S. Triantafyllou, D. K. P. Yue, M. A. Grosenbaugh, and M. J. Wolfgang, Drag Reduction in Fish-like Locomotion, *Journal of Fluid Mechanics*, vol. 392, 1999, pp. 183-212.
- [8] J. Liu and H. Hu. Novel Mechatronics Design for a Robotic Fish. *IEEE/RSJ International Conference on Intelligent Robots and Systems (IROS)*, Edmonton, Canada, 2005, pp. 2077-2082.
- [9] Pablo Valdivia y Alvarado, Design of Biomimetic Compliant Devices for Locomotion in Liquid Environments, *Ph.D. Thesis*, MIT, 2007.
- [10] J. Y. Cheng, T. J. Pedley and J. D. Altringham, A Continuous Dynamic Beam Model for Swimming Fish, *Philosophical Transactions of the Royal Society B: Biological Sciences*, vol. 353, 1998, pp. 981-997.
- [11] Pablo Valdivia y Alvarado, and Kamal Youcef-Toumi, Design of Machines With Compliant Bodies for Biomimetic Locomotion in Liquid Environments, *Journal of Dynamic Systems, Measurement and Control*, vol. 128, 2006, pp. 3-13.
- [12] Brenden P. Epps, Pablo Valdivia y Alvarado, Kamal Youcef-Toumi, and Alexandra H. Techet, Swimming Performance of a Biomimetic Compliant Fish-like Robot, *Experimental Fluids*, 2009.
- [13] Miomeetria AS., Myoton:Inventions for Performance, available at www.myoton.ee.
- [14] Zenija Roja, Valdis Kalkis, Arved Vain, Henrijs Kalkis, and Maija Eglite, Assessment of skeletal muscle fatigue of road maintenance workers based on heart rate monitoring and myotonometry, *Journal of Occupational Medicine and Toxicology*, vol. 1:20, 2006, pp. 1-9.
- [15] Georg Gavronski, Alar Veraksit, Eero Vasar, and Jaak Maaros, Evaluation of viscoelastic parameters of the skeletal muscles in junior triathletes, *Physiological Measurement*, vol. 28, 2007, pp. 625-637.
- [16] Mario Bizzini, and Anne F. Mannoni, Reliability of a new, hand-held device for assessing skeletal muscle stiffness, *Clinical Biomechanics*, vol. 18, 2003, 459-461.

APPENDIX C

T. Salumäe and M. Kruusmaa, “A Flexible Fin with Bio-Inspired Stiffness Profile and Geometry,” *J. Bionic Eng.*, vol. 8, no. 4, pp. 418–428, Dec. 2011.

A Flexible Fin with Bio-Inspired Stiffness Profile and Geometry

T. Salumäe, M. Kruusmaa

Centre for Biorobotics, Tallinn University of Technology, Akadeemia tee 15A-111, 12618, Tallinn, Estonia

Abstract

Biological evidence suggests that fish use mostly anterior muscles for steady swimming while the caudal part of the body is passive and, acting as a carrier of energy, transfers the momentum to the surrounding water. Inspired by those findings we hypothesize that certain swimming patterns can be achieved without copying the distributed actuation mechanism of fish but rather using a single actuator at the anterior part to create the travelling wave. To test the hypothesis a pitching flexible fin made of silicone rubber and silicone foam was designed by copying the stiffness distribution profile and geometry of a rainbow trout. The kinematics of the fin was compared to that of a steadily swimming trout. Fin's propulsive wave length and tail-beat amplitude were determined while it was actuated by a single servo motor. Results showed that the propulsive wave length and tail-beat amplitude of a steadily swimming 50 cm rainbow trout was achieved with our biomimetic fin while stimulated using certain actuation parameters (frequency 2.31 Hz and amplitude 6.6 degrees). The study concluded that fish-like swimming can be achieved by mimicking the stiffness and geometry of a rainbow trout and disregarding the details of the actuation mechanism.

Keywords: biomimetics, stiffness profile, fin, robotics, fish

Copyright © 2011, Jilin University. Published by Elsevier Limited and Science Press. All rights reserved.

doi: 10.1016/S1672-6529(11)60047-4

1 Introduction

Most of marine and underwater mechanisms, such as ships, submarines, or underwater robots use screw propellers for propulsion. Although these devices work sufficiently well for most purposes, the systems designed by nature still outperform them. Fish are able to swim with high velocities while maintaining superior agility and efficiency. Therefore they can be taken as inspiration when designing new kind of propulsion mechanisms.

Based on the theoretical knowledge of fish swimming^[1,2], a variety of studies on devices mimicking fish to generate propulsion in liquid environments have been conducted. Most of these devices use rigid links and discrete mechanisms to achieve fish-like motion, dynamics and behaviour^[3–7]. The complexity of these systems increases along with the increasing similarity with fish kinematics and therefore in turn decreases the swimming efficiency of the device.

Another alternative is to use compliant bodies which, when actuated from a single point, carry a travelling wave. This wave is similar to the propulsion wave

in the body of fish, which instead of median or pectoral fins use their body and the caudal fin for generating propulsion. The oscillating wave travels through the body with a velocity higher than the swimming speed of the fish^[1]. Compliant bodies carrying a similar travelling wave using single-point actuation can be modelled as dynamically bending beams^[8], which have vibrational characteristics determined by the external and internal forces of the system. The vibrational characteristics in turn are related to geometry, material properties and actuation. The geometry and material properties together define the stiffness of the body which has a high impact on the swimming of both biological fishes^[9–11] and compliant fish-like bodies^[12,13]. Therefore the stiffness of compliant underwater fin propulsors has been studied thoroughly to increase the efficiency and control of fish-like devices and flapping foils.

McHenry *et al.* showed that body stiffness controls swimming kinematics and therefore the speed and performance of elastic models of pumpkinseed sunfish during steady, undulatory swimming^[13] and Prempraneerach *et al.* proved the same for an oscillating NACA0014 foil by demonstrating that the efficiency of

Corresponding author: T. Salumäe

E-mail: taavi@biorobotics.ttu.ee

a pitching and heaving foil can be higher than that of a screw propeller^[12]. Both studies investigated the influence of global stiffness on a compliant body. Riggs *et al.*^[14] investigated the importance of stiffness profile along the elastic fin by taking experimental stiffness profile of a pumpkinseed sunfish from McHency *et al.*^[13], casting flapping foils with the same profile but with a different absolute stiffness value, and comparing the performance with NACA profiles. They showed that fish-like stiffness profile can increase the performance of flapping foils. However, they did not take into account the geometry of the fin and the exact stiffness values. Biomimetic stiffness variation along the body was also justified by Akanyeti *et al.*^[15]. They showed that the increasing elasticity towards the tail will increase the performance of a foil.

As an alternative to an experimental approach, a theoretical analysis can be used to find properties of a compliant propulsor. Alvarado and Youcef-Toumi created a beam model of a compliant single-actuation mechanism and calculated the design parameters of a carangiform-swimming fish-robot^[16–18]. The resulting mechanism's swimming performance attained one third of the real fish's performance and considerable errors in the targeted kinematics were reported. This may indicate that our current theoretical knowledge of nonlinear compliant vibrating systems with water interactions is not advanced enough to accurately describe the required kinematics and dynamics of the system.

Motivated by the above mentioned theoretical and empirical studies on fishlike motion of compliant flapping foil propulsion systems, this study presents a method for biomimetic design of these mechanisms. In Ref. [15] we argued that stiffness, stiffness profile and geometry are design parameters interrelated with each other in a complex manner and they all have impacts on the resultant kinematic characteristics of the propulsor. We therefore show a method of experimentally determining those characteristics from a rainbow trout and a method of building an artificial propulsor with the same parameters. The general methodology is as follows:

(1) Geometry and stiffness distribution along the body of a 50 cm long rainbow trout is characterized experimentally.

(2) An artificial fish tail (flapping foil) following the same geometry and stiffness profile is produced. A composite model made of two silicone materials with

different properties is used to mimic both the desired geometry and stiffness profiles.

(3) Kinematics and swimming performance of artificial tail are determined and compared to those of a real steadily swimming rainbow trout.

The hypothesis of the study is that if the stiffness distribution and geometry of a flapping foil are the same as those of a real trout and the foil is actuated from a single point using sinusoidal angular motion, the foil will produce undulatory motion with kinematic parameters similar to those of a real swimming fish. The hypothesis is based on the fact that fish are able to swim at low cruising speeds with undulatory motions using only their anterior muscles^[19,20]. Posterior body acts passively to carry a travelling wave and transmits locomotor power from the anterior muscle to the caudal fin^[21]. In our mechanism, the rotational single-point actuation acts as an anterior muscle and the flapping foil should respond to actuation similarly to the body of a living fish due to the same geometry and stiffness properties. If the similar kinematic behaviour of a steadily swimming rainbow trout is achieved with the single point actuator, it will show that for a biomimetic caudal fin propulsor the body stiffness and geometry play greater role than the actuation mechanism and a complicated undulatory motion can be achieved without copying the complex distributed actuation system of real fish. Those results can then be taken into account when designing biomimetic propulsors for low mechanical complexity.

2 Materials and methods

2.1 Test subject

To determine the stiffness and stiffness profile, the properties of a rainbow trout (*Oncorhynchus mykiss*) were measured. The specimen with the length of 0.5 m and the weight of 1.58 kg was caught from a fish farm. The experiments were conducted shortly after the death to prevent the change of body properties that might affect the characterisation results.

2.2 Bending stiffness experiment

The first experiment carried out on the test subject was the characterisation of the bending stiffness distribution along the body. The bending stiffness $\kappa(x)$ along the longitudinal axis x of the fish body can be evaluated as the ratio of moment $M(x)$ applied at single point to the

resulting body curvature $k(x)$ at this point

$$\kappa(x) = \frac{M(x)}{k(x)}. \quad (1)$$

The longitudinal coordinate x starts from the tip of the snout and measures the distance along the midline of the body.

The stiffness can be measured using various methods. The most comprehensive and direct method would be gripping the fish and bending it while measuring the applied bending moment and the resulting midline curvature as reported by Long *et al.*^[22–24] and McHenry *et al.*^[13]. With this method it is possible to conduct dynamic measurements and to find stiffness-deformation ratio, which for fish is not constant because of the complex structure of the backbone and flesh. However, the method used in our study to mimic the stiffness distribution of a real trout does not allow designing the stiffness-deformation ratio easily. Therefore, for the simplicity of the experimental procedure, another stiffness determination method was used.

Gravitational force was used to apply a moment to the fish while measuring the curvature of the body using image processing. The trout was laid on the horizontal plate so that its anterior part of the body was resting on the plate and the posterior part of the body was left hanging over the edge. The anterior part was fixed rigidly with clamps and the posterior part bent freely due to gravitational forces. The bending part of the body was photographed using Nikon's digital single-lens reflex camera with 300 mm focal length lens from a relatively far distance of 5 m to minimize image deformation. The experiment was conducted 5 times with a different percentage of the posterior part left over the edge of the horizontal plate so that the bending started from different distance along the longitudinal coordinate x . Measurements were taken at distances 0.20 m, 0.25 m, 0.30 m, 0.35 m and 0.40 m. After the experiment the fish was removed and a photograph of a dot grid was taken for the spatial calibration. Dot grid calibration allows eliminating the image deformation problems because the real distance and the distance measured on image are matched in every position of the image.

The images were analysed using the LabVIEW software. The midline of the freely hanging part of the body was extracted by finding the upper and lower edges of the body using the vertical rake algorithm and taking

their average position on the vertical axis. Points along the midline were detected with the horizontal step of 1 mm. An example of an extracted body midline can be seen in Fig. 1. To give an analytical description to a fish bending, the extracted midline points were fitted using a quadratic polynomial. For all the 5 polynomial fits the coefficient of determination was $R^2 > 0.99$, showing the goodness of a fit. This polynomial is later used to find a curvature of the fish body at different locations.

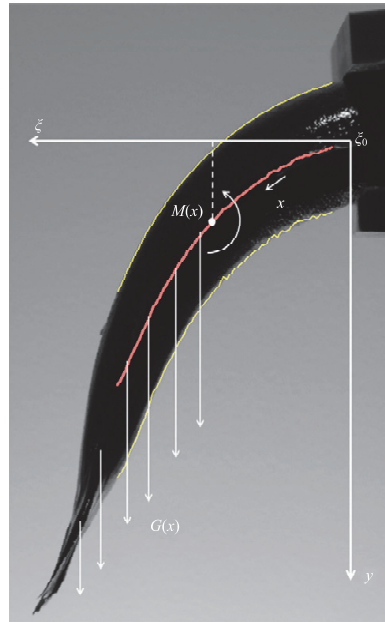


Fig. 1 Experimental setup for measuring the bending stiffness distribution and explanation of symbols used in calculations. Gravitational force $G(x)$ induces the moment $M(x)$. x -axis along the midline of the trout is a function of body deflection $y(\xi)$.

2.3 Mass distribution

To calculate the moment, caused by the gravitational force, acting on the fish's body at various locations, the mass distribution of the test subject had to be determined. For this purpose, the fish was sliced into pieces with a length of 20 mm in the longitudinal direction. The 80 mm caudal fin and the head of the fish were not sliced. The beginning and the end of every piece along the x -axis were measured and slices were weighted using a digital scale.

To describe the mass distribution, the mass per unit length, m_b , was calculated for every measured trout slice from the mass and the length of that slice. The value was

assigned to the centre of every slice and the results are presented in Fig. 2. It is noticeable from the graph that until the 2/5 of the Body Length (BL) the variance of the data points is high, but in the posterior part of the body the values are decreasing with the linear trend. The high variance is caused by the fact that the internal organs of a fish can move in the slicing process. The linear analytical model for mass distribution for the posterior 3/5 of the body was fitted. To avoid the appearance of negative mass in the end of the body, it was assumed that the weight of fish at the tip of the caudal fin equals zero, thus the line must intercept the point (0.5; 0).

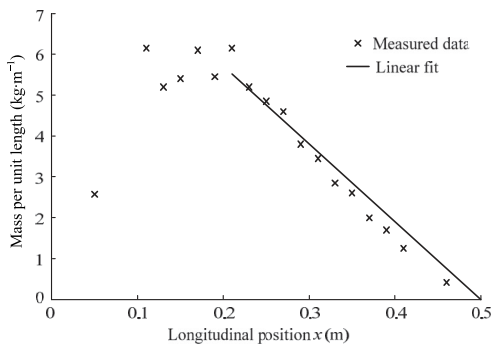


Fig. 2 Mass per unit length of a rainbow trout. Linear regression is applied to the experimental data for the 300 mm of the posterior part of the test subject.

As the result of the linear regression, the relation of mass per unit length m_l to the x -coordinate ($x > 0.2\text{m}$) of the fish is governed by

$$m_l = -19.06x + 9.53 \quad (R^2 = 0.94) \quad (2)$$

2.4 Stiffness profile calculation

Next, the static bending stiffness distribution was calculated from body bending and mass distribution. The fish bending curves fitted above as quadratic polynomials have a general form

$$y(\xi) = a\xi^2 + b\xi + c, \quad (3)$$

where ξ is the horizontal axis, and y is the vertical axis, which measures the fish's body deflection. The reference of the ξ -axis is set to the tip of a snout and the bending starts from the point ξ_0 . The variable ξ_1 marks the tip of the fish tail, where $x=l$. The variable x is the distance from the fish nose along the body midline as mentioned before. The coordinate frame and the sig-

nificant points are shown on Fig. 1.

The moment $M(x)$ is induced by the gravitational force G which depends on the mass distribution of the body $m(x)$. The force per unit length acting on the fish body is

$$G(x) = gm(x), \quad (4)$$

where g is the acceleration of gravity.

Because the load on the fish tail $G(x)$ is distributed, the moment $M(x)$ acting on point x has to be calculated by summing the effect of infinitesimal forces which are parts of this distributed load. The moment is calculated as a product of force and its distance from the point where the moment is to be found, therefore the moment induced by a distributed load is a sum of all infinitesimal parts of this distributed load multiplied by their distances from the point x_i to the point x along the horizontal ξ -axis. Mathematically it can be done by integrating the product of infinitesimal load $G(x_i)$ and distance from the integration variable x_i to the point x . The integral has to be taken over the x -coordinate starting from the point x , where the moment is to be calculated up to the end of the tail x_l .

$$M(x) = \int_x^{x_l} G(x_i)[\xi(x_i) - \xi(x)]dx_i, \quad (5)$$

where x_i is the variable of integration; x is the point where the moment is calculated; $[\xi(x_i) - \xi(x)]$ is the distance from x_i to x along ξ .

The relationship $\xi(x)$ between the horizontal coordinate ξ and the fish body coordinate x was found as an inverse function of $x(\xi)$ which can be defined as a length of function $y(\xi)$. This is governed by the following equation

$$x(\xi) = \int_{\xi_0}^{\xi} \sqrt{1 + \left(\frac{dy}{dx}\right)^2} d\xi + \xi_0, \quad (6)$$

where ξ_0 is added to take into account the straight part of the fish on the table.

Substituting y in Eq. (6) with Eq. (3) and taking a derivative, the equation becomes

$$x(\xi) = \int_{\xi_0}^{\xi} \sqrt{4a^2\xi^2 + 4abx + b^2} d\xi + \xi_0. \quad (7)$$

Since relation $\xi(x)$ is also needed, the $x = f(\xi)$ must be inverted to get $\xi = f^{-1}(x)$. The function was inverted using computational methods.

The curvature of the bending fish body was calcu-

lated from quadratic polynomials using a general curvature equation. To find a curvature depending on the x instead of ζ , the function $\zeta(x)$ was substituted in the curvature equation. The resulting equation for finding body curvature from image processing results is then

$$\kappa(x) = \frac{\left| \frac{d^2}{d\xi^2} y[\zeta(x)] \right|}{\left\{ 1 + \left[\frac{d}{d\xi} y[\zeta(x)] \right]^2 \right\}^{\frac{3}{2}}}. \quad (8)$$

The bending stiffness $\kappa(x)$ of a fish was calculated from the experimental data by substituting the derived bending moment $M(x)$ and body curvature $k(x)$ in Eq. (1). Calculations were performed separately for all 5 photographs taken during the experiments. Results were combined to find the stiffness distribution of the 300 mm of the posterior body. Stiffness could not be reliably calculated for the last 50 mm of the body because of a very small moment and curvature due to a small mass of a caudal fin. To minimize the errors, not all the data from every measurement was used for calculations. In the posterior part the body deflection is very large and the curvature is small, therefore the errors due to uncertainty of the curvature measurement increase. For that reason only the part of data where the body deflection is small (20% of a maximum deflection) was used.

The results showed that the stiffness of the body decreases towards the caudal fin and a linear fit could be used to describe this distribution (Fig. 3). The decreasing linear trend in stiffness is consistent also with previous

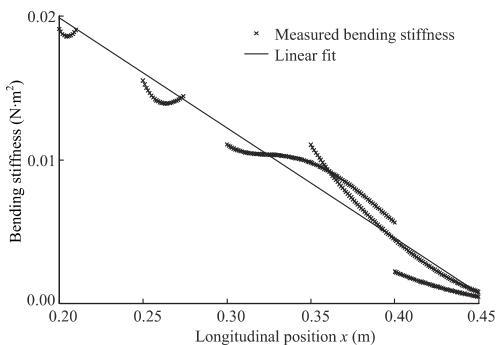


Fig. 3 Bending stiffness distribution of a 500 mm long rainbow trout. Data from 5 measurements between 300 mm and 450 mm of a tail is combined and a linear fit is applied.

studies of fish bending stiffness^[13]. The bending stiffness $\kappa_f(x)$ of a 500 mm rainbow trout can be thus described as

$$\kappa_f(x) = (3.52 - 7.66x)10^{-2}. \quad (9)$$

2.5 Geometry

Besides the bending stiffness, the outer geometry of a test subject was determined. During the mass distribution experiment where the trout was sliced, the cross-sectional height and width of all the slices were measured. These dimensions were used to define the shape of the biomimetic fin. To give an analytical description for further calculation and design process, the model proposed in Ref. [25] was used. The model has been previously used for defining the geometry of flapping foils and it fits the experimental data well.

The Fish body is defined by elliptical cross-sections with minor radius $r(x)$ and major radius $R(x)$. Experimental data for 17 cross-sections of our test subject was fitted using this model. The resulting descriptions for major and minor radii of cross-sections are

$$R(x) = 0.037 \sin(9.603x) + 0.013(e^{4.578x} - 1), \quad (10)$$

$$r(x) = 0.014 \sin(10.74x) + 0.026 \sin(4.99x). \quad (11)$$

The goodness of the fit for major radius $R(x)$ (height of the fish) was $R^2=0.96$ and for minor radius $r(x)$ (width of the fish) was $R^2=0.92$.

2.6 Biomimetic fin

Using the data from a real fish a hydrofoil with the biomimetic stiffness profile and geometry was designed. This artificial tail had a length of 300 mm to mimic the posterior part of the trout's body. That specific length was chosen because rainbow trout as a subcarangiform swimmer uses only 3/5 of the length of its body for swimming while the anterior 2/5 of the body is rigid^[1]. Therefore only the part of the fish, where the travelling wave is generated was copied. The outer geometry of an artificial tail follows the shape described by Eqs. (10) and (11). To copy also the stiffness profile of a trout the foil was composed of two concentric soft silicone bodies. The stiffness of the body at every position along the longitudinal axis can therefore be varied by changing the ratio of inner and outer material. The design of a fin can be seen in Fig. 4.

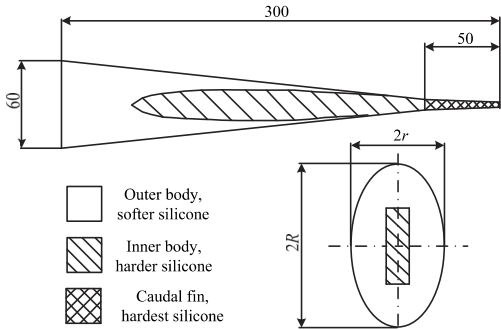


Fig. 4 Design of the biomimetic foil. The image above shows the top view of the foil and the image below a cross-section of the tail design. The tail is composed of two silicones with different elasticities. The outer shape is made of softer silicone and inside the soft silicone there is a harder silicone structure with a rectangular cross-section. By varying the width of the rectangular section we fine-tune the stiffness profile.

Stiffness of such a composite model is governed by

$$\kappa_m(x) = E_1 I_1(x) + E_2 [I_m(x) - I_1(x)], \quad (12)$$

where E_1 and E_2 are the Young's moduli of the inner and outer material respectively, $I_m(x)$ is the second moment of area of the model's cross-section and $I_1(x)$ is the second moment of area of the cross-section of the inner body. As the outer geometry of the model is defined by Eq. (10) and Eq. (11), its second moment of area $I_m(x)$ is known. Young's moduli of materials E_1 and E_2 are constants, therefore the stiffness distribution of the model can be varied by changing the second moment of area I_1 of the inner structure.

The second moment of area I_1 can be varied along the length of the tail by changing the geometry of the inner structure. The geometry itself can have any symmetrical shape and it is important that the moment can only be changed by changing its dimensions. Therefore, for easiest fabrication it is reasonable to use a rectangular cross-section and to change its width along the length of the fish to achieve the right stiffness distribution.

To find materials with most suitable Young's moduli for the inner and outer structures, tensile experiments on Instron 5822 mechanical servo-electric testing system were carried out. Specimens of six different silicone materials were attached between mechanical wedge action grips and were pre-tensioned with 1 N force. They were stretched with the speed of 500 mm per minute up to the elongation of 100%. Recom-

mendations of ISO standard for measuring stress-strain properties of rubbers^[26] were taken into consideration when choosing the parameters of the experiment. A relatively high speed of 500 mm per minute was used to avoid the relaxation effect (a property of polymers to relieve stress under constant strain) of silicone materials. The force was measured using a 50 N load cell with the resolution of 0.001 N. Elongation was measured using the INSTRON non-contact video extensometer from the dots marked on the specimens. The distance between the dots before tensing was 50 mm. As the bending stiffness of a fish is small, a material with smallest Young's modulus, Smooth-On Soma Foama 15, was chosen for outer body. Soma Foama 15 is 2-component silicone foam with a Young's modulus $E_2 = 26$ kPa. For the inner material a Smooth-On Dragon Skin 10 2-component silicone rubber with a Young's modulus $E_1 = 353$ kPa was used. As there was no data about the stiffness profile of the 50 mm caudal fin, but the fin seems to be stiffer than flesh, a material with higher Young's modulus was most probably needed. Therefore Smooth-On Dragon Skin 30 with a Young's modulus of 577 kPa was chosen for casting the caudal fin.

Using Eq. (12), geometry of the tail and Young's moduli of materials, the desired geometry of the inner body of the foil was calculated. Even though the Young's modulus of the chosen silicone foam is very low, it was not sufficient to copy the exact stiffness profile of the trout. The Young's modulus of the foam is still too high to achieve the very low bending stiffness at the given geometry. The comparison of the stiffness measured from the trout and the stiffness of the biomimetic tail is shown in Fig. 5. In the anterior part the stiffness of the artificial tail is relatively higher than that of the real trout, but the difference decreases quickly dropping to zero at approximately 1/3 of the length of the tail.

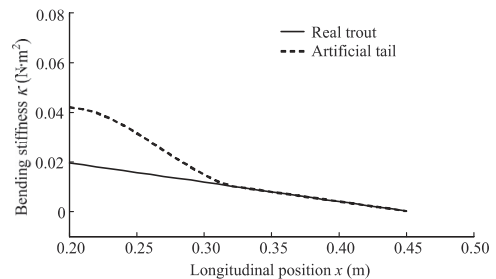


Fig. 5 Stiffness of a real trout and the artificial tail.

To fabricate the biomimetic foil, a negative plastic mould with the outer geometry of the tail was produced using CNC-milling and the positive mould for inner geometry was made manually. First, the negative mould was treated with a release agent and was coated with a thin layer of silicone rubber. This layer was needed, because the silicone foam used for the outer geometry absorbs water. A thin layer of silicone will form a “skin” around the foam to avoid water absorption. After the “skin” was dry, the caudal fin part of the mould was filled with silicone. Positive mould for inner body was fixed inside the outer mould. The silicone foam was cast into the mould and was left drying. After that, the positive mould was removed and the inner material was cast into the hollowness that the positive mould created inside the silicone foam. A metal bracket for mounting the tail to the actuation mechanism was cast into the silicone at the front face of the foil. The fabricated biomimetic fin can be seen in Fig. 6.

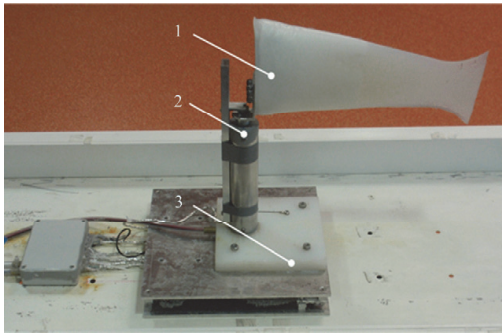


Fig. 6 Fish actuation and force measurement device. 1-artificial fish tail; 2-DC motor actuator; 3-force plate.

2.7 Performance experiments

The kinematics and swimming performance of the biomimetic flapping foil were characterised by conducting underwater experiments in the water tank of Centre for Biorobotics of Tallinn University of Technology. The tank is 4 meter long, 1.5 meter wide and 1.5 meter high. Inside the tank there is a flow tunnel with 1.5 meter long, 0.5 meter wide and 0.5 meter high working section. The flow inside the tunnel is generated using a screw propeller driven by 4 kW induction motor with variable frequency drive capable of producing laminar flow velocities up to $0.48 \text{ m}\cdot\text{s}^{-1}$. Flow velocity was previously calibrated using digital particle image velocimetry.

The foil was mounted on a DC motor using a metal bracket casted inside the front part of the tail. The position feedback controlling motor generated sinusoidal oscillating pitch motion. The system was fixed on a steel plate with 4 load cells under every corner measuring the vertical reaction force. The lateral and longitudinal forces generated by the tail were calculated from the readings of these sensors. The foil actuator and water flow velocity were controlled and force readings were acquired using National Instruments LabVIEW software with NI PCIe 6363 DAQ card. The biomimetically shaped head was mounted in front of the foil to reduce the turbulence and drag acting on the tail.

To evaluate the predicted swimming velocity of the robotic fish with the designed flapping foil, the experiments with flowing water and sinusoidally actuated tail were carried out. Water flow speed and tail-beat amplitude was fixed while the tail-beat frequency was controlled using a PI controller implemented in LabVIEW so that the average measured force in longitudinal direction would be zero (drag and thrust forces are balanced). The frequency resulting in balanced force was thus considered to give the robot a still water swimming velocity equal to the flow speed set in the experiment.

This method does not give the true value of swimming velocity of a freely swimming robot with our biomimetic tail, because the thrust force generated does not have to balance only the drag force acting on the robot, but also the drag force acting on the rod on which the mechanism is mounted on. Therefore it may be predicted that the real swimming velocity would be higher by amount, which cannot be determined with this experimental setup. However, the drag acting on the head and tail of the robot are bigger compared to the drag acting on the mounting, so the swimming speed estimation was considered to be reasonable.

2.8 Kinematics

To determine the kinematics of the foil, its movement was recorded in still water from above using PointGrey Research Dragonfly Express camera with a frame rate of 120 fps.

The kinematics of the tail was characterised by the length λ of the propulsive wave in the foil and the tail's trailing edge amplitude a_L . The same parameters were used by Webb *et al.*^[27] to characterise the kinematics of a steadily swimming rainbow trout and they were

chosen in this study to allow comparison between our biomimetic foil and a biological fish. Identical methods were used also for determining these parameters from a video.

To measure the length of the propulsive wave, half of the wave length was measured directly from video frames and was multiplied by 2 to get the full wave length. Measurements were performed using software developed in LabVIEW environment. Markers on the midline of the foil were used for tracing. The tail's trailing edge amplitude was measured manually from video frames by finding the distance between the leftmost and the rightmost position of the tail's tip.

3 Results

3.1 Length of the propulsive wave

The propulsive wave length λ of the biomimetic foil compared to that of the trout with a length of 500 mm is shown in Fig. 7. The propulsive wave length of a real rainbow trout is reported in Ref. [27]. The results did not show a significant relationship between the wavelength λ and the tail's actuation amplitude a ($r=0.07$). However, the wavelength is linearly correlated to the actuation frequency f ($r=-0.94$). The resulting relation with degree of freedom adjusted coefficient of multiple determination $R^2=0.88$ is

$$\lambda = -0.06f + 0.51. \quad (13)$$

Wavelength values of the biomimetic foil were similar to the wavelength of a biological trout. At actuation frequencies $2.1 \text{ Hz} < f < 2.3 \text{ Hz}$ the difference at every amplitude was below 3% and in all other measurements the difference stayed below 17%.

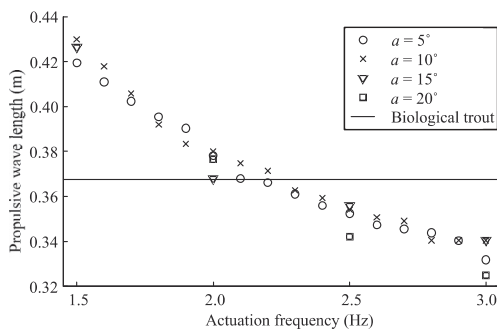


Fig. 7 Length λ of a propulsive wave in the body of the biomimetic flapping foil. Propulsive wavelength of a rainbow trout reported by Webb *et al.*^[27] is added for comparison.

3.2 Tail-beat amplitude

The tail-beat amplitude a_L of the biomimetic foil compared to that of a steadily swimming trout obtained from Ref. [27] is shown in Fig. 8. Amplitude a_L was linearly dependent on the actuation amplitude a ($r=0.97$) and was also in correlation with the actuation frequency f ($r=0.99$). The relation was described using a surface fit ($R^2=0.994$)

$$a_L = 0.0546 - 0.01429f + 0.006536a. \quad (14)$$

Tail-beat amplitude values were exceeding that of a rainbow trout at most actuation amplitudes and frequencies. However, with an actuation amplitude $a=5$ deg the difference less than 3% was achieved.

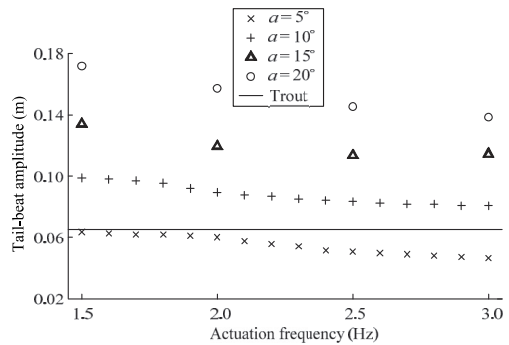


Fig. 8 Tail-beat amplitude a_L of the biomimetic flapping foil.

3.3 Swimming velocity

The tail-beat frequency balancing the drag forces with respect to different flow velocities can be seen in Fig. 9. The results show a linear relationship between the swimming speed and the actuation frequency up to 2 Hz at all actuation amplitudes. While the frequency is increased above this limit the linear relation discontinues to hold and the increase in frequency has to be bigger to achieve the same increase in velocity. This phenomenon is consistent with the thrust measurements taken in still water (Fig. 10) that show the nearly constant thrust force in the frequency interval between 2 and 3 Hz while using lower actuation amplitudes.

When comparing the predicted swimming velocity of our mechanism to that of real trout with the same size it is visible that although the linear trend holds for both, the slope of velocity to frequency fit of our tail is lower making our tail less frequency-dependent.

The highest swimming speed that could be tested in

our flow tunnel, $0.48 \text{ m}\cdot\text{s}^{-1}$ ($0.96 \text{ BL}\cdot\text{s}^{-1}$), was achieved at the actuation amplitude of 15 degree and the actuation frequency of 3.2 Hz. This means that our robotic tail is capable of swimming at biological swimming speeds.

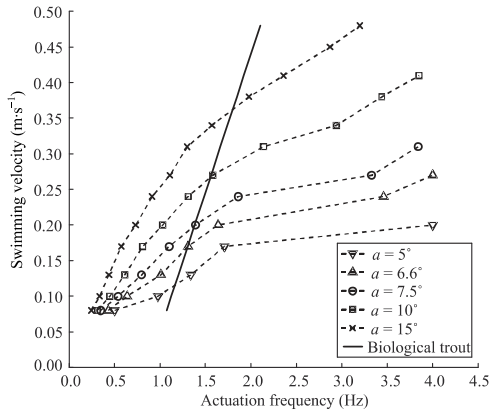


Fig. 9 Swimming velocity of the biomimetic foil.

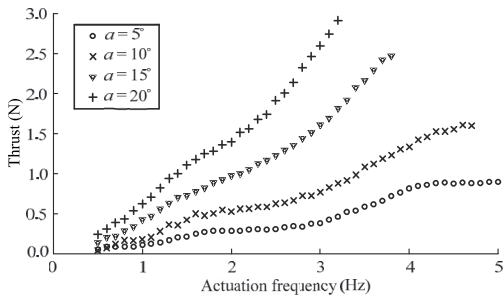


Fig. 10 Generated thrust force of the biomimetic foil.

4 Discussion

The design method proposed in this study allows varying the stiffness of the artificial tail along the body to mimic that of real trout. However, materials soft enough to copy the stiffness profile in full length of the tail were not found and the designed prototype has a higher stiffness in the anterior part of the tail. The difference is definitely high enough to change the experimental results. It probably affects all parameters, the tail-beat amplitude, length of the propulsive wave and the swimming velocity. Nevertheless, the overall trend and order of magnitude of values will not change and they will probably stay within the biological range reported in results. This is supported by the fact that the deformation of the anterior part of the tail of subca-

rangiform swimmers and flapping foils is relatively small compared to that of the posterior part of the tail. This means that the error caused by the stiffness difference is also small.

Despite of that, the increase in the accuracy of mimicking the stiffness is important to determine the magnitude of errors. This could be achieved by finding a material with lower Young's modulus. With a biological geometry the elastic modulus of that material has to be not more than 11.8 kPa. No commercially available silicone rubbers or foams with such a low value can be found. Therefore, new custom-made silicones should be implemented or other types of materials should be used. Another way would be using a smaller fish so with the same material the bending stiffness would be smaller because of the reduced geometry.

The accuracy of copying the stiffness profile is also reduced because of the limitations of the method used to measure the stiffness of a real trout. The method does not allow measuring the stiffness of the caudal fin because its deflection caused by the gravitational force is too small for precise measurement. In this study, however, mostly the body kinematics is investigated and the effect of the caudal fin properties on kinematic parameters of the flapping foil's body is considered to be small.

The kinematical parameters of our biomimetic tail were compared to those of a real steadily swimming trout reported by Webb *et al.* [27].

The propulsive wave length of the biomimetic tail was linearly related to actuation frequency. Wavelength of the rainbow trout, however, is not related to swimming speed and thus frequency, but to fish's size only. Therefore, by choosing the right actuation frequency using Eq. (13), the wavelength equal to that of the trout with the same size as our tail was achieved. For our foil that frequency was 2.31 Hz, which falls into the biological range and according to Ref [27] would result in steady swimming speed of $1.3 \text{ BL}\cdot\text{s}^{-1}$ on a trout. Nearly the same velocity can be achieved with our fin at the same tail-beat frequency while increasing the actuation amplitude up to 15 degrees.

The tail-beat amplitude of a biological trout, however, is constant. That amplitude can be achieved on our biomimetic tail when choosing the right pitch actuation amplitude using the relation (14) and keeping the frequency constant. The biomimetic foil matches the amplitude value $6.5\cdot 10^{-2} \text{ m}$ of a trout at actuation amplitude

6.6 deg. Unlike the tail-beat amplitude of a real trout, the tail-beat amplitude of the artificial tail is dependent on the actuation frequency. This trend is explained by theoretical mechanics, which says that in the driven oscillatory system, the amplitude of the wave reaches its maximum value at the resonance frequency of the system^[28]. This effect is also experimentally shown in previous studies about flapping foils, for example in Ref. [13]. Experiments in the current study revealed that the tail-beat amplitude decreases with the increase in driving frequency. Therefore the fin was actuated over its natural frequency. It was hypothesized in Ref. [13] that fish increase the stiffness of their body while swimming at higher frequencies in order to increase the natural frequency and to avoid the reduction of body wave amplitude.

Results of kinematics measurements show that for certain actuation parameters, the kinematics of our biomimetic trout tail is exactly the same as the kinematics of a real trout tail. However, the number of kinematic parameters used in this paper is limited by the comparative data on real fish found in literature. Kinematics is well known only for relatively small fish^[29]. Determining the properties of small fish is more complicated due to relatively bigger errors in mass distribution and geometry measurements. Also a small foil is harder to use as a propulsor of a robotic fish, because the robot has to accommodate also mechanics and electronics. Using three parameters to evaluate the similarity of kinematics of a fish and a foil is enough to conclude that the foil mimicking the fish body is sufficient to generate the same locomotion principle as fish - using a travelling wave. However, conclusions about the absolute similarity in kinematics of fish and biomimetic foil cannot be drawn. Still, using available data, the main hypothesis of this study is proven – by mimicking the stiffness profile and geometry of the rainbow trout on the pitching foil, similar kinematics will be achieved at certain actuation properties.

It may be expected that if the kinematics of the artificial tail is the same as that of the biological trout, also the swimming velocity should be equal. The velocity of our tail at actuation properties resulting in the biological kinematics (6.6 deg, 2.31 Hz) is in the range of 0.2...0.24 m·s⁻¹ (0.4...0.48 BL·s⁻¹), which is only 30% to 37% of that of the real trout with same size. Although the drag forces of our robotic fish were big due to experimental

mechanism attached to it, the real velocity would probably not rise above 50% of that of the real fish. This result complements the idea that kinematics of large-scale rainbow trout have to be described in more detail to get more descriptive data for comparison.

In addition to developing better methods for kinematics similarity assessment, the future work should concentrate on additional performance experiments of flapping foils with biomimetic stiffness and geometry profile. This includes efficiency, thrust and wake structure analysis in comparison with other similar foils.

5 Conclusion

In this study a novel type of composite-structure pitching foil was presented. Stiffness profile and geometry of this foil are independent design parameters and the distributions of their values in this study were copied from a rainbow trout. It was shown that such artificial tail, while actuated from a single point using a sinusoidal pitch motion, exhibits swimming kinematics similar to that of a live rainbow trout. This proves experimentally that by abandoning the distributed actuation mechanism of the fish it is still possible to achieve its complicated motion by simply copying stiffness and geometry distributions from a biological trout.

Acknowledgments

This work is supported by European Union 7th Framework program under FP7-ICT-2007-3 STREP project FILOSE (Robotic Fish LOcomotion and SENSing).

References

- [1] Sfakiotakis M, Lane D M, Davies J B C. Review of fish swimming modes for aquatic locomotion. *IEEE Journal of Oceanic Engineering*, 1999, **24**, 237–252.
- [2] Lauder G V, Madden P G A. Learning from fish: Kinematics and experimental hydrodynamics for roboticists. *International Journal of Automation and Computing*, 2006, **4**, 325–335.
- [3] Barrett D S. *Propulsive Efficiency of a Flexible Hull Underwater Vehicle*, PhD Thesis, Massachusetts Institute of Technology, Cambridge, USA, 1996.
- [4] Anderson J M, Chhabra N K. Maneuvering and stability performance of a robotic tuna. *Journal of Integrative and Comparative Biology*, 2002, **42**, 118–126.
- [5] Kumph J M. *Maneuvering of a Robotic Pike*, MS Thesis,

- Massachusetts Institute of Technology, Cambridge, USA, 2000.
- [6] Yu J, Tan M, Wang S, Chen E. Development of a biomimetic robotic fish and its control algorithm. *IEEE Transactions on Systems, Man, and Cybernetics - Part B: Cybernetics*, 2004, **34**, 1798–1810.
- [7] Liu J, Dukes I, Hu H. Novel mechatronics design for a robotic fish. *IEEE International Conference on Intelligent Robots and Systems*, Edmonton, Canada, 2005, 2077–2082.
- [8] Cheng J Y, Pedley T J, Altringham J D. A continuous dynamic beam model for swimming fish. *Philosophical Transactions of the Royal Society of London: B*, 1998, **353**, 981–997.
- [9] Long J H Jr, Nipper K S. The importance of body stiffness in undulatory propulsion. *American Zoologist*, 1996, **36**, 678–694.
- [10] Long J H Jr, Koob T J, Irving K, Combie K, Engel V, Livingston N, Lammert A, Schumacher J. Biomimetic evolutionary analysis: Testing the adaptive value of vertebrate tail stiffness in autonomous swimming robots. *Journal of Experimental Biology*, 2006, **209**, 4732–4746.
- [11] Long J H Jr, Porter M E, Root R G, Liew C W. Go reconfigure: How fish change shape as they swim and evolve. *Integrative and Comparative Biology*, 2010, **50**, 1120–1139.
- [12] Prempraneerach P, Hover F S, Triantafyllou M S. The effect of chordwise flexibility on the thrust and efficiency of a flapping foil. *13th International Symposium on Unmanned Untethered Submersible Technology*, Durham, USA, 2003.
- [13] McHenry M J, Pell C A, Long J H Jr. Mechanical control of swimming speed: Stiffness and axial wave form in undulating fish models. *Journal of Experimental Biology*, 1995, **198**, 2293–2305.
- [14] Riggs P, Bowyer A, Vincent J. Advantages of a biomimetic stiffness profile in pitching flexible fin propulsion. *Journal of Bionic Engineering*, 2010, **7**, 113–119.
- [15] Akanyeti O, Ernits A, Fiazza C, Toming G, Kulikovskis G, Listak M, Raag R, Salumäe T, Fiorini P, Kruusmaa M. Myometry-driven compliant-body design for underwater propulsion. *IEEE International Conference on Robotics and Automation*, Anchorage, USA, 2010.
- [16] Alvarado P V, Youcef-Toumi K. Performance of machines with flexible bodies designed for biomimetic locomotion in liquid environments. *Proceedings of the IEEE International Conference on Robotics and Automation*, Barcelona, Spain, 2005.
- [17] Alvarado P V, Youcef-Toumi K. Design of machines with compliant bodies for biomimetic locomotion in liquid environments. *Journal of Dynamic Systems, Measurement, and Control*, 2006, **128**, 3–13.
- [18] Epps B P, Alvarado P V. Swimming performance of a biomimetic compliant fish-like robot. *Experiments in Fluids*, 2009, **47**, 927–939.
- [19] Blight A R. Undulatory swimming with and without waves of contraction. *Nature*, 1976, **264**, 352–354.
- [20] Blight A R. The muscular control of vertebrate swimming movements. *Biological Reviews*, 1977, **52**, 181–218.
- [21] Long J H Jr, Mchenry M J, Boetticher N C. Undulatory swimming: How traveling waves are produced and modulated in sunfish (*Lepomis gibbosus*). *Journal of Experimental Biology*, 1994, **192**, 129–145.
- [22] Long J H Jr. Stiffness and damping forces in the intervertebral joints of blue marlin (*Makaira nigricans*). *Journal of Experimental Biology*, 1992, **162**, 131–155.
- [23] Long J H Jr, Hale M E, McHenry M J, Westneat M W. Functions of fish skin: Flexural stiffness and steady swimming of longnose gar (*Lepisosteus osseus*). *Journal of Experimental Biology*, 1996, **199**, 2139–2151.
- [24] Long J H Jr. Muscles, elastic energy and the dynamics of body stiffness in swimming eels. *American Zoologist*, 1998, **38**, 771–792.
- [25] Alvarado P V. *Design of Biomimetic Compliant Devices for Locomotion in Liquid Environments*, PhD Thesis, Massachusetts Institute of Technology, Cambridge, USA, 2007.
- [26] ISO 37:2005 *Rubber, vulcanized or thermoplastic – Determination of tensile stress-strain properties*, 2008.
- [27] Webb P W, KostECKI P T, Stevens E D. The effect of size and swimming speed on locomotor kinematics of rainbow trout. *Journal of Experimental Biology*, 1984, **109**, 77–95.
- [28] Meirovitch L. *Fundamentals of Vibrations*, McGraw-Hill international edition, McGraw-Hill Higher Education, Singapore, 2001.
- [29] Liao J C, Beal D N, Lauder G V, Triantafyllou M S. The Karman gait: Novel body kinematics of rainbow trout swimming in a vortex street. *Journal of Experimental Biology*, 2003, **206**, 1059–1073.

APPENDIX D

H. El Daou, T. Salumae, G. Toming, and M. Kruusmaa, “A bio-inspired compliant robotic fish: Design and experiments,” in *Proc. IEEE Int. Conf. on Robotics and Automation (ICRA)*, 2012, pp. 5340–5345.

A Bio-inspired Compliant Robotic Fish: Design and Experiments

Hadi El Daou, Taavi Salumäe, Gert Toming and Maarja Kruusmaa

Abstract—This paper studies the modelling, design and fabrication of a bio-inspired fish-like robot propelled by a compliant body. The key to the design is the use of a single motor to actuate the compliant body and to generate thrust. The robot has the same geometrical properties of a subcarangiform swimmer with the same length. The design is based on rigid head and fin linked together with a compliant body. The flexible part is modelled as a non-uniform cantilever beam actuated by a concentrated moment. The dynamics of the compliant body are studied and a relationship between the applied moment and the resulting motion is derived. A prototype that implements the proposed approach is built. Experiments on the prototype are done to identify the model parameters and to validate the theoretical modelling.

I. INTRODUCTION

Underwater robots provide an engineering tool to practical applications in marine and military fields, such as monitoring the environment, harvesting natural resources, undersea operation, pipe inspection and many other applications.

With millions of years of evolution, aquatic animals, in particular fish, are very efficient swimmers. This has inspired scientists to study fish locomotion and build fish-like robots. MIT's RoboTuna I and II are the best known bio-inspired underwater robots [1]. These are tethered robots, mimicking the thunniform swimmers and use a system of pulleys and cable tendons actuated by DC-motors. MIT also developed Robot pike to learn more about the fluid mechanics that fish use to propel themselves with a purpose to develop small fish-like autonomous vehicles for reduced energy consumption and increased operation time [3]. The Vorticity Control Unmanned Undersea Vehicle (VCUUV) was produced in Draper Laboratory; it was the first autonomous mission-scale UUV that utilizes fish-like swimming and manoeuvring [2]. The University of Essex has developed a series of autonomous robots G1 to G9 and MT1. The G series have a multi-motor-multi-joint tail structure, which employs 4 servo motors to drive 4 tail joints separately according to a predetermined swimming wave sequence [4][5][6][7][8]. The Japanese National Maritime Research Institute developed many kinds of robotic fish prototypes to increase swimming efficiency [9].

Most of these designs use rigid links and discrete mechanisms to achieve fish-like swimming. The complexity of these systems increases proportionally with the kinematic

similarity to fish. An alternative is to use compliant structures; These bodies can be modelled as dynamically bending beams [10] whose vibration characteristics are determined by external and internal forces of the system, which in turn are related to the geometry, material properties and actuation.

This alternative design concept also has some biological relevance. The EMG studies of muscle activity of swimming fish reveal that for swimming at cruising speeds (1 to 2 body lengths per second) fish use mainly anterior muscles while the posterior part of the body acts like a carrier of the travelling wave conveying the momentum to the surrounding fluid [11], [12], [13]. A robotic fish using smart materials for caudal fin design was developed in Michigan State University [14] to increase efficiency, focusing on unique physics of Ionic polymer metal composite (IPMC) materials and its interaction with the fluid. A subclass of swimmers that exploits the use of compliant bodies and one servo-motor for actuation was developed at MIT [15]. It assumes that a compliant body can be modelled by a cantilever beam actuated by a single point and studies the dynamics in order to mimic swimming fish motions.

In this study, the design of a robot with a flexible body excited by a concentrated moment is studied. It makes use of the models developed in [16] but differs in many aspects. In fact, in [16] the mechanical modelling does not take into account the elasticity of the rigid plate used for actuation and neglected the hydrodynamic effect on the rigid fin. In this work, a different approach is used. It takes into account the non-homogeneity in the material distribution and the effect of a rigid fin in the end of the compliant body. The dynamics of the compliant body are studied to find a relationship between the applied force and the resulting deflections. Moreover in this study it is believed, that a compliant body cannot be forced to deform to a random shape but has defined mode shapes that are determined by the actuation frequencies and the modal properties of the system.

The objectives of this paper are to:

- study the dynamics of the compliant body and derive the relationship between the applied forces and the resulting motion.
- propose a design that implements the proposed approach and build a fish-like robot prototype.
- identify the model parameters and validate the model through physical experiments.

The remainder of this paper is organized as follows: In section II the dynamics of the compliant body are developed. In section III the prototype of robotic fish is described. Results from physical experiments on the prototype are

This work is supported by European Union 7th Framework program under FP7-ICT-2007-3 STREP project FILOSE (Robotic Fish LOcomotion and SEnsing), www.fiLOSE.eu.

Authors are with Center for Biorobotics, Tallinn University of Technology, Tallinn, Estonia. maarja.kruusmaa@ttu.ee, hadi.daou@ttu.ee

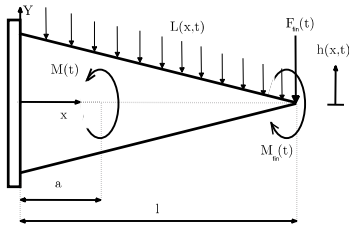


Fig. 1. Structural model of the compliant body. a =actuation point, l =length of the compliant body, $M(t)$ =actuation moment, $L(x,t)$ hydrodynamic distributed forces, $F_{fin}(t)$, $M_{fin}(t)$ =concentrated force and moment resulting from the hydrodynamic forces acting on the fin and $h(x,t)$ =lateral line deflection

presented in section IV. Finally, section V discusses the contributions and future work.

II. DYNAMICS OF THE COMPLIANT BODY

Fig.1 shows the structural model of the compliant body. The "assumed modes" method is used to derive the equations of motion of the compliant body [17] [18] [19] [20] [21]. It aims at deriving such equations by first discretizing the kinetic energy, potential energy and the virtual work and making use of the Lagrange's equation of motion. The Elastic deformations are modelled by a finite series:

$$h(x,t) = \sum_{r=1}^n \varphi_r(x) q_r(t) \quad 0 < x < l \quad (1)$$

where:

- $\varphi_r(x)$: are known trial functions. The eigenfunctions of a uniform cantilever beam are chosen as trial functions.
- $q_r(t)$: are unknown generalized coordinates.
- n : is the order of the expansion.
- l : is the length of the compliant body.

Considering that the passive fin is rigid compared to the compliant body, its lateral deflection $h(x,t)$ can be expressed as:

$$h(x,t) = h(l,t) + \frac{\partial h(l,t)}{\partial x} (x-l) \quad l < x < l + \Delta l$$

$$= \sum_{i=1}^n (\varphi_i(l) q_i(t) + \varphi_i'(l) q_i(t) (x-l)) \quad (2)$$

where Δl is the length of the rigid fin.

The external forces acting on the compliant body are: the time varying moment $M(t)$, the distributed hydrodynamic forces $L(x,t)$, the concentrated moment $M_{fin}(t)$ and the concentrated force $F_{fin}(t)$. $M_{fin}(t)$ and $F_{fin}(t)$ are the concentrated moment and force resulting from the action of the hydrodynamic forces on the rigid fin. The hydrodynamic forces are modelled in terms of added mass and expressed as:

$$L(x,t) = D(m(x)\dot{h}(x,t)) \approx m(x) \frac{\partial^2 h}{\partial t^2} \quad (3)$$

where $m(x)$ is the apparent mass of the cross section per unit length. It is approximated by $m(x) = C_0 \rho_f A(x)$ where C_0 is a constant that can be determined experimentally, ρ_f is the fluid density and $A(x)$ is the cross area of a fluid cylinder surrounding the body at x .

The concentrated force $F_{fin}(t)$ is:

$$F_{fin}(t) = - \int_l^{l+\Delta l} m(x) \frac{\partial^2 h}{\partial t^2} dx = - \sum_{i=1}^n \ddot{q}_i(t) [\alpha \varphi_i(l) + \beta \varphi_i'(l)] \quad (4)$$

where:

$$\alpha = \int_l^{l+\Delta l} m(x) dx \quad \beta = \int_l^{l+\Delta l} m(x)(x-l) dx \quad (5)$$

The concentrated moment $M_{fin}(t)$ is:

$$M_{fin}(t) = - \int_l^{l+\Delta l} m(x) \frac{\partial^2 h}{\partial t^2} (x-l) dx$$

$$= - \sum_{i=1}^n \ddot{q}_i(t) [\beta \varphi_i(l) + \gamma \varphi_i'(l)] \quad (6)$$

where:

$$\gamma = \int_l^{l+\Delta l} m(x)(x-l)^2 dx \quad (7)$$

The kinetic and potential energies can be written as:

$$T(t) = \frac{1}{2} \int_0^l \mu(x) \left(\frac{\partial h(x,t)}{\partial t} \right)^2 dx$$

$$= \frac{1}{2} \sum_{i=1}^n \sum_{j=1}^n \dot{q}_i(t) \dot{q}_j(t) \int_0^l \mu(x) \varphi_i(x) \varphi_j(x) dx \quad (8)$$

$$V(t) = \frac{1}{2} \int_0^l EI(x) \left(\frac{\partial^2 h(x,t)}{\partial x^2} \right)^2 dx$$

$$= \frac{1}{2} \sum_{i=1}^n \sum_{j=1}^n q_i(t) q_j(t) \int_0^l EI(x) \varphi_i''(x) \varphi_j''(x) dx \quad (9)$$

$\mu(x)$ and $EI(x)$ are the mass per unit length and the stiffness at x respectively.

The total virtual work can be expressed as:

$$\delta W = \delta W_1 + \delta W_2 + \delta W_3 + \delta W_4$$

where δW_1 is the virtual work of $M(t)$:

$$\delta W_1 = \int_0^l M(t) \delta \underline{h}(x-a) \delta h'(x,t) dx = \sum_{j=1}^n M(t) \varphi_j'(a) \delta q_j \quad (10)$$

δW_2 is the virtual work of $L(x,t)$:

$$\delta W_2 = - \int_0^l L(x,t) \delta h(x,t) dx = - \int_0^l m(x) \frac{\partial^2 h}{\partial t^2} \delta h(x,t) dx$$

$$= - \sum_{i=1}^n \sum_{j=1}^n \ddot{q}_i(t) \int_0^l m(x) \varphi_i(x) \varphi_j(x) dx \delta q_j \quad (11)$$

δW_3 is the virtual work of F_{fin} :

$$\begin{aligned} \delta W_3 &= \int_0^l F(t) \underline{\delta}(x-l) \delta h(x,t) dx \\ &= - \sum_{i=1}^n \sum_{j=1}^n \ddot{q}_i(t) [\alpha \varphi_i(l) \varphi_j(l) + \beta \varphi_i'(l) \varphi_j'(l)] \delta q_j \end{aligned} \quad (12)$$

δW_4 is the virtual work of $M_{fin}(t)$:

$$\begin{aligned} \delta W_4 &= \int_0^l M_{fin}(t) \underline{\delta}(x-l) \delta h'(x,t) dx = \sum_{j=1}^n M_{fin}(t) \varphi_j'(l) \delta q_j \\ &= - \sum_{i=1}^n \sum_{j=1}^n \ddot{q}_i(t) [\beta \varphi_i(l) \varphi_j'(l) + \gamma \varphi_i'(l) \varphi_j'(l)] \delta q_j \end{aligned} \quad (13)$$

$\underline{\delta}$ denotes the Dirac delta function and $h'(x,t) = \frac{\partial}{\partial x} h(x,t)$.

The Lagrange's equations are used to write the equations of motion of the approximate system:

$$[M]\{\ddot{q}(t)\} + [K]\{q(t)\} = \{Q(t)\} \quad (14)$$

where:

$$\begin{aligned} m_{ij} &= \int_0^l (\mu(x) + \rho_f A(x)) \varphi_i(x) \varphi_j(x) dx + \alpha \varphi_i(l) \varphi_j(l) \\ &\quad + \beta (\varphi_i'(l) \varphi_j(l) + \varphi_i(l) \varphi_j'(l)) + \gamma \varphi_i'(l) \varphi_j'(l) \end{aligned}$$

$$k_{ij} = \int_0^l EI(x) \varphi_i''(x) \varphi_j''(x) dx$$

and

$$Q_i(t) = - \int_0^l M(t) \underline{\delta}'(x-a) \varphi_i(x) dx$$

To find the response of (14), the eigenvalue problem is first solved introducing:

$$q(t) = ae^{\lambda t}$$

This leads to the following characteristic equation:

$$\det(\lambda^2 M + K) = 0$$

where $\lambda_r = -iw_r$ and w_r are the undamped natural frequencies of the approximate system. To obtain the solution of (14), the following linear transformation is used:

$$q(t) = U\eta(t) \quad (15)$$

where:

$$U = [a_1 \ a_2 \ a_3 \ a_4 \ a_5 \ \dots \ a_n]$$

Where a_n is the eigenvector associated with the eigenvalue $\lambda_n = -iw_n$. The eigenvectors are orthogonal with respect

to the mass and stiffness matrices. They are normalized to yield:

$$a_r^T \cdot M \cdot a_s = \delta_{rs} \quad a_r^T \cdot K \cdot a_s = w_r^2 \delta_{rs}$$

Where δ_{rs} is defined as the Kronecker delta.

Introducing (15) in (14) and premultiplying by U^T , the independent modal equations are then obtained:

$$\ddot{\eta}(t) + \Lambda \eta(t) = N(t) \quad (16)$$

in which :

$$\Lambda = \text{diag}[w_1^2 \ w_2^2 \ w_3^2 \ w_4^2 \ w_5^2 \ w_6^2 \ \dots \ w_n^2]$$

and

$$N(t) = U^T Q(t) \quad (17)$$

The model must include some damping [22]. It is convenient to assume proportional damping: a special type of viscous damping [23]. The proportional damping model expresses the damping matrix as a linear combination of the mass and stiffness matrices, that is:

$$C = \alpha_1 M + \alpha_2 K \quad (18)$$

Where α_1 and α_2 are constant scalars. The result is that for the i th mode:

$$\ddot{\eta}_i(t) + 2\zeta_i w_{ni} \dot{\eta}_i(t) + w_{ni}^2 \eta_i(t) = N_i(t) \quad (19)$$

The solution of (19) can be written by components in the form of convolution integrals as follows:

$$\eta_i(t) = \frac{1}{w_{di}} \int_0^t e^{-\zeta_i w_{ni} \tau} N_i(t-\tau) \sin(w_{di} \tau) d\tau \quad (20)$$

where $w_{di} = \sqrt{1 - \zeta_i^2} w_{ni}$ is the damped natural angular frequency.

Finally using (15), the generalized coordinates are calculated. The motions of the compliant body are then calculated using (1).

III. PROTOTYPE DESIGN

A prototype that implements the proposed theoretical approach is built. Its dimensions are acquired from those of a sub-carangiform swimmer with the same dimensions. Fig-2, shows the CAD of the prototype; It consists of:

- a compliant body attached to a passive rigid caudal fin. The length of the compliant body is 0.22 m and that of the fin is 0.08m;
- a rigid head accommodating the electronics and a servomotor used to actuate the compliant body. The servomotor actuates the compliant body by pulling two cables attached to the rigid plate casted inside the flexible body;
- an aluminium part connecting the head and the compliant body.

The dimensions of the robot are chosen to allow it to accommodate the electronics and the motor and to swim

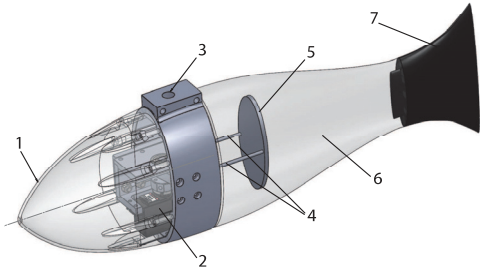


Fig. 2. CAD view of the fish-like robot. 1-Rigid head of the robot; 2-Servo-motor; 3-Middle part made from aluminum holding the head, the compliant body and a servo-motor; 4-Steel cables; 5-Actuation plate; 6-Compliant body; 7-Rigid fin.

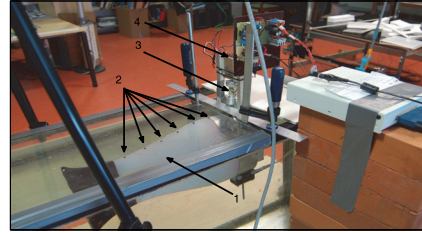


Fig. 3. The experimental setup composed of: 1- An compliant body, 2- Six metallic markers, 3- A custom torque sensor, 4- a servo motor

freely in the test tank. The Young's modulus of elasticity is chosen experimentally. Trials on compliant bodies with different modulus are performed. The compliant bodies with a high modulus of elasticity are hard to deform while those with a low elasticity don't generate enough thrust.

A compromise solution is a Young's modulus of 83Kpa. The flexible part is casted from commercial platinum cure silicon rubber Dragon Skin[®] 20 and a special additive Slacker[®] used to alter the elasticity of the rubber. The distance between the actuation point and the compliant body base is chosen to be $a=0.07m$.

IV. EXPERIMENTS AND RESULTS

In this section, the experiments carried out on the compliant body are described. These experiments aim to:

- estimate the natural frequencies and damping ratios of the system;
- validate the theoretical modelling;
- measure the average thrusts and velocities as a function of actuation frequencies.

A. Parameter Identification

A special experimental setup is used. It consists of (see Fig.3):

- a compliant body attached to a passive rigid caudal fin;
- six metallic markers attached to the compliant body and used to track its motions;
- a custom torque sensor;
- a servo motor used for actuation.
- a digital camera filming at a rate of 50 frames per second.
- a water tank.

To estimate the damping ratios, experiments are carried out on the compliant body in air. The undamped natural frequencies are calculated using the approach developed earlier in this paper. Tab-I summarizes the undamped natural frequencies in air. An expansion series of order $n=6$ is used.

The servo-motor is controlled to oscillate in the range of a given interval $[-\theta, +\theta]$ for different actuation frequencies. For each frequency the compliant body is excited for a given

TABLE I

UNDAMPED NATURAL FREQUENCIES OF THE COMPLIANT BODY IN AIR

f_{n1} [Hz]	f_{n2} [Hz]	f_{n3} [Hz]	f_{n4} [Hz]	f_{n5} [Hz]	f_{n6} [Hz]
4.0696	11.1351	33.9573	71.1087	813.4664	17556

number of actuation periods and the maximum value of the torque is recorded. Two trials are performed: In the first referred to as Exp-1, the compliant body is actuated using harmonic torques with different actuation frequencies close to the first undamped natural frequency f_{n1} . The maximum values of the torques are then drawn as a function of the actuation frequency as shown in fig.4. The minimum value on the graph corresponds to $f_1=3.3$ Hz equal to $f_{n1} \sqrt{1-2\zeta_1^2}$ [24]. The first damping ratio is then calculated as $\zeta_1 = 0.41$. In the second trial, referred to as Exp-2, the compliant body is actuated using harmonic torques with different actuation frequencies close to the second undamped natural frequency f_{n2} . The maximum values of the torques are then drawn as a function of the actuation frequency as shown in fig.5. The minimum value on the graph corresponds to $f_2=9.96$ Hz equal to $f_{n2} \sqrt{1-2\zeta_2^2}$. The second damping ratio is then calculated as $\zeta_2 = 0.3$. This approach is not applied to measure the damping ratios for higher frequencies to prevent damaging the system. Instead $\zeta_3, \zeta_4, \zeta_5$ and ζ_6 are assumed to be equal to ζ_2 .

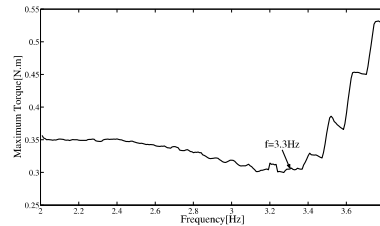


Fig. 4. Maximum torque measured in Exp-1 as a function of actuation frequency.

To estimate the constant C_0 defining the added mass used to model the hydrodynamic forces, experiments are carried

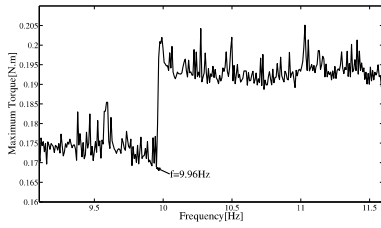


Fig. 5. Maximum torque measured in Exp-2 as a function of actuation frequency.

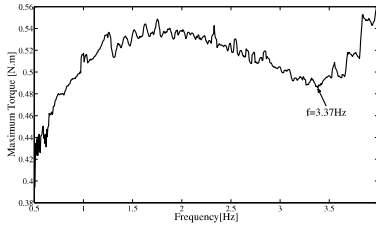


Fig. 6. Maximum torque measured in Exp-3 as a function of actuation frequency.

out on the compliant body in water and are referred to as Exp-3. The same approach applied to measure the damping ratio is used. The compliant body is excited with actuation frequencies close to the second undamped natural frequency in water. The maximum values of the torques are then drawn as a function of the actuation frequency as shown in fig. 6. The minimum value on the graph corresponds to $f_{n2} = \frac{3.37}{\sqrt{1-2*0.31^2}}$. The first undamped natural frequency is small and not easy to identify. Having f_{n2} , C_0 is the constant that makes the calculated and measured second undamped frequencies equal. In the present case, C_0 is equal to 0.8. Tab-II summarizes the calculated values of the undamped natural frequencies of the compliant body in water.

TABLE II
UNDAMPED NATURAL FREQUENCIES OF THE COMPLIANT BODY IN WATER

f_{n1} [Hz]	f_{n2} [Hz]	f_{n3} [Hz]	f_{n4} [Hz]	f_{n5} [Hz]	f_{n6} [Hz]
0.7924	3.7495	12.2776	33.0006	457.6453	9634

B. Experimental Model Validation

These experiments are carried out to validate the proposed theoretical modelling. In this framework, the robot is fixed in a steady position and the compliant body is actuated by a known torque. The motion of the midline is tracked using a video-camera filming at a rate of 50 frames/second. The videos are then processed manually using Matlab. Torques with different amplitudes and frequencies are applied to the compliant body. The measured lateral deflections are

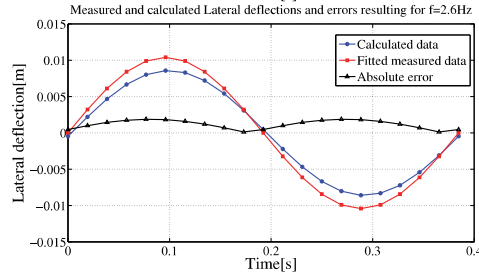
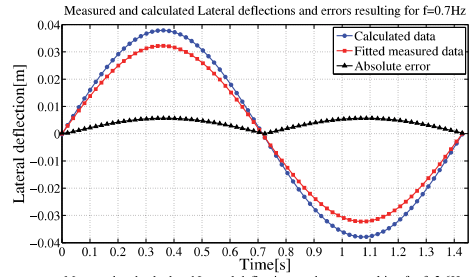


Fig. 7. Experimental, calculated lateral deflections and absolute errors in water of the bottom of the compliant body for $M(t) = \sin(w*t)$.

then compared to those calculated by the assumed modes method. The results show that for large deflections (20% of the compliant body length) the absolute errors between the measured and calculated motions are relatively small (around 17% of the compliant body length). These errors become more important in the case of small lateral deflections (5% of the flexible part length) and are around 40% of the compliant body length. This is because the tracking is done manually and in the case of small deflection the imprecision becomes more important. Fig.7 shows the graphs of the calculated and measured lateral deflection of the midline's point at the bottom of the compliant body during one actuation period with $M = \sin(wt)$.

C. Experiments on the Robot

The experimental setup shown in fig.8 is used to measure the thrust generated by the compliant body while the robot being held in a static position on a force plate. Experiments are carried out while the compliant body is actuated with different frequencies f and amplitudes M_0 . Fig.9 shows the average speed and thrust as a function of actuation frequency for $M_0=1Nm$. One can see that the speed and thrust increase with the frequency.

V. CONCLUSION AND FUTURE WORK

This paper describes the design and experiments carried out on a bio-inspired fish-like robot. It brings many contributions to the field of compliant underwater robots modelling and control in particular:

- an analytical approach to model the dynamics of robots with non-homogeneous compliant parts;

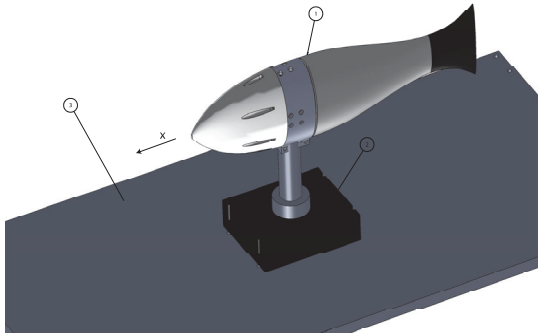


Fig. 8. Experimental setup used to measure the static thrust. 1-the biomimetic fish robot; 2-force sensor; 3-metallic plate

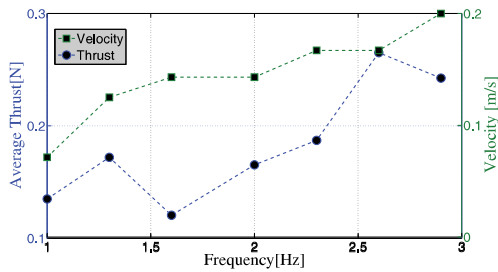


Fig. 9. Average thrust and velocity as function of actuation frequency

- experimental methods to estimate the internal damping and hydrodynamic forces;
- a model for the effect of adding a passive rigid fin to the end of the compliant body;
- a prototype for bio-inspired fish like robot.

Future work should address the problem of adding flexible parts with variable elasticity to the design to force the system to vibrate near its natural frequencies and to reduce energy consumption.

REFERENCES

[1] K. Streitlien, G.S. Triantafyllou, M.S. Triantafyllou, "Efficient foil propulsion through vortex control", *AIAA Journal*, vol. 34, pp. 2315-2319, 1996.

[2] J.M. Anderson, "Vorticity control for efficient propulsion", Ph.D. dissertation, Massachusetts Institute of Technology, Department of Ocean Engineering, 1996.

[3] J.M. Kumph, "Maneuvering of a robotic pike", Master of Science dissertation, Massachusetts Institute of Technology, Department of Ocean Engineering, 2003.

[4] J. Liu and H. Hu, "Novel mechatronics design for a robotic fish". In Proceedings of IEEE/RSJ International Conference on Intelligent Robots and Systems (IROS), Edmonton, Canada, pp. 2077-2082, 2005.

[5] J. Liu and H. Hu, "Mimicry of sharp turning behaviours in a robotic fish". In Proceedings of IEEE International Conference on Robotics and Automation Barcelona, Spain, pp. 3329-3334, April 2005.

[6] J. Liu and H. Hu, "A 3D Simulator for autonomous robotic fish". *International Journal of Automation and Computing*, Vol.1, No.1, pp. 42-50, 2004.

[7] J. Liu and H. Hu, "Building a 3D simulator for autonomous navigation of robotic fishes". In Proceedings of IEEE/RSJ International Conference on Intelligent Robots and Systems (IROS), pp. 613-618, 2004.

[8] J. Liu and H. Hu, "Building a simulation environment for optimising control parameters of an autonomous robotic fish", Proceedings of CACSCUK, Luton, pp. 317-322, 2003

[9] <http://www.nmri.go.jp/eng/khirata/fish/>

[10] J.Y. Cheng, T.J. Pedley and J.D. Altringham, "A continuous dynamic beam model for swimming fish". *Philosophical Transactions of the Royal Society of London Series B: Biological Sciences*, Vol. 353, pp. 981-997, 1998.

[11] A.R. Blight, "Undulatory swimming with and without waves of contraction", *Nature*, Vol. 264, pp. 352-354, 1976.

[12] A.R. Blight, "The muscular control of vertebrate swimming movements", *Biological Reviews*, Vol. 52, Issue 2, pp. 181-218, 1977.

[13] J.H. Jr.Long, M.J. McHenry and N.C. Boetticher, "Undulatory swimming: How traveling waves are produced and modulated in sunfish (*Lepomis Gibbosus*)". *Journal of Experimental Biology*, Vol. 192, pp. 129-145, 1994.

[14] Z. Chen, S. Shatara and X. Tan, "Modelling of biomimetic robotic fish propelled by an Ionic Polymer-Metal composite caudal fin", *IEEE/ASME Transactions on Mechatronics*, Vol. 15, No. 3, pp. 448-459, 2010.

[15] P. V y Alvarado, and K. Youcef-Toumi, *Design of Machines with Compliant Bodies for Biomimetic Locomotion in Liquid Environments*, *ASME Journal of Dynamic Systems, Measurement, and Control*, 128, 3-13, March 2006.

[16] P. Valdivia y Alvarado. "Design of biomimetic compliant devices for locomotion in liquid environments". PhD thesis, Massachusetts Institute of Technology, 2007.

[17] W.T. Thomson, "Theory of vibration with applications", 2nd edition, Prentice-Hall, Englewood Cliffs, NJ, 1981.

[18] A.R. Fraser and R.W. Daniel, "Perturbation Techniques for Flexible Manipulators", Kluwer International Series in Engineering and Computer Science, Vol. 138, Kluwer, Boston, MA, 1991.

[19] J.L. Junkins and Y. Kim, "Introduction to dynamics and control of flexible structures", Education Series, J. S. Przemieniecki, Editor-in-Chief, AIAA, Washington, DC, 1993.

[20] R.D. III Robinett, C. Dohrmann, G.R. Eisler, J. Feddema, G.G. Parker, D.G. Wilson, and D. Stokes, "Flexible Robot Dynamics and Controls", International Federation for Systems Research, International Series on Systems Science and Engineering, Vol. 19, Kluwer, Dordrecht, 2002.

[21] H. Baruh, "Analytical Dynamics", McGraw-Hill International Editions, 1999.

[22] D.J. Wagg, S.A. Neild, "Nonlinear vibration with control for flexible and adaptive structures". Series: Solid Mechanics and Its Applications, Vol. 170. A Springer-SBM - Canopus Academic Publishing Ltd co-publication 1st Edition, 2010.

[23] S. Adhikari and A.S. Phani, "Experimental identification of generalised proportional viscous damping matrix". *Transactions ASME: Journal of Vibration and Acoustics*, Vol. 131, pp. 011008-01-011008-11, 2009.

[24] S. S. Rao, "Mechanical vibrations", Pearson Prentice Hall, 2004.

APPENDIX E

H. El Daou, T. Salumäe, L. D. Chambers, W. M. Megill, and M. Kruusmaa, “Modelling of a biologically inspired robotic fish driven by compliant parts.,” *Bioinspiration & Biomimetics.*, vol. 9, no. 1, p. 016010, Mar. 2014.

Modelling of a biologically inspired robotic fish driven by compliant parts

Hadi El Daou^{1,3}, Taavi Salumäe¹, Lily D Chambers², William M Megill²
and Maarja Kruusmaa¹

¹ Centre of Biorobotics, Tallinn University of Technology, 12618, Tallinn, Estonia

² Department of Mechanical Engineering, University of Bath, BA2 7AY, UK

E-mail: h.el-daou@imperial.ac.uk, taavi.salumae@ttu.ee, l.chambers@bristol.ac.uk,
william.megill@hsrw.eu and maarja.kruusmaa@ttu.ee

Received 18 July 2013, revised 2 December 2013

Accepted for publication 6 December 2013

Published 22 January 2014

Abstract

Inspired by biological swimmers such as fish, a robot composed of a rigid head, a compliant body and a rigid caudal fin was built. It has the geometrical properties of a subcarangiform swimmer of the same size. The head houses a servo-motor which actuates the compliant body and the caudal fin. It achieves this by applying a concentrated moment on a point near the compliant body base. In this paper, the dynamics of the compliant body driving the robotic fish is modelled and experimentally validated. Lighthill's elongated body theory is used to define the hydrodynamic forces on the compliant part and Rayleigh proportional damping is used to model damping. Based on the assumed modes method, an energetic approach is used to write the equations of motion of the compliant body and to compute the relationship between the applied moment and the resulting lateral deflections. Experiments on the compliant body were carried out to validate the model predictions. The results showed that a good match was achieved between the measured and predicted deformations. A discussion of the swimming motions between the real fish and the robot is presented.

Keywords: biologically inspired robots, underwater, robotics, dynamics of flexible robots

(Some figures may appear in colour only in the online journal)

1. Introduction

The high efficiency, manoeuvrability and agility of fish exceed by far those of existing underwater vehicles and ships [1]. These characteristics make fish a good source of inspiration for engineers and scientists aiming to design and build underwater vehicles capable of manoeuvring in complex environments without the limitations involved in using conventional propellers [2, 3]. In recent years, robotics researchers and biologists have studied fish locomotion with the aim of building more efficient devices copying the shape of fish bodies and mimicking their motion [4].

Most of the early designs used rigid links and discrete mechanisms to achieve fish-like motion, dynamics and behaviour [5–9]. While mimicking the motion of fish was successful, these systems had relatively high energy

consumptions, large bodies and were noisy. As the robots increased in complexity to better mimic the natural swimming, this increased the complexity of their control.

To overcome these limitations, researchers in robotics investigated the use of flexible parts in their designs. Compared to their rigid counterparts, flexible robots have the advantage of lower cost, higher speed, less complexity in the design, lighter weight, no joints and fewer actuators, all of which contribute to reducing the power consumption [10].

The use of flexible materials in robots began with space robotics research [11, 12] and expanded into other disciplines including nuclear maintenance [13, 14], micro surgery [15, 16], micro motion devices [17], mechanical amplifiers [18], painting and drawing robots and pattern recognition through haptics and many other applications [19]. Currently, soft robotics is an emerging field receiving progressively more attention [20].

³ Author to whom any correspondence should be addressed.

Several studies have addressed the use of compliant materials in the design of underwater robots. Chen *et al* [21] developed a robotic fish using smart materials for caudal fin design. The purpose of their study was to increase efficiency by focusing on the unique physics of ionic polymer metal composite (IPMC) materials and their interaction with the fluid. Their robot was 0.2 m long, 0.052 m wide and 0.063 m tall; it had a maximum speed of 0.11 BL s^{-1} when operated at 1.6 Hz. Zhang *et al* [22] built a bio-inspired prototype fish using a flexible matrix composite muscle technology for fin and body actuation. A coupled fluid-structure model was developed to predict the response and understand the dynamics of the system. The overall response of the artificial fish agreed with the predicted response. Ahlborn *et al* [23] carried out experiments to measure thrust and forward impulse of a computer controlled fish-tail. They showed that the propulsive forces of fast-start swimming can be optimized by using a flexible tail with moderate elasticity. Lauder *et al* [24] presented new experimental and hydrodynamic data for bluegill sunfish and used particle image velocimetry to show that continuous thrust production is due to fin flexibility. Park *et al* [25] conducted experiments to find the optimal compliance of a fin that maximized thrust. They reported that the maximum thrust was achieved when the fin-bending angle, due to the movement of the caudal fin, lags behind the driving angle, which is driven by the motor, by approximately $\frac{\pi}{2}$. Aureli *et al* [26] developed a modelling framework for studying free-locomotion of biomimetic underwater vehicles propelled by vibrating IPMCs. The model predictions were validated through experimental results on a miniature remotely controlled fish-like robotic swimmer. Youngsu Cha *et al* [27] studied energy harvesting from the beating of a biomimetic fish tail using IPMCs. They designed and modelled the dynamics of a tail inspired by the morphology of the heterocercal tail of thresher sharks. Their models predictions were in a good agreement with their experimental results for a wide range of frequencies and for moderately large-amplitude oscillation. Other examples of soft underwater robots include a compliant octopus arm [28] and the FESTO Aqua-Ray [29]. A series of fish robots using compliant bodies was developed at MIT [30], inspired by bony fish that use carangiform swimming motion. The assumption in that study was that the posterior part could be modelled by a cantilever beam actuated at a single point and studied the dynamics in order to mimic fish swimming motions. They reported that the swimming performance of their robot was comparable to that of a real fish despite considerable errors in the targeted kinematics.

The present study investigates the use of several compliant design concepts to build simple and efficient underwater vehicles [36, 37]. It tackles the similar problem of single-point actuated compliant tails [38] and uses the findings in [39, 40] to present a general framework for modelling and validating the dynamics of the compliant part. This design approach is inspired by studies in which electromyography muscle activity measurements of swimming fish have revealed that for swimming at cruising speeds (1 to $2 \text{ body length s}^{-1}$) fish use mainly anterior muscles while the posterior part of the body carries the travelling wave passively to transfer the

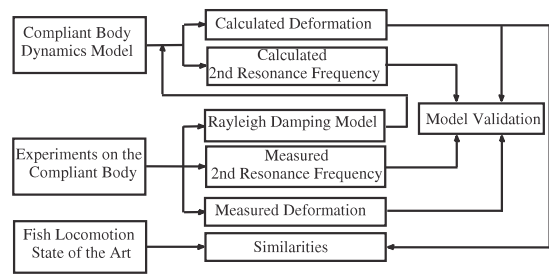


Figure 1. Basic summary of the study.

momentum to the surrounding fluid [31–33]. Other studies emphasize the importance of the material properties of fish (in particular stiffness) in determining the operating frequency of the fish body and tail [34, 35].

In [30] and [39], it is assumed that it is possible to duplicate fish swimming motion with a robot by using a model that acquires fish motion as an input and the desired motor torque as the output. In the present study, we show that the compliant body is limited in motion and can only deform in defined shapes or modes that are dependent on the actuation frequency and the natural frequencies of the system. The dynamics of the compliant body are studied using the assumed modes method to find a relationship between the applied force and the resulting deflections.

In contrast to previous work, the mechanical modelling in this study takes into account the inhomogeneous distribution of material along the compliant body and the effects of attaching a rigid caudal fin to its trailing end. This has not been previously modelled to the authors' knowledge but has a significant effect on the hydrodynamics of swimming. The use of a rigid plate for actuating the compliant body is also taken into account: its own elasticity was measured and included in the model. If this parameter was neglected, inaccurate modelling of the system could occur.

Lighthill's elongated body theory [43] is used in the present study to model the interaction between the fish-like robot and the surrounding water. In previous studies [30, 39, 40], the hydrodynamic forces have been modelled in terms of added mass, or in [38], in a term analogous to viscous damping. In the present study, Lighthill's elongated body theory is used to model the interaction between the fish-like robot and the surrounding water, since it is more general and suited for the geometry and dynamics of subcarangiform and carangiform swimmers [43].

Damping is of great importance in the dynamic design of compliant structures. The effect of damping was not considered in [30, 39]. A more general damping model than that in [40] is presented in this paper.

The remainder of this paper is organized as follows (figure 1). In section 2 the prototype is presented. A model for the compliant body is presented in section 3 and the equations of motion are derived. Section 4 describes the experiments which were carried out on the compliant body to validate the proposed theoretical approach. An analysis of similarities in behaviour between the robot and subcarangiform swimmers

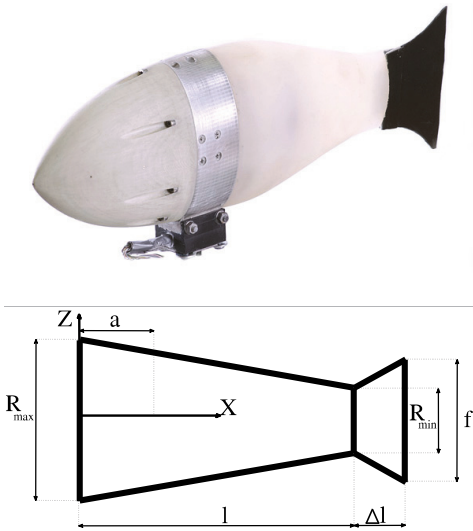


Figure 2. Photograph of the FILOSE fish-like robot and a schematic illustrating the compliant part's definition of dimensions.

is presented in section 5. Finally, section 6 highlights the contributions and future perspectives.

2. Robot description

Figure 2 shows the robot's prototype and the definitions of its dimensions. It is based on the design described in [30, 38] and mimics subcarangiform swimmers by incorporating a rigid $\frac{2}{5}$, and $\frac{3}{5}$ compliant body and caudal fin to pass the travelling wave.

The fish-like robot has five pressure sensors (MS5407-AM, Measurement Specialities Inc., Hampton, USA) incorporated in the head and was designed to use readings from flow to control its robot's motion in real time [41, 42]. No flow measurements were used in this study.

The physical prototype consists of an aluminium joiner connecting a rigid head to a compliant body and a rigid fin. The actuation mechanism is composed of an aluminium plate cast within the compliant body and actuated using two steel cables and a servo-motor housed in the head. The head was machined using CNC and rapid prototyping techniques whereas the compliant part was cast together with the actuation plate in special moulds copying the dimensions of a subcarangiform swimmer. A platinum cure silicon rubber Dragon Skin 20 (Smooth-On Inc., Easton, Pennsylvania, USA) was used to build the compliant part and Slacker Tactile Mutator (Smooth-On Inc., Easton, Pennsylvania, USA) was added to alter its elasticity.

Young's modulus of elasticity was chosen experimentally by compromising between the mechanical properties of the rubber and the maximum motor torque. Experiments were carried out on different compliant bodies with different modulus of elasticity. The optimal value was defined as the

Table 1. Compliant part's dimensions and material properties.

Dimensions of the compliant body	
Length l	0.22 m
Max. height R_{\max}	0.15 m
Min. height R_{\min}	0.075 m
Max. width	0.08 m
Dimensions of the rigid fin	
Length Δl	0.08 m
Max. height f	0.14 m
Material properties	
$E_{\text{compliant body}}$	83 Kpa
$\rho_{\text{compliant body}}$	1080 kg m ⁻³
Actuation properties	
E_{plate}	63 Gpa
ρ_{plate}	2700 kg m ⁻³
a	0.07 m

one that generated the highest thrust without overloading the servo-motor.

The motor used for actuation is a Futaba BLS152 brushless servo with a maximum torque of 3 Nm. The robot's head also houses a 400 MHz miniature ARM computer and voltage regulators for the motor and electronics.

The caudal fin is made of light plastic materials. The robot is tethered by a cable and is controlled using NI Labview software (National Instruments Corporation, Austin, Texas, USA) running on an external PC. Table 1 summarizes the dimensions and materials properties of the compliant part.

3. Compliant body modelling and dynamics

In this section, a model for the compliant body is presented and the equations of motion are derived. The fish-like robot designed in this study copies the geometrical properties of a subcarangiform swimmer. A subcarangiform swimmer produces propulsion by undulating approximately $\frac{2}{3}$ of its body to produce the propulsive wave responsible for forward motion while the movement of the anterior part of the body is reduced. Therefore this paper focuses on modelling the undulating motion of the compliant body and the rigid caudal fin.

3.1. The model

Figure 3 shows the compliant body model used in this study. The compliant body is modelled as a cantilever beam with variable cross-section actuated by a time varying moment applied at a distance a from the base. The external forces acting on the compliant body are: the hydrodynamic forces $L(x, t)$, the concentrated force and moment $F_{\text{fin}(t)}$ and $M_{\text{fin}(t)}$ resulting from the hydrodynamic forces on the rigid caudal fin. The inertial properties of the rigid caudal fin are ignored.

It is assumed that the fish-like robot swims at a fixed depth and thus moves only in the x - y plane. Lighthill's elongated body theory predicts that the hydrodynamic force $L(x, t)$, for an inviscid steady flow with small amplitude lateral motion, can be modelled by the material derivative of the

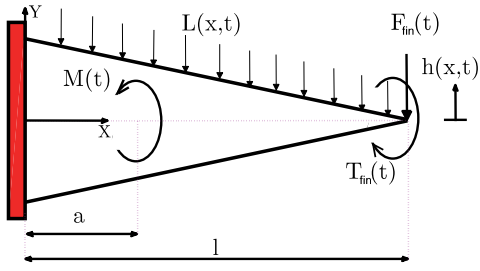


Figure 3. Structural model of the compliant body. $a =$ distance between the base of the compliant body and the actuation point, $l =$ length of the compliant body, $M(t) =$ actuation moment, $L(x, t) =$ hydrodynamic distributed forces, $F_{fin}(t)$, $M_{fin}(t) =$ concentrated force and moment resulting from the hydrodynamic forces on the rigid caudal fin and $h(x, t) =$ lateral line deflection.

lateral momentum. This theory considers elongated bodies that are laterally symmetric, with small body surface slopes, and zero cross-sectional areas at both ends. The distributed hydrodynamic force $L(x, t)$ per unit length for an inviscid steady flow is considered perpendicular to the compliant body midline and expressed as [43]:

$$\begin{aligned}
 L(x, t) &= \left(\frac{\partial}{\partial t} + U \frac{\partial}{\partial x} \right) \left[m(x) \left(\frac{\partial h}{\partial t} + U \frac{\partial h}{\partial x} \right) \right] \\
 &= m(x) \left(\frac{\partial^2 h}{\partial t^2} + 2U \frac{\partial^2 h}{\partial x \partial t} + U^2 \frac{\partial^2 h}{\partial x^2} \right) \\
 &\quad + U \frac{\partial m(x)}{\partial x} \left(\frac{\partial h}{\partial t} + U \frac{\partial h}{\partial x} \right) \quad (1)
 \end{aligned}$$

where $m(x)$ is the added mass of the cross-section per unit length, U the uniform free stream velocity relative to the fish and $h(x, t)$ is the lateral displacement of the compliant body. The existence of a shedding vortex at sections along the contracting part of the body makes the material rate of change in fluid momentum independent of the longitudinal variation of the cross-flow added mass (due to body shape alone) [44]. Equation (1) can be further simplified to give an expression of the hydrodynamic force $L(x, t)$:

$$L(x, t) = m(x) \left(\frac{\partial^2 h}{\partial t^2} + 2U \frac{\partial^2 h}{\partial x \partial t} + U^2 \frac{\partial^2 h}{\partial x^2} \right). \quad (2)$$

Since the rigid fin is very light, its inertial properties are negligible compared to the propelled virtual fluid and are thus ignored in the present study. The concentrated force and moment resulting from the hydrodynamic forces on the rigid caudal fin are:

$$F_{fin}(t) = - \int_l^{l+\Delta l} L(x, t) dx \quad l < x < l + \Delta l \quad (3)$$

$$M_{fin}(t) = - \int_l^{l+\Delta l} L(x, t)(x - l) dx \quad l < x < l + \Delta l \quad (4)$$

where Δl is the length of the rigid caudal fin. From (2), (3) and (4), one can see that the concentrated force and moment resulting from the hydrodynamic forces on the caudal fin depend on its length and on the added mass of the cross-section $m(x)$.

3.2. Dynamics of the compliant body

The robotic fish is a continuous dynamic system with infinite degrees of freedom. An exact solution for such a system is not feasible; approximate techniques and a discretization method are used instead. Three discretization formulations exist: assumed modes, finite elements and lumped-parameter methods.

The lumped-parameter approach uses pseudo joints and linear springs to model the flexibility of compliant parts. This technique is simple but its difficulty is in determining the optimal number of joints and springs' constants [45, 46].

Theodore *et al* [46] compared the assumed mode to the finite element method, their study showed that the assumed modes formulation is suitable for systems with one flexible link and for numerical simulation purposes while the finite element formulation is recommended for flexible multilink systems with complex cross-sectional geometries. The robot fish has only one flexible body and its cross-sectional geometry is relatively simple; for these reasons the assumed mode approach was used in this study.

The method of assumed-modes aims at deriving the equations of motion by first discretizing the kinetic energy, potential energy and the virtual work and making use of Lagrange's equation of motion. Elastic deformations are modelled by a finite series of space-dependent admissible functions multiplied by a specific set of time dependent amplitude functions resulting in amplitudes that form the generalized configuration coordinates in the Lagrange dynamics formulation [47]:

$$h(x, t) = \sum_{r=1}^n \varphi_r(x) q_r(t) \quad 0 < x < l \quad (5)$$

where:

- $\varphi_r(x)$: are known trial functions. In this study, the eigenfunctions of a uniform cantilever beam are chosen as trial functions.
- $q_r(t)$: are unknown generalized coordinates.
- n : is the order of the expansion.

Considering that the passive caudal fin is rigid compared to the compliant body, its lateral deflection $h(x, t)$ can be expressed as:

$$\begin{aligned}
 h(x, t) &= h(l, t) + \frac{\partial h(l, t)}{\partial x} (x - l) \quad l < x < l + \Delta l \\
 &= \sum_{i=1}^n (\varphi_i(l) q_i(t) + \varphi_i'(l) q_i(t) (x - l)). \quad (6)
 \end{aligned}$$

The external forces acting on the compliant body are the time varying moment $M(t)$, the distributed hydrodynamic forces $L(x, t)$, the concentrated moment $M_{fin}(t)$ and the concentrated force $F_{fin}(t)$. Substituting (6) and (2) into (3) and (4) yields:

$$\begin{aligned}
 F_{fin}(t) &= - \sum_{i=1}^n \ddot{q}_i(t) [\alpha \varphi_i(l) + \beta \varphi_i'(l)] - 2U \sum_{i=1}^n \dot{q}_i(t) \alpha \varphi_i'(l) \quad (7)
 \end{aligned}$$

$$M_{\text{fin}}(t) = -\sum_{i=1}^n \dot{q}_i(t) [\beta \varphi_i(l) + \gamma \varphi_i'(l)] - 2U \sum_{i=1}^n \dot{q}_i(t) \beta \varphi_i'(l) \quad (8)$$

where:

$$\alpha = \int_l^{l+\Delta l} m(x) dx \quad \beta = \int_l^{l+\Delta l} m(x)(x-l) dx$$

$$\gamma = \int_l^{l+\Delta l} m(x)(x-l)^2 dx.$$

The kinetic and potential energies of the beam can be written as:

$$T(t) = \frac{1}{2} \int_0^l \mu(x) \left(\frac{\partial h(x,t)}{\partial t} \right)^2 dx$$

$$= \frac{1}{2} \sum_{i=1}^n \sum_{j=1}^n \dot{q}_i(t) \dot{q}_j(t) \int_0^l \mu(x) \varphi_i(x) \varphi_j(x) dx \quad (9)$$

$$V(t) = \frac{1}{2} \int_0^l EI(x) \left(\frac{\partial^2 h(x,t)}{\partial x^2} \right)^2 dx$$

$$= \frac{1}{2} \sum_{i=1}^n \sum_{j=1}^n q_i(t) q_j(t) \int_0^l EI(x) \varphi_i''(x) \varphi_j''(x) dx. \quad (10)$$

Note that $\mu(x)$ and $EI(x)$ are the mass per unit length and the stiffness at x respectively.

The total virtual work can be expressed as:

$$\delta W = \delta W_1 + \delta W_2 + \delta W_3 + \delta W_4$$

where δW_1 , δW_2 , δW_3 and δW_4 are respectively the virtual works of the actuation moment $M(t)$, the hydrodynamic forces $L(x, t)$, the concentrated force F_{fin} and the concentrated moment $M_{\text{fin}}(t)$. See appendix for the detailed derivation of the virtual work.

The kinetic and potential energies are now expressed in terms of n coordinates, thus the system is approximated as an n -dimensional discrete one. The discretized forms of the kinetic and potential energies and the virtual work are used together with the Lagrange's equations to write the equations of motion of the approximate system as:

$$[M]\{\ddot{q}(t)\} + [C]\{\dot{q}(t)\} + [K]\{q(t)\} = \{Q(t)\} \quad (11)$$

where:

$$m_{ij} = \int_0^l (\mu(x) + m(x)) \varphi_i(x) \varphi_j(x) dx + \alpha \varphi_i(l) \varphi_j(l)$$

$$+ \beta (\varphi_i'(l) \varphi_j(l) + \varphi_i(l) \varphi_j'(l)) + \gamma \varphi_i'(l) \varphi_j'(l)$$

are the mass coefficients and

$$k_{ij} = \int_0^l EI(x) \varphi_i''(x) \varphi_j''(x) dx + U^2 \int_0^l m(x) \varphi_i(x) \varphi_j''(x) dx \quad (12)$$

are the stiffness coefficients. $\int_0^l m(x) \varphi_i(x) \varphi_j''(x) dx \ll \int_0^l EI(x) \varphi_i''(x) \varphi_j''(x) dx$, (12) can be further simplified to yield:

$$k_{ij} = \int_0^l EI(x) \varphi_i''(x) \varphi_j''(x) dx. \quad (13)$$

The generalized force associated with the generalized coordinate $q_i(t)$ is:

$$Q_i(t) = -\int_0^l M(t) \underline{\underline{\delta}}'(x-a) \varphi_i(x) dx.$$

The damping of the compliant body in water includes both internal damping due to the structural material and external damping caused by energy loss to the surrounding fluid;

$$C = C_i + C_e$$

where C_i and C_e are respectively the internal and external damping matrices. The external damping coefficients are:

$$C_{eij} = 2U \left[\int_0^l m(x) \varphi_i(x) \varphi_j'(x) dx + (\alpha \varphi_i(l) + \beta \varphi_i'(l)) \varphi_j'(l) \right].$$

Proportional damping is used to model both internal and external damping; it is a particular type of viscous damping [48]. The proportional damping model expresses the damping matrix as a linear combination of the mass and stiffness matrices, that is for the internal damping:

$$C_i = \alpha_1 M + \alpha_2 K \quad (14)$$

where α_1 and α_2 are constant scalars. The procedure to calculate these two constants is discussed later in this paper. To find the response of (11), the eigenvalue problem for the undamped case is first solved introducing:

$$q(t) = ae^{\lambda t}.$$

This leads to the following characteristic equation:

$$\det(\lambda^2 M + K) = 0$$

where $\lambda_r = -iw_{nr}$ and w_{nr} are the undamped natural frequencies of the approximate system. To obtain the solution of (11), the following linear transformation is used:

$$q(t) = \chi \eta(t) \quad (15)$$

where:

$$\chi = [a_1 a_2 a_3 a_4 a_5 \dots a_m].$$

Where a_r is the eigenvector associated with the eigenvalue $\lambda_r = -iw_{nr}$. The eigenvectors are orthogonal with respect to the mass and stiffness matrices. They are normalized to yield:

$$a_r^T M a_s = \delta_{rs} \quad a_r^T K a_s = w_{nr}^2 \delta_{rs}$$

δ_{rs} is defined as the Kronecker delta.

Substituting (15) into (11) and multiplying by χ^T , the independent modal equations are then obtained:

$$\ddot{\eta}(t) + \Lambda \eta(t) = N(t) \quad (16)$$

in which :

$$\Lambda = \text{diag}[w_{n1}^2, w_{n2}^2, w_{n3}^2, w_{n4}^2, w_{n5}^2, w_{n6}^2, \dots, w_{nm}^2]$$

and

$$N(t) = \chi^T Q(t) \quad (17)$$

The result is that for the i th mode:

$$\ddot{\eta}_i(t) + 2\zeta_i w_{ni} \dot{\eta}_i(t) + w_{ni}^2 \eta_i(t) = N_i(t). \quad (18)$$

The solution of (18) can be written by components in the form of convolution integrals as follows:

$$\eta_i(t) = \frac{1}{w_{di}} \int_0^t e^{-\zeta_i w_{ni} \tau} N_i(t-\tau) \sin(w_{di} \tau) d\tau \quad (19)$$

where $w_{di} = \sqrt{1 - \zeta_i^2} w_{ni}$ is the damped natural angular frequency.

Finally using (15), the generalized coordinates are calculated. The lateral deflections of the compliant body are then computed using (5).

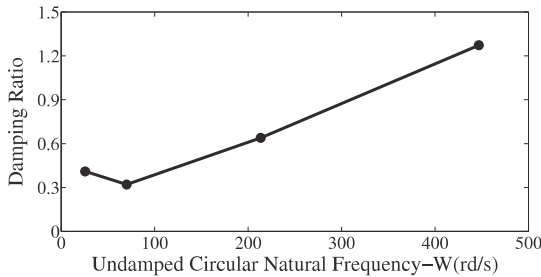


Figure 4. Damping ratio versus undamped natural frequency.

4. Parameters identification and experimental validation

This section describes the experiments carried out on the compliant body to estimate the internal damping factors and to validate the proposed theoretical modelling.

4.1. Internal damping estimation

With the assumption of Rayleigh proportional damping, the two constants α_1 and α_2 from (14) can be calculated using the following equation [47, 49]:

$$2\zeta_i w_{ni} = \alpha_1 + w_{ni}^2 \alpha_2. \quad (20)$$

From (20), it can be observed that α_1 and α_2 depend on the natural frequencies and damping ratios of the system. Computing Rayleigh damping coefficients is then a procedure that involves experiments to measure a sufficient number of damping factors and solving the eigenvalue problem to calculate the undamped natural frequencies using the approach developed earlier in this paper.

Only the first two damping factors were estimated using a frequency response method described in [40], measuring the remaining factors was not possible as appropriate measurement instruments were not available during this study. These limitations resulted in errors when estimating the Rayleigh damping coefficients, however, when the theoretical results were compared to experimental results a good approximation was achieved. α_1 and α_2 are then calculated using:

$$\begin{pmatrix} \alpha_1 \\ \alpha_2 \end{pmatrix} = \begin{pmatrix} 1 & w_{n1}^2 \\ 1 & w_{n2}^2 \end{pmatrix}^{-1} \times \begin{pmatrix} 2\zeta_1 w_{n1} \\ 2\zeta_2 w_{n2} \end{pmatrix}.$$

Figure 4 shows the graph of the damping ratios calculated using (20) versus the undamped natural frequencies, the first portion of the graph shows marked nonlinearity and thereafter the variation becomes linear.

4.2. Theoretical model experimental verification

In this section, two kinds of experiments were performed to validate the theoretical modelling of the compliant body dynamics. These experiments were carried out in still water.

4.2.1. Second natural frequency in water. The overall objective is to compare the calculated and measured second

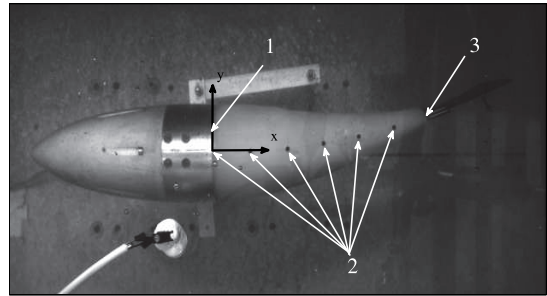


Figure 5. Video image of the fish-like robot in motion top view. 1-reference frame, 2-metallic markers, 3-tip of the compliant body.

resonant frequency of the compliant body immersed in water. The second resonance frequency was examined as it was the simplest to measure; in fact the first resonance frequency in water was small while the higher natural frequencies create a lot of resonance in the water tank and may damage the system. It was also important to choose the actuation frequency of the compliant body close to the second resonance frequency in water to decrease the energy consumption of the servo-motor.

The second resonant frequency of the immersed compliant body was measured in an earlier study[40] to be 3.37 ± 0.1 Hz. To calculate the second resonant frequency, the second undamped natural frequency f_{n2} was calculated using the approach developed in section 3 and found to be equal to 3.45 Hz. The second resonant frequency is then calculated as $f_{n2} \sqrt{1 - 2 \times \zeta_2^2} = 3.45 \sqrt{1 - 2 \times 0.32^2} = 3.1$ Hz. The relative percentage of error between the measured and calculated second resonance frequency is equal to 8%.

4.2.2. Comparison of experimental and theoretical lateral deflections.

In this framework, the robot was fixed in a steady position (see figure 5) and the compliant body was actuated by a torque of known value $M(t) = M_0 \sin(2\pi ft)$. The motion of the compliant body midline was tracked using a video camera recording at 50 frames s^{-1} . The videos were then processed and the midline trajectories measured and compared to those computed by the theory developed in section 2. The tracking was performed manually using software custom-written in Matlab.

Trials on the compliant body were carried out with different frequencies f and amplitudes M_0 . The lateral deflection of a point was defined as the y component toward a frame attached to the compliant body base as shown in figure 5.

In figure 6, the theoretical solution is compared to the average measured lateral deflection of the compliant body's tip for an actuation period $T = \frac{1}{f}$ s and for a torque amplitude $M_0 = 1$ Nm.

In tables 2 and 3, the ratio between the maximum theoretical and experimental lateral deflections and the compliant body's length ($l = 0.22$ m) were reported for the tip of the compliant body and markers 5, 4 and 3 at different actuation frequencies; where marker 5 designated the nearest metallic marker to the tip of the compliant body. The number of tests performed for each amplitude and frequency varied from

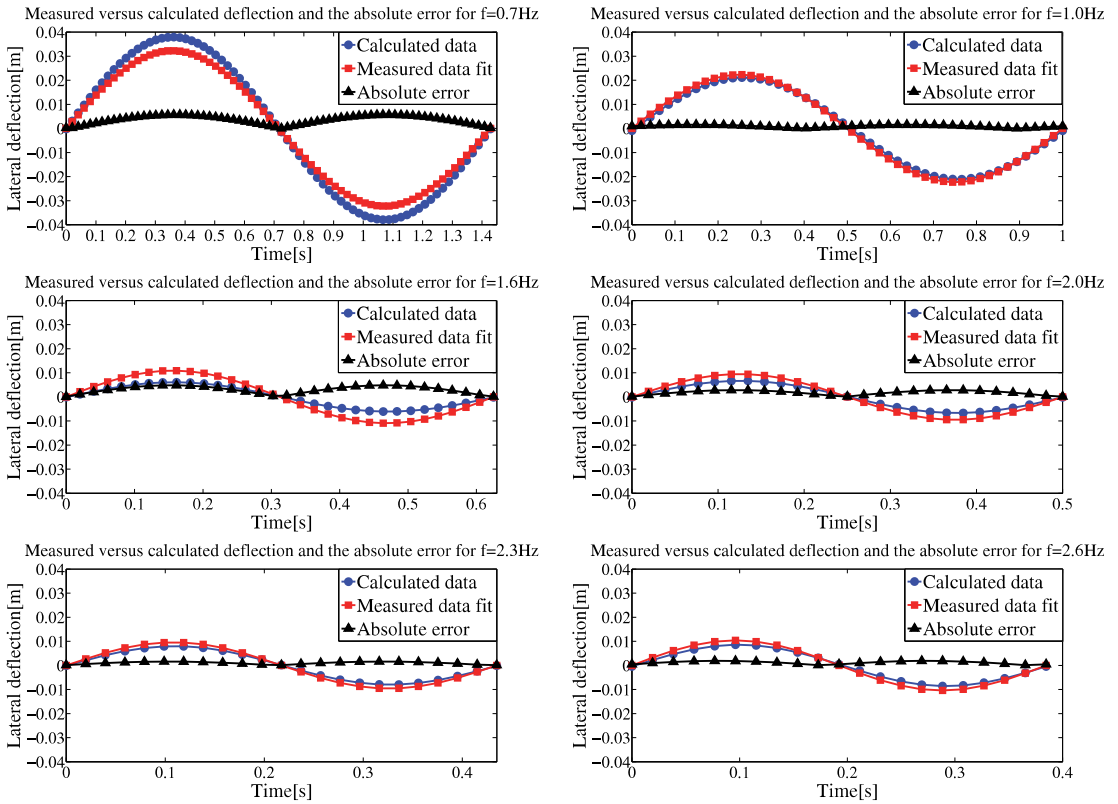


Figure 6. Graphs showing the values of experimental, calculated lateral deflection and absolute error (absolute value of the difference between the measured and calculated lateral deflection) in water of the tip of the compliant body midline during an actuation period for different values of actuation frequencies. The compliant body is actuated by a time varying moment $M(t) = \sin(\omega t)$.

Table 2. Ratio between the maximum theoretical lateral deflection and the compliant body’s length over a period.

Frequency	Marker3	Marker4	Marker5	Tip of the compliant body
0.7 Hz	0.0678	0.1010	0.1431	0.1690
1.0 Hz	0.0536	0.0667	0.0755	0.0934
1.6 Hz	0.0598	0.0689	0.0385	0.0281
2.0 Hz	0.0739	0.0878	0.0520	0.0326
2.3 Hz	0.0719	0.0871	0.0550	0.0348
2.6 Hz	0.0772	0.0960	0.0636	0.0418

5 to 15. In general the errors for the low frequencies are less than those of the higher frequencies. The maximum percentage of absolute errors between the theoretical and experimental results for the tip of the compliant body for $f = 0.7$ Hz and 1 Hz are 12% and 11% respectively. It increases for higher frequencies and reaches 48%, 42%, 28% and 32% for $f = 1.6$ Hz, 2.0 Hz, 2.3 Hz and 2.6 Hz respectively. The results for low frequencies $f = 0.7$ and 1 Hz are accurate and more reliable because the corresponding amplitude of deflection are considerably larger. The maximum lateral deflections of the compliant body’s tip for $f = 1.6, 2, 2.3$ and 2.6 Hz are

equal to 1.2, 1.24, 1 and 1.36 cm respectively. In contrast, the lateral deflection for $f = 0.7$ and 1 Hz are equal to 3.3 and 2.31 cm respectively. These results are also observed for the other markers and when actuating the compliant body with different torque amplitudes. It is believed that the source of error lies within the manual tracking used to measure the deformation of each marker and due to the difficulty in determining the damping ratios for the higher harmonics. Figure 7 shows graphs where the calculated motions of the robot’s compliant body midline are plotted against measured experimental deflections, during one period of tail oscillation, for $M_0 = 1$ Nm and $f = 0.7$ Hz.

5. Discussion

In this paper, the dynamics of a fish-like robot composed of a rigid head, a compliant body and a rigid caudal fin were developed using the assumed modes method. The hydrodynamic forces acting on the compliant body were modelled using Lighthill’s elongated body theory. Rayleigh proportional damping was used to model the dissipative forces in the structure and those resulting from the interaction with the surrounding fluid. The modelling was simplified by assuming

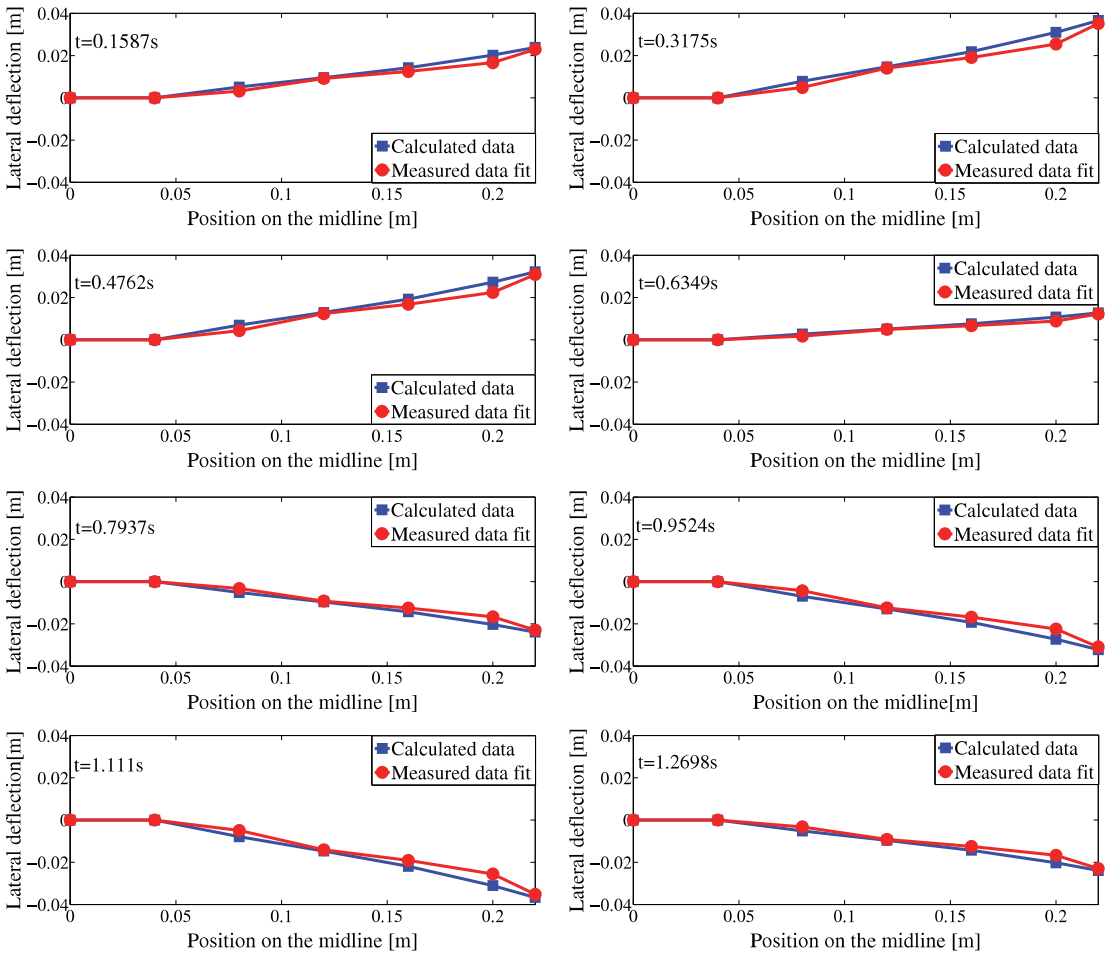


Figure 7. Comparison of predicted and measured kinematic behaviour of the compliant body for $f = 0.7$ Hz and $M_0 = 1$ Nm.

Table 3. Ratio between the maximum experimental lateral deflection and the compliant body's length over a period.

Frequency	Marker3	Marker4	Marker5	Tip of the compliant body
0.7 Hz	0.0550 ± 0.0009	0.0877 ± 0.0013	0.1168 ± 0.0011	0.1500 ± 0.0019
1.0 Hz	0.0459 ± 0.0015	0.0677 ± 0.0032	0.0814 ± 0.0032	0.1050 ± 0.0045
1.6 Hz	0.0555 ± 0.0136	0.0759 ± 0.0182	0.0773 ± 0.0182	0.0541 ± 0.0018
2.0 Hz	0.0473 ± 0.0091	0.0618 ± 0.0091	0.0591 ± 0.0114	0.0564 ± 0.0077
2.3 Hz	0.0455 ± 0.0045	0.0545 ± 0.0045	0.0532 ± 0.0014	0.0455 ± 0.0014
2.6 Hz	0.0559 ± 0.0045	0.0955 ± 0.0227	0.0782 ± 0.0014	0.0618 ± 0.0182

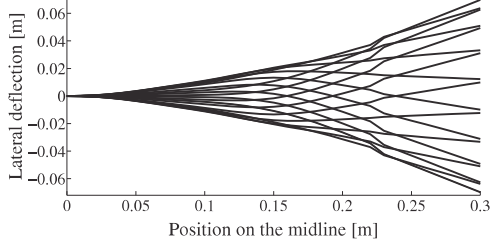
that the rigid caudal fin had negligible inertial properties, that a shedding vortex existed along the contracting part of the body and that computing Rayleigh damping coefficients can be achieved by measuring only two damping ratios. Despite these limitations, experiments on the compliant body showed a good agreement between the predicted and measured motions.

The kinematic envelope generated over 1 tail beat cycle by the robot's compliant body and caudal fin is shown in figure 8. In both cases of low (0.7 Hz) and high (1.6 Hz) frequencies,

the magnitude of the torques actuating the compliant body was $M_0 = 1$ Nm.

As the design is bio-inspired, a discussion of similarities with biological swimmers is important to adjust the current model in the future and to improve the design and performance. In comparison, in the kinematic envelope of a swimming trout the tail beat frequency increases linearly with swimming speed [50]. The wavelength (λ) on the body of the fish is independent of its swimming speed and is related to its size (L_f) by [51]:

Robot's compliant body and caudal fin midline through 1 beat cycle for $f=0.7$ Hz



Robot's compliant body and caudal fin midline through 1 beat cycle for $f=1.6$ Hz

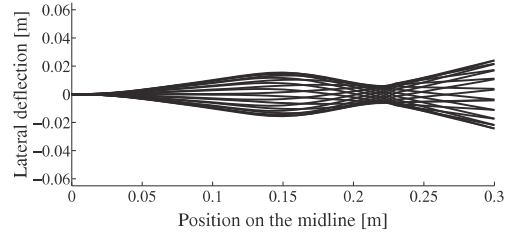


Figure 8. Robot's compliant body and caudal fin midline through 1 tail beat cycle for $f = 0.7$ Hz and 1.6 Hz.

$$\lambda = 1.43 \times L_f^{0.83}. \quad (21)$$

As the frequency increases the wavelength is maintained, providing the evidence as discussed by [52] that it is controlled by flexural stiffness. This is not the case for a material with constant elasticity as is clearly seen by the change from the lower to higher frequencies of the robot tail. The fish is a poly-articulated system that has a skeleton as well as higher elasticity than the robot tail. As proposed by [52], a fish is able to modify its stiffness profile to maintain the tail amplitude with increasing tail beat frequency. Many animals are known to actively tune their locomotive frequencies through control of their elastic oscillations [53]. At present, we demonstrate how this active tuning is possible with a robot composed from a body of constant elasticity and a model, and highlight the disparity between the elastic oscillations generated and those necessary to reproduce a fish's kinematic envelope. At the lower frequency of 0.7 Hz of the robot tail is vibrating in the first mode and at the higher frequency of 1.6 Hz (figure 8) it has moved to the second mode as is evident by the presence of a node at 0.22 m on the midline. However, as the tail beat increases on a swimming trout the fish remains in the first mode of vibration. The amplitude (A) of the tail beat is independent of swimming speed as well and is relatively smaller in larger fish, as is described in the equation from [51]:

$$A = 0.36 \times L_f^{0.74}. \quad (22)$$

The relative amplitude (A/L_f) decreases with increasing size of the fish where the tail beat amplitude for a trout of a size similar to that of the robot at 50 cm body length would be around 0.13. The robot as designed at present operates at a specific amplitude of 0.12 at low frequency, but it could not maintain this at the higher frequency and dropped to a relative amplitude of 0.04.

The mode shapes of the simplistic robot and biological subcarangiform swimming motion are of course different. One way to better achieve the propulsive mechanism of a fish would be to develop a variable stiffness robot body. The dynamic model developed in this research provides the building blocks from which to formulate and test which stiffness profile would be best suited. Moreover, the methodology used to elaborate the model can be generalized for the case of compliant bodies with variable stiffness. Lighthill's hydrodynamic forces, Rayleigh damping and the assumed method combined together with an energetic approach could be used to model the dynamics in the case of variable elasticity by introducing a variable term for the modulus of elasticity.

6. Conclusion and future work

A model for a robot fish with compliant parts was presented and a coupled fluid-structure model was developed to predict the response and understand the dynamics of the system. A comparison between the experimental and predicted response of the compliant part was achieved and a good agreement is found. The modelling technique is not specific and is applicable to similar fluid-structure coupling problems.

In this research the initial steps have been made, however many improvements still need to be made. In particular, future work should address the problem of adding flexible sections with variable elasticity to the design to force the system to vibrate near its natural frequencies and to reduce energy consumption. Another perspective is to study alternative designs for the compliant body especially the use of a flexible skeleton and addition of fins for stability control. Another area of interest is to research the energy efficiency of the robot and ways to increase it.

Acknowledgments

This work was carried out under the FILOSE project, supported by the European Union, seventh framework programme (FP7-ICT-2007-3). The authors thank Andres Ernits for his contributions on developing the electronics and the flow tank.

Appendix. Derivation of the virtual work

The virtual work of the actuation moment $M(t)$ is:

$$\delta W_1 = \int_0^l M(t) \underline{\delta}(x-a) \delta h'(x,t) dx = \sum_{j=1}^n M(t) \varphi_j'(a) \delta q_j. \quad (A.1)$$

The virtual work of the hydrodynamic forces $L(x,t)$ is:

$$\begin{aligned} \delta W_2 &= - \int_0^l L(x,t) \delta h(x,t) dx \\ &= - \sum_{i=1}^n \sum_{j=1}^n \ddot{q}_i(t) \int_0^l m(x) \varphi_i(x) \varphi_j(x) dx \delta q_j \end{aligned}$$

$$\begin{aligned}
 & -2U \sum_{i=1}^n \sum_{j=1}^n \dot{q}_i(t) \int_0^l m(x) \varphi'_i(x) \varphi_j(x) dx \delta q_j \\
 & -U^2 \sum_{i=1}^n \sum_{j=1}^n \dot{q}_i(t) \int_0^l m(x) \varphi''_i(x) \varphi_j(x) dx \delta q_j. \quad (A.2)
 \end{aligned}$$

The virtual work of the concentrated force F_{fin} is:

$$\begin{aligned}
 \delta W_3 &= \int_0^l F_{fin}(t) \underline{\delta}(x-l) \delta h(x,t) dx \\
 &= - \sum_{i=1}^n \sum_{j=1}^n \dot{q}_i(t) [\alpha \varphi_i(l) + \beta \varphi'_i(l)] \varphi_j(l) \delta q_j \\
 & - 2U \sum_{i=1}^n \sum_{j=1}^n \dot{q}_i(t) \alpha \varphi'_i(l) \varphi_j(l) \delta q_j. \quad (A.3)
 \end{aligned}$$

The virtual work of the concentrated moment $M_{fin}(t)$ is:

$$\begin{aligned}
 \delta W_4 &= \int_0^l M_{fin}(t) \underline{\delta}(x-l) \delta h'(x,t) dx \\
 &= \sum_{j=1}^n M_{fin}(t) \varphi'_j(l) \delta q_j \\
 &= - \sum_{i=1}^n \sum_{j=1}^n \dot{q}_i(t) [\beta \varphi_i(l) + \gamma \varphi'_i(l)] \varphi'_j(l) \delta q_j \\
 & - 2U \sum_{i=1}^n \sum_{j=1}^n \dot{q}_i(t) \beta \varphi'_i(l) \varphi'_j(l) \delta q_j \quad (A.4)
 \end{aligned}$$

$\underline{\delta}$ denotes the Dirac delta function and $h'(x,t) = \frac{\partial}{\partial x} h(x,t)$.

References

[1] Colgate J E and Lynch K M 2004 Mechanics and control of swimming: a review *IEEE J. Ocean. Eng.* **29** 660–73

[2] Sfakiotakis M, Lane D M and Davies J B C 1999 Review of fish swimming modes for aquatic locomotion *IEEE J. Ocean. Eng.* **24** 237–52

[3] Triantafyllou M S and Triantafyllou G S 1995 An efficient swimming machine *Sci. Am.* **272** 64–70

[4] Lauder G V and Madden P G A 2006 Learning from fish: kinematics and experimental hydrodynamics for roboticists *Int. J. Autom. Comput.* **4** 325–35

[5] Streitlien K, Triantafyllou G S and Triantafyllou M S 1996 Efficient foil propulsion through vortex control *AIAA J.* **34** 2315–9

[6] Anderson J M 1996 Vorticity control for efficient propulsion *PhD Dissertation*, Department of Ocean Engineering, Massachusetts Institute of Technology p 194

[7] Kumph J M 2003 Maneuvering of a robotic pike *Master of Science Dissertation*, Department of Ocean Engineering, Massachusetts Institute of Technology p 77

[8] Liu J L and Hu H 2005 Novel mechatronics design for a robotic fish *Proc. IEEE/RSJ Int. Conf. on Intelligent Robots and Systems (Edmonton, Canada)* pp 2077–82

[9] Liu J and Hu H 2005 Mimicry of sharp turning behaviours in a robotic fish *Proc. IEEE Int. Conf. on Robotics and Automation (Barcelona, Spain)* pp 3329–34

[10] Dwivedya S K and Eberhard P 2006 Dynamic analysis of flexible manipulators, a literature review *Mech. Mach. Theory* **41** 749–77

[11] Dubowsky S 1994 Dealing with vibrations in the deployment structures of space robotic systems *5th Int. Conf. on Adaptive Structures (Sendai, Japan)* pp 5–7

[12] Mavrodís C, Dubowsky S and Raju V 1995 End-point control of long reach manipulator systems *Proc. 9th World Congress on the Theory of Machines and Mechanisms (Milan, Italy)* vol 2 pp 71–76

[13] Meggiolaro M A and Dubowsky S 2001 Improving the positioning accuracy of powerful manipulators with application in nuclear maintenance *Proc. 16th Brazilian Congress of Mechanical Engineering on Robotics and Control* vol 15 pp 210–9

[14] Chalfoun J, Bidard C, Keller D, Perrot Y and Piolain G 2007 Design and flexible modeling of a long reach articulated carrier for inspection *IEEE/RSJ Int. Conf. on Intelligent Robots and Systems* pp 4013–9

[15] Riviere C N, Ang W T and Khosla P K 2003 Towards active tremor canceling in handheld microsurgical instruments *IEEE Trans. Robot. Autom.* **19** 793–800

[16] Kumar R, Berkelman P, Gupta P, Barnes A, Jensen P S, Whitcomb L L and Taylor R H 2000 Preliminary experiments in cooperative human/robot force control for robot assisted micro-surgical manipulation *Proc. IEEE Int. Conf. on Robotics and Automation* vol 1 pp 610–7

[17] Ouyang P R, Tjiptoprodjo R C, Zhang W J and Yang G S 2008 Micro-motion devices technology: the state of arts review *Int. J. Adv. Manuf. Technol.* **38** 463–78

[18] Ouyang P R, Zhang W J and Gupta M M 2008 A new compliant mechanical amplifier based on a symmetric five bar topology *Trans. ASME, J. Mech. Des.* **130** 104501

[19] Fukuda T 1985 Flexibility control of elastic robot arms *J. Robot. Syst.* **2** 73–88 <http://adsabs.harvard.edu/abs/1985JRoS...2...73F>

[20] Pfeifer R, Lungarella M and Iida F 2012 The challenges ahead for bio-inspired ‘soft’ robotics *Commun. ACM* **55** 76–87

[21] Chen Z, Shatara S and Tan X 2010 Modelling of biomimetic robotic fish propelled by an ionic polymer-metal composite caudal fin *IEEE/ASME Trans. Mechatronics* **15** 448–59

[22] Zhang Z, Philen M and Neu W 2010 A biologically inspired artificial fish using flexible matrix composite actuators: analysis and experiment *Smart Mater. Struct.* **19** 1–11

[23] Ahlborn B, Chapman S, Stafford R and Harper R 1997 Experimental simulation of the thrust phases of fast-start swimming of fish *J. Exp. Biol.* **200** 2301–12 www.ncbi.nlm.nih.gov/pubmed/9320219

[24] Lauder G V and Madden P G A 2006 Learning from fish: kinematics and experimental hydrodynamics for roboticists *Int. J. Autom. Comput.* **3** 325–35

[25] Park Y J, Jeong U, Lee J, Kwon S R, Kim H Y and Cho K J 2012 Kinematic condition for maximizing the thrust of a robotic fish using a compliant caudal fin *IEEE Trans. Robot.* **28** 1216–27

[26] Aureli M, Kopman V and Porfiri M 2010 Free-locomotion of underwater vehicles actuated by ionic polymer metal composites *IEEE/ASME Trans. Mechatronics* **15** 603–14

[27] Cha Y, Verotti M, Walcott H, Peterson S D and Porfiri M 2013 Energy harvesting from the tail beating of a carangiform swimmer using ionic polymermetal composites *Bioinspir. Biomim.* **8** 036003

[28] Calisti M, Giorelli M, Levy G, Mazzolai B, Hochner B, Laschi C and Dario P 2011 An octopus-bioinspired solution to movement and manipulation for soft robots *Bioinspir. Biomim.* **6** 036002

[29] www.festo.com/cms/en_corp/9786.htm

[30] Valdivia y Alvarado P 2007 Design of biomimetic compliant devices for locomotion in liquid environments *PhD Thesis* Massachusetts Institute of Technology p 194

- [31] Blight A R 1976 Undulatory swimming with and without waves of contraction *Nature* **264** 352–4
- [32] Blight A R 1977 The muscular control of vertebrate swimming movements *Biol. Rev.* **52** 181–218
- [33] Long J H Jr, Mchenry M J and Boetticher N C 1994 Undulatory swimming: how traveling waves are produced and modulated in sunfish (*Lepomis Gibbosus*) *J. Exp. Biol.* **192** 129–45 www.ncbi.nlm.nih.gov/pubmed/9317485
- [34] Long J H Jr 1992 Stiffness and damping forces in the intervertebral joints of blue marlin (*Makaira Nigricans*) *J. Exp. Biol.* **162** 131–55 <http://jeb.biologists.org/content/162/1/131.abstract>
- [35] Long J H Jr 1998 Muscles, elastic energy and the dynamics of body stiffness in swimming eels *Am. Zool.* **38** 771–92 <http://citeseerx.ist.psu.edu/viewdoc/summary?doi=10.1.1.155.2904>
- [36] Fiazza C, Salumäe T, Listak M, Kulikovskis G, Templeton R, Akanyeti O, Megill W, Fiorini P and Kruusmaa M 2010 Biomimetic mechanical design for soft-bodied underwater vehicles *Proc. IEEE Oceans Conf. (Sydney)* pp 1–7
- [37] Akanyeti O, Ernits A, Fiazza C, Toming G, Kulikovskis G, Listak M, Raag R, Salumäe T, Fiorini P and Kruusmaa M 2010 Myometry-driven compliant-body design for underwater propulsion *Proc. IEEE Int. Conf. on Robotics and Automation (Anchorage, Alaska)* pp 84–9
- [38] Valdivia y Alvarado P and Youcef-Toumi K 2006 Design of machines with compliant bodies for biomimetic locomotion in liquid environments *Trans. ASME, J. Dyn. Syst. Meas. Control* **128** 3–13
- [39] El Daou H, Salumäe T, Ristolainen A, Toming G, Listak M and Kruusmaa M 2011 A Bio-mimetic design and control of a fish-like robot using compliant structures *15th IEEE Int. Conf. on Advanced Robotics (Tallinn, Estonia)* pp 563–8
- [40] El Daou H, Salumäe T, Toming G and Kruusmaa M 2012 Bio-inspired compliant robotic fish: design and experiments *IEEE Int. Conf. on Robotics and Automation (St. Paul, MN, USA)* pp 5340–45
- [41] Salumäe T and Kruusmaa M 2013 Flow-relative control of an underwater robot *Proc. R. Soc. A* **469** 20120671
- [42] Jung D S, Pott P P, Salumäe T and Kruusmaa M 2013 Flow aided path following of an underwater robot *ICRA: Proc. IEEE Int. Conf. of Robotics and Automation* pp 4602–7
- [43] Lighthill M J 1960 Note on the swimming of slender fish *J. Fluid Mech.* **9** 305–17
- [44] Wu T Y 2001 Mathematical biofluidynamics and mechanophysiology of fish locomotion *Math. Methods Appl. Sci.* **24** 1541–64
- [45] Meirovitch L 2001 *Fundamentals of Vibrations* (New York: McGraw-Hill) p 806
- [46] Theodore R J and Ghosal A 1995 Comparison of the assumed modes and finite element models for flexible multilink manipulators *Int. J. Robot. Res.* **14** 91–111
- [47] Baruh H 1999 *Analytical Dynamics* (New York: McGraw-Hill) p 744
- [48] Adhikari S and Phani A S 2009 Experimental identification of generalised proportional viscous damping matrix *Trans. ASME, J. Vib. Acoust.* **131** 011008
- [49] Rao S S 2004 *Mechanical Vibrations* (Englewood Cliffs, NJ: Prentice-Hall) p 1104
- [50] Bainbridge R 1958 The speed of swimming of fish as related to size and to the frequency and amplitude of the tail beat *J. Exp. Biol.* **35** 109–33 <http://jeb.biologists.org/content/35/1/109>
- [51] Webb P W, KostECKI P T and Stevens E D 1984 The effect of size and swimming speed on the locomotor kinematics of rainbow trout *J. Exp. Biol.* **109** 77–95 <http://jeb.biologists.org/content/109/1/77>
- [52] McHenry M J, Pell C A and Long J Jr 1995 Mechanical control of swimming speed: stiffness and axial wave form in undulating fish models *J. Exp. Biol.* **198** 2293–305 <http://jeb.biologists.org/content/198/11/2293>
- [53] Ahlborn B K, Blake R W and Megill W M 2006 Frequency tuning in animal locomotion *Zoology* **109** 43–53

APPENDIX F

T. Salumae, I. Ranó, O. Akanyeti, and M. Kruusmaa, “Against the flow: a Braitenberg controller for a fish robot,” in *Proc. IEEE Int. Conf. on Robotics and Automation (ICRA)*, 2012, pp. 4210–4215

Against the flow: A Braitenberg controller for a fish robot

Taavi Salumäe

Iñaki Rañó

Otar Akanyeti

Maarja Kruusmaa

Abstract—Underwater vehicles do not localise or navigate with respect to the flow, an ability needed for many underwater tasks. In this paper we implement rheotaxis behaviour in a fish robot, a behaviour common to many aquatic species. We use two pressure sensors on the head of the robot to identify the pressure differences on the left and right side and control the heading of the fish robot by turning a servo-motor actuated tail. The controller is inspired by the Braitenberg vehicle 2b, a simple biological model of tropotaxis, that has been used in many robotic applications. The experiments, conducted in a flow pipe with a uniform flow, show that the robot is able to orient itself, and keep the orientation, to the incoming current. Our results demonstrate that guidance of a fish robot relative to a flow can be implemented as a simple rheotaxis behaviour using two sensors and a Braitenberg 2b controller.

I. INTRODUCTION

Underwater vehicles developed so far do not localise or navigate with respect to the flow. Completing an underwater mission, like; docking, transect inspection or pipeline inspection, implies moving with respect to some global reference frame. Under these assumptions the flow can be seen just as a disturbance to be compensated for, however, sometimes the global reference information might not be available. Also, most of the underwater robots are large rigid vehicles that are not sensitive to local flow disturbances. Soft, flexible and compliant robots, on the other hand, are tested only in laboratory conditions in still water [1], [2], [3]. However, with a trend of miniaturisation, the effect of the local flow to the robot becomes more relevant.

With the increasing interest in bioinspiration in robotics, the effect of the environment to the robot's design is revised in the light of new biological evidence. The findings suggest that fish do more than just compensate disturbances caused by the flow. They exploit their special flow-sensing organ, the lateral line, for a diversity of behaviours, such as localisation in the flow, object detection, catching prey and schooling [4], [5], [6], [7]. Recently, several attempts have been made to develop lateral line flow and pressure sensors [8], [9], [10], [11]. With the maturation of this technology it becomes more realistic to obtain information about the local flow and consequently, develop methods for flow sensor signal processing and control. At a time though, the artificial lateral line technology has not yet been integrated to any underwater robot, and so far there exists no underwater robot that uses

local flow sensing to negotiate the flow, an issue we will address in this paper through the use of Braitenberg vehicles.

Because of their apparent simplicity, Braitenberg vehicles [12] have been used in robotics for decades as sensor based steering control mechanisms. As they are probably more intuitive for the newcomer than the potential based methods, they were not formalised but used instead on an empirical basis, which turned their use into an educated guess of parameter adjustment. This is the reason why they are mainly used for teaching robotics [13]. Recently it has been shown that our intuitive understanding of Braitenberg vehicles can be wrong [14], that unexpected behaviours can appear even in the simplest cases [15] and ways of adjusting the parameters to obtain desired behaviours have been identified [16].

Since Braitenberg vehicles model, in their simplest form, tropotaxis behaviours [17], the orientation of animals towards, or away from, the source of stimulation, they are well suited to implement fish rheotaxis. Rheotaxis is a widespread behaviour in various fish species accomplished by using visual and tactile cues and lateral line sensing [18]. This behaviour helps fish to migrate upstream, to hold a position in the stream and not to be swept away or stay in a favourable place to detect odours and food carried with the flow.

It is well known that animals have good moving performances in the real world, and, therefore, they are good models to implement robot motion. Seeking behaviours can be implemented as positive taxis whilst escaping behaviours correspond to negative taxis, moreover, as Braitenberg vehicles work at the steering or guidance level they can be used with any locomotive configuration which can be interfaced to the steering level control. However, most applications of Braitenberg vehicles use wheeled robots in the tradition of the original work to implement different abilities. Phototaxis for target acquisition through vehicle 3a is used in [19] in order to avoid relying on odometry. This work uses a modified version of Braitenberg vehicle 2b for obstacle avoidance based on infrared sensors, the same technique used in [20], where an artificial stimulus built up from laser and sonar proximity readings. In both cases the stimulus to implement vehicle 2b is just a weighted integration of the free area in front of the robot, measured with different kinds of proximity sensors. [21] presents a hardware version of vehicle 3b that avoids obstacles and performs wall following behaviour using infrared sensors. The power supply of the wheels is connected in a decreasing way to sensors at the front of the robot making the vehicle to slow down in the presence of obstacles.

Through the literature we find multiple empirical applications of Braitenberg vehicles to wheeled robots, ranging from

Taavi Salumäe and Maarja Kruusmaa are with the Centre for Biorobotics, Tallinn University of Technology, Tallinn, Estonia. {taavi, maarja.kruusmaa}@biorobotics.ttu.ee

Iñaki Rañó is with the Institute für Neuroinformatik, Ruhr-Universität Bochum, Germany. inaki.rano@ini.rub.de

Otar Akanyeti is with the Department of Computer Science, University of Verona, Verona, Italy. otarakanyeti@yahoo.com

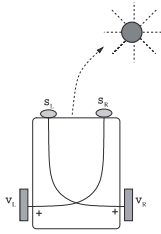


Fig. 1. Braitenberg vehicle 2b. Left and right motor velocities V_L and V_R are directly proportional to the light sensor signals S_L and S_R on the opposite sides of the robot. Therefore the robot is always turning in the direction of a light source (stimulus) and is moving towards it.

target seeking, wandering, and sound source localisation to obstacle avoidance. The few underwater robot examples of Braitenberg vehicles provide aquatic robots with light following competences using Lego Mindstorms as part of a robotics teaching program [22]. This is possible because Braitenberg vehicles are well suited to implement the steering control abstracting the specific locomotive subsystem.

This paper presents two major contributions. First, we implement a control mechanism for an underwater robot using flow sensors to orient the robot with respect to oncoming flow. Second, this work presents the first application of Braitenberg vehicles to fish robots, as these control mechanisms were previously used in wheeled robots only. We show, therefore, that the rheotaxis behaviour can be achieved by using a simple Braitenberg vehicle like controller using the feedback provided by a pressure difference around the nose of the robot. The rest of the paper is organised as follows. Section II reviews the qualitative description of Braitenberg vehicle 2b, its mathematical model and sets up the framework to use it as a controller for our fish robot. Section III presents the materials and methods used, namely the fish robot and the experimental setup, while the results are presented in section IV. A summary of the contributions, their implications and further working lines are presented in Section V.

II. BRAITENBERG VEHICLE 2B TO STEER A FISH ROBOT UPSTREAM

In this section we will review the state of the art of theoretical Braitenberg 2b vehicles and will apply its basic ideas to develop a controller enabling fish robot to swim upstream.

A. Braitenberg 2b Controller for Wheeled robots

We use Braitenberg vehicle 2b (see figure 1) to steer the fish as this vehicle performs a hill climbing on the scalar stimulus it is immersed in, i.e. moves towards high stimulus values. In general the stimulus $S(\mathbf{x})$, $\mathbf{x} \in \mathbb{R}^2$ is a scalar value at each point (light or sound intensity, pressure...), and the controller relating the sensor inputs and outputs is modelled as a smooth function of the stimulus $F(s)$. In the case of a wheeled vehicle this represents the velocity of

the wheels, and each wheel is controlled using the sensorial input on the opposite side, a contralateral direct connection. Approximating the velocity of each wheel by a first order Taylor series and computing the velocity of the vehicle we obtain:

$$\dot{x} = F(S(\mathbf{x})) \cos \theta \quad (1)$$

$$\dot{y} = F(S(\mathbf{x})) \sin \theta \quad (2)$$

$$\dot{\theta} = \frac{\delta}{d} \nabla F(S(\mathbf{x})) \cdot \hat{e}_p \quad (3)$$

where d is the wheelbase of the vehicle, $\mathbf{x} = (x, y)$ is the midpoint between the sensors, δ is the distance between the sensors, $\nabla F(S(\mathbf{x}))$ is the gradient of the compound connection-stimulus function and $\hat{e}_p = [-\sin \theta \cos \theta]^T$ is a unitary vector orthogonal to the vehicle's head direction pointing to its left (see [14] for more details). These equations describe the behaviour of Braitenberg vehicle 2b provided the function $F(s)$ has non-negative derivative. In general, we can assume both, the stimulus $S(\mathbf{x})$ and the function $F(s)$, take non-negative values, there are no negative stimuli and the robot will not move backwards. Unless the function $F(s)$ actually vanishes for some stimulus value the dynamical system describing the behaviour of the vehicle has no stability point since equations (1) and (2) never vanish simultaneously. This behaviour is well suited as we do not want the fish to stop moving.

When the stimulus is linear, i.e. it has a constant gradient, the angular equation controlling the heading of the vehicle can be stated as:

$$\dot{\theta} = \frac{\delta}{d} F'(S(\mathbf{x})) \|\nabla S(\mathbf{x})\| \sin(\theta_0 - \theta) \quad (4)$$

where $\|\nabla S(\mathbf{x})\|$ is the norm of the gradient and θ_0 is its direction. Equation (4) has two equilibrium points, namely, the vehicle heading the gradient or the opposite direction. It can be seen that in the case of the vehicle 2b the stable equilibrium point makes the vehicle head the gradient, while the robot heading the direction to the gradient is an unstable point.

B. Application to a Fish Robot

In order to apply this exact taxis technique to the robotic fish we would need to be able to access a relation between the measured pressure and the flow velocity and to have a precise velocity control. However, as our main goal is only controlling the heading of the fish to make it swim upstream, we will analyse the relation between the heading of the fish relative to the flow and the pressure readings. If the robot is immersed in a uniform flow, the flow velocity and pressure in the boundary layer around the robot's head are inversely proportional to each other according to the Bernoulli's law. If the robot is aligned parallel with the flow streamlines (facing the flow), the streamlines around the head are symmetric and the pressure at both sides of the head is equal. The stagnation point (the point with zero velocity and maximum pressure)

is at the nose of the robot. The scalar stimulus we can use to implement the Braitenberg vehicle 2b is the measured pressure. Provided the fish is symmetric and the sensors are symmetrically placed w.r.t. the flow. We will denote P_0 the pressure values obtained in two corresponding sensors. If the robot turned with respect to the flow, the stagnation point moves to one side of the robot, and the pressure readings on both sides are different. Apart from the morphological characteristics, the change in the pressure measured on each sensor will depend on the heading of the robot relative to the flow direction. The pressure difference between the left and right side sensor therefore measures the angle of the robot with respect to the flow. If we select the heading of the robot $\theta = 0$ in the opposite direction of the flow, we can express the pressure on each side sensor as $P_r(\theta)$ and $P_l(\theta)$ such that $P_l(0) = P_r(0) = P_0$. As the effect of the pressure change is different for the right and left sensors, it can be seen that they have different signs on their derivatives w.r.t. θ . If we approximate the two functions as Taylor series around $\theta = 0$, we obtain the following expression for a Braitenberg like controller as a first order approximation:

$$\dot{\theta} = F'(P_0) \left[\frac{dP_r}{d\theta} - \frac{dP_l}{d\theta} \right] \theta \quad (5)$$

where we omitted the morphological parameters δ and d , and where $F(p)$ is the connection function between the sensors and the motor. It can be seen that for the standard angle definitions, the derivatives of $P_r(\theta)$ and $P_l(\theta)$ should be negative and positive respectively, and since $F'(p) > 0$ for Braitenberg vehicle 2b, the above equation has an stable equilibrium point at the origin, the fish heading the flow. This simple analysis indicates that Braitenberg vehicle 2b could be an adequate controller for the robot fish. However, since the motion of the fish itself will be oscillatory a deeper analysis has to be performed to ensure the stability of the controller. In current study we exclude this analysis and show experimentally that on average the fish will head the flow using this type of reactive controller.

III. THE ROBOT IN THE FLOW

The robot used in the experiments is a biomimetic fish robot developed in the research project FILOSE with the purpose to investigate fish and flow interaction. The schematic of the robot is represented in Figure 2. It consists of a rigid head and a compliant tail driven by a single servo-motor in the anterior part of the tail. The head is watertight and contains on-board electronics for sensor signal pre-processing and the servo-motor drive circuits controlled by the atmega324 micro-controller.

The tail consists of a compliant silicon body and a passive rigid caudal fin and it is bended by the servo-motor. The kinematics and dynamics of the robot tail are presented in [23]. The flexible tail is modelled as a cantilever beam with a variable cross-section actuated by a time varying moment $M(t)$. Taking now into account the hydrodynamic forces acting on the tail and the fin, we can calculate the lateral

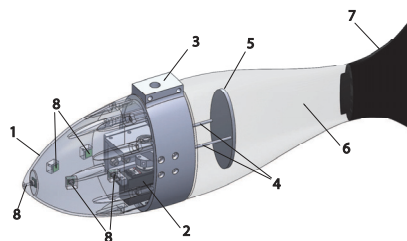


Fig. 2. CAD view of the fish-like robot. 1-Rigid head of the robot; 2-Servo-motor; 3-Middle part made from aluminium holding the head, the tail and a servo-motor; 4-Steel cables; 5-Actuation plate; 6-Compliant tail; 7-Rigid fin; 8-Pressure sensors.

deflection $h(x, t)$ of the fin using a method of assumed modes as described in [23] and consequently the heading of the robot in the global reference frame.

The moment $M(t)$ is applied to the tail by controlling the angle φ of the servo-motor using sinusoidal motion

$$\varphi = A \sin(2\pi ft) + \varphi_0 \quad (6)$$

By controlling the tail-beat amplitude A or frequency f the velocity of the robot can be varied while changing the tail offset φ_0 turns the fish in a desired direction.

A. Pressure sensors

Two pressure sensors are mounted on the each side of the rigid head of the robot and one on the tip of the nose. In this study only anterior two sensors on the sides were used. Other 3 sensors were not used. For experiments we are using small size commercial pressure sensors MS5407-AM from Intersema that are designed to be used in diving watches. The sensing unit is micro machined from silicon, mounted on 6.2×6.4 mm ceramic carrier and protected with a metal cap. The sensor is gel protected against humidity and water. The sensing unit is connected as a Wheatstone bridge to give the sensor a high sensitivity of 56 mV/bar in the full scale (0 to 7 bar). We are using a 22-bit differential analog-digital input converter with 124.5 mV reference voltage so that we can measure pressure with LSB of about 0.106 Pa. For the best signal-to-noise ratio, the analog-digital converter is soldered on PCB directly under the pressure sensor so that analog signal wires are as short as possible. Digitalised pressure information is carried from AD converter to a micro controller over SPI.

Theoretical relation between the heading of the robot and the pressure difference was experimentally tested by continuously changing the heading of the fish in flow while measuring pressure difference. The relation is presented in figure 3. It can be seen that the pressure signal is very noisy and there is a drift in sensors creating a hysteresis on the graph. However, a correlation between the angular position of the fish relative to the flow and the pressure difference is

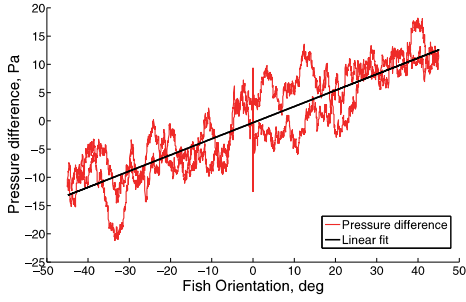


Fig. 3. Pressure difference on the left and the right side of the robot head versus the orientation of the robot.

apparent. The relation was found to be linear and described by the equation

$$\theta = f(P_R - P_L) = 3.48(P_R - P_L) \quad (7)$$

where P_R and P_L are, respectively, the average pressures on the right and left sides.

Our preliminary experiments show that the pressure difference is also related to the lateral velocity and acceleration of the fish. We filtered noise as well as the velocity and acceleration effects by averaging the pressure readings over 7 seconds observation window.

B. The experimental setup

The experiments with our robotic fish are conducted in a flow tunnel with a working section of $0.5m \times 0.5m \times 1.5m$. The tunnel is embedded into a test tank. Uniform flow in the working section is created with the help of a U-shaped flow strengthener and two sequential laminators. An AC motor is used to create the circulation inside the flow tunnel and it permits controlling the flow speed with 0.04 m/s accuracy. The uniformity of the flow is checked and the flow speed is calibrated using a digital particle image velocimetry (DPIV) system.

The fish robot is placed into the working section of the flow tunnel which is represented on figure 4. An expanded polystyrene bar is attached to the upper part of the fish as a floater. It makes the robot positively buoyant so that the bar touches the glass ceiling of the flow tunnel. The friction between the bar and the tunnel ceiling is negligible due to the ball-shaped crew heads. Two LEDs are mounted to the bar. An overview camera tracks the LEDs and the position and orientation of the robot is determined according to the LEDs positions on the bar. Wires under the bar connect the robot to an off-board PC running control algorithms and a video tracking software in LabView environment.

IV. BRAITENBERG CONTROLLER

We implemented a pressure-driven controller to achieve the rheotaxis behaviour. The aim of the controller was to keep the robot's angular deviation θ as close as possible to

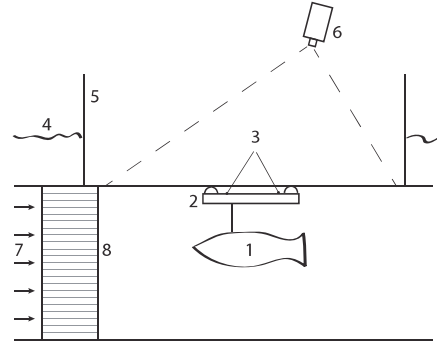


Fig. 4. Side-view of the flow tunnel. x -axis is parallel to the flowstream and y -axis is perpendicular to the flowstream, parallel to the horizontal plane. 1-Robotic fish; 2-floater; 3-LED's on the floater for position tracking using camera; 4-water level; 5-glass through which the working area is filmed; 6-camera for position tracking of the fish; 7-flow direction; 8-flow laminator.

the direction of the incoming flow by controlling the offset of the actuation signal φ_0 . Derived from Equation (7), θ can be represented in terms of pressure difference on the left and right side of the robot, therefore the setpoint of the controller was chosen as $P_R - P_L = 0$, leading to the control law,

$$\varphi_0 = [0 - (P_R - P_L)_c]K_\varphi, \quad (8)$$

where $(P_R - P_L)_c$ was drift-compensated pressure difference. To minimize the drift in sensor readings, an integral component has been added to the controller as,

$$(P_R - P_L)_c = C_d \int_0^\tau [0 - (P_R - P_L)] d\tau + (P_R - P_L) \quad (9)$$

where both K_φ and C_d were chosen to be constant.

Due to limited length of the flow tank, the robot was programmed to maintain its distance from the beginning of the flow tunnel rather than swimming upstream. Holding station at predetermined position was achieved using a feedback controller based on the overhead camera. The tail beat amplitude (A) was adjusted using,

$$A = (x_{sp} - x_{pv})K_A, \quad (10)$$

where x_{sp} and x_{pv} were, respectively, the desired and actual position of the robot. K_A was chosen to be constant.

To evaluate the performance of the Braitenberg controller (Equation (8)), we tested it on the robot. We compared the robot behaviour with two other extreme cases when the robot was driven with:

- 1) No offset control: only holding station controller was active. This controller set the minimum performance level. We expected that the Braitenberg controller would perform better than this level.
- 2) Offset control using feedback from the overhead camera: a PID controller was developed to maintain the

orientation of the robot with respect to a global reference frame, in this case parallel to the oncoming flow. The control setpoints were chosen as x and y coordinates in the flow tunnel.

All three controllers were tested in the flow tunnel at flow velocity 0.16 m/s. The tail-beat frequency for holding station was set to 2.0 Hz. The setpoint for the flow-directional position was 500 mm from the beginning of the tunnel. The controller parameters K_A , C_d , K_φ and PID parameters were fine-tuned to get the most stable behaviour.

During experiments, the robot was actuated first. Then water-pump was switched on. The robot was moved to the holding station distance and the controllers were tested at least for 5 minutes. As the water-pump was switched off, the robot moved forward due to decreasing drag. The experiments were ended after observing the forward motion.

The performance was measured by computing the standard deviation of the heading of the robot. The smaller the deviation, the better the controller.

A. Results

Figure 6 presents the typical trajectories of the robot while being driven by the three candidate controllers. Downstream position was well-kept with camera feedback and braitenberg controller. However, with no offset control slight deviations from the setpoint were apparent, although the same camera-feedback control was used for holding downstream position. This instability is due to large deviations of the fish orientation resulting in fluctuations of drag forces and flow-directional thrust component.

The heading of the robot as a function of time while holding station is given in Figure 5 (above). Compared to no offset control, both Braitenberg and camera-based controllers achieved better results by reducing the fluctuations from the desired set point ($\theta = 0$). Due to the more confined heading, the lateral deviations of the robot while driven by the both controllers were also limited 5 (below). Table 1 presents the mean and standard deviation of both heading and lateral position of the robot. It is seen that the standard deviation has reduced greatly with both controllers compared to no offset control.

The steady state performance (after $t = 50$ s) of the both controllers were similar, there was no statistical difference. Yet, camera-based controller converged to the steady state faster than the Braitenberg controller. The main reason for slower response of the Braitenberg controller is most likely the averaging of pressure sensor signals over 7 seconds. This was necessary to filter out the periodic oscillations of the pressure values caused by the motion of the fish. Controller can be made faster by analysing these self-motion signals and taking them into consideration inside the controller instead of filtering them out. However, this analysis was not included in this study.

Overall the results clearly demonstrates that the rheotaxis behaviour was achievable through a feedback controller driven by the local flow information, in this case pressure readings, and the performance of the controller was similar

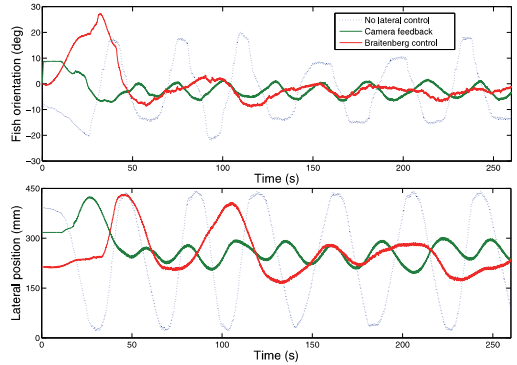


Fig. 5. Heading (above) and lateral position (below) of the robot in time.

TABLE I
MEAN AND STANDARD DEVIATION OF THE HEADING AND LATERAL POSITION OF THE ROBOT FOR THREE CONTROLLERS

	No offset	Braitenberg	Camera feedback
Mean y	237.7 mm	250.3 mm	253.5 mm
Mean θ	-2.8 deg	-2.9 deg	-2.7 deg
Standard deviation y	146.3 mm	59.2 mm	26.7 mm
Standard deviation θ	11.3 deg	2.9 deg	2.7 deg

to the performance of a controller based on a global reference point.

V. CONCLUSIONS AND FURTHER WORK

This paper presents the first implementation of rheotaxis behaviour of a fish robot using Braitenberg vehicle 2b. The controller is based on two pressure sensors to detect and compute pressure differences on both sides of the robot's nose under the assumption that the difference is only a function of the heading of the fish relative to the flow. Even though this is a simplistic approach, experimental evidence pinpoints its validity for our settings. This backs up the philosophy of Braitenberg vehicles, namely that complex behaviour is the result of simple controllers interacting with their environment. Since Braitenberg vehicles are steering control mechanisms, the computed angular velocity has to be converted to single point actuated tail. The results, compared to an open-loop controlled robot and a visually guided robot, show that the robot is able to align itself against the stream. Its average heading as well as lateral deflection are smaller than of a robot without a sensor feedback. This work contributes to underwater robotics by stating navigation and localisation with respect to the flow as a relevant problem to increase autonomy. It also presents one of the first applications of Braitenberg vehicles to non wheeled robots by implementing rheotaxis. The final contribution is an empirical proof that rheotaxis behaviour for an underwater robot, does not need complex techniques and therefore it is achievable with a currently available technology.

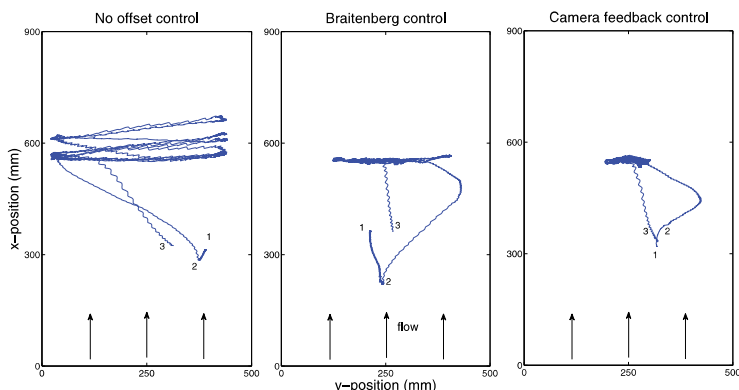


Fig. 6. Trajectories of the fish robot driven by: a) no offset control, b) Braitenberg control and c) Camera-based feedback control. In all three cases, station holding controller given in Equation (10) was active. 1. Position of the robot at the beginning of the experiment, 2. Position of the robot when flow was started. 3. Final position of the robot at the end of the experiment.

It is not clear if our approach scales up to more challenging tasks such as navigating in complex flows or when robot motion contains high velocity and accelerations. The signal to noise ratio of the sensors would decrease with the more rapid self-motion of the body and turbulence and it is possible that more complicated mechanisms underlie in rheotaxis phenomena when it becomes to navigation with respect to eddies and waves. Complexity will also increase when extending the study to 3D environment. Dynamic pressure changes caused by the flow are relatively small compared to the changes in the static pressure as the robot rolls, yaws or pitches.

REFERENCES

- [1] J. Yu, M. Tan, S. Wang, and E. Chen, "Development of a biomimetic robotic fish and its control algorithm," *IEEE Transactions on Systems, Man, and Cybernetics - Part B: Cybernetics*, vol. 34, no. 4, pp. 1798–1810, 2004.
- [2] A. Crespi, D. Lachat, A. Pasquier, and A. Ijspeert, "Controlling swimming and crawling in a fish robot using a central pattern generator," *Autonomous Robots*, vol. 25, pp. 3–13, 2008.
- [3] V. Alvarado, "Design of biomimetic compliant devices for locomotion in liquid environments," Ph.D. dissertation, Massachusetts Institute of Technology, 2007.
- [4] J. Goulet, J. Engelmann, B. P. Chagnaud, J. P. Fransch, M. D. Suttner, and J. L. van Hemmen, "Object localization through the lateral line system of fish: Theory and experiment," *Journal of Computational Physiology*, vol. 194, pp. 1–17, 2008.
- [5] A. B. Sichert, R. Bamler, and J. L. van Hemmen, "Hydrodynamic object recognition," *Physical Review Letters*, 2009.
- [6] A. J. Kalmijn, *Hydrodynamic and acoustic field detection. Sensory Biology of Aquatic Animals*. New York, Springer, 1988, pp. 83–130.
- [7] H. Bleckmann, *Role of the lateral line in fish behaviour*. Chapman and Hall, 1993, ch. 7, pp. 201–235.
- [8] A. Qualtieri, F. Rizzi, M. Todaro, A. Passaseo, R. Cingolani, and M. D. Vittorio, "Stress-driven aln cantilever-based flow sensor for fish lateral line system," *Microelectron. Eng.*, 2011.
- [9] Z. Fan, J. Chen, J. Zou, D. Bullen, C. Liu, and F. Delcomyn, "Design and fabrication of artificial lateral line flow sensors," *Journal of Micromechanics and Microengineering*, vol. 12, pp. 655–661, 2002.
- [10] Y. Yang, N. Nguyen, N. Chen, M. Lockwood, C. Tucker, H. Hu, H. Bleckmann, C. Liu, and D. L. Jones, "Artificial lateral line with biomimetic neuromasts to emulate fish sensing," *Bioinspiration & Biomimetics*, vol. 5, 2010.
- [11] G. Krijnen, T. Lammerink, R. Wiegrenik, and J. Casas, "Cricket-inspired flow sensor array," in *Proc. IEEE 6th Sensors Conference*, 2007, pp. 539–546.
- [12] V. Braitenberg, *Vehicles. Experiments in synthetic psychology*. The MIT Press, 1984.
- [13] C. Buiu, "Hybrid educational strategy for a laboratory course on cognitive robotics," *IEEE Transactions on Education*, vol. 51, no. 1, pp. 100–107, 2008.
- [14] I. Raňó, "A steering taxis model and the qualitative analysis of its trajectories," *Adaptive Behavior*, vol. 17, no. 3, pp. 197–211, 2009.
- [15] —, *An empirical evidence of Braitenberg vehicle 2b behaving as a billiard ball*. Springer, 2010, pp. 293–302.
- [16] —, "On the convergence of braitenberg vehicle 3a immersed in parabolic stimuli," in *Proceedings of the IEEE International Conference on Intelligent Robots and Systems (IROS)*, 2011.
- [17] G. Fraenkel and D. Gunn, *The orientation of animals. Kineses, taxes and compass reactions*. Dover publications, 1961.
- [18] J. C. Montgomery, C. F. Baker, and A. G. Carton, "The lateral line can mediate rheotaxis in fish," *Nature*, vol. 389, pp. 960–963, 1997.
- [19] E. Bicho and G. Schöner, "The dynamic approach to autonomous robotics demonstrated on a low-level vehicle platform," *Robotics and Autonomous Systems*, vol. 21, pp. 23–35, 1997.
- [20] I. Raňó and T. Smithers, "Obstacle avoidance through Braitenberg's aggression behavior and motor fusion," in *Proc. of the 2nd European Conf. on Mobile Robots*, 2005, pp. 98–103.
- [21] L. Capozzo, G. Attolico, and G. Cicirelli, "Building low cost vehicles for simple reactive behaviors," in *Proceedings of the IEEE International Conference on Systems, Man, and Cybernetics*, vol. 6, 1999, pp. 675–680.
- [22] R. Stolkin, R. Sheryll, and L. Hotaling, "Braitenbergian experiments with simple aquatic robots," in *Proceedings of the IEEE OCEANS conference*, 2007.
- [23] H. E. Daou, T. Salumae, A. Ristolainen, G. Toming, M. Listak, and M. Kruusmaa, "A bio-mimetic design and control of a fish-like robot using compliant structures," in *Proceedings of The 15th IEEE International Conference on Advanced Robotics*, 2011, pp. 563 – 568.

APPENDIX G

T. Salumäe and M. Kruusmaa, “Flow-relative control of an underwater robot,” *Proceedings of the Royal Society. A*, vol. 469, no. 2153, 2013.

Research



Cite this article: Salumäe T, Kruusmaa M.
2013 Flow-relative control of an underwater
robot. *Proc R Soc A* 469: 20120671.
<http://dx.doi.org/10.1098/rspa.2012.0671>

Received: 9 November 2012

Accepted: 7 February 2013

Subject Areas:

ocean engineering

Keywords:

biomimetics, robot sensing systems,
underwater robotics

Author for correspondence:

Taavi Salumäe

e-mail: taavi.salumae@ttu.ee

This paper describes flow-relative and flow-aided navigation of a biomimetic underwater vehicle using an artificial lateral line for flow sensing. Most of the aquatic animals have flow sensing organs, but there are no man-made analogues to those sensors currently in use on underwater vehicles. Here, we show that artificial lateral line sensing can be used for detecting hydrodynamic regimens and for controlling the robot's motion with respect to the flow. We implement station holding of an underwater vehicle in a steady stream and in the wake of a bluff object. We show that lateral line sensing can provide a speed estimate of an underwater robot thus functioning as a short-term odometry for robot navigation. We also demonstrate navigation with respect to the flow in periodic turbulence and show that controlling the position of the robot in the reduced flow zone in the wake of an object reduces a vehicle's energy consumption.

1. Introduction

All fishes have developed a lateral line organ for detecting and processing hydrodynamic events [1]. Also, some crustaceans [2] and aquatic mammals have flow-sensitive organs [3]. At the same time, man-made underwater vehicles mostly rely on ultrasonic sensing and vision for getting feedback from the environment [4,5]. The standard method for flow detection of underwater vehicles is using an acoustic Doppler current profiler (ADCP). ADCPs measure the global flow speed and its readings are incorporated into the vehicle's navigational system to compensate for the drift [6,7]. As opposed to the highly distributed lateral line organ of fish, ADCP does not measure local flow. Also, ADCPs are expensive, bulky devices consuming lots of energy and are therefore not suitable for small vehicles.

At the same time, many possible application scenarios require miniature, efficient and manoeuvrable autonomous underwater vehicles. For example, pipeline inspection, shipwreck penetration and harbour monitoring are such kinds of tasks.

Small vehicles become more dependent on the environment as currents and eddies can easily deviate them away from their desired path. This is especially relevant to riverine technology where flow is often rapid, turbulent and obstructed by objects.

Rheotropism is a tendency of fish to react to mechanical stimuli of the flow [8]. For example, it is shown that fish can detect the direction of flow and face towards the oncoming current [9], known as the rheotaxis behaviour. This helps migrating upstream or holding a position in a favourable place in the stream to detect odours and food carried with the flow. In the study of Chagnaud *et al.* [10], it is also discussed that fish are able to detect the velocity of the flow and keep their position without drifting down- or upstream.

One of the most interesting expressions of rheotropism for both biologists and engineers is the fish' behaviour behind a bluff object in flow [11]. An object in the flow generates a repeating pattern of swirling vortices, known as the Kármán vortex street (KVS). The KVS is a well-studied hydrodynamic effect that can be realized in laboratory conditions with high repeatability [12]. In rivers such vortex streets can be generated by rocks or other objects. Some fish, for example, rainbow trout *Oncorhynchus mykiss*, are shown to use KVS to reduce their energy consumption [13] by taking advantage of the reduced flow speeds behind the object or adapting a specific locomotion pattern (called Kármán gaiting) when interacting with the vortices [14–16].

Such behaviours demonstrate high sensitivity, discrimination ability and redundancy of the biological lateral line and have inspired researchers to mimic its working principles and functionality.

The biological lateral line is a dual system consisting of superficial neuromasts, which are sensitive to flow speed and canal neuromasts responding to pressure changes [17]. Several types of artificial superficial MEMS-based neuromasts have been developed [18,19] and demonstrated to be capable of detecting hydrodynamic events, such as a dipole source [20]. Pressure sensors [21] or optical flow sensors placed in artificial canals [22] have been also used, and it is demonstrated that the presence of KVS can be detected and the position of the cylinder generating the street can be estimated from those sensor readings [21].

Although several artificial lateral line systems have been developed, to the best of our knowledge, they have never been mounted on an underwater robot and used for controlling the robot in the flow.

In this paper, we demonstrate flow-relative control of an underwater robot (figure 1). We use on-board pressure sensors for local flow sensing for

- identification and discrimination of flow regimens (uniform flow and periodic turbulence);
- detecting the orientation of the robot with respect to the flow direction in a steady stream;
- measuring the flow speed; and
- estimating the position of the robot in a wake of an object.

With the feedback from the lateral line sensors, we control the robot to hold its position with respect to the flow by first identifying the flow regimen and then compensating for its downstream drift and the lateral displacement in the wake.

The robotic platform used in this study is a biomimetic underwater robot FILOSE (Robotic FIsh LOcomotion and SEnsing) developed to study fish and flow interaction and to extract bioinspired design principles using a reductionist approach. As opposed to the traditional mechanical design of using serial chain kinematics for generating undulating motion [23,24], the FILOSE robot uses a compliant tail driven by a single motor. Thrust is generated using vibrations at a resonance frequency mimicking the kinematics of a trout at cruising speeds [25,26].

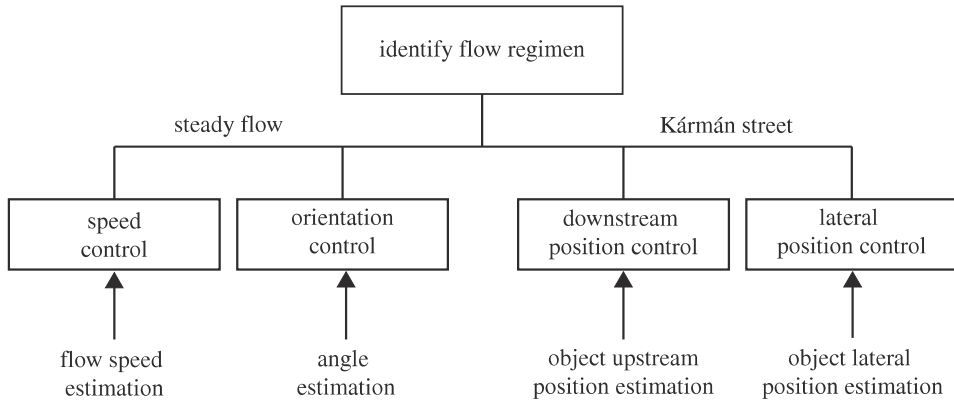


Figure 1. Control architecture. The robot identifies the flow regimen to choose between two station-holding approaches (control in steady flow or in Kármán street).

We have also applied the principle of minimal complexity to the sensor and controller design. Though fish lateral line is generally very elaborate, its morphology varies from species to species in design and complexity [27]. For example, some species, such as Ruffe have been observed to have short lateral line canals consisting of only three neuromasts (S. Van Netten 2012, private communication). In our previous work, we have shown that rheotaxis behaviour (facing upstream) can be achieved using only two pressure sensors on the sides of the robot and a simple Braitenberg 2b controller [28]. Here, we use standard linear control methods to investigate to what extent the seemingly complex behaviours of flow-based control can be achieved with the low-complexity artificial lateral line configuration and control. The artificial lateral line here consists of pressure sensors, but as they record absolute pressure values translated to the flow speeds their functionality is rather analogous to the superficial neuromasts.

2. Experimental set-up

(a) The robot

The 50 cm long FILOSE robot mimics the geometry and swimming mode of a rainbow trout (*Oncorhynchus mykiss*). Rainbow trout is a subcarangiform swimmer. It generates thrust by undulating three-fifths of its posterior body [29]. Similarly, the FILOSE robot has a 30 cm long compliant posterior body where the motion is generated using only a single actuator. The servomotor creates vibrations in the tail through steel cables. The tail actuation can be expressed by sinusoidal motion.

$$\varphi = A \cdot \sin(2\pi ft) + \varphi_0, \quad (2.1)$$

where φ is the motor angle, A the actuation amplitude, f the frequency and φ_0 the motor angle offset. As the system is, in principle, a non-homogeneous cantilever beam with a decreasing cross section, the amplitude of oscillations increase towards the end of the tail. Varying the amplitude and the frequency of the oscillations changes the swimming speed of the robot, whereas adding an offset to the actuation signal will make the robot turn left or right. Modelling of the tail and the selection of geometry and compliant materials is described in more detail in [30].

The fish robot is equipped with piezoresistive silicon absolute pressure sensors. These sensors form an artificial lateral line. The sensors are mounted inside the rigid plastic head of the robot and are connected to the 1 mm pressure taps on the surface of the head. There are all together five pressure taps: one at the tip of the nose, two on the sides of the head 50 mm from the nose and two on the sides of the head 100 mm from the nose (figure 2).

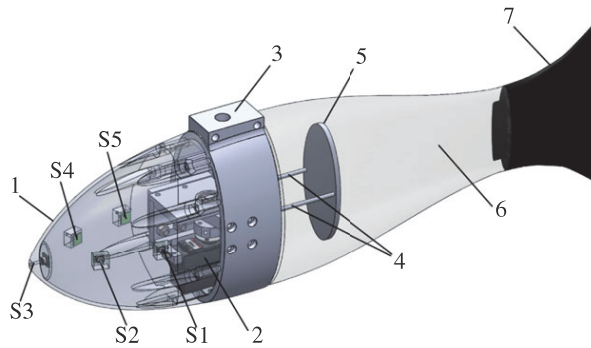


Figure 2. CAD view of the robot. 1, rigid head of the robot; 2, servo-motor; 3, middle part for holding the head and the tail; 4, steel cables; 5, actuation plate; 6, compliant tail; 7, rigid fin; S1–S5, pressure sensors. (Online version in colour.)

We use Intersema MS5407-AM miniature low-noise, high-sensitivity, high-linearity sensors. The signals are digitized by using a 22-bit differential analog–digital converter mounted directly on the printed circuit board (PCB) under the sensor to minimize noise. The range of the sensors is 7 bar and the sensitivity is 0.1 Pa. As the pressure sensors are sensitive to temperature changes, a temperature sensor was attached on the PCB of every sensor, and the pressure is compensated for temperature drifts.

The sensors are connected to a 400 MHz miniature ARM computer mounted inside the FILOSE fish head. The ARM processor also controls a high-torque brushless servo motor used for tail actuation. The on-board computer communicates with the external computer over a serial interface through a cable connected to the robot. The cable is relatively thin to minimize its effect on the robot's motion. All the higher level control and processing is implemented in LabView on board the external computer for runtime debugging, monitoring and analysis.

(b) Test tank

The experiments with the robotic fish were conducted in a flow tunnel with a closed working section 0.5 m wide and high and 1.5 m long. The ceiling of the tunnel is transparent. Flow speed calibration using digital particle image velocimetry (DPIV) system confirmed that up to 50 cm s^{-1} uniform flow can be created with our set-up. As the maximum speed of the fish robot is 19 cm s^{-1} , the maximum flow speed in the experiments was also limited to 19 cm s^{-1} .

For the control experiments, the robot was mounted on a slender polystyrene bar that gave it a positive buoyancy of 0.2 N (figure 3). The robot with the bar was placed in the tunnel so that the bar was supported against the upper glass wall of the flow tunnel with two sharp-ended plastic tips. The depth of the robot was thus fixed and it only moved in the horizontal plane. This type of set-up simplifies the experiments as the robot does not need to have active buoyancy control. The effect of the bar on the swimming dynamics is small because of the much smaller size of the bar compared with the fish robot and minor friction against the glass. This set-up also permits trajectory tracking and motion analysis of the robot with the help of two LEDs mounted on the polystyrene bar detectable with an overview camera through the transparent ceiling.

(c) Kármán vortex street

KVS is a repeating pattern of vortices in the wake of an object. We used two types of objects to create the KVS. First, we experimented with the vertical half-cylinder, which is a classic, well-repeatable approach described thoroughly in the literature [12]. We used a half-cylinder with a diameter of 10 cm and a flow speed of 0.15 cm s^{-1} . DPIV was used to characterize the flow behind the cylinder. The DPIV data were analysed using a custom-made toolbox described

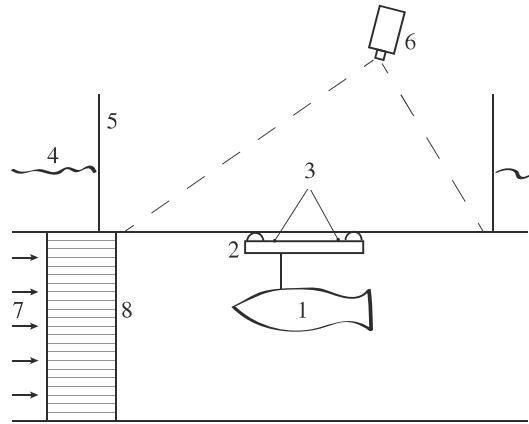


Figure 3. Side-view of the flow tunnel. 1, robotic fish; 2, floater; 3, LED's on the floater for position tracking; 4, water level; 5, transparent glass box on top of the tunnel for filming; 6, camera for position tracking; 7, flow direction; 8, collimators.

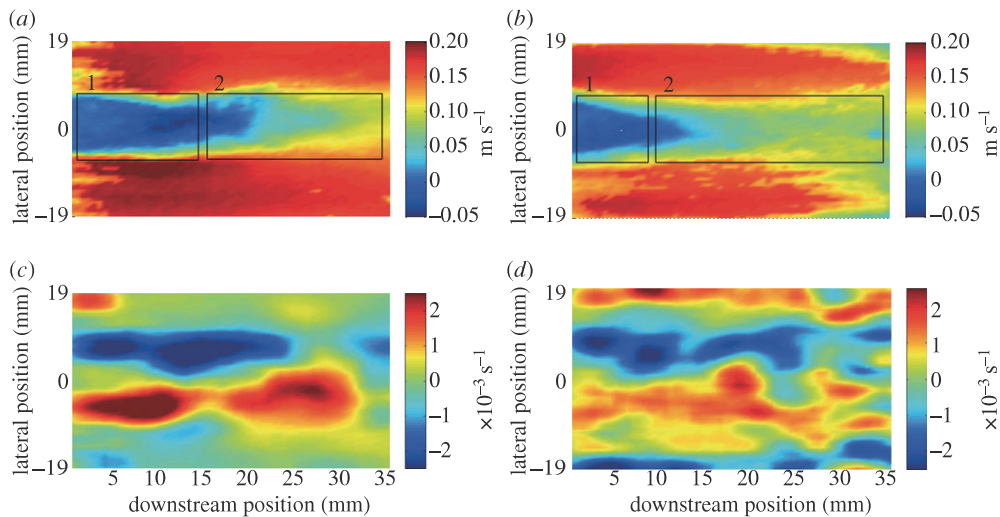


Figure 4. Results of the DPIV analyses. (a,b) The mean downstream velocity behind the cylinder (a) and the cuboid (b). (c,d) The vorticity behind the cylinder (c) and the cuboid (d). On the mean velocity (a,b): 1, suction zone; 2, reduced flow area.

in [31]. In figure 4, an instant vorticity (below) and the mean downstream velocity (above) are shown. Table 1 indicates the parameters required for our study. Figure 4c illustrates that the cylinder generates well-developed vortices. Figure 4a shows that the velocity behind the cylinder is considerably slower (blue colour) than the velocity next to the cylinder outside the vortex street (red colour). When moving closer than 13.7 cm to the cylinder (the suction point), the downstream flow becomes negative. This is an important distance to consider in the controller design because an object placed into the suction zone will be sucked against the cylinder. Downstream from the suction zone is the area of reduced flow. This is the most favourable place for the fish robot station holding because of the decreased drag.

To test our artificial lateral line robot control also in less perfect and thus more natural conditions, we replaced a cylinder with a cuboid. The height of the cuboid was 155 mm and the width and length were 100 mm. The centre of the cuboid was placed at the same height as the robot's centre plane. Figure 4d demonstrates that no well-developed vortex street exists behind

Table 1. KVS description.

parameter	behind the cylinder	behind the the cuboid
incoming flow speed (cm s ⁻¹)	15	15
tank width (cm)	50	50
object width (cm)	10	10
vortex shedding frequency (Hz)	0.4	0.3
vortex street width (cm)	(13.7 ± 1.2)	(14.8 ± 1.3)
suction point (cm)	(13.7 ± 0.6)	(6.5 ± 0.6)
vortex shedding point (cm)	(42.4 ± 0.6)	(35.5 ± 0.6)
mean velocity inside KVS (cm s ⁻¹)	9.4	6.1
mean velocity outside KVS (cm s ⁻¹)	16.4	14.4

the cuboid. From the velocity image in figure 4b, it can be seen that the suction zone is shorter than behind the cylinder. Also the flow speed in the area of reduced flow is narrower and not as stable as behind the cylinder.

3. Station holding in steady flow

(a) Flow speed detection

From our previous studies with a fixed robotic fish with pressure sensors, we know that the flow speed can be estimated by the pressure drop on the sides of the robot or by the pressure difference between the tip of the nose and on the sides [32]. Here, we study if the same relations hold for the freely swimming robot and if they can be used to design a controller for station holding.

If the robot is facing directly towards the flow, the pressure sensor at the tip of the nose measures the stagnation pressure p_0 . It is equal to the sum of the free-stream static pressure p_{fs} and the free-stream dynamic pressure: $p_0 = p_{fs} + 1/2\rho V^2$, where ρ is the density of water and V the free-stream velocity. From that we can find the flow speed

$$V = \sqrt{\frac{2(p_0 - p_{fs})}{\rho}}, \quad (3.1)$$

where p_{fs} can be measured at the point on the robot's head, where the flow speed is equal to the free flow speed. None of our sensors is mounted at this point, meaning that pressure difference ($p_0 - p_{fs}$) cannot be directly measured. We measure the difference between the nose sensor and the average pressure of the side sensors ($p_0 - p_a$) instead. Within the velocity range of our robot, we have found that the difference of these two values can be approximated by a constant multiplier C_s , giving $(p_0 - p_{fs}) = C_s(p_0 - p_a)$.

To experimentally validate the relation (3.1), we fixed the robot in the flow tunnel and recorded the pressure sensor signals at different flow rates. The results are shown in figure 5. With a correction coefficient $C_s = 0.45$, the theoretical relation (3.1) fitted the experimental data with a goodness of fit $R^2 = 0.975$.

We also estimate the speed using only the average pressure on the sides of the robot. The relationship between the average pressure drop ΔP_a and the flow speed is also plotted in figure 5. We can see that it can be well fitted ($R^2 = 0.993$) with an equation

$$V = 1.74\sqrt{\Delta P_a} + 0.07609\Delta P_a. \quad (3.2)$$

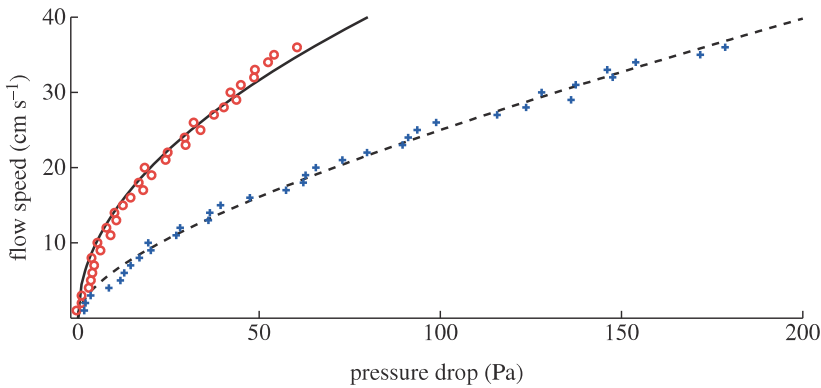


Figure 5. Pressure difference between the tip of the nose and the sides of the robot. Solid line, equation (3.1); dashed line, equation (3.2); circles, $C_s(P_0 - P_a)$; plus symbols, ΔP_a . (Online version in colour.)

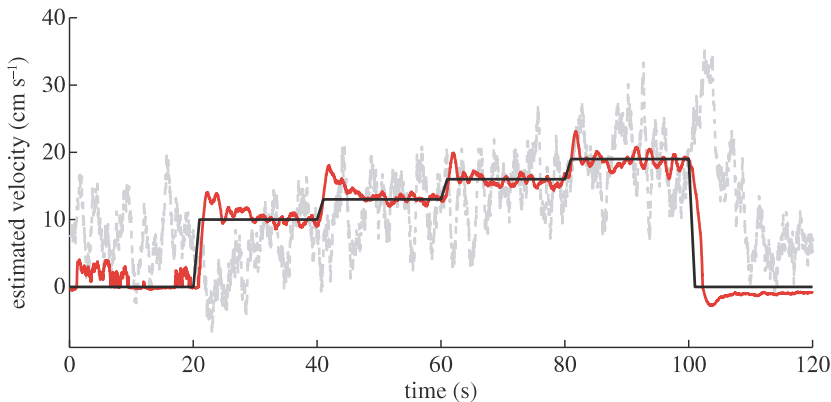


Figure 6. Flow speed estimated using two different methods (estimated velocity: dashed line, difference at nose and on sides; thick solid line, average pressure on sides) while the robot is actuated. The thin solid line marks the actual velocity. (Online version in colour.)

The sensors also measure the environmental pressure, which changes at different velocities because of the motor that is generating flow. Therefore, equation (3.2) is not proportional to the square root of pressure drop as derived from Bernoulli's law, but includes also another component describing the change in environmental pressure.

A validation experiment was conducted with a freely swimming robot. The robot fish was placed in the flow tunnel and its downstream position was kept constant using a proportional, integral, derivative (PID) controller with the feedback from the overhead camera, while the speed of the flow was gradually changed. The controller changed the amplitude of the tail to match the velocity of the robot with that of the flow. The pressure data were recorded and the estimated flow speed was calculated using equations (3.1) and (3.2). The results are shown in figure 6. It can be seen that by using the estimation (3.2) (the average pressure on the sides) the water flow can be estimated with a rather high precision, whereas the estimation from (3.1) is noisy and deemed not to provide high enough precision to be used for downstream position control.

Another set of experiments was conducted to establish the relationship between the flow speed estimation and the orientation angle of the robot. This is important to see whether the estimation also holds when the robot is not directly aligned with the flow. The robot was fixed to the motor using a stiff rod, while the angle of the motor was changed by the control software. The

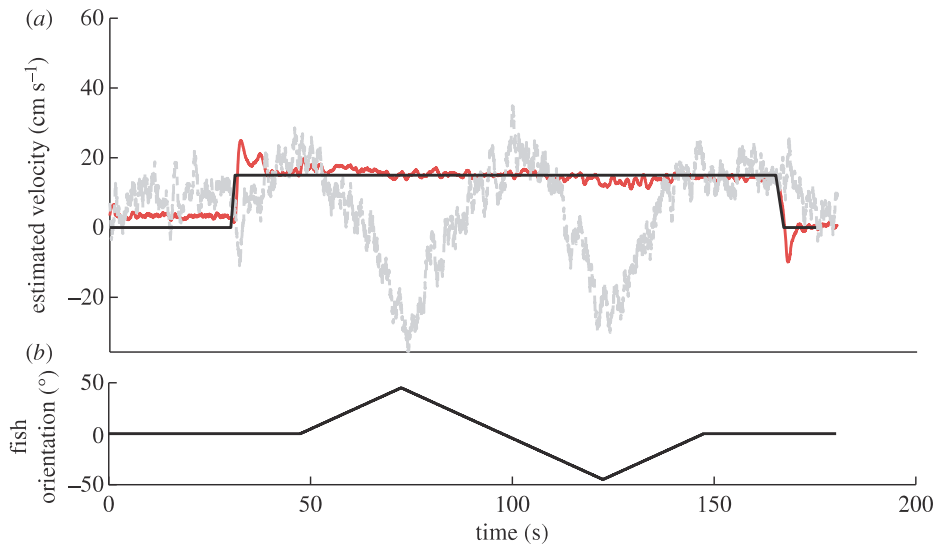


Figure 7. Flow speed estimated using two different methods (estimated velocity: dashed line, difference at nose and on sides; thick solid line, average pressure on sides; thin solid line, actual velocity) while the robot is fixed and its orientation with respect to the flow is changed. (a) The estimated flow speed and the real flow speed, and (b) the deviation from the flow direction. (Online version in colour.)

experiments were carried out with a constant flow speed of 15 cm s^{-1} . The maximum orientation angle with respect to the flow direction was $\pm 45^\circ$. The pressure readings were recorded and the flow speed estimations were calculated. The results are presented in figure 7, where figure 7a shows the speed estimation and figure 7b shows the corresponding robot's orientation. As we can see, equation (3.2) estimates the flow speed with a high precision even if the robot is not oriented towards the flow. There is only a slight increase in error when the angle gets larger. We can also see that equation (3.1) cannot accurately estimate the flow speed unless the robot is facing directly upstream.

The high noise of the estimation (3.1) with a moving robot and the high angle dependability comes from the fact that the stagnation point moves away from the robot's nose when it turns or when its head oscillates. The usage of this relation for robot control is therefore limited to a static robot facing the flow or could be applied with highly distributed lateral line that is able to detect the moving stagnation point. Otherwise the method is very versatile as it does not depend on the depth of the robot or other parameters affecting the environmental pressure.

The estimation (3.2), on the other hand, depends on the environmental pressure and has to be calibrated for every specific environment. However, it is much less orientation-dependent as the pressure drop on the one side of the robot is compensated by the increase in the other side. Also the signal-to-noise ratio of that method is better as the average value of four sensors can be used.

(b) Flow direction detection

When the robot is not directly heading against the flow, the pressure on the side turned towards the flow will be higher. To find the relation between the pressure readings and the robot's orientation, we placed the robot in a steady flow, changed the angle of the robot and recorded the pressure data. The experiment was repeated with three different flow speeds. The anterior sensor pair (S2 and S4) and the posterior sensor pair (S1 and S5) were analysed separately. The correlations are shown in figure 8. We can see that there is a linear relationship between the pressure difference and the robot's orientation. The slope of the trend increases with the increasing flow speed and is larger for the anterior sensor pair.

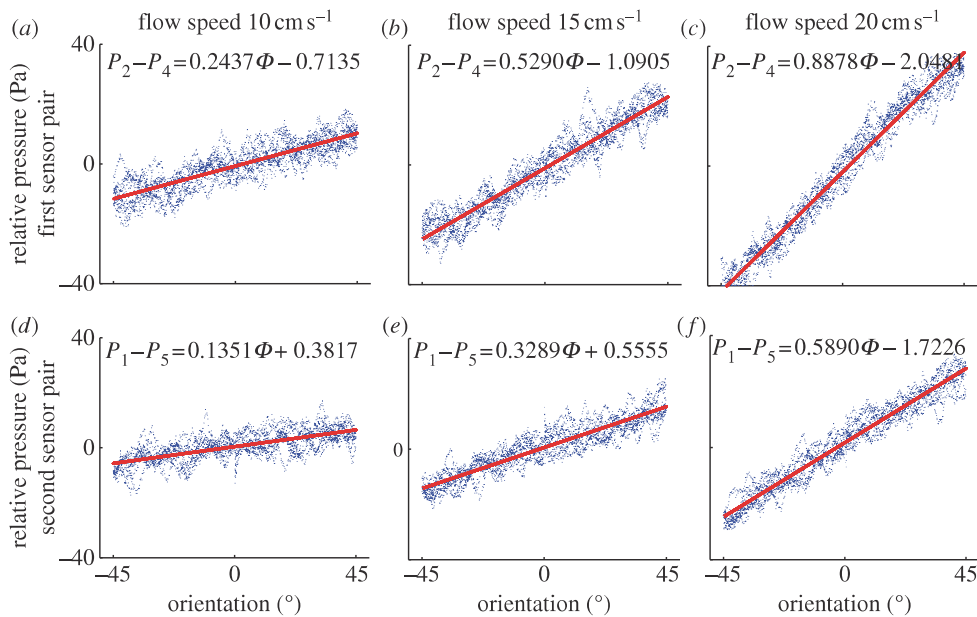


Figure 8. The pressure difference on left- and right-hand sides of the robots head relative to the fish orientation with respect to the flow direction. (a–c) Anterior sensor pair and (d–f) posterior sensor pair at three flow speeds. (Online version in colour.)

Using these relations, we can measure the angle of the robot for the given flow speed and robot geometry. For every different situation, the relation has to be recalibrated. However, if the aim is to orient the robot towards the flow, the exact relation is not necessary as the controller can work only by equalizing the pressure on both sides.

(c) Actuation characterization

The robotic fish was characterized by measuring the swimming velocity at different actuation parameters. The velocity can be varied by changing the amplitude or the frequency of the robot's tail. We have identified that our fish robot is most efficient at the tail-beat frequency of 2 Hz, therefore we fixed the frequency and only found the relation between the robot's forward speed and the actuation amplitude. We placed the robot into the flow tunnel and actuated it with the 2 Hz frequency, while the flow speed was changed and the amplitude was controlled by a PID controller using the position feedback from the camera to keep the robot's downstream position constant. This gave us the amplitude required to make the robot swim at the desired flow speed and actuation frequency. The results show a linear relationship ($R_2 = 0.9885$) between the swimming velocity and the actuation amplitude, making it a reliable control output. The relationship between the velocity and amplitude are described by

$$V = \frac{A + 9.1}{1.56}. \quad (3.3)$$

(d) Control

We implemented a controller for station holding in a steady flow consisting of two parts: the speed controller and the orientation controller (figure 1).

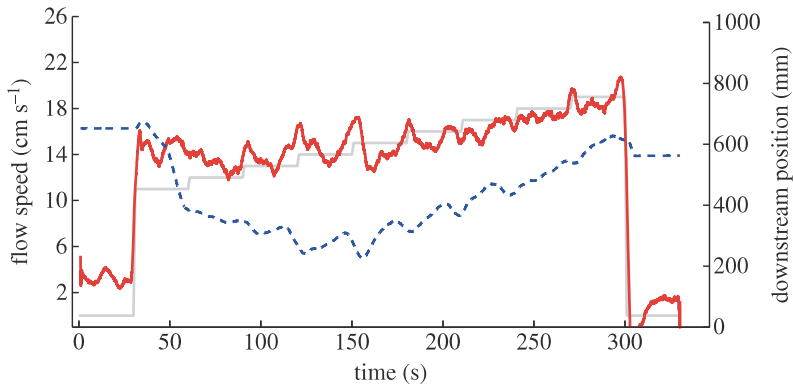


Figure 9. Downstream position of the robot controlled by the station-holding controller while the flow speed is gradually increased over 270 s. The actual flow speed and the estimated flow speed are marked on the left axis and the downstream position is marked on the right axis. Dashed line, downstream position; grey line, actual flow speed; thick solid line, estimated flow speed. (Online version in colour.)

(i) Speed control

The speed controller matches the velocity of the robot to the velocity of the flow $U = V$. This can be achieved by substituting the estimated velocity V from equation (3.2) into equation (3.3) and finding the actuation amplitude A

$$A = 1.56V - 9.1. \quad (3.4)$$

To test the performance of our method for station holding, the freely swimming robot was controlled in flow while the flow speed was gradually changed. The initial flow speed was 11 cm s^{-1} and it was increased after every 30 s by 1 up to 19 cm s^{-1} . The results are shown in figure 9. From the graph, we can see that when the flow was started, the robot overestimated the flow speed and started quickly drifting forward. However, shortly after that the position of the robot became very stable. When the flow was increased further, the robot started slowly drifting backwards owing to small underestimation of the flow speed. This is characteristic to the odometry-based robot localization where the error is integrated over time. In general, the downstream position was very stable. The maximum error over 270 s was about 400 mm (four of five body lengths) and the downstream drift in the end of the experiment was 100 mm (one of five body lengths).

(ii) Orientation

The aim of the orientation control is to control the heading of the robot with respect to the flow. The flow direction estimations presented in §3*b* can be used as an input to the controller. The output will be the offset of the tail's motor. To test the principle and the robustness of the method, we used a simple proportional control

$$\varphi_0 = (\theta_s - \theta_e)K_p, \quad (3.5)$$

where θ_s is the desired orientation angle; θ_e the estimated orientation angle and K_p the proportional gain. We experimentally identified the controller gain for 15 cm s^{-1} flow and tested the controller in the flow tunnel with a desired orientation angle of 0° . Using different angles is problematic in our set-up as the robot would swim quickly against the wall of the tunnel. The controller's performance is demonstrated in figure 10. The graph shows a comparison between the controlled and the uncontrolled orientation angle. When the angle was not controlled, the robot started to oscillate between the walls of the flow tunnel. With a simple pressure-feedback sensor, however, the robot's angle was very stable. The standard deviation of the angle of the

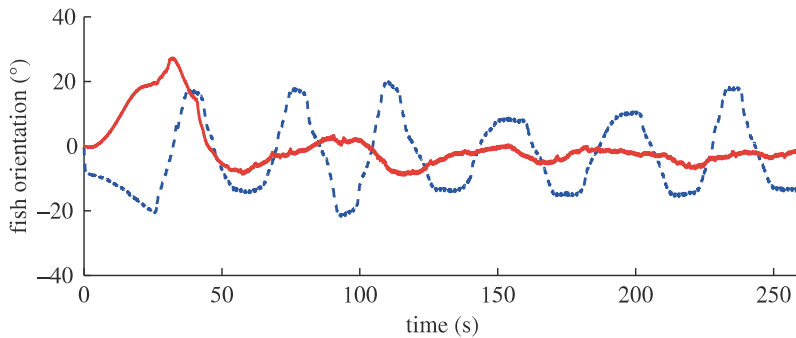


Figure 10. Orientation angle of the robot fish with respect to the flow direction. Dashed line denotes no orientation and solid line denotes pressure-feedback control. (Online version in colour.)

uncontrolled robot was 11.3° while adding the simple controller reduced the standard deviation to 2.9° . The lateral deviation was reduced from 146.3 to 59.2 mm. The excursion from the set angle in the beginning of the dataset is caused by the disturbance when the flow was started. We can see that the controller was able to quickly recover from the disturbance and stabilize the angle.

4. Station holding in the Kármán street

(a) Kármán vortex street detection

From the previous experiments with static pressure sensor arrays, two approaches have been proposed for the KVS detection: frequency spectrum analysis and turbulence intensity analysis [21]. We conducted an experiment with a swimming fish robot in the KVS behind the cylinder to study the feasibility of those approaches for real-time control. The distance from the cylinder was 30 cm and the translational movement was restricted by fixing the floater with a magnet. The robot was actuated and the pressure data were logged. A comparative experiment was conducted in steady flow.

A fast Fourier transform of the recorded data was computed to see whether it is possible to detect dominant frequencies from the frequency spectrum. It was discovered that peak frequencies are present in pressure sensor readings at 2 Hz (actuation frequency) and at 0.4 Hz (vortex shedding frequency), but the minimum time window of the fast Fourier transform was about 30–50 s. This window is obviously too long and not suitable for real-time control.

Another method for KVS detection in [21] analysed the turbulence intensity using the standard deviation of the pressure readings. We compared the standard deviation over different timeframes and detected a 10 per cent average increase in the standard deviation when the robot was in KVS. However, to get a stable difference, a long timeframe (more than 30 s) was needed. When the deviation was calculated from shorter time series, the KVS detection was not reliable enough.

As the proposed methods for KVS detection did not meet the requirements of a real-time application, we developed an alternative approach to KVS detection by measuring the absolute pressure and identifying the reduced flow area behind the object. To test the usability of such an approach, we conducted an experiment, where the tail's offset was controlled manually inside and outside KVS. The tail-beat amplitude was controlled automatically using a camera-feedback control to keep the distance from the cylinder constant at 50 cm. The results of the experiment are shown in figure 11. Figure 11*a* shows the lateral position of the robot with respect to the KVS midline while figure 11*b* presents the corresponding pressure at the tip of the nose. The red line on the lateral position graph is the outer limit (6.8 cm from the midline) of the KVS identified

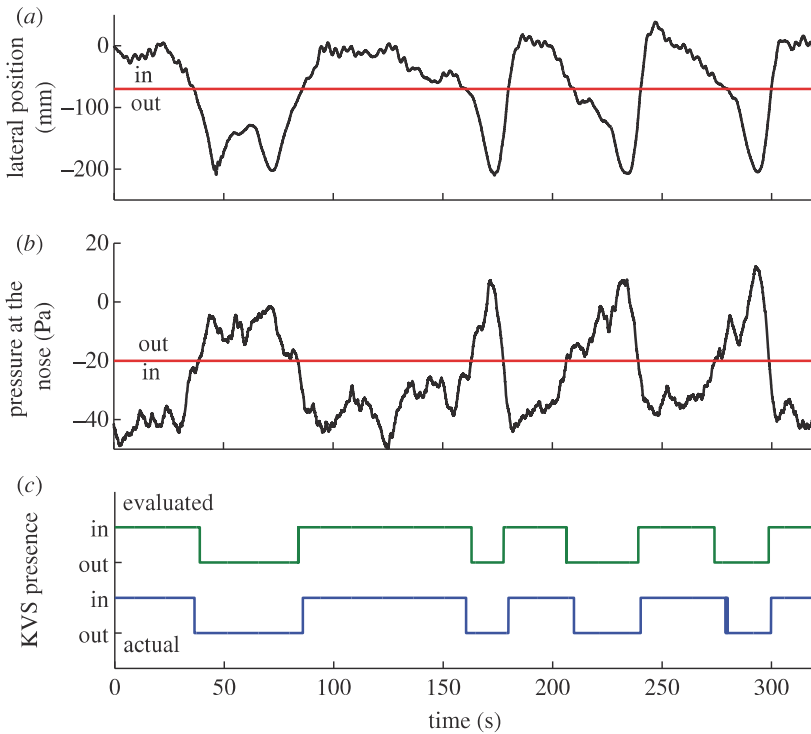


Figure 11. KVS detection using the pressure at the nose. (a) The lateral position of the robot with respect to the KVS midline, and (b) the corresponding pressure at the nose of the robot. The thick solid line on (a) is the limit of the KVS and on (b) it is marking a threshold below which the robot is considered to be in the KVS. (c) Whether the robot is actually in the KVS and its evaluation about the presence of the KVS. (Online version in colour.)

from the DPIV data. It can be seen that the pressure data correlates very well with the presence of the vortex street. We manually determined a pressure threshold for KVS identification. From figure 11c, it can be seen that the estimation matches with the actual presence of the KVS.

(b) Downstream distance estimation

To implement the station-holding controller in the KVS, the robot needs to have an estimate of its distance from the cylinder. To find the correlation between the pressure on the head of the robot and the distance, the robot was placed in KVS at the incoming flow speed 15 cm s^{-1} . The robots downstream position was varied by manipulating it with a magnet through the upper glass wall of the flow tunnel and the pressure data were recorded at various distances. From the results (figure 12), we see that when approaching the cylinder, the average pressure on the sides of the robot is slightly decreasing owing to the lower flow speed behind the cylinder. Another trend is the pressure drop at the tip of the nose when going closer to the cylinder, which is also an expected result because the static pressure behind the cylinder is lower compared with the areas outside the KVS. By combining these two trends, we get a good estimation about the distance from the cylinder:

$$D_{xe} = \frac{(P_3 - P_{\text{avg}}) + 36.29 + C}{0.09815}, \quad (4.1)$$

where D_{xe} is estimated distance from the cylinder; P_3 pressure at the nose and P_{avg} average pressure on the sides. The constant C takes into account the reduced dynamic pressure at the nose resulting from the lateral oscillation of the head. It was identified by actuating the robot in still water and comparing the sensor signals with a steady robot and the actuated robot.

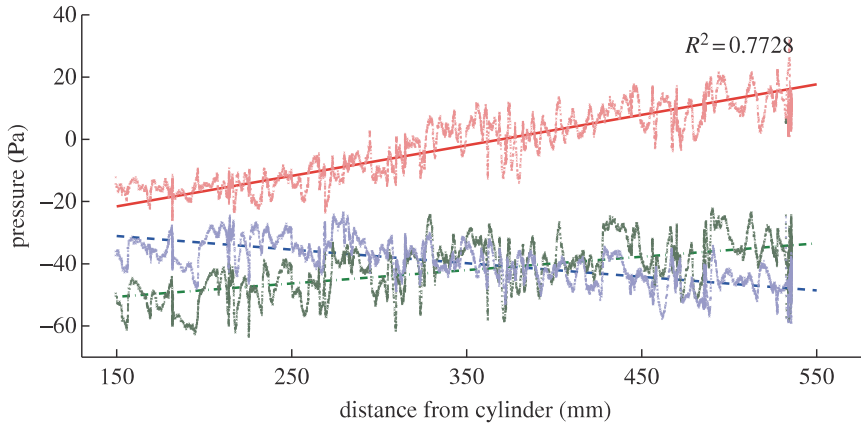


Figure 12. Pressure data in KVS with respect to the distance from the cylinder. Dashed line denotes average pressure on sides, dash-dotted line denotes pressure on nose and solid line denotes difference on nose and sides. (Online version in colour.)

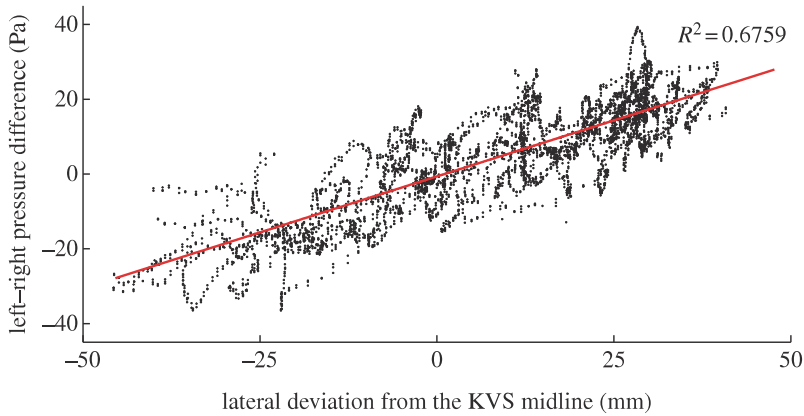


Figure 13. Pressure difference on the left- and on the right-hand sides of the fish robot head versus the lateral deviation from the midline of the KVS. (Online version in colour.)

(c) Lateral position estimation

Another input for the controller is the estimation of the lateral position of the robot with respect to the cylinder or in other words the sideways deviation from the midline of the KVS. As it may be predicted, the sideways movement will cause the asymmetry in the pressure on the left- and on the right-hand sides of the robot owing to the reduced pressure behind the cylinder and increased flow speed when deviating from the midline. To identify this asymmetry, the robot was moved laterally in the KVS at the distance of 200 mm from the cylinder while the pressure data were recorded. The relationship between the lateral position and the pressure difference is presented in figure 13 and is described by the equation

$$D_{ye} = \frac{(P_l - P_r) + 0.63}{0.59}, \quad (4.2)$$

where D_{ye} is the deviation from the midline of the KVS; P_l the average pressure on the left-hand side of the robot and P_r the average pressure on the right-hand side of the robot.

(d) Control

The station-holding controller for the KVS again consists of two parts: the downstream position control and the lateral control (figure 1).

(i) Downstream position control

The downstream position controller keeps the robot in the KVS at the desired distance from the cylinder, which is somewhere between the suction zone and the end of the street, by changing the actuation amplitude of the motor and therefore the forward velocity V of the robot. When the robot is aligned along the midline of the KVS, then there is an actuation amplitude A for every distance D from the cylinder that gives the robot's velocity V equal to the water flow speed U at this point. This stable amplitude is dependent on two components: the water flow speed outside the KVS and the distance from the cylinder. The water flow speed defines the maximum amplitude required to make the robot hold station. When getting closer to the cylinder, the required amplitude gets smaller because of reduced flow behind the cylinder. It is implemented in the controller design by adding another component A_2 to the tail-beat amplitude A_1 .

To find A_2 , we characterized two points in the KVS. The distance D_1 was chosen at the border of the suction zone. This is the distance, where theoretically no actuation is needed to hold the robot at the same location (figure 4). The second point is the minimum distance D_2 where the effect of KVS is becoming insignificant. When increasing the distance beyond this point, the stable amplitude is equal to the free-stream amplitude A_1 . We assumed the decrease in amplitude between these points to be linear giving the component A_2 a form of

$$A_2 = (D_x - D_2) \frac{A_1}{D_2 - D_1}, \quad (4.3)$$

where D_x is the distance from the cylinder. In the controller, D_x is equal to the distance estimation D_{xe} described by equation (4.1). Distances D_1 and D_2 were determined from DPIV images.

The third component of the actuation signal A_3 is introduced to compensate for the up- or downstream drift of the robot. It consists of a proportional and an integral part.

$$A_3 = K_p(D_x - D_{xs}) + K_i \int_0^t (D_x - D_{xs}) dt, \quad (4.4)$$

where D_{xs} is the setpoint; K_p and K_i are experimentally determined controller gains.

The final control law is therefore a combination of all the three described components:

$$A_c = A_1 + A_2 + A_3. \quad (4.5)$$

(ii) Lateral control

The task of the lateral position controller is to keep the fish robot aligned along the midline of the cylinder. We use lateral position estimation described by equation (4.2) as a controller input and turn the robot towards the midline using a proportional control algorithm

$$\varphi = (D_{ys} - D_{ye}) K_p, \quad (4.6)$$

where φ is the tail actuation offset for turning the robot; D_{ys} the set point for lateral position and K_p the experimentally determined proportional gain.

(e) Controller testing

(i) Station holding behind a cylinder

A typical trajectory of a robotic fish holding station in the KVS can be seen in figure 14. We can see that the robot is holding its position during the whole 270 s long experiment. The standard deviation of the downstream position is 40.5 mm and that of the lateral position is 12.7 mm.

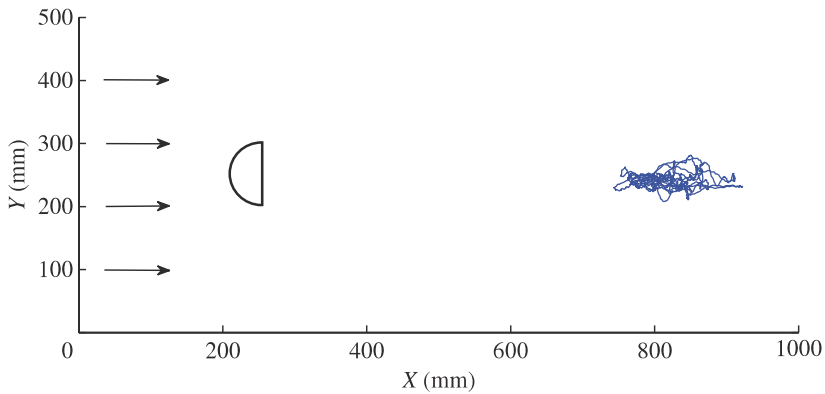


Figure 14. Centre of mass trajectory of a robotic fish over 270 s in a KVS generated by the cylinder with a station-holding control in action. Flow direction and a position of the cylinder are marked on the graph. (Online version in colour.)

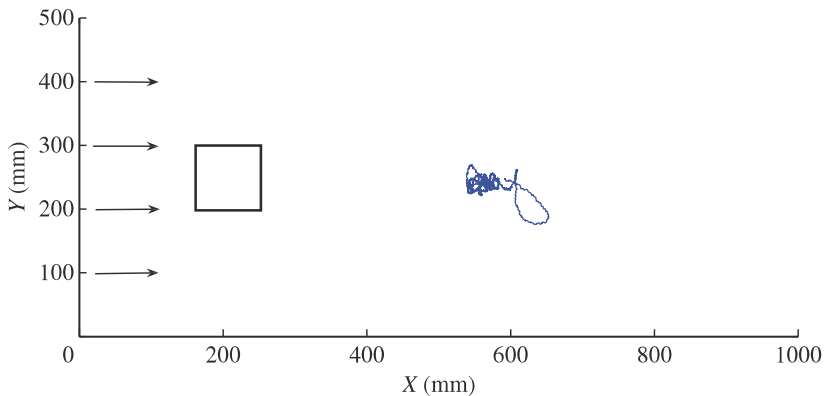


Figure 15. Trajectory of the robot's centre of mass over 270 s holding station behind a cuboid. (Online version in colour.)

(ii) Station holding behind a cuboid

To test the robustness of our control, we repeated the experiment with a cuboid in the flow. The cuboid was placed in uniform flow as described in figure 4. Owing to its non-streamlined shape, it creates a less perfect KVS—the dominant frequency varies and the turbulence is less predictable.

We tested the control with the same controller parameters as behind the cylinder, but the robot was not able to keep a stable position. This is mainly because the area of the reduced flow behind the cuboid is different and more turbulent flow increases the drag. Therefore, we again characterized the environment by identifying D_1 and D_2 . All the other controller parameters were kept the same.

The trajectory of the robot behind the cuboid is presented in figure 15. It can be seen that the robot is able to keep its position for the whole length of the test trial, 270 s. The standard deviation of the downstream position was 21.2 mm and that of the lateral position was 13.3 mm.

(f) Energy consumption in Kármán vortex street

During the experiments, we also monitored the total energy consumption by recording the current consumption of the motor. We compared the energy consumption in the steady flow and in KVS behind the cylinder and behind the cuboid (figure 16). The results show 7 per cent reduced energy

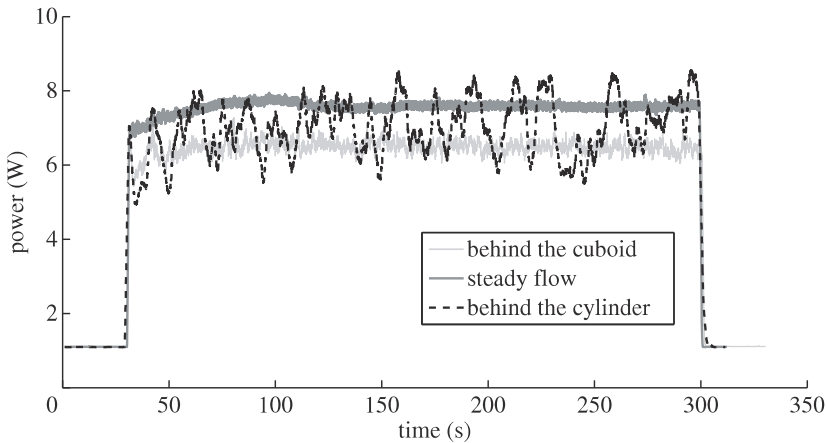


Figure 16. Energy consumption of a robot holding station in the steady flow (thick line) and behind the cuboid (thin line) at equal incoming flow velocity (dashed line, behind the cylinder).

consumption in the reduced flow region behind the cylinder and 17 per cent behind the cuboid. We assume that the better performance behind the cuboid is mainly caused by the well-defined suction zone behind the cylinder. The steeper pressure drop in the cylinder's shadow made it too difficult to approach the suction zone without been sucked in.

5. Discussion

The experiments described in this paper test the feasibility of flow-related control using an artificial lateral line. We designed simple proportional controllers and conducted a series of experiments.

The flow speed detection experiments showed that two different methods can be used for speed estimation. The first approach is finding the difference between the stagnation pressure and the static pressure. The second approach would be measuring only the average pressure drop on the sides of the robot. The first approach is applicable in every environment without the need for calibration. However, it gives reasonable results only with a static robot facing directly the flow. To use it in a more general situation, the measurements have to be combined with data about the fish orientation in flow. The second method needs to be calibrated for the specific environment, but is less angle-dependent. For a more general situation, the usage of these two estimations could be combined together with other sensors of the robot, for example, the inertial measurement unit.

For the moving platform, the pressure measurements provide the odometry reading estimating the robot's relative position with respect to the flow with the accuracy less than one body length of the robot over a duration of 270s with varying flow speeds. The downstream drift in the end of the experiment was one-fifth of the robot's body length. It suggests that the method can provide an accurate enough odometry estimate to be used in case of the absent global reference. As such, it may propose a low cost alternative for the Doppler effect-based odometry [6,7] and for small underwater vehicles for which ADCP devices are too bulky.

We showed that the orientation with respect to the flow can be estimated using the pressure difference on the left- and the right-hand sides. To test if this estimate can be used for orientation control, a set of experiments has to be conducted at varying flow speeds and angle setpoints. The width limits of our test tank do not allow us to experiment with different desired orientation angles. Therefore, we tested the controller only with a robot oriented directly towards the flow, where the robot was able to keep a desired orientation. A variation of this experiment was previously reported in [33], where a simple Braitenberg controller was used to keep the robot facing upstream.

Furthermore, we implemented a controller for station holding in KVS as well as a method for discriminating KVS from uniform flow. Our results showed that periodic turbulence (KVS) can be detected by simply monitoring the pressure readings in the nose of the robot. As opposed to the spectral and turbulence analyses proposed in [21], this method works in real time owing to the very fast response and the very distinctive change in pressure readings at the nose when entering the KVS. If the change is caused solely by the changing speed of the uniform flow, then there will also be difference in the pressure on the sides of the robot, making the identification of those two different events possible. The negative side of our proposed method is that the robot has to be aware of the initial flow properties. It can only detect when the environment changes from one flow regimen to another, because we have manually adjusted the discrimination threshold. The threshold value is valid only for the specific object geometry and flow speed, but the method gives instantaneous feedback about the change of flow regimen. It could be combined with more advanced methods for identification and classification of flow regimens using, e.g. supervised learning or state vector machines. For example, visual data or obstacle detection sensor data could be used to adapt the threshold value for a specific situation.

When the robot has detected the presence of the KVS in the flow, it can switch controlling its position behind an object. The distance from the object as well as the deviation from the KVS midline can be estimated using pressure sensors. The robustness of the controller was tested by repeating the experiment under less perfect, and more natural, environmental conditions, in turbulence generated by a rectangular object. The performance of the robot was stable. However, this conclusion holds only when the properties of the specific KVS are known and the controller parameters are identified based on the specific flow conditions. In our case, we used DPIV imaging to detect the important parameters of the vortex street, but in reality the size of the object generating vortices, its shape and the flow speed can vary. More advanced control methods can be based upon those test results for detecting the parameters of the KVS and fine tuning, e.g. an adaptive controller.

6. Conclusion

In this paper, we demonstrated a flow-based control of an underwater vehicle using artificial lateral line pressure sensors. Various technological solutions have been proposed for implementing artificial lateral lines and their ability to detect hydrodynamic events have been tested, but their application for robot control has not been studied so far. We show that flow regimen identification and flow-related control can be achieved with a simple control architecture using the pressure distribution around the body of a moving robot. This approach for flow-based navigation could be used on any underwater vehicle but is especially valuable for small-scale underwater vehicles in turbulent flows.

We have shown that flow-related control can be achieved in various flow regimens using a simple linear control. Increased signal-to-noise ratio of the sensors and more sophisticated control would improve the performance and make it applicable in a greater variety of hydrodynamic environments. The main limitation of the present approach is the need of calibration for specific conditions. In different situation, the calibration is not valid, however in principle the relations will hold. This allows the use of pressure sensors without exact calibration, for example, when orienting towards the flow or aligning itself behind the object. Our lateral line could be combined with other sensing mechanisms to create adaptive control based on learning algorithms. The biomimetic approach could also be used here as fish have also no awareness of absolute pressures and exact relations.

Our experiments in KVS also showed that station holding behind the object resulted in the reduced energy consumption of the robot. This is consistent with the biological evidence of fish flow refuging [34], where fish are observed to exploit regions of reduced flow to save energy. In real world applications, the artificial lateral line can be used for detecting reduced flow and

holding station in the hydrodynamic shadow similar to the fish refuging behaviour to reduce energy consumption of underwater vehicles. This would lead to increased autonomy and longer missions of the robots.

This work was supported in part by European Commission 7th Framework program under FP7-ICT-2007-3 STREP project FILOSE (Robotic Fish Locomotion and Sensing) and Estonian Information Technology Foundation under Tiger University program.

References

1. Mogdans J, Bleckmann H. 2012 Coping with flow: behavior, neurophysiology and modeling of the fish lateral line system. *Biol. Cybern.* **106**, 627–642. (doi:10.1007/s00422-012-0525-3)
2. Denton EJ, Gray J. 1985 Lateral-line-like antennae of certain of the Penaeidea (Crustacea, Decapoda, Natantia). *Proc. R. Soc. Lond. B* **226**, 249–261. (doi:10.1098/rspb.1985.0094)
3. Dehnhardt G, Mauck B, Bleckmann H. 1998 Seal whiskers detect water movements. *Nature* **394**, 235–236. (doi:10.1038/28303)
4. Folkesson J, Leonard J. 2011 Autonomy through SLAM for an underwater robot. In *Robotics research. The 14th Int. Symp. ISRR* (eds C. Pradalier, R. Siegwart & G. Hirzinger). Springer Tracts in Advanced Robotics, no. 70, pp. 55–70. Berlin, Germany: Springer. (doi:10.1007/978-3-642-19457-3_4)
5. Shkurti F, Rekleitis I, Scaccia M, Dudek G. 2011 State estimation of an underwater robot using visual and inertial information. In *Int. Conf. on Intelligent Robotics and Systems (IROS), San Francisco, CA, USA, 2011*, pp. 5054–5060. New York, NY: Institute of Electrical and Electronic Engineers.
6. Stanway JM. 2010 Water Profile Navigation with an Acoustic Doppler Current Profiler. In *OCEANS 2010 IEEE, Sydney, Australia, 2010*, pp. 1–5. New York, NY: Institute of Electrical and Electronic Engineers.
7. Medagoda L, Williams SB, Pizarro O, Jakuba MV. 2011 Water column current aided localisation for significant horizontal trajectories with Autonomous Underwater Vehicles. In *OCEANS 2011. Sydney, Australia, 2011*, pp. 1–10. New York, NY: Institute of Electrical and Electronic Engineers.
8. Arnold GP. 1974 Rheotaxis in fishes. *Biol. Rev.* **49**, 515–576. (doi:10.1111/j.1469-185X.1974.tb01173.x)
9. Montgomery J, Baker C, Carton A. 1997 The lateral line can mediate rheotaxis in fish. *Nature* **389**, 960–963. (doi:10.1038/40135)
10. Chagnaud BP, Brücker C, Hofmann MH, Bleckmann H. 2008 Measuring flow velocity and flow direction by spatial and temporal analysis of flow fluctuations. *J. Neurosci.* **28**, 4479–4487. (doi:10.1523/JNEUROSCI.4959-07.2008)
11. Liao JC. 2006 The role of the lateral line and vision on body kinematics and hydrodynamic preference of rainbow trout in turbulent flow. *J. Exp. Biol.* **209**, 4077–4090. (doi:10.1242/jeb.02487)
12. Zdravkovich M. 1997 *Flow around circular cylinders: volume 1: fundamentals*. Oxford, UK: Oxford University Press.
13. Cook CL, Coughlin DJ. 2010 Rainbow trout *Oncorhynchus mykiss* consume less energy when swimming near obstructions. *J. Fish Biol.* **77**, 1716–1723. (doi:10.1111/j.1095-8649.2010.02801.x)
14. Liao JC. 2004 Neuromuscular control of fish swimming in a vortex street: implications for energy economy. *J. Exp. Biol.* **207**, 3495–3506. (doi:10.1242/jeb.01125)
15. Liao JC. 2007 A review of fish swimming mechanics and behavior in altered flows. *Phil. Trans. R. Soc. B* **362**, 1973–1993. (doi:10.1098/rstb.2007.2082)
16. Liao JC, Beal DN, Lauder GV, Triantafyllou MS. 2003 The Kármán gait; novel kinematics of rainbow trout swimming in a vortex street. *J. Exp. Biol.* **206**, 1059–1073. (doi:10.1242/jeb.00209)
17. Bleckmann H, Zelick R. 2009 Lateral line system of fish. *Integr. Zool.* **4**, 13–25. (doi:10.1111/j.1749-4877.2008.00131.x)
18. Quattieri A, Rizzi F, Todaro MT, Passaseo A, Cingolani R, De Vittorio M. 2011 Stress-driven AlN cantilever-based flow sensor for fish lateral line system. *Microelectron. Eng.* **88**, 2376–2378. (doi:10.1016/j.mee.2011.02.091)
19. Quattieri A, Rizzi F, Epifani G, Ernits A, Kruusmaa M, De Vittorio M. 2012 Parylene-coated bioinspired artificial hair cell for liquid flow sensing. *Microelectron. Eng.* **98**, 516–519. (doi:10.1016/j.mee.2012.07.072)

20. Yang Y, *et al.* 2010 Artificial lateral line with biomimetic neuromasts to emulate fish sensing. *Bioinspiration Biomimetics* **5**, 16001. (doi:10.1088/1748-3182/5/1/016001)
21. Venturelli R, *et al.* 2012 Hydrodynamic pressure sensing with an artificial lateral line in steady and unsteady flows. *Bioinspiration Biomimetics* **7**, 1–21.
22. Klein A, Bleckmann H. 2011 Determination of object position, vortex shedding frequency and flow velocity using artificial lateral line canals. *Beilstein J. Nanotechnol.* **2**, 276–283. (doi:10.3762/bjnano.2.32)
23. Yu J, Tan M, Shuo W, Erkui C. 2004 Development of a biomimetic robotic fish and its control algorithm. *IEEE Trans. Syst. Man Cybern. B Cybern.* **34**, 1798–1810. (doi:10.1109/TSMCB.2004.831151)
24. Crespi A, Lachat D, Pasquier A, Jispeert AJ. 2007 Controlling swimming and crawling in a fish robot using a central pattern generator. *J. Autonomous Robots* **25**, 3–13. (doi:10.1007/s10514-007-9071-6)
25. El Daou H, Salumäe T, Toming G, Kruusmaa M. 2012 Bio-inspired compliant robotic fish: design and experiments. In *IEEE Int. Conf. on Robotics and Automation (ICRA), Saint Paul, MN, USA, 2012*, pp. 5340–5345. New York, NY: Institute of Electrical and Electronic Engineers.
26. Salumäe T, Kruusmaa M. 2011 A flexible fin with bio-inspired stiffness profile and geometry. *J. Bionic Eng.* **8**, 418–428. (doi:10.1016/S1672-6529(11)60047-4)
27. Coombs S, Janssen J, Webb JF. 1988 Diversity of lateral line systems: evolutionary and functional considerations. In *Sensory biology of aquatic animals* (eds J Atema, RR Fay, AN Popper, WN Tavolga), pp. 553–593. New York, NY: Springer.
28. Braitenberg V. 1984 *Vehicles. Experiments in synthetic psychology*. Cambridge, MA: MIT Press.
29. Sfakiotakis M, Lane DM, Davies JBC. 1999 Review of fish swimming modes for aquatic locomotion. *IEEE J. Oceanic Eng.* **24**, 237. (doi:10.1109/48.757275)
30. El Daou H, Salumäe T, Ristolainen A, Toming G, Listak M, Kruusmaa M. 2011 A Bio-mimetic design and control of a fish-like robot using compliant structures. In *IEEE Int. Conf. on Advanced Robotics, Tallinn, Estonia, 2011*, pp. 563–568. New York, NY: Institute of Electrical and Electronic Engineers.
31. Visentin F, Fiazza MC, Akanyeti O, Venturelli R, Fiorini P. 2011 Towards flow-sensing robots: situated analysis for PIV flow imaging. In *15th Int. Conf. on Advanced Robotics (ICAR), Tallinn, Estonia, 2011*, pp. 606–612. New York, NY: Institute of Electrical and Electronic Engineers.
32. Kruusmaa M, Toming G, Salumäe T, Ježov J, Ernits A. 2011 Swimming speed control and on-board flow sensing of an artificial trout. In *IEEE Int. Conf. on Robotics and Automation (ICRA), Shanghai, China, 2011*, pp. 1791–1797. New York, NY: Institute of Electrical and Electronic Engineers.
33. Salumäe T, Rañó I, Akanyeti O, Kruusmaa M. 2012 Against the flow: a Braitenberg controller for a fish robot. In *2012 IEEE Int. Conf. of Robotics and Automation, Saint Paul, MN, USA, 2012*, pp. 4210–4215. New York, NY: Institute of Electrical and Electronic Engineers.
34. Liao JC, Cotel A. 2013 Effects of turbulence on fish swimming in aquaculture. In *Swimming physiology of fish: part 2, vol. 5* (eds AP Palstra, JV Planas), pp. 109–127. Berlin, Germany: Springer.

APPENDIX H

M. Kruusmaa, G. Toming, T. Salumae, J. Jezov, and A. Ernits, “Swimming speed control and on-board flow sensing of an artificial trout,” in *Proc. IEEE Int. Conf. on Robotics and Automation (ICRA)*, 2011, pp. 1791–1796.

Swimming Speed Control and on-board Flow Sensing of an Artificial Trout

Maarja Kruusmaa, Gert Toming, Taavi Salumäe, Jaas Ježov, Andres Ernits

Abstract—This paper describes a sensing-actuation coupling of a robotic trout that detects changes of the laminar flow speed using an on-board pressure sensor and adjusts its tail-beat frequency for steady swimming.

The caudal fin actuator closely mimics the morphology of a real trout, in particular the geometry, stiffness and stiffness distribution of the body and the caudal fin. We hypothesize that the linear relationship between the tail-beat frequency and speed, well-known and proven to hold for all fish studied so far, also holds for an artificial fish. We validate the hypothesis and use the results to derive a linear control law to adjust the tail-beat frequency to the swimming speed. We use an onboard pressure sensor to detect the flow speed and test the actuation in a controlled hydrodynamic environment in a flow pipe.

I. INTRODUCTION

FISH exhibit remarkable ability to interact with the flow to achieve efficient locomotion [1,2,3]. Proof-of-concept fish robot prototypes and their control together with the theoretical foundations of fish locomotion have been studied for several decades with the intention to improve efficiency [4,6,8], stability [12], agility [14], controllability [5,7,11,13] or maneuverability [9,10] of the underwater robots. While most of the work in underwater robotics focuses on mechanical design and locomotion, and to some extent, locomotion control, there is very little work done for coupling sensing and locomotion to achieve the desired locomotion patterns. To our knowledge, there is no work so far that couples fish robot flow sensing and locomotion using on-board sensors.

Flow sensing is an important source of information of real fish. The lateral line, consisting of superficial and canal neuromasts, is capable of feeling both flow velocity and pressure around the fish [22]. By using this information, fish are able to hold station in turbulent waters, adjust its swimming speed with respect to the surrounding flow, detect nearby obstacles [24, 25], predators and prey by their wake signatures or hold formation while swimming in schools. Blind fish are shown to have most of those abilities [23]. This gives a sufficient rationale to investigate the flow around a robotic fish and we see it as an inevitable prerequisite for efficient fish robot locomotion.

Real-time flow sensing proposes severe engineering

This work is supported by European Union 7th Framework program under FP7-ICT-2007-3 STREP project FILOSE (Robotic Fish Locomotion and Sensing), www.filose.eu

Authors are with Center for Biorobotics, Tallinn University of Technology, Tallinn, Estonia. Email: Maarja.kruusmaa@biorobotics.ttu.ee

challenges due to the instability of the environment, high signal to noise ratio and lack of suitable velocity and pressure sensors with high resolution and low noise level. Recently, some promising attempts are made to develop artificial lateral line sensors [15,16,17]. Flow sensing mechanisms of the lateral line is gaining more and more interests also outside the community of biologists with the aim to put those biologically inspired sensing paradigms into a practical use [18,19,20,21]. Lateral line sensors thus offer a promising perspective for efficient sensing-actuation coupling, but they are still in the early phase of their technological development and have not yet shown to function reliably for such a purpose. A feasible intermediate step would be to study the flow sensing – actuation coupling using more mature technology.

This paper is motivated by the biological evidence of the importance lateral line sensing. So far, underwater robots do not have flow sensing, but fish studies suggest that sensing the flow around the robot can lead to more efficient and stable swimming. In this paper we report an experiment of closing the flow sensing-actuation loop of a fish robot with the help of a commercially available on-board pressure sensor detecting the speed of the laminar flow and correlating the tail beat frequency to the sensor output. The control law is derived from biology literature. The fish robot used in these experiments mimics the morphology of a rainbow trout (*Oncorhynchus mykiss*) and is built with the purpose of studying the computational morphology of fish robots.

II. FISH LOCOMOTION KINEMATICS

Rainbow trout is using BCF (body and caudal fin) propulsion. BCF swimmers use their body and the caudal fin for creating a travelling wave that, by conveying the momentum to the surrounding water, creates the thrust force. Further, rainbow trout is classified as a subcarangiform swimmer, which means that two thirds of its body is used for propulsion while the first, anterior, third of the body stays rigid during swimming [1].

Our fish robot uses a single point actuation by a servo motor placed at the origin of the travelling wave, i.e. at the first third of the robot's body. This design was inspired by the biological studies showing that at steady swimming at cruising speeds, fish engage only the anterior muscles, using the posterior part of the body as a carrier of the travelling wave [26]. Such a design,

as opposed to the segmented serial link actuation is also proposed in [14] as an alternative to simplify the mechanics and control of the robot.

Our aim was, as closely as possible, to replicate the kinematics of the rainbow trout and in our previous work we have investigated how the material properties, such as stiffness and stiffness distribution change the kinematics of the tail fin. We have measured the material properties of the real trout, designed a tail propulsor with similar parameters and shown that the kinematics of the artificial propulsor is similar to the one of the biological fish [27].

Steady swimming occurs when the fish's undulatory movement is repetitive. We can express the kinematics of the steady swimming fish as proposed in [29]:

$$h(x, t) = a(x)\sin(kx - \omega t), \quad (1)$$

where $h(x, t)$ represents displacement in space and time, ω is proportional to the tail-beat frequency, $k = \frac{2\pi}{\lambda}$ is the wave number, with λ representing the wavelength and $a(x)$ is the amplitude envelope expressed by a quadratic function. The amplitude envelope shows the range of motion of a caudal fin and is directly related to the volume of water moved by the fish.

The relationship of tail-beat frequency to swimming velocity is called stride length and it is a kinematic parameter widely studied in biology literature. The stride length is inversely related to the Strouhal number, another parameter commonly investigated in kinematic studies. Strouhal number is defined as

$$St = \frac{fL}{v}, \quad (2)$$

where L is the characteristic length and V is velocity. It has been found that the relationship between tail-beat frequency and velocity is linear and can be expressed in the general form as

$$f = \alpha + \beta V, \quad (3)$$

where f is the tail-beat frequency. Brainbridge studied dace, trout and sunfish and reported for a trout the equation to have the specific form

$$f = 0.32 + 1.44 \frac{V}{L}, \quad (4)$$

where L is the length [31]. Later on the law has been confirmed for many other species [32, 33, 34]. At very low speeds the rule has shown to have exceptions since fish at very low swimming speeds also tend to use pectoral fins to power swimming and their trailing edge amplitude covaries with the frequency.

Webb et al. have studied the locomotor kinematics of the rainbow trout and concluded that for the rainbow trout with

the length $0.055m < L < 0.56m$ in the laminar flow $0.1 \text{ m/s} - 0.7 \text{ m/s}$, the linear relationship between the tail beat frequency and the swimming velocity can be expressed as

$$f = 3.19L^{-\frac{1}{3}} + 1.29 \frac{V}{L}. \quad (5)$$

At the same time, they found the amplitude to be independent of V [30].

The expression (3) in the general form holds for all species studied so far. Thus, Nature gives us a general linear control law that can be used for controlling the motion of the fish-like robot with respect to speed. Since the morphology of our trout robot is similar to a real trout and shown to have similar locomotion kinematics [27], we hypothesize that the linear relationship could be also used for the robot. If this is the case, we have derived a simple, linear, bio-inspired control law for closing the control loop and testing the flow sensing-actuation coupling.

III. MATERIALS AND METHOD

A. Method

The work in this paper is governed by the following methodology:

- We investigate the relationship between f and V to confirm or reject the hypothesis that the biology-inspired linear control law (3) can be also used to control our fish robot prototype. In case the linear relationship holds we use the test results for parameter identification of (3).
- For fish swimming at a constant speed, thrust equals drag. We can therefore determine the tail-beat frequency corresponding to a specific swimming speed by force readings. We design a PI controller and close the control loop minimizing the differences between thrust and drag. The force control test results give us the control law with the accurate gains for steady swimming.
- We test the pressure sensor for stability, sensitivity and accuracy on an underwater cylinder to investigate its suitability for our application.
- We mount the pressure sensor to the head of the artificial trout and test its ability to adjust the swimming speed to flow speed changes using (3) and force plate measurement signals as the observer.

Next sections describe the materials and equipment used in this work.

B. Flow pipe

The experiments are conducted in a flow pipe with a working section of $0.5m \times 0.5m \times 1.5m$. The pipe is embedded into a test tank (see Fig. 1). Laminar flow in the working section is created with the help of a U-shaped flow strengthener and two sequential laminators. The AC motor is used to create the circulation inside the flow pipe and permits controlling the laminar flow speed with 0.04 m/s accuracy. The laminarity of the flow is checked and the flow speed is calibrated using a digital particle image velocimetry (DPIV) system.

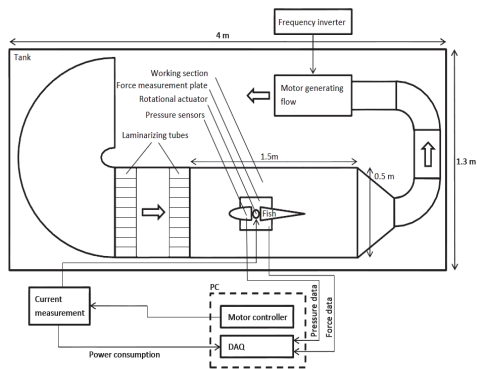


Fig. 1. Top view of the experimental tank. Fish robot is placed inside the flow tunnel where the flow is produced using a screw driven by an AC motor. Robot together with an DC actuator is mounted rigidly on the force measurement system. The system is controlled and force is measured using LabVIEW software and DAQ interface.

C. The Robot

The robot and its fabrication method are described in [27] and [28]. It consists of a rigid head and a compliant tail actuated by a servomotor. The 100 mm long tail is made of a mixture of silicon foam (Soma Foama 15 by Smooth On) and Dragon Skin Silicon Rubber Shore hardness 10A so that it as closely as possible resembles the stiffness and stiffness distribution of a real rainbow trout. As for subcarangiform swimmers, the first third of the anterior part is rigid and made of fiber glass according to the head of a real rainbow trout.

The robot with the size $L = 0.5\text{m}$ is steadily fixed on a rigid rod in the middle of the working section from below (see Fig. 2). The rod is attached to a force plate in the bottom of the test tank. Load cells are mounted in every corner of the rectangular force place, which permits deriving thrust and drag forces by combining the individual force readings.

D. Pressure sensor

We detect the flow speed by using a pressure sensor mounted in the rigid head of the fish and determine the freestream velocity from the pressure sensor readings. We use a small size (6.4mm x 6.2 mm x 2.88 mm), high-sensitivity pressure sensor Intersema MS5407-AM in 7 bar absolute pressure range. The pressure sensor signal is processed with 18 bit ADC with 8 times gain, the reference voltage for ADC is 2,048 V, which gives us pressure sensor sensitivity 3.57 Pa. The supply voltage is 5V. All the electronics is closed into a watertight package and mounted in the head of the robot fish.

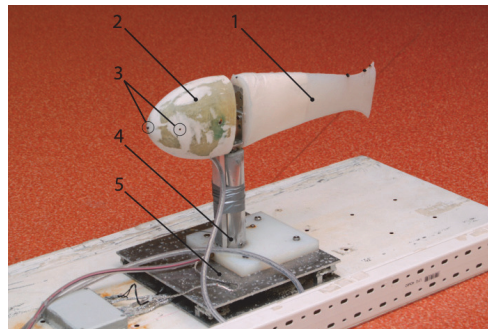


Fig. 2. Robotic fish prototype. 1 – Rotationally-actuated compliant tail; 2 – Head enclosing the electronics for pressure sensors; 3 – Pressure sensors mounted on the tip of the head and on the side of the head; 4 – Rotational actuation mechanism; 5 – Force measurement plate with 4 load to measure longitudinal and lateral forces.

The sensor was chosen because it was the only commercially available sensor getting close to our requirements for sensitivity. However, even here, the repeatability $\pm 0.2\%$ (0.014 bar), 40 mV pressure offset and pressure hysteresis 0.2 %, caused us significant long-term drift problems so that the sensors had to be repeatedly calibrated. The sensor was sensitive to mechanical vibration and acoustic noise from the flow pipe engine, electromagnetic field and disturbances of the power supply voltage. To achieve a tolerable signal to noise ratio, ADC and amplifiers were mounted in the fish head, the wires were shielded, and the electronics of the sensors decoupled. The test tank was bolstered with rubber cushions.

E. Limitations of the Biological Analogy

Though the mechanical design and control of the trout are bio-inspired, there are differences that should be taken into account when interpreting the experimental results and drawing conclusions. In particular:

- Our robot is attached to the rod and the head is steadily fixed because accuracy of the pressure sensor is too low to translate the signals from the moving head into velocity values. Real fish rotate head and move laterally while swimming.
- The rod keeping the robot in place contributes to the overall drag and the system becomes less efficient.
- Real fish hardly aim at achieving some absolute quantitative swimming speed. Rather, they solve the inverse control problem, balancing out thrust and drag or holding station with respect to some visual cues. The problem in this paper was chosen to demonstrate the usability of on-board pressure sensors for control.
- Biological canal lateral line pressure difference detection threshold is 0.1-1mPa whereas our sensor's sensitivity is 10^4 - 10^5 times lower [35].

IV. SENSOR CALIBRATION

Flow speed around the fish head is determined using a pressure sensor, assuming that the flow in the boundary layer around the fish head is laminar and thus the pressure and the laminar flow speed are inversely proportional according to the Bernoulli's law

$$P + \frac{1}{2}\rho V^2 + \rho gh = \text{const.} \quad (6)$$

Here P denotes pressure, ρ is water density and h is the height of the water column. If we assume that the third term expressing the constant atmospheric pressure does not change, we can take it equal to a constant. For the dynamic pressure we thus obtain

$$\text{const} - P_d = \frac{1}{2}\rho V^2, \quad (7)$$

which gives us the relation between pressure and velocity.

The pressure sensor was first tested and calibrated using a well-defined fluid dynamics benchmark measuring pressure around a 80 mm cylinder in a laminar flow at 0.21 m/s. The pressure sensor was mounted inside a motorized cylinder detecting the pressure through a 2mm hole. The cylinder was turned around by 10 degrees, obtaining and averaging over 60 measurements at every step. The 0 degree angle was perpendicular to the flow.

Figure 3 shows experimental results together with the standard deviation obtained experimentally (blue line) and in simulations with the Open Foam computational fluid dynamics solver (red).

The comparison of the experimental and simulation results confirm that the sensor readings are accurate enough when used in region before the separation point.

It can be seen that until 70-90 degree angle the deviations are small and the experimental values quite closely coincide with theoretical estimates. The highest pressure is, as theory predicts, at the leading edge stagnation point at 0 degrees where the theoretical local flow velocity is zero.

The error margins start diverging along with the increasing gap between theoretical and experimental results at 70-90 degree angle. This region corresponds to the separation point of the cylinder, i.e. the point where the boundary layer breaks apart and the cylinder is going to shed a vortex wake, so called von Karman vortex street.

Given the signal to noise ratio of the sensor readings in that region it is rather hard to detect the exact dynamics of the flow topology. The cylinder tests confirm that the signals are stronger and more noise free in the boundary layer while they become too noisy at the turbulent region. This suggests the placement of the pressure sensor in the nose of the fish, close to the stagnation point or on the side, where the flow is still laminar but the pressure drop is steeper along the cylinder profile and thus smaller changes in the flow speed could be detected.

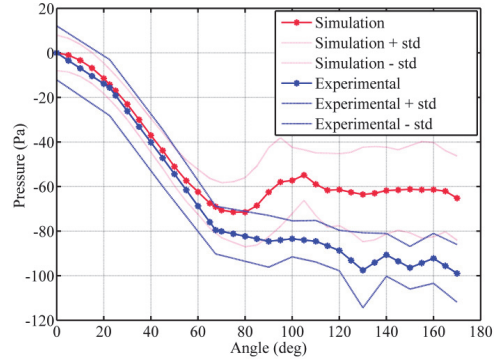
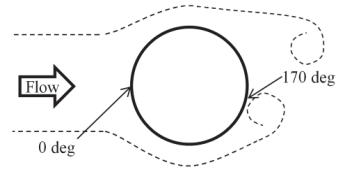


Fig. 3. Pressure sensor calibration setup (above). Pressure around the cylinder in flow with 0.21 m/s velocity (below).

We therefore tested the sensor both in the nose of the fish head, close to the stagnation point and on the side in the laminar flow region. The sensor on the side was better as the differences at low flow speeds got better articulated.

Side looking pressure sensor was mounted into the fish and connected to the environment through a 2mm hole. The head was calibrated in the flume pipe at speeds 0.1 m/s – 0.5 m/s. The pressure sensor readings were recorded while increasing the flow speed by 0.04m/s interval. The pressure – freestream flow speed relationship obtained with curve fitting was

$$V = -0.0001946P^2 - 0.01768P + 0.004003 \quad (8)$$

with the coefficient of determination $R^2 = 0.9902$. As such, the method of determining the freestream velocity from a pressure sensor readings in a laminar region of the flow was confirmed to be very accurate.

V. FORCE CONTROL

Assuming that the linear control law (1) holds also for an artificial fish, a force feedback loop was implemented using a PI controller with the aim of keeping the drag and thrust forces balanced when the flow velocity is changed (see Fig. 4). The flow velocity in the test flume is determined from the flow motor frequencies calibrated with DPIV readings. The flow speed range from 0.1 – 0.5 m/s is determined by the test conditions. The flow velocity 0.5 m/s is currently the upper limit where our flume tank flow is guaranteed to be linear over the whole working section. At every flow condition, the test was ran 10 minutes and the frequency readings were averaged over the measurement interval.

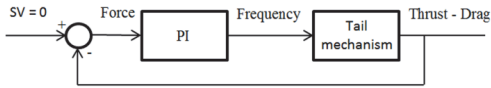


Fig. 4. Force feedback controller.

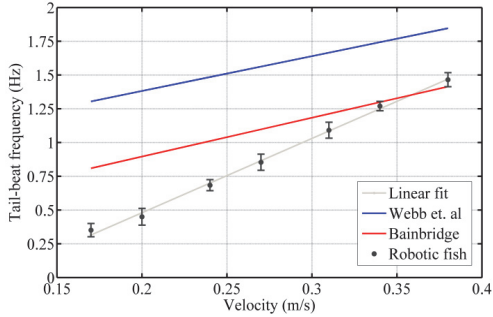


Fig. 5. Average tail-beat frequency required to balance thrust and drag forces. Experimental data is compared to fish tail-beat frequencies at different swimming speeds.

The test results confirm that the general law $f = \alpha + \beta V$ also holds in case of our artificial trout. The control law with the following gains

$$f = -0.6206 + 5.502V \quad (9)$$

was found to be very stable and linear ($R^2 = 0.998$).

Figure 5 shows the test results plotted against the biological evidence from trout kinematics by Webb et al. [30] and Bainbridge [31]. The Strouhal number of our artificial trout is higher than the ones of the real trout with the same length, which renders our artificial trout less efficient than its biological counterparts of the same size ($L = 0.5\text{m}$). Obviously, the differences can be contributed to the dissimilarities between the embodiment, actuation mechanism and experimental setup but also to the fact that at low frequencies the amplitude is found to co-vary with the frequency while in case of our experiment the amplitude is kept constant (10 deg).

VI. SWIMMING CONTROL WITH THE ONBOARD FLOW/PRESSURE SENSING

In this experiment the control law derived and calibrated in section V is used to make the trout to adapt its swimming speed obtained from pressure sensor readings using (9) as shown on Fig. 6. Figure 7 shows the test results plotted against the force control experiments of Section V. The force feedback control and flow sensor control series show only slight dissemblance, which, since the force control appeared to be almost perfectly stable, should be attributed to the flow disturbances and sensor imprecision. The simultaneous force should in an ideal case be exactly zero, but show occasional slight deviations between 0.015 – 0.037N.

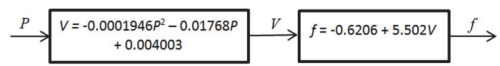


Fig. 6. Tail-beat frequency control with onboard pressure sensing. P – Pressure; V – flow speed; f – tail-beat frequency.

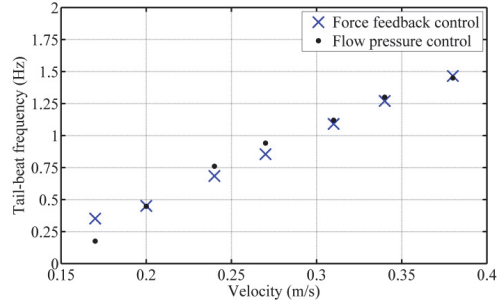


Fig. 7. Tail-beat frequencies using force feedback control and flow pressure control.

VII. CONCLUSIONS

In this paper we demonstrated the speed control of an artificial trout by adjusting its swimming speed with respect to the on-board pressure sensor signals. The contributions of this paper are the following:

1. We derive a linear control law from biology literature and show that it is also applicable on an robotic artifact.
2. We use on-board pressure sensing to control the swimming speed.

Our experimental results show that in a controlled hydrodynamic environment the control of the fish is almost perfectly linear which confirms that both the sensor and the linear control method are suitable for this task. However, our artificial trout is much less efficient than the biological ones. Besides the obvious technological reasons, some of the inefficiency can be attributed to that, while the robot can adjust only its tail-beat frequency, a real fish has many more control parameters, such as the amplitude, amplitude envelope, local stiffness and hence the speed of the travelling wave propagation [34]. Some of those parameters can be also made controllable with the same or a more advanced fish robot, thus also offering a valuable tool for decoupling those influences and studying them separately from the perspective of efficient swimming.

A commercially available pressure sensor turned out to be sufficiently accurate and stable for our purpose, that is, for a simple test in an almost perfectly controllable hydrodynamic environment. Real fish have lateral and recoil motion while they swim and we found the sensor to be too inaccurate to translate the translational and rotational motion in the boundary layer of the fish head into the freestream velocity. Also, the noise to signal ratio is too high for extracting information in a turbulent flow as it could be seen from the

measurements taken near the separation point of the cylinder. Lateral line MEMS sensors could hold the potential to more complicated signal analysis and flow pattern recognition in the future. The testing methods described in this paper can also be used to test and benchmark new types of sensors. In future we plan to use the same method for control in more complicated flows and also in comparison with the MEMS lateral line sensors developed in [36]

REFERENCES

- [1] Michael Sfakiotakis, David M. Lane, and J. Bruce C. Davies, "Review of Fish Swimming Modes for Aquatic Locomotion," *IEEE Journal of Oceanic Engineering*, vol. 24, no. 2, pp. 237-252, April 1999.
- [2] G. V. Lauder, P. G. A. Madden, Learning from Fish: Kinematics and Experimental Hydrodynamics for Roboticists, *International Journal of Automation and Computing* 4 (2006) 325-33
- [3] J.E. Colgate, K.M.Lynch, Mechanics and Control of Swimming, *IEEE Journal of Oceanic Engineering*, Vol. 29, No. 3, July 2004.
- [4] Michael S. Triantafyllou, and George S. Triantafyllou, An Efficient Swimming Machine, *Scientific American*, vol. 272:3, 1995, pp. 272-3.
- [5] K. A. Morgansen, V. Duindam, R. J. Mason, J. W. Burdick, R. M. Murray, Nonlinear Control Methods for Planar Carangiform Robot Fish Locomotion, Proceedings of the 2001 IEEE International Conference on Robotics and Automation, pp. 427-434
- [6] D. S. Barrett, M. S. Triantafyllou, D. K. P. Yue, M. A. Grosenbaugh, and M. J. Wolfgang, Drag Reduction in Fish-like Locomotion, *Journal of Fluid Mechanics*, vol. 392, 1999, pp. 183-212.
- [7] J. Liu and H. Hu. Novel Mechatronics Design for a Robotic Fish. IEEE/RSJ International Conference on Intelligent Robots and Systems (IROS), Edmonton, Canada, 2005, pp. 2077-2082.
- [8] D. S. Barrett, Propulsive Efficiency of a Flexible Hull Underwater Vehicle, PhD Thesis. Massachusetts: Institute of Technology, 1996.
- [9] J. M. Anderson and N. K. Chhabra, "Maneuvering and Stability Performance of a Robotic Tuna," *Integrative and Comparative Biology*, vol. 42, pp. 118-126, 2002.
- [10] J. M. Kumph, Maneuvering of a Robotic Pike, MS Thesis. Massachusetts: Institute of Technology, 2000.
- [11] J. Yu, M. Tan, S. Wang, and E. Chen, "Development of a Biomimetic Robotic Fish and Its Control Algorithm," *IEEE Transactions on Systems, Man, and Cybernetics - Part B: Cybernetics*, vol. 34, no. 4, pp. 1798-1810, 2004.
- [12] N. Kato, "Control performance in the horizontal plane of a fish robot with mechanical pectoral fins," *IEEE J. Oceanic Eng.*, vol. 25, pp. 121-129, Jan. 2000.
- [13] A. Crespi, D. Lachat, A. Pasquier, A.J. Ijspeert, Controlling swimming and crawling in a fish robot using a central pattern generator, *Auton Robot* (2008) 25: 3-13
- [14] V. Alvarado, Design of biomimetic compliant devices for locomotion in liquid environments, Phd Thesis. Massachusetts: Institute of Technology, 2007
- [15] Z. Fan, J. Chen, J.Zou, D. Bullen, C. Liu, F. Delcomyn, Design and fabrication of artificial lateral line flow sensors, *IoP, Journal of Micromechanics and Microengineering*, 12 (2002) 655-661
- [16] Y. Yang, N. Nguyen, N. Chen, M. Lockwood, C. Tucker, H. Hu, H. Bleckmann, C. Liu, D. L. Jones, Artificial lateral line with biomimetic neuromasts to emulate fish sensing, *Iop Publishing, Bioinspiration & Biomimetics*, 5 (2010).
- [17] G. Krijnen, T. Lammerink, R. Wiegrenik, J. Casas, Cricket-inspired flow sensor array, Proc. IEEE Sensors Conference, Atlanta, Georgia; Oct. 28 - 31, p. 539 - 546.
- [18] N. Martiny, S. Sosnowski, K. Khlentz, S. Hirche, Y. Nie, J. P. Franosch, J. L. van Hemmen, Design of a Lateral-Line Sensor for an Autonomous Underwater Vehicle. Preprints of the 8th IFAC International Conference on Manoeuvring and Control of Marine Craft, Brazil, 292-297, 2009.
- [19] J. Goulet, J. Engelmann, B. P. Chagnaud, J. P. Franosch, M. D. Suttner and J. L. van Hemmen, Object localization through the lateral line system of fish: theory and experiment, *Journal of Computational Physiology*, vol. 194, 1-17, 2008.
- [20] A. B. Sichert, R. Bamler and J. L. van Hemmen, Hydrodynamic object recognition, *Physical Review Letters*, 2009.
- [21] A. J. Kalmijn, Hydrodynamic and acoustic field detection, *Sensory Biology of Aquatic Animals*, ed. J. Atema, R. R. Fay, A. N. Popper and W. N. Tavolga, New York, Springer, 83-130, 1988.
- [22] H. Bleckmann, Role of the lateral line in fish behaviour, in "Behavior of Teleost Fishes," Chapter 7, pp. 201 - 235, T. J. Pitcher Ed., Chapman and Hall, 1993
- [23] Theresa Burt de Perera, Spatial parameters encoded in the spatial map of the blind Mexican cave fish, *Astyanax fasciatus*, *Animal Behaviour* Volume 68, Issue 2, August 2004, Pages 291-295
- [24] J. Goulet, J. Engelmann, B. P. Chagnaud, J-M. P. Franosch, M. D. Suttner, J. L. van Hemmen, Object localization through the lateral line system of fish: theory and experiment, *J Comparative Physiology A* (2008) 194:1-17
- [25] A.M. Sutterlin, S. Waddy, , 1975. Possible role of posterior lateral line in obstacle entrainment by brook trout (*Salvelinus fontinalis*). *Journal of the Fisheries Research Board of Canada*, 32 (12), pp 2441.
- [26] J Long, M Mchenry and N Boetticher, Undulatory Swimming: How Traveling Waves are Produced and Modulated in Sunfish (*Lepomis gibbosus*), *Journal of Experimental Biology*, Vol 192, Issue 1, pp. 129-145
- [27] O. Akanyeti, A. Ernits, C. Fiazza, G. Toming, G. Kulikovskis, M. Listak, R. Raag, T. Salumäe, P. Fiorini, M. Kruusmaa, Myometry-Driven Compliant-Body Design for Underwater Propulsion, In Proc. of IEEE Int. Conf on Robotics and Automation, IEEE ICRA 2010, Anchorage, Alaska, May 2010.
- [28] Taavi Salumäe, Design of a compliant underwater propulsion mechanism by investigating and mimicking the body of a rainbow trout (*Oncorhynchus mykiss*). MS Thesis, Tallinn University of Technology, 2010.
- [29] M. Mchenry, C. Pell, J. Jr, Mechanical control of swimming speed: stiffness and axial wave form in undulating fish models, *J Exp Bio*, 198, pp. 2293-2305, 1995.
- [30] P. W. Webb and P. T. Kostecki, "The Effect of Size and Swimming Speed on Locomotor Kinematics of Rainbow Trout," *Journal of Experimental Biology*, vol. 109, pp. 77-95, 1984.
- [31] R. Bainbridge, The speed of swimming of fish as related to size and to the frequency and amplitude of the tail beat. *J. Exp. Bio.*, 35, pp. 109-133, 1958
- [32] J.R. Hunter, J.R. Zweifel, 1971. Swimming speed, tail beat frequency, tail beat amplitude and size in jack mackerel, *Trachurus symmetricus*, and other fishes. *Fishery Bulletin Fish Wildlife Resv. U.S.* 69, pp253-266.
- [33] B. Jayne and G. Lauder, 1995. Speed effects on midline kinematics during steady undulatory swimming of largemouth bass, *The Journal of Experimental Biology*, no. 198, pp. 585-602.
- [34] J. H. Long, Jr, M. E. Porter, R. G. Root, C. W. Liew, Go Reconfigure: How Fish Change Shape as They Swim and Evolve, *Integrative and Comparative Biology*, pp. 1-20, published online, June 24, 2010
- [35] S. M. van Netten, Hydrodynamic detection by cupulae in a lateral line canal: functional relations between physics and physiology, *Biological Cybernetics*, Vol. 94, No 1, pp. 67 - 85.
- [36] A. Quattieri; F. Rizzi; M. Teresa Todaro; A. Passaseo; Massim De Vittorio, Stress-driven AIN cantilever-based flow sensor for fish lateral line system. 36th Int. Conf. on Micro and Nano Engineering 19-22 September 2010, Genova, Italy.

CURRICULUM VITAE

Personal data

Name: Taavi Salumäe
Date of birth: 20.09.1986
Place of birth: Rapla, Estonia
Citizenship: Estonian

Contact data

Address: Kivimäe talu, Oola küla, Rapla vald, Raplamaa 79643, Estonia
Phone: +372 525 44 18
E-mail: taavi@salumae.com

Education

2010 - 2015	Tallinn University of Technology	PhD
2008 - 2010	Tallinn University of Technology	MSc in Mechatronics, <i>Cum Laude</i>
2005 - 2008	Tallinn University of Technology	BSc in Mechatronics
1993 - 2005	Rapla Vesiroosi Gümnaasium	Highschool

Language competence

Estonian	Native
English	Fluent
German	Basic skills
Russian	Basic skills

Professional employment

2012 - ...	Tallinn University of Technology, Centre for Biorobotics	Junior Researcher
2010 - 2012	Tallinn University of Technology, Centre for Biorobotics	Engineer
2009 - 2010	Inserv OÜ	Automation Engineer

ELULOOKIRJELDUS

Isikuandmed

Nimi: Taavi Salumäe
Sünniaasta: 20.09.1986
Sünnikoht: Rapla, Eesti
Kodakondsus: Eesti

Kontaktandmed

Address: Kivimäe talu, Oola küla, Rapla vald, Raplamaa 79643, Eesti
Telefon: +372 525 44 18
E-mail: taavi@salumae.com

Hariduskäik

2010 - 2015	Tallinna Tehnikaülikool	PhD
2008 - 2010	Tallinna Tehnikaülikool	MSC, Mehhatroonika, <i>Cum Laude</i>
2005 - 2008	Tallinna Tehnikaülikool	BSc, Mehhatroonika
1993 - 2005	Rapla Vesiroosi Gümnaasium	Keskharidus

Keeleoskus

Eesti keel	Emakeel
Inglise keel	Kõrgtase
Saksa keel	Algtase
Vene keel	Algtase

Teenistuskäik

2012 - ...	Tallinna Tehnikaülikool, Biorobootika Keskus	Nooremteadur
2010 - 2012	Tallinna Tehnikaülikool, Biorobootika Keskus	Insener
2009 - 2010	Inserv OÜ	Automaatikainsener

**DISSERTATIONS DEFENDED AT
TALLINN UNIVERSITY OF TECHNOLOGY ON
*INFORMATICS AND SYSTEM ENGINEERING***

1. **Lea Elmik**. Informational Modelling of a Communication Office. 1992.
2. **Kalle Tammemäe**. Control Intensive Digital System Synthesis. 1997.
3. **Eerik Lossmann**. Complex Signal Classification Algorithms, Based on the Third-Order Statistical Models. 1999.
4. **Kaido Kikkas**. Using the Internet in Rehabilitation of People with Mobility Impairments – Case Studies and Views from Estonia. 1999.
5. **Nazmun Nahar**. Global Electronic Commerce Process: Business-to-Business. 1999.
6. **Jevgeni Riipulk**. Microwave Radiometry for Medical Applications. 2000.
7. **Alar Kuusik**. Compact Smart Home Systems: Design and Verification of Cost Effective Hardware Solutions. 2001.
8. **Jaan Raik**. Hierarchical Test Generation for Digital Circuits Represented by Decision Diagrams. 2001.
9. **Andri Riid**. Transparent Fuzzy Systems: Model and Control. 2002.
10. **Marina Brik**. Investigation and Development of Test Generation Methods for Control Part of Digital Systems. 2002.
11. **Raul Land**. Synchronous Approximation and Processing of Sampled Data Signals. 2002.
12. **Ants Ronk**. An Extended Block-Adaptive Fourier Analyser for Analysis and Reproduction of Periodic Components of Band-Limited Discrete-Time Signals. 2002.
13. **Toivo Paavle**. System Level Modeling of the Phase Locked Loops: Behavioral Analysis and Parameterization. 2003.
14. **Irina Astrova**. On Integration of Object-Oriented Applications with Relational Databases. 2003.
15. **Kuldar Taveter**. A Multi-Perspective Methodology for Agent-Oriented Business Modelling and Simulation. 2004.
16. **Taivo Kangilaski**. Eesti Energia käiduhaldussüsteem. 2004.
17. **Artur Jutman**. Selected Issues of Modeling, Verification and Testing of Digital Systems. 2004.
18. **Ander Tenno**. Simulation and Estimation of Electro-Chemical Processes in Maintenance-Free Batteries with Fixed Electrolyte. 2004.
19. **Oleg Korolkov**. Formation of Diffusion Welded Al Contacts to Semiconductor Silicon. 2004.

20. **Risto Vaarandi**. Tools and Techniques for Event Log Analysis. 2005.
21. **Marko Koort**. Transmitter Power Control in Wireless Communication Systems. 2005.
22. **Raul Savimaa**. Modelling Emergent Behaviour of Organizations. Time-Aware, UML and Agent Based Approach. 2005.
23. **Raido Kurel**. Investigation of Electrical Characteristics of SiC Based Complementary JBS Structures. 2005.
24. **Rainer Taniloo**. Ökonoomsete negatiivse diferentsiaaltakistusega astmete ja elementide disainimine ja optimeerimine. 2005.
25. **Pauli Lallo**. Adaptive Secure Data Transmission Method for OSI Level I. 2005.
26. **Deniss Kumlander**. Some Practical Algorithms to Solve the Maximum Clique Problem. 2005.
27. **Tarmo Veskioja**. Stable Marriage Problem and College Admission. 2005.
28. **Elena Fomina**. Low Power Finite State Machine Synthesis. 2005.
29. **Eero Ivask**. Digital Test in WEB-Based Environment 2006.
30. **Виктор Войтович**. Разработка технологий выращивания из жидкой фазы эпитаксиальных структур арсенида галлия с высоковольтным р-п переходом и изготовления диодов на их основе. 2006.
31. **Tanel Alumäe**. Methods for Estonian Large Vocabulary Speech Recognition. 2006.
32. **Erki Eessaar**. Relational and Object-Relational Database Management Systems as Platforms for Managing Softwareengineering Artefacts. 2006.
33. **Rauno Gordon**. Modelling of Cardiac Dynamics and Intracardiac Bio-impedance. 2007.
34. **Madis Listak**. A Task-Oriented Design of a Biologically Inspired Underwater Robot. 2007.
35. **Elmet Orasson**. Hybrid Built-in Self-Test. Methods and Tools for Analysis and Optimization of BIST. 2007.
36. **Eduard Petlenkov**. Neural Networks Based Identification and Control of Nonlinear Systems: ANARX Model Based Approach. 2007.
37. **Toomas Kirt**. Concept Formation in Exploratory Data Analysis: Case Studies of Linguistic and Banking Data. 2007.
38. **Juhan-Peep Ernits**. Two State Space Reduction Techniques for Explicit State Model Checking. 2007.

39. **Innar Liiv**. Pattern Discovery Using Seriation and Matrix Reordering: A Unified View, Extensions and an Application to Inventory Management. 2008.
40. **Andrei Pokatilov**. Development of National Standard for Voltage Unit Based on Solid-State References. 2008.
41. **Karin Lindroos**. Mapping Social Structures by Formal Non-Linear Information Processing Methods: Case Studies of Estonian Islands Environments. 2008.
42. **Maksim Jenihhin**. Simulation-Based Hardware Verification with High-Level Decision Diagrams. 2008.
43. **Ando Saabas**. Logics for Low-Level Code and Proof-Preserving Program Transformations. 2008.
44. **Ilja Tšahhirov**. Security Protocols Analysis in the Computational Model – Dependency Flow Graphs-Based Approach. 2008.
45. **Toomas Ruuben**. Wideband Digital Beamforming in Sonar Systems. 2009.
46. **Sergei Devadze**. Fault Simulation of Digital Systems. 2009.
47. **Andrei Krivošei**. Model Based Method for Adaptive Decomposition of the Thoracic Bio-Impedance Variations into Cardiac and Respiratory Components. 2009.
48. **Vineeth Govind**. DfT-Based External Test and Diagnosis of Mesh-like Networks on Chips. 2009.
49. **Andres Kull**. Model-Based Testing of Reactive Systems. 2009.
50. **Ants Torim**. Formal Concepts in the Theory of Monotone Systems. 2009.
51. **Erika Matsak**. Discovering Logical Constructs from Estonian Children Language. 2009.
52. **Paul Annus**. Multichannel Bioimpedance Spectroscopy: Instrumentation Methods and Design Principles. 2009.
53. **Maris Tõnso**. Computer Algebra Tools for Modelling, Analysis and Synthesis for Nonlinear Control Systems. 2010.
54. **Aivo Jürgenson**. Efficient Semantics of Parallel and Serial Models of Attack Trees. 2010.
55. **Erkki Joason**. The Tactile Feedback Device for Multi-Touch User Interfaces. 2010.
56. **Jürgo-Sören Preden**. Enhancing Situation – Awareness Cognition and Reasoning of Ad-Hoc Network Agents. 2010.
57. **Pavel Grigorenko**. Higher-Order Attribute Semantics of Flat Languages. 2010.

58. **Anna Rannaste.** Hierarcical Test Pattern Generation and Untestability Identification Techniques for Synchronous Sequential Circuits. 2010.
59. **Sergei Strik.** Battery Charging and Full-Featured Battery Charger Integrated Circuit for Portable Applications. 2011.
60. **Rain Ottis.** A Systematic Approach to Offensive Volunteer Cyber Militia. 2011.
61. **Natalja Sleptšuk.** Investigation of the Intermediate Layer in the Metal-Silicon Carbide Contact Obtained by Diffusion Welding. 2011.
62. **Martin Jaanus.** The Interactive Learning Environment for Mobile Laboratories. 2011.
63. **Argo Kasemaa.** Analog Front End Components for Bio-Impedance Measurement: Current Source Design and Implementation. 2011.
64. **Kenneth Geers.** Strategic Cyber Security: Evaluating Nation-State Cyber Attack Mitigation Strategies. 2011.
65. **Riina Maigre.** Composition of Web Services on Large Service Models. 2011.
66. **Helena Kruus.** Optimization of Built-in Self-Test in Digital Systems. 2011.
67. **Gunnar Piho.** Archetypes Based Techniques for Development of Domains, Requirements and Software. 2011.
68. **Juri Gavšin.** Intrinsic Robot Safety Through Reversibility of Actions. 2011.
69. **Dmitri Mihhailov.** Hardware Implementation of Recursive Sorting Algorithms Using Tree-like Structures and HFSM Models. 2012.
70. **Anton Tšertov.** System Modeling for Processor-Centric Test Automation. 2012.
71. **Sergei Kostin.** Self-Diagnosis in Digital Systems. 2012.
72. **Mihkel Tagel.** System-Level Design of Timing-Sensitive Network-on-Chip Based Dependable Systems. 2012.
73. **Juri Belikov.** Polynomial Methods for Nonlinear Control Systems. 2012.
74. **Kristina Vassiljeva.** Restricted Connectivity Neural Networks based Identification for Control. 2012.
75. **Tarmo Robal.** Towards Adaptive Web – Analysing and Recommending Web Users` Behaviour. 2012.
76. **Anton Karputkin.** Formal Verification and Error Correction on High-Level Decision Diagrams. 2012.
77. **Vadim Kimlaychuk.** Simulations in Multi-Agent Communication System. 2012.

78. **Taavi Viilukas**. Constraints Solving Based Hierarchical Test Generation for Synchronous Sequential Circuits. 2012.
79. **Marko Kääramees**. A Symbolic Approach to Model-based Online Testing. 2012.
80. **Enar Reilent**. Whiteboard Architecture for the Multi-agent Sensor Systems. 2012.
81. **Jaan Ojarand**. Wideband Excitation Signals for Fast Impedance Spectroscopy of Biological Objects. 2012.
82. **Igor Aleksejev**. FPGA-based Embedded Virtual Instrumentation. 2013.
83. **Juri Mihhailov**. Accurate Flexible Current Measurement Method and its Realization in Power and Battery Management Integrated Circuits for Portable Applications. 2013.
84. **Tõnis Saar**. The Piezo-Electric Impedance Spectroscopy: Solutions and Applications. 2013.
85. **Ermo Täks**. An Automated Legal Content Capture and Visualisation Method. 2013.
86. **Uljana Reinsalu**. Fault Simulation and Code Coverage Analysis of RTL Designs Using High-Level Decision Diagrams. 2013.
87. **Anton Tšepurov**. Hardware Modeling for Design Verification and Debug. 2013.
88. **Ivo Mürsepp**. Robust Detectors for Cognitive Radio. 2013.
89. **Jaas Ježov**. Pressure sensitive lateral line for underwater robot. 2013.
90. **Vadim Kaparin**. Transformation of Nonlinear State Equations into Observer Form. 2013.
92. **Reeno Reeder**. Development and Optimisation of Modelling Methods and Algorithms for Terahertz Range Radiation Sources Based on Quantum Well Heterostructures. 2014.
93. **Ants Koel**. GaAs and SiC Semiconductor Materials Based Power Structures: Static and Dynamic Behavior Analysis. 2014.
94. **Jaan Übi**. Methods for Coepetition and Retention Analysis: An Application to University Management. 2014.
95. **Innokenti Sobolev**. Hyperspectral Data Processing and Interpretation in Remote Sensing Based on Laser-Induced Fluorescence Method. 2014.
96. **Jana Toompuu**. Investigation of the Specific Deep Levels in p -, i - and n -Regions of GaAs p^+pin-n^+ Structures. 2014.